The Development of Iron Catalysts for Suzuki-Miyaura Cross-Coupling and the Reactivity Discovered Along the Way

Michael Crockett

A dissertation

submitted to the Faculty of

the department of Chemistry

in partial fulfillment

of the requirements for the degree of

Doctor of Philosophy

Boston College

Morrissey College of Arts and Sciences
Graduate School

May 2020

The Development of Iron Catalysts for Suzuki-Miyaura Cross-Coupling and the Reactivity Discovered Along the Way

Michael Crockett

Advisor: Professor Jeffery Byers

Abstract: This dissertation discusses the development of iron-based catalysts for Suzuki-Miyaura cross-coupling reactions and some of the unique reactivity that was discovered as a direct result of these studies. Chapter one will review the area of iron-catalyzed cross-coupling with an emphasis placed on areas where iron provides complimentary reactivity to other metals. Chapter two will detail the initial discovery of conditions that allow for iron-catalysts to participate in the cross-coupling of aryl boronic esters and alkyl halides. Chapter three will discuss the the development of ligands for iron that allow for more general cross-coupling reactivity to be observed. Finally, chapter four will discuss the unique C-H funtionalization reactivty that has been observed as byproducts in chapters two and three. Digging deeper into this reactivty lead to the discovery of a completely novel three-component coupling reaction mediated by the iron complexes discovered in chapter three.

Table of Contents

List of Tables

List of Figures

Acknowledgements

I would like to thank everyone who made this thesis possible and enabled the completion of my Ph.D. at Boston College. Firstly, I would like to thank the members of my thesis committee. Prof. Zhang and Prof. Liu have provided extensive feedback that has served to strengthen the writing here. Additionally, Prof. Liu and Prof. Kelly provided very helpful feedback on my original research proposal that will undoubtedly be very helpful in my career.

I would like to thank Prof. Jeffery Byers for his indefatigable support of the chemistry that I have worked on. Anytime that I would hit a wall in the research his door was always open for advice. He consistently challenged me to be the best chemist that I can be and provided numerous opportunities for me to showcase the skills I acquired in his group. Most importantly, he showed me that research didn't have to be your exclusive passion through his commitment to teaching and outreach.

I would like to thank the faculty and staff in the Boston College Chemistry Department. In particular, Dale, Ian and Lynne in the main office have always been very helpful and have made the last 5 years enjoyable. Additionally, I would like to thank John and TJ in the NMR lab for a tremendous amount of support over the last 5 years. TJ additionally was always someone that I could talk to and his emails could often be a bright spot in my day. I would also like to thank Sally Wyman. Her commitment to helping us find what we need in the literature is commendable and I was grateful that she was always around when I had questions.

I would additionally like to thank Prof. Neil Wolfman. I had the pleasure of teaching with him for 4 years during my time at Boston College and in that time he showed me what it meant to be an ally and mentor. His commitment to teaching and people in general amazed me. I hope that I can be even 10 % of the teacher and friend that he was. He will be sorely missed.

None of the work presented in the following pages would have been possible without the help of a tremendous number of people. In particular, working with Teresa Make, Chet Tyrol, Alex Wong, and Nancy Yone on the so called "small molecule" projects has been tremendously enjoyable and productive. I also had the great privilege of working with excellent collaborators, including Jeffery Sears and Mike Neidig in Rochester as well as Hongtu Zhand and Christine Thomas at Ohio State. I would also like to thank Brian Sparling and Jason Tedrow for a tremendous amount of help with the projects discussed in chapters 2 and 3. I would also like to thank the Byers group members past and present for helping to create a space that was always welcoming to me. In particular, I would like to thank Miao Qi for being a great friend and always helping to push me on chemistry. Without her support a number of the more outlandish experiments in this thesis might not have been performed.

I would like to express my deepest gratitude to the tremendous number of friends I have made in my time at Boston College. It has been amazing to relocate so far from home and find a new home out here. From bar crawls to barbeques and ski trips, I will remember my time out here forever and hope to visit this now very extensive network wherever we may find each other in the world!

I am overwhelmed by the support, love, and encouragement my family has given me throughout my education. I am so grateful to have a family that truly values my education and helped remove the many obstacles that stood before me. Trips to the mountains and the beach were an always welcome reprieve.

Finally, I would like to thank my wonderful girlfriend Hannah for the support she has given me for the last 5 years. Though it wasn't easy living apart for the first three years, I always felt as though she had my back and that we would get through this together.

Chapter 1. The Development of Iron-Catalyzed Coupling Reactions and Comparisons to State-of-the-Art Nickel-Based Systems.

1.1.   Introduction

The advent of metal-catalyzed coupling reactions has had broad reaching influence in pharmaceutical and natural product synthesis.[1] Due to the tremendous success of palladium-catalyzed couplings between two sp^2-hybridized carbon centers, some have postulated that the breadth of explored pharmaceutical targets has been limited by these methods.[2] As a result, the exploration of coupling reactions that can be applied to sp^3-hybridized carbon centers has been a central focus of the last three decades. In particular, methods utilizing abundant first-row transition metals have shown tremendous promise for addressing this challenge.[3] Methods using nickel-based catalysts have taken a dominant position in this field and represent the lion's share of all papers published for these sp^3 containing coupling reactions.[3] While nickel-catalyzed methods have been tremendously useful, many groups have been interested in developing alternative methods based on the other first-row transition metals.[4-6] While considerations such as the toxicity of nickel catalysts are inportant to consider, the purpose of this overview is to highlight the development of iron-catalyzed coupling methods with an emphasis in how these methods can offer complementary reactivty to the developed nickel-catalyzed systems.

1.2.   The initial development of iron-catalyzed cross-coupling

While tremendous effort has been applied to the development of palladium-based catalysts for cross-coupling, the initial discovery of reactivity that could be considered cross-coupling was made by Kharasch using simple metal salts including iron salts (Scheme 1.1).[7] Further developments were made in the 1970s by Kochi for the alkylation of vinyl halides (Scheme 1.1).[8-9] However, after these developments, the field of iron-catalyzed coupling reactions stagnated for many years. The delay in development is likely due to the discovery of similar palladium-catalyzed transformations that were more readily understood mechanistically.[10] Alongside the developments

2

in nickel-catalyzed cross-coupling, the field of iron-catalyzed cross-coupling enjoyed a renaissance in the early 2000s. The primary driving force behind this resurgence was work performed by Fürstner and co-workers,[11] who demonstrated that simple iron salts could be used as effective precatalysts for a variety of Kumada-type cross-couplings. The mechanistic differences that may be responsible for the differences in reactivity are still being fully explored, but a summary of what is known mechanistically has been the subject of a recent review.[5]

Scheme 1.1. Karasch's[7] report of C-C bond formation from Grignards and metal salts. Kochi's[9] report of alkylation of vinyl halides.

Karasch 1941

60 %

Kochi 1976

R = 1°, 2°, 3°, alkyl

8 examples
50-80% yield
mixture of E/Z isomers

Fe(DMB)$_3$
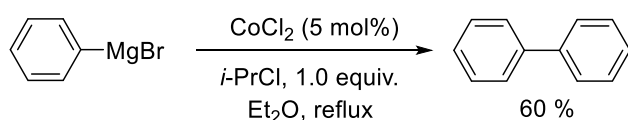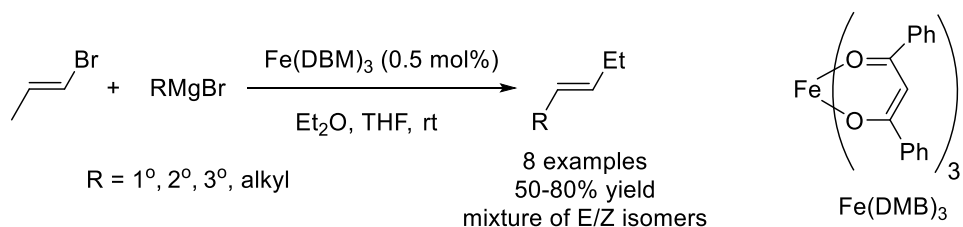
1.3. Kumada cross-coupling reactions mediated by iron

Kumada-Corriu cross-coupling reactions are characterized by the utlilization of organomagnesium based nucleophiles in conjunction with organic electrophiles, usually aryl, alkenyl, or alkyl halides and pseudohalides.[12-13] The nucleophilic nature of the organomagnesium reagent typically results in very fast transmetallation.[14] The fast transmetallation is likely a reason that Kumada-type couplings are the most represented in the iron-catalyzed cross-coupling literature.

1.3.1. Aryl-aryl Kumada-type cross-coupling reactions

While there is by no means an abundance of literature on examples of iron-catalyzed aryl-aryl Kumada-type cross-couplings,[5] a few such systems have been reported using iron-based complexes (Scheme 1.2a).[15-17] The majority of the reported systems utilize NHC ligands and high temperatures to effect the transformation as well as an additional ligand that is used to disrupt aggregation. When compared to similar nickel-based systems, the nickel catalysts operate at lower temperature with similar functional group tolerance.[18] The propensity for nickel-based catalysts to activate aryl chlorides at lower temperature may also be why similar complexes have been reported for the activation of aryl ethers (Scheme 1.2b).[19]

Scheme 1.2. a) Nakamura group's report[15] of iron-catalyzed aryl-aryl coupling. b) Ong group's report[19] of nickel catalyzed aryl ether coupling.
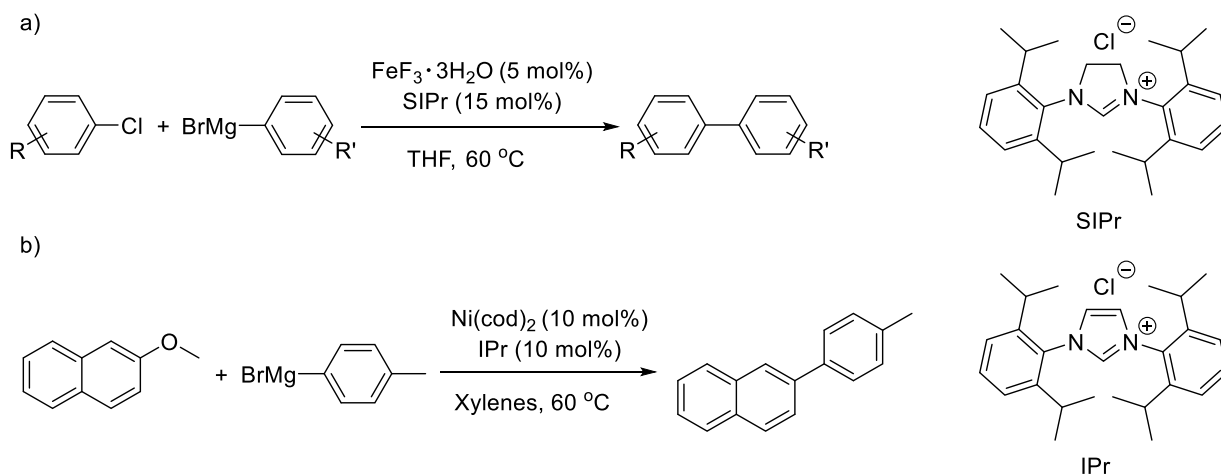
1.3.2. Aryl-alkyl Kumada-type cross-coupling reactions

In comparison to aryl-aryl Kumada reactions, there exists an abundance of iron-mediated alkyl-aryl Kumada couplings. The initial example of Kumada-type couplings using alkyl Grignards with aryl electrophiles was reported by Fürstner.[11] Importantly, Fürstner's work also showcased the ability of these iron precatalysts to undergo reactivity that was previously known to nickel, but with drastically increased rates (Scheme 1.3).[11] The enhanced reactivty allowed for

Scheme 1.3. Furstner group's reported[11] system for alkyl-aryl Kumada couplings as compared to Kumada's orginal conditions reported using nickel based catalysts.
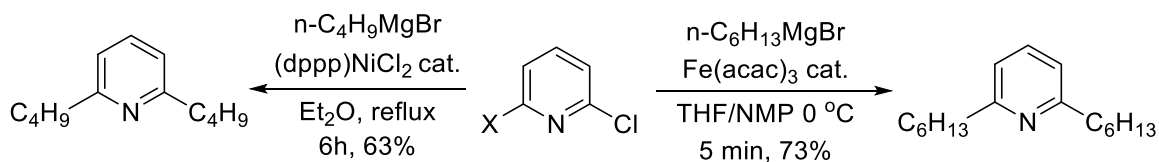
the coupling of very challenging heteroaromatic substrates with rates that far surpassed those of the reported nickel systems.[20] The drastic difference in reactivity provides the basis for investigation of iron's complementary reactivity for other transformations. In work by the Perry group,[21] it was also demonstrated that secondary alkyl Grignards could be employed in these reactions (Scheme 1.4). However, high levels of isomerization was observed when acyclic secondary nucleophiles were employed. The authors postulate that this is due to β-hydride elimination- reinsertion events taking place.[21] This limitation was later addressed by the Cook group through the use of fluoride ligands which they propose extend catalyst lifetime (Scheme 1.5).[22] This report also demonstrated that aryl tosylates were suitable substrates for these Kumada-type couplings. By comparison, a nickel-based system for identical substrates was reported in 2019 by the Szostak group.[23] The primary difference between the two systems is that the nickel-based catalyst appears to activate the electrophile at lower temperatures. However, the difference in rate is minor in this case.

Scheme 1.4. Perry group's reported[21] system for the coupling of aryl chlorides with alkyl Grignards.

5
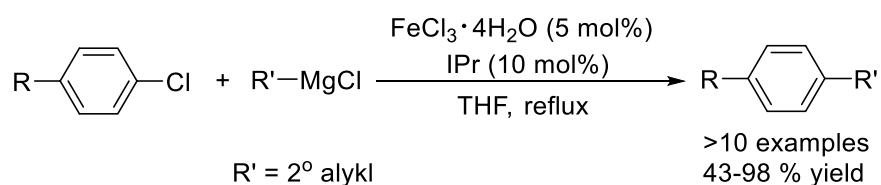
Scheme 1.5. Cook group's reported[22] system for the coupling of aryl tosylates with alkyl Grignards and a comparison to the Szostak[23] system.

Cook 2013

>20 examples
45-81 % yield

Szostak 2019

>30 examples
61-95 % yield
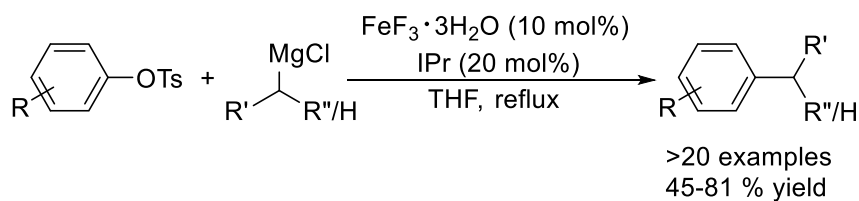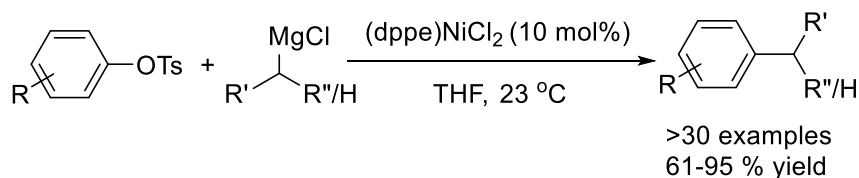
The converse reaction that employs aryl Grignards with alkyl electrophiles has been investigated to a much greater extent in recent years. In 2011, the groups of Nakamura[24] and Yamaguchi[25] both reported the coupling of aryl Grignards with secondary electrophiles (Scheme 1.6). These two examples were the first to demonstrate that ligand design played a critical role in the successful coupling of these more challenging substrates. Furthermore, the Nakamura group demonstrated that a tertiary electrophile could be used in these reactions and still achieve high yields.[24] Tertiary electrophiles were not tolerated under these conditions. Denmark and coworkers then demonstrated that similar iron salts were superior in the coupling of alkyl sulfones.[26] This work also demonstrated the first formal oxidative addition into a C-S bond mediated by a first-row transition metal (Scheme 1.7).

Scheme 1.6. Nakamura group's reported[24] system for the coupling of aryl Grignards with alkyl halides.

>10 examples
76-98 % yield
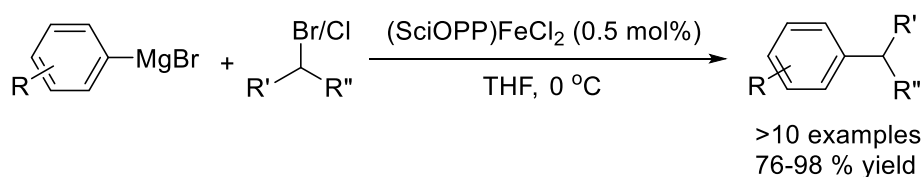
Scheme 1.7. Denmark group's reported[26] system for the coupling of aryl Grignards with alkyl sulfones.

>20 examples
25-84 % yield
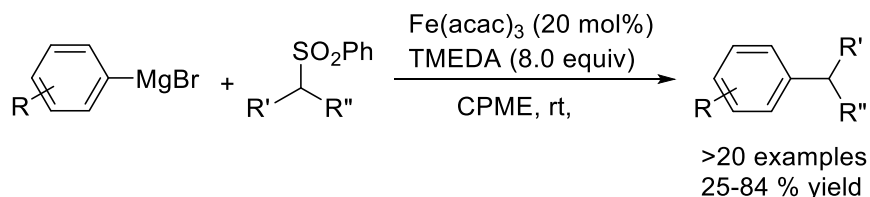
More recent work in this area has focused on enantioconvergent Kumada-type cross-couplings. In 2015, the Nakamura group reported the first enantioselective cross-coupling mediated by an iron-based catalyst (Figure 1.8).[27] In their system, they demonstrated the enantioconvergent coupling of racemic α-halo esters with aryl Grignards in the presence of a chiral bisphosphine ligand and iron acetoacetonate mixture. Importantly, they demonstrate that the ligands that are typically used for a similar nickel-catalyzed transformation[28] are ineffective at producing the products with high enantioselectivty. The different outcomes for the same ligand may indicate that different parameters are important for each metal in these reactions. Mechanistic studies of both the nickel[29] and iron[30-32] systems seem to corroborate the idea that there are subtle

Scheme 1.8. Nakamura group's reported[27] system for the enantioselective coupling of aryl Grignards with α-chloroesters with a comparison to the Fu group's reported system.[28]

Nakamura 2015

>25 examples
25-92 % yield
48-82% e.e.

BenzP

Fu 2010

>30 examples
72-91 % yield
72-95% e.e.

R-(Box)
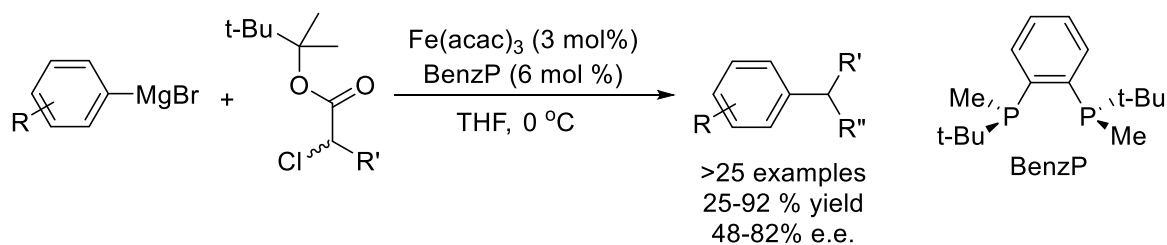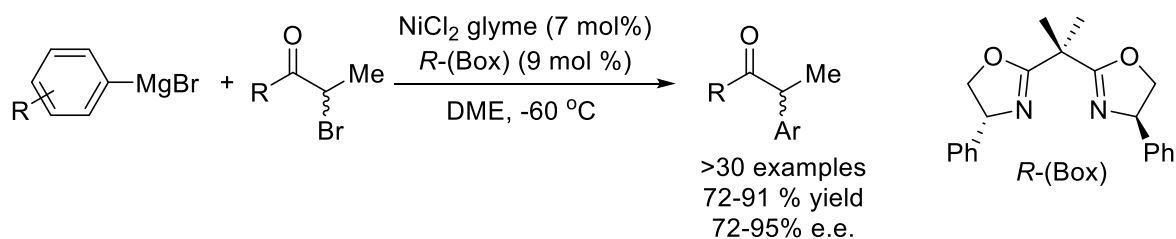
differences in mechanism between the two metals. In particular, while both mechanistic studies point toward a M(I/II/III) radical chain mechanism, how these metals access that manifold is different. Ultimately, differences in the metal electronic structure may allow for the development of new classes of ligands that result in higher enantioselectivities in the iron-based systems.

1.3.3. Alkyl-alkyl Kumada-type cross-coupling reactions mediated by iron

In comparison to aryl-aryl and alkyl-aryl cross-couplings, alkyl-alkyl coupling reactions are still rare.[3] The dearth of reactions of this type is even more apparent when considering only iron-based systems for this transformation. After the first report from the Chai group in 2007,[33] the Cardenas group reported the successful coupling of unactivated alkyl halides with alkyl Grignard reagents that had functionality embedded in the molecules (Scheme 1.9).[34] After this advancement, there has only been one other report of alkyl-alkyl Kumada coupling mediated by iron.[35] There still remain no reports of secondary Grignards being tolerated as substrates in these reactions. By comparison, nickel-based systems exist for the coupling of secondary electrophiles.[36-38] Despite the advances with respect to the substitution of the electrophile, there still are no examples of a reaction where both substrates are secondary. Nevertheless, stereospecific[37] and diastereoselective[38] reactions in this class do exist for the primary-secondary bond forming reactions.

Scheme 1.9. Cárdenas group's reported[34] system for the cross-coupling of alkyl Grignards with alkyl halides.

$$\text{R'/H} \quad \underset{R}{\overset{\text{R'/H}}{\diagdown}}\text{I} \; + \; \text{BrMg}\diagup\text{R''} \xrightarrow[\text{THF, rt}]{\begin{array}{c}\text{Fe(OAc)}_2\text{ (2.5 mol\%)}\\ \text{IMes (6 mol \%)}\end{array}} \; \underset{R}{\overset{\text{R'/H}}{\diagdown}}\diagup\text{R''}$$

>15 examples
36-88% yield
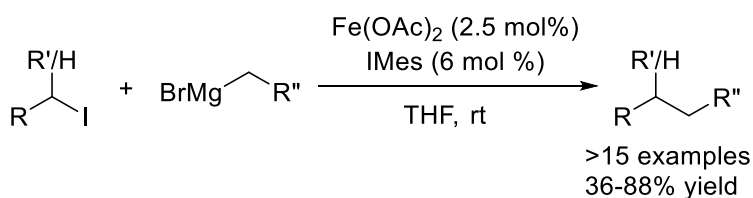
1.4.   Negishi cross-coupling reactions mediated by iron

Negishi cross-coupling reactions are characterized by the use of organozinc based nucleophiles in conjunction with organic electrophiles, usually aryl, alkenyl, or alkyl halides and pseudohalides.[39] The zinc nucleophile is often considered to be softer than the organomagnesium nucleophiles from which they are derived.[40] Many researchers that are attempting to improve functional group tolerance often focus their efforts on this class of nucleophiles.[41]

Unlike Kumada-type coupling reactions, there is only one example of an alkyl-alkyl Negishi-type coupling mediated by iron.[42] Furthermore, there is only one substrate in any iron-catalyzed Negishi coupling that constitutes an aryl-aryl coupling.[43] This subsection of the field is dominated by alkyl-aryl couplings.[44-46] In all cases, the aryl or vinyl fragment is derived from the zinc nucleophile. Despite this limitation, a wide variety of electrophiles are able to participate in these reactions. The Nakamura group reported the first iron-catalyzed Negishi coupling in 2005.[47] A variety of aryl and heteroaryl zinc reagents were tolerated under these conditions. The scope also included a variety of secondary alkyl halides. Interestingly, all of the secondary halides they used are in 6-membered rings and no acyclic examples are reported. In 2008, the Bedford group extended this work to tolerate benzylic electrophiles.[45] Since then, there have been numerous studies into the mechanistic features of these reactions and incremental improvements were made as a result of these studies.[43, 46, 48-49]

In 2009, the Nakamura group reported the first example of alkenyl zinc reagents in iron-catalyzed Negishi coupling.[44] In this work, they were able to couple a variety of configurationally stable vinyl zinc reagents with alkyl electrophiles. In all cases they observed nearly complete retention of the configuration in the olefin starting material (Scheme 1.10). Vinyl nucleophiles are otherwise quite rare in the literature when first-row transition metals are used.[50-52]

Scheme 1.10. Nakamura group's reported[44] system for the Nehishi coupling of vinyl organozinc reagents with alkyl halides.

>15 examples
73-98 % yield
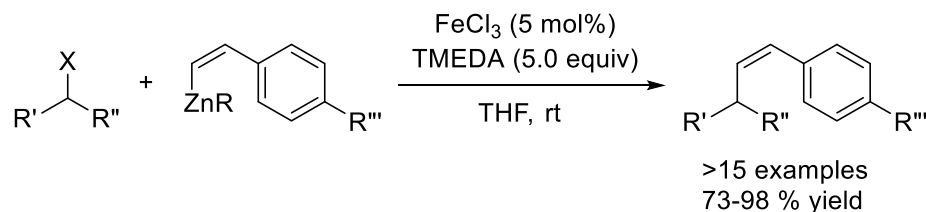
In contrast to the relatively few reports of iron-catalyzed Negishi coupling reactions, there are numerous examples of nickel-catalyzed Negishi couplings. Aryl-aryl[41], aryl-alkyl[53], and alkyl-alkyl[54] couplings can all be readily achieved using reported nickel catalysts. Furthermore, diastereoselective[55], enantioselective[56], and enantioconvergent[57] reactions have all been reported using nickel-based catalysts. It is difficult to see where iron catalysts for similar transformations could be advantageous over the already developed nickel catalysts, though there are examples where the nickel-catalyzed reactions exhibit deleterious isomerization side reactions.[53, 58]

1.5.   Suzuki-Miyaura cross-coupling reactions mediated by iron

Suzuki-Miyaura cross-coupling reactions are characterized by the utilization of organoboron based nucleophiles in conjunction with organic electrophiles, usually aryl, alkenyl, or alkyl halides and pseudohalides.[59] Boron-based nucleophiles have numerous advantages over zinc- and magnesium-based nucleophiles. Boronic esters in particular are typically air-stable, have long shelf lives, and provide non-toxic byproducts when used in coupling reactions.[60] The drawback to the stability they provide is often lower reactivity, which is evidenced by the base that is typically required in reactions that involve boronic esters. Despite this drawback of requiring an activator, the Suzuki-Miyaura reaction is now one of the most utilized reactions in the pharmaceutical industry.[61]

10

By comparison to palladium- and nickel-based systems, the development of iron-based catalysts for Suzuki-Miyaura coupling has been slow. To date, there are only seven reported examples for this transformation. The first example of a Suzuki-type coupling was reported by the Bedford group in 2009 (Scheme 1.11).[62] This report utilized tetra-aryl borates as the transmetallating nucleophile with the addition of a zinc co-catalyst. The Nakamura group improved upon this initial development through the discovery that alkyl lithium reagents and magnesium salts could be used to activate boronic esters (Scheme 1.12).[63] The Bedford group then extended this methodology to tolerate more widely available ligands and provided some mechanistic insight.[64] Both systems, however, still rely on alkyl lithium reagents to activate the boronic ester. The use of alkyl lithium reagents is a significant disadvantage when compared to the alkoxides that are tolerated in similar transformations using nickel-based catalysts.[65]

Scheme 1.11. Bedford group's reported[62] system for the Suzuki-Miyaura coupling of tetra-arylboron reagents with alkyl halides.
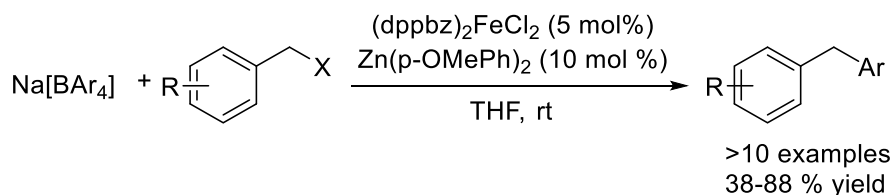
An area that iron catalysis has lagged behind the reported nickel-based systems is in alkyl-alkyl[66] and aryl-aryl[67] Suzuki-Miyaura cross-coupling. Both methods have limitations that prevent their more wide-scale adoption by the pharmaceutical industry. In contrast, nickel-based catalysts for similar transformations are already quite advanced.[68] There is also only one example of an

Scheme 1.12. Nakamura group's reported[63] system for the Suzuki-Miyaura coupling of aryl boronic esters with alkyl halides.

11
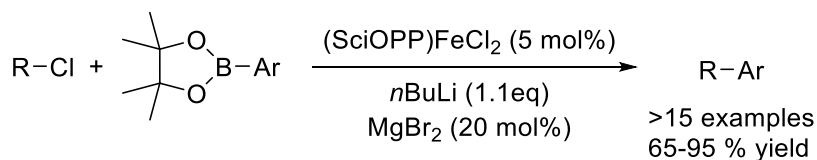
enantioselective Suzuki-Miyaura cross-coupling mediated by iron (Scheme 1.13).[69] This example

is very similar to a previously reported reaction from the same group that utilized Grignard

reagents. As with other types of cross-coupling, the technologies for enantioselective couplings

are still more advanced with nickel based-catalysts; however, nickel-based catalysts for

enantioselective Suzuki-Miyaura couplings are also still quite rare.[70]

Scheme 1.13. Nakamura group's reported system for the enantioselective cross-coupling of
boronic esters with α-bromooesters.
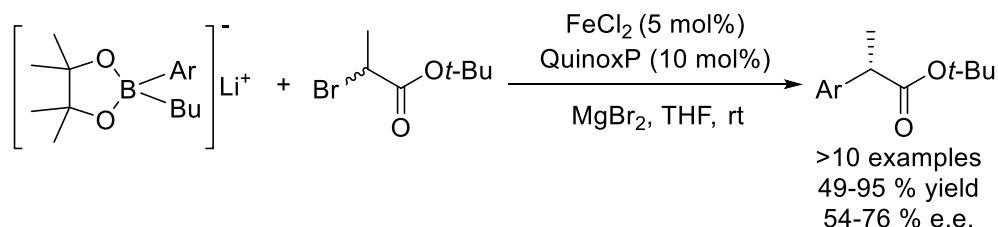
1.6.   Cross-electrophile coupling reactions mediated by iron

An emerging subfield in cross-coupling methodology is cross-electrophile coupling,

wherein two different organic electrophiles are coupled with cross-selectivity.[71] This methodology

has significant advantages when the typical nucleophile/electrophile pairs are difficult to access.

The main limitation in the development of this branch of cross-coupling has been reactions that

are exclusively cross-selective.[72] In recent years, this challenge has been met by a variety of groups

and there are now robust methods for alkyl-aryl couplings using nickel-based catalysts.[73]

Additionally, enantioselective methods have also been developed as an extension of the $C(sp^2)$-

$C(sp^3)$ couplings.[74] While the nickel-based systems are quite advanced, iron-based systems for

cross-electrophile coupling are underdeveloped. There are only two systems reported in the

literature. [75-76] The first reported system utilized a magnesium reductant to couple aryl bromides

with alkyl chlorides (Scheme 1.14).[76] However, the authors propose that the magnesium additive

Scheme 1.14. Shen group's reported[76] system for the reductive coupling of unactivated aryl bromides with alkyl chlorides.
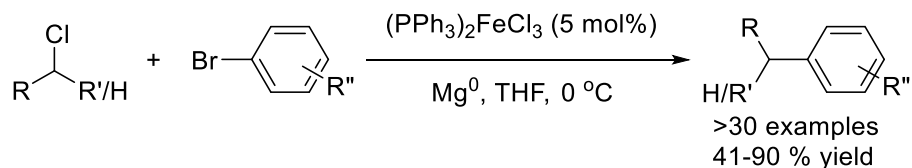
is simply forming a Grignard *in situ* and as a result this may be considered to be a Kumada coupling. The second example is from the Gong group for the vinylation of tertiary oxalates (Scheme 1.15).[75] Interestingly, the Gong group had previously reported a nickel-based system for the arylation of tertiary oxalates, but found that those conditions led to exclusive dimerization when vinyl halides were used.[77]

Scheme 1.15. Gong group's reported[75] system for the reductive coupling of unactivated aryl bromides with alkyl chlorides.
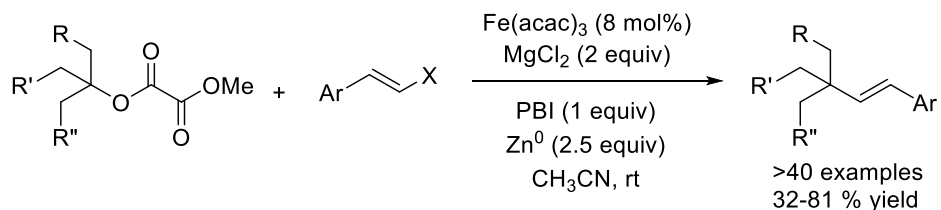
1.7. Conclusions

In the past 30 years, the first-row transition metals have received more attention for the cross-coupling of $C(sp^3)$-hybridized centers. At the forefront of most of these developments has been nickel catalysis. The ability to add into very stable bonds has been instrumental in this arena. Nevertheless, there are still limitations to the nickel chemistry that has been discovered. The study of metals like iron can help to address some of these limitations. This overview aimed to highlight some of the reported systems where complimentary reactivty has been discovered serendipitously. Table 1.1 summarizes the available methods for both iron and nickle. Studies in the future should focus on further developing the strengths and weaknesses of each metal. As can be seen from the areas where there are no known methods, a particular emphasis should be placed on coupling

13

reactions that can furnish contiguos sterically encumbered sites. In particular, methods that exploit the different propensity for isomerization of the substrates will be promising for accessing different products from the same starting materials.

Table 1.1. Summary table of known methods with iron- and nickel- based catalysts for cross-coupling.

	Aryl Nucleophile	1° Nucleophile	2° Nucleophile	3° Nucleophile
Aryl Electrophile	Ni cat. Kumada Ni cat. Negishi Ni cat. Suzuki Fe cat. Kumada Fe cat. Suzuki	Ni cat. Kumada Ni cat. Negishi Fe cat. Kumada	Ni cat. Kumada Ni cat. Negishi Fe cat. Kumada	Ni cat. Kumada Fe cat. Kumada
1° Electrophile	Ni cat. Kumada Ni cat. Negishi Ni cat. Suzuki Fe cat. Kumada Fe cat. Negishi Fe cat. Suzuki	Ni cat. Kumada Ni cat. Negishi Ni cat. Suzuki Fe cat. Kumada Fe cat. Negishi Fe cat. Suzuki	Ni cat. Kumada Ni cat. Negishi	**No Known Examples**
2° Electrophile	Ni cat. Kumada Ni cat. Negishi Ni cat. Suzuki Fe cat. Kumada Fe cat. Negishi Fe cat. Suzuki	Ni cat. Kumada Ni cat. Negishi Ni cat. Suzuki Fe cat. Kumada Fe cat. Suzuki	Ni cat. Negishi	**No Known Examples**
3° Electrophile	Ni cat. Suzuki	Fe cat. Kumada	**No Known Examples**	**No Known Examples**

1.8. References

1.   King, A. O.; Yasuda, N., Palladium-Catalyzed Cross-Coupling Reactions in the Synthesis of Pharmaceuticals. In *Organometallics in Process Chemistry*, Springer Berlin Heidelberg: Berlin, Heidelberg, 2004; pp 205-245.

2.   Lovering, F.; Bikker, J.; Humblet, C., Escape from Flatland: Increasing Saturation as an Approach to Improving Clinical Success. *Journal of Medicinal Chemistry* **2009,** *52* (21), 6752-6756.

3.   Jana, R.; Pathak, T. P.; Sigman, M. S., Advances in Transition Metal (Pd,Ni,Fe)-Catalyzed Cross-Coupling Reactions Using Alkyl-organometallics as Reaction Partners. *Chemical Reviews* **2011,** *111* (3), 1417-1492.

4.   Cahiez, G.; Moyeux, A., Cobalt-Catalyzed Cross-Coupling Reactions. *Chemical Reviews* **2010,** *110* (3), 1435-1462.

5.   Mako, T. L.; Byers, J. A., Recent advances in iron-catalysed cross coupling reactions and their mechanistic underpinning. *Inorganic Chemistry Frontiers* **2016,** *3* (6), 766-790.

6.   Santilli, C.; Beigbaghlou, S. S.; Ahlburg, A.; Antonacci, G.; Fristrup, P.; Norrby, P.-O.; Madsen, R., The Manganese-Catalyzed Cross-Coupling Reaction and the Influence of Trace Metals. *European Journal of Organic Chemistry* **2017,** *2017* (35), 5269-5274.

7.   Kharasch, M. S.; Fields, E. K., Factors Determining the Course and Mechanisms of Grignard Reactions. IV. The Effect of Metallic Halides on the Reaction of Aryl Grignard Reagents and Organic Halides1. *Journal of the American Chemical Society* **1941,** *63* (9), 2316-2320.

8.   Smith, R. S.; Kochi, J. K., Mechanistic studies of iron catalysis in the cross coupling of alkenyl halides and Grignard reagents. *The Journal of Organic Chemistry* **1976,** *41* (3), 502-509.

9.   Tamura, M.; Kochi, J., Iron catalysis in the reaction of grignard reagents with alkyl halides. *Journal of Organometallic Chemistry* **1971,** *31* (3), 289-309.

10.   Johansson Seechurn, C. C. C.; Kitching, M. O.; Colacot, T. J.; Snieckus, V., Palladium-Catalyzed Cross-Coupling: A Historical Contextual Perspective to the 2010 Nobel Prize. *Angewandte Chemie International Edition* **2012,** *51* (21), 5062-5085.

11.   Fürstner, A.; Leitner, A.; Méndez, M.; Krause, H., Iron-Catalyzed Cross-Coupling Reactions. *Journal of the American Chemical Society* **2002,** *124* (46), 13856-13863.

12.   Corriu, R. J. P.; Masse, J. P., Activation of Grignard reagents by transition-metal complexes. A new and simple synthesis of trans-stilbenes and polyphenyls. *Journal of the Chemical Society, Chemical Communications* **1972,** (3), 144a-144a.

13.   Tamao, K.; Sumitani, K.; Kumada, M., Selective carbon-carbon bond formation by cross-coupling of Grignard reagents with organic halides. Catalysis by nickel-phosphine complexes. *Journal of the American Chemical Society* **1972,** *94* (12), 4374-4376.

14.   Hedström, A.; Bollmann, U.; Bravidor, J.; Norrby, P.-O., Iron-Catalyzed Coupling of Aryl Grignard Reagents with Alkyl Halides: A Competitive Hammett Study. *Chemistry – A European Journal* **2011,** *17* (43), 11991-11993.

15.   Agrawal, T.; Cook, S. P., Iron-Catalyzed Coupling of Aryl Sulfamates and Aryl/Vinyl Tosylates with Aryl Grignards. *Organic Letters* **2014,** *16* (19), 5080-5083.

16.   Chua, Y.-Y.; Duong, H. A., Selective Kumada biaryl cross-coupling reaction enabled by an iron(iii) alkoxide–N-heterocyclic carbene catalyst system. *Chemical Communications* **2014,** *50* (61), 8424-8427.

17.   Hatakeyama, T.; Nakamura, M., Iron-Catalyzed Selective Biaryl Coupling: Remarkable Suppression of Homocoupling by the Fluoride Anion. *Journal of the American Chemical Society* **2007,** *129* (32), 9844-9845.

18.   Yamaguchi, J.; Muto, K.; Itami, K., Recent Progress in Nickel-Catalyzed Biaryl Coupling. *European Journal of Organic Chemistry* **2013,** *2013* (1), 19-30.

19.   Ambre, R.; Yang, H.; Chen, W.-C.; Yap, G. P. A.; Jurca, T.; Ong, T.-G., Nickel Carbodicarbene Catalyzes Kumada Cross-Coupling of Aryl Ethers with Grignard Reagents through C–O Bond Activation. *European Journal of Inorganic Chemistry* **2019,** *2019* (30), 3511-3517.

20.   Tamao, K.; Kodama, S.; Nakajima, I.; Kumada, M.; Minato, A.; Suzuki, K., Nickel-phosphine complex-catalyzed Grignard coupling—II: Grignard coupling of heterocyclic compounds. *Tetrahedron* **1982,** *38* (22), 3347-3354.

21.   Perry, M. C.; Gillett, A. N.; Law, T. C., An unprecedented iron-catalyzed cross-coupling of primary and secondary alkyl Grignard reagents with non-activated aryl chlorides. *Tetrahedron Letters* **2012,** *53* (33), 4436-4439.

22.   Agrawal, T.; Cook, S. P., Iron-Catalyzed Cross-Coupling Reactions of Alkyl Grignards with Aryl Sulfamates and Tosylates. *Organic Letters* **2013,** *15* (1), 96-99.

23.   Piontek, A.; Ochędzan-Siodłak, W.; Bisz, E.; Szostak, M., Nickel-Catalyzed C(sp2)−C(sp3) Kumada Cross-Coupling of Aryl Tosylates with Alkyl Grignard Reagents. *Advanced Synthesis & Catalysis* **2019,** *361* (10), 2329-2336.

24.   Takuji, H.; Yu-ichi, F.; Yoshihiro, O.; Takuma, I.; Toru, H.; Shintaro, K.; Kazuki, O.; Hikaru, T.; Masaharu, N., Kumada–Tamao–Corriu Coupling of Alkyl Halides Catalyzed by an Iron–Bisphosphine Complex. *Chemistry Letters* **2011,** *40* (9), 1030-1032.

25.   Yoshitaka, Y.; Hiroaki, A.; Makoto, N.; Hideto, H.; Takashi, I.; Masatoshi, A., Synthesis of Iron(III) Complex Bearing Tridentate β-Aminoketonato Ligand: Application to Iron-catalyzed Cross-coupling Reaction of Arylmagnesium Bromides with Alkyl Halides. *Chemistry Letters* **2011,** *40* (9), 983-985.

26.   Denmark, S. E.; Cresswell, A. J., Iron-Catalyzed Cross-Coupling of Unactivated Secondary Alkyl Thio Ethers and Sulfones with Aryl Grignard Reagents. *The Journal of Organic Chemistry* **2013,** *78* (24), 12593-12628.

27.   Jin, M.; Adak, L.; Nakamura, M., Iron-Catalyzed Enantioselective Cross-Coupling Reactions of α-Chloroesters with Aryl Grignard Reagents. *Journal of the American Chemical Society* **2015,** *137* (22), 7128-7134.

28.   Lou, S.; Fu, G. C., Nickel/Bis(oxazoline)-Catalyzed Asymmetric Kumada Reactions of Alkyl Electrophiles: Cross-Couplings of Racemic α-Bromoketones. *Journal of the American Chemical Society* **2010,** *132* (4), 1264-1266.

29.   Yin, H.; Fu, G. C., Mechanistic Investigation of Enantioconvergent Kumada Reactions of Racemic α-Bromoketones Catalyzed by a Nickel/Bis(oxazoline) Complex. *Journal of the American Chemical Society* **2019,** *141* (38), 15433-15440.

30.   Lee, W.; Zhou, J.; Gutierrez, O., Mechanism of Nakamura's Bisphosphine-Iron-Catalyzed Asymmetric C(sp2)–C(sp3) Cross-Coupling Reaction: The Role of Spin in Controlling Arylation Pathways. *Journal of the American Chemical Society* **2017,** *139* (45), 16126-16133.

31.   Sharma, A. K.; Sameera, W. M. C.; Jin, M.; Adak, L.; Okuzono, C.; Iwamoto, T.; Kato, M.; Nakamura, M.; Morokuma, K., DFT and AFIR Study on the Mechanism and the Origin of

Enantioselectivity in Iron-Catalyzed Cross-Coupling Reactions. *Journal of the American Chemical Society* **2017,** *139* (45), 16117-16125.

32.   Sears, J. D.; Neate, P. G. N.; Neidig, M. L., Intermediates and Mechanism in Iron-Catalyzed Cross-Coupling. *Journal of the American Chemical Society* **2018,** *140* (38), 11872-11883.

33.   Dongol, K. G.; Koh, H.; Sau, M.; Chai, C. L. L., Iron-Catalysed sp3–sp3 Cross-Coupling Reactions of Unactivated Alkyl Halides with Alkyl Grignard Reagents. *Advanced Synthesis & Catalysis* **2007,** *349* (7), 1015-1018.

34.   Guisán-Ceinos, M.; Tato, F.; Buñuel, E.; Calle, P.; Cárdenas, D. J., Fe-catalysed Kumada-type alkyl–alkyl cross-coupling. Evidence for the intermediacy of Fe(i) complexes. *Chemical Science* **2013,** *4* (3), 1098-1104.

35.   Przyojski, J. A.; Veggeberg, K. P.; Arman, H. D.; Tonzetich, Z. J., Mechanistic Studies of Catalytic Carbon–Carbon Cross-Coupling by Well-Defined Iron NHC Complexes. *ACS Catalysis* **2015,** *5* (10), 5938-5946.

36.   Ren, P.; Vechorkin, O.; Allmen, K. v.; Scopelliti, R.; Hu, X., A Structure–Activity Study of Ni-Catalyzed Alkyl–Alkyl Kumada Coupling. Improved Catalysts for Coupling of Secondary Alkyl Halides. *Journal of the American Chemical Society* **2011,** *133* (18), 7084-7095.

37.   Greene, M. A.; Yonova, I. M.; Williams, F. J.; Jarvo, E. R., Traceless Directing Group for Stereospecific Nickel-Catalyzed Alkyl−Alkyl Cross-Coupling Reactions. *Organic Letters* **2012,** *14* (16), 4293-4296.

38.   Perez Garcia, P. M.; Di Franco, T.; Orsino, A.; Ren, P.; Hu, X., Nickel-Catalyzed Diastereoselective Alkyl–Alkyl Kumada Coupling Reactions. *Organic Letters* **2012,** *14* (16), 4286-4289.

39.   King, A. O.; Okukado, N.; Negishi, E.-i., Highly general stereo-, regio-, and chemo-selective synthesis of terminal and internal conjugated enynes by the Pd-catalysed reaction of alkynylzinc reagents with alkenyl halides. *Journal of the Chemical Society, Chemical Communications* **1977,** (19), 683-684.

40.   Blechert, S., Synthese mit Metallorganika: Organometallics in Organic Synthesis, Vol. 1. Von E.–I. Negishi. John Wiley & Sons, New York – Chichester – Brisbane – Toronto 1980. 532 S., zahlr. Formeln, Tab., geb. £ 15, 85. *Nachrichten aus Chemie, Technik und Laboratorium* **1981,** *29* (3), 178-179.

41.   Negishi, E., Palladium- or nickel-catalyzed cross coupling. A new selective method for carbon-carbon bond formation. *Accounts of Chemical Research* **1982,** *15* (11), 340-348.

42.   Agata, R.; Kawamura, S.; Isozaki, K.; Nakamura, M., Iron-catalyzed Alkyl–Alkyl Negishi Coupling of Organoaluminum Reagents. *Chemistry Letters* **2019,** *48* (3), 238-241.

43.   Adams, C. J.; Bedford, R. B.; Carter, E.; Gower, N. J.; Haddow, M. F.; Harvey, J. N.; Huwe, M.; Cartes, M. Á.; Mansell, S. M.; Mendoza, C.; Murphy, D. M.; Neeve, E. C.; Nunn, J., Iron(I) in Negishi Cross-Coupling Reactions. *Journal of the American Chemical Society* **2012,** *134* (25), 10333-10336.

44.   Hatakeyama, T.; Nakagawa, N.; Nakamura, M., Iron-Catalyzed Negishi Coupling Toward an Effective Olefin Synthesis. *Organic Letters* **2009,** *11* (20), 4496-4499.

45.   Bedford, R. B.; Huwe, M.; Wilkinson, M. C., Iron-catalysed Negishi coupling of benzylhalides and phosphates. *Chemical Communications* **2009,** (5), 600-602.

46.   Brown, C. A.; Nile, T. A.; Mahon, M. F.; Webster, R. L., Iron catalysed Negishi cross-coupling using simple ethyl-monophosphines. *Dalton Transactions* **2015,** *44* (27), 12189-12195.

17

47.   Nakamura, M.; Ito, S.; Matsuo, K.; Nakamura, E., Iron-Catalyzed Chemoselective Cross-Coupling of Primary and Secondary Alkyl Halides with Arylzinc Reagents. *Synlett* **2005,** *2005* (11), 1794-1798.

48.   Messinis, A. M.; Luckham, S. L. J.; Wells, P. P.; Gianolio, D.; Gibson, E. K.; O'Brien, H. M.; Sparkes, H. A.; Davis, S. A.; Callison, J.; Elorriaga, D.; Hernandez-Fajardo, O.; Bedford, R. B., The highly surprising behaviour of diphosphine ligands in iron-catalysed Negishi cross-coupling. *Nature Catalysis* **2019,** *2* (2), 123-133.

49.   Bedford, R. B.; Carter, E.; Cogswell, P. M.; Gower, N. J.; Haddow, M. F.; Harvey, J. N.; Murphy, D. M.; Neeve, E. C.; Nunn, J., Simplifying Iron–Phosphine Catalysts for Cross-Coupling Reactions. *Angewandte Chemie International Edition* **2013,** *52* (4), 1285-1288.

50.   Phapale, V. B.; Cárdenas, D. J., Nickel-catalysed Negishi cross-coupling reactions: scope and mechanisms. *Chemical Society Reviews* **2009,** *38* (6), 1598-1607.

51.   Haas, D.; Hammann, J. M.; Greiner, R.; Knochel, P., Recent Developments in Negishi Cross-Coupling Reactions. *ACS Catalysis* **2016,** *6* (3), 1540-1552.

52.   Yang, B.; Wang, Z.-X., Nickel-Catalyzed Cross-Coupling of Allyl Alcohols with Aryl- or Alkenylzinc Reagents. *The Journal of Organic Chemistry* **2017,** *82* (9), 4542-4549.

53.   Joshi-Pangu, A.; Ganesh, M.; Biscoe, M. R., Nickel-Catalyzed Negishi Cross-Coupling Reactions of Secondary Alkylzinc Halides and Aryl Iodides. *Organic Letters* **2011,** *13* (5), 1218-1221.

54.   Zhou, J.; Fu, G. C., Cross-Couplings of Unactivated Secondary Alkyl Halides: Room-Temperature Nickel-Catalyzed Negishi Reactions of Alkyl Bromides and Iodides. *Journal of the American Chemical Society* **2003,** *125* (48), 14726-14727.

55.   Gong, H.; Gagné, M. R., Diastereoselective Ni-Catalyzed Negishi Cross-Coupling Approach to Saturated, Fully Oxygenated C-Alkyl and C-Aryl Glycosides. *Journal of the American Chemical Society* **2008,** *130* (36), 12177-12183.

56.   Arp, F. O.; Fu, G. C., Catalytic Enantioselective Negishi Reactions of Racemic Secondary Benzylic Halides. *Journal of the American Chemical Society* **2005,** *127* (30), 10482-10483.

57.   Cordier, C. J.; Lundgren, R. J.; Fu, G. C., Enantioconvergent Cross-Couplings of Racemic Alkylmetal Reagents with Unactivated Secondary Alkyl Electrophiles: Catalytic Asymmetric Negishi α-Alkylations of N-Boc-pyrrolidine. *Journal of the American Chemical Society* **2013,** *135* (30), 10946-10949.

58.   Joshi-Pangu, A.; Wang, C.-Y.; Biscoe, M. R., Nickel-Catalyzed Kumada Cross-Coupling Reactions of Tertiary Alkylmagnesium Halides and Aryl Bromides/Triflates. *Journal of the American Chemical Society* **2011,** *133* (22), 8478-8481.

59.   Miyaura, N.; Yamada, K.; Suzuki, A., A new stereospecific cross-coupling by the palladium-catalyzed reaction of 1-alkenylboranes with 1-alkenyl or 1-alkynyl halides. *Tetrahedron Letters* **1979,** *20* (36), 3437-3440.

60.   Soriano-Ursúa, M. A.; Farfán-García, E. D.; López-Cabrera, Y.; Querejeta, E.; Trujillo-Ferrara, J. G., Boron-containing acids: Preliminary evaluation of acute toxicity and access to the brain determined by Raman scattering spectroscopy. *NeuroToxicology* **2014,** *40*, 8-15.

61.   Lima, C. F. R. A. C.; Rodrigues, A. S. M. C.; Silva, V. L. M.; Silva, A. M. S.; Santos, L. M. N. B. F., Role of the Base and Control of Selectivity in the Suzuki–Miyaura Cross-Coupling Reaction. *ChemCatChem* **2014,** *6* (5), 1291-1302.

62.   Bedford, R. B.; Hall, M. A.; Hodges, G. R.; Huwe, M.; Wilkinson, M. C., Simple mixed Fe–Zn catalysts for the Suzuki couplings of tetraarylborates with benzyl halides and 2-halopyridines. *Chemical Communications* **2009,** (42), 6430-6432.

63.   Hatakeyama, T.; Hashimoto, T.; Kondo, Y.; Fujiwara, Y.; Seike, H.; Takaya, H.; Tamada, Y.; Ono, T.; Nakamura, M., Iron-Catalyzed Suzuki−Miyaura Coupling of Alkyl Halides. *Journal of the American Chemical Society* **2010,** *132* (31), 10674-10676.

64.   Bedford, R. B.; Brenner, P. B.; Carter, E.; Carvell, T. W.; Cogswell, P. M.; Gallagher, T.; Harvey, J. N.; Murphy, D. M.; Neeve, E. C.; Nunn, J.; Pye, D. R., Expedient Iron-Catalyzed Coupling of Alkyl, Benzyl and Allyl Halides with Arylboronic Esters. *Chemistry – A European Journal* **2014,** *20* (26), 7935-7938.

65.   Zhou, J.; Fu, G. C., Suzuki Cross-Couplings of Unactivated Secondary Alkyl Bromides and Iodides. *Journal of the American Chemical Society* **2004,** *126* (5), 1340-1341.

66.   Hatakeyama, T.; Hashimoto, T.; Kathriarachchi, K. K. A. D. S.; Zenmyo, T.; Seike, H.; Nakamura, M., Iron-Catalyzed Alkyl–Alkyl Suzuki–Miyaura Coupling. *Angewandte Chemie International Edition* **2012,** *51* (35), 8834-8837.

67.   O'Brien, H. M.; Manzotti, M.; Abrams, R. D.; Elorriaga, D.; Sparkes, H. A.; Davis, S. A.; Bedford, R. B., Iron-catalysed substrate-directed Suzuki biaryl cross-coupling. *Nature Catalysis* **2018,** *1* (6), 429-437.

68.   Zultanski, S. L.; Fu, G. C., Nickel-Catalyzed Carbon–Carbon Bond-Forming Reactions of Unactivated Tertiary Alkyl Halides: Suzuki Arylations. *Journal of the American Chemical Society* **2013,** *135* (2), 624-627.

69.   Iwamoto, T.; Okuzono, C.; Adak, L.; Jin, M.; Nakamura, M., Iron-catalysed enantioselective Suzuki–Miyaura coupling of racemic alkyl bromides. *Chemical Communications* **2019,** *55* (8), 1128-1131.

70.   Lundin, P. M.; Fu, G. C., Asymmetric Suzuki Cross-Couplings of Activated Secondary Alkyl Electrophiles: Arylations of Racemic α-Chloroamides. *Journal of the American Chemical Society* **2010,** *132* (32), 11027-11029.

71.   Jutand, A., Contribution of Electrochemistry to Organometallic Catalysis. *Chemical Reviews* **2008,** *108* (7), 2300-2347.

72.   Everson, D. A.; Weix, D. J., Cross-Electrophile Coupling: Principles of Reactivity and Selectivity. *The Journal of Organic Chemistry* **2014,** *79* (11), 4793-4798.

73.   Goldfogel, M.; Huang, L.; Weix, D., Cross-Electrophile Coupling: Principles and New Reactions. 2020; pp 183-222.

74.   Cherney, A. H.; Reisman, S. E., Nickel-Catalyzed Asymmetric Reductive Cross-Coupling Between Vinyl and Benzyl Electrophiles. *Journal of the American Chemical Society* **2014,** *136* (41), 14365-14368.

75.   Ye, Y.; Chen, H.; Yao, K.; Gong, H., Iron-Catalyzed Reductive Vinylation of Tertiary Alkyl Oxalates with Activated Vinyl Halides. *Organic Letters* **2020,** *22* (5), 2070-2075.

76.   Li, Z.; Sun, H.-M.; Shen, Q., Iron-mediated inter- and intramolecular reductive cross-coupling of unactivated alkyl chlorides with aryl bromides. *Organic & Biomolecular Chemistry* **2016,** *14* (12), 3314-3321.

77.   Liu, J.; Ren, Q.; Zhang, X.; Gong, H., Preparation of Vinyl Arenes by Nickel-Catalyzed Reductive Coupling of Aryl Halides with Vinyl Bromides. *Angewandte Chemie International Edition* **2016,** *55* (50), 15544-15548.

19

Chapter 2. Iron-Catalyzed Suzuki-Miyaura Cross-Coupling Reactions Between Alkyl Halides and Unactivated Aryl Boronic Esters

2.1   Introduction

Transition metal catalyzed cross-coupling reactions between aryl or vinyl halides and organometallic reagents have emerged as robust methodologies for the efficient construction of carbon-carbon and carbon-heteroatom bonds in organic synthesis.[1] These methods have been heavily utilized in industrial and academic settings, which has led to the production of large libraries of structural motifs available to synthetic chemists.[2] A particularly attractive cross-coupling variant is the Suzuki-Miyaura cross-coupling reaction, which employs nucleophilic organoboron reagents and organohalide electrophiles.[3] This type of catalysis is particularly appealing due to the low toxicity, broad functional-group tolerance, ease of synthesis, and ease of handling of organoboron reagents compared to the alternatives.[4]

Although the Suzuki-Miyaura cross-coupling reactions have been successfully employed across industry,[5] the reactions typically make use of palladium-based catalysts. While these reactions can be carried out at low catalyst loadings, are tolerant of many functional groups, and are well understood mechanistically,[6] palladium is toxic[7] and expensive, and the reaction is limited with respect to substrate scope.[8] In particular, palladium-based cross-coupling reactions have not been used widely for cross-coupling reactions involving alkyl halide substrates due to byproduct formation that results from facile β-hydride elimination reactions. Advances in ligand design have resulted in new palladium-catalyzed cross-coupling reactions that tolerate many alkyl nucleophiles[9] and some alky electrophiles,[8, 10-12] but the latter examples are typically limited to primary alkyl halides due to the tendency for palladium to undergo oxidative addition with alkyl halides by an S_N2-type mechanism.[13]

To address these limitations, many groups have explored other catalysts based on different transition metals. Particularly promising are cross-coupling reactions that involve first row

transition metals.[1] Pioneering work from the Fu group greatly advanced the use of nickel-based catalysts for the productive and enantioselective cross-coupling of primary and secondary alkyl halides with aryl[14] and alkyl[15] organoboron reagents, primarily boranes, used in Suzuki-Miyaura cross-coupling reactions. Similarly, iron-based catalysts have enjoyed a recent renaissance in popularity since their original discovery by Kochi as competent metals for cross-coupling reactions.[16] Fürstner,[17] Nakamura,[18-22] Bedford,[23-24] and others[25-27] have pioneered the use of iron-based catalysts for a variety of cross-coupling reactions. Being an earth-abundant metal, iron is more abundant and therefore inexpensive compared to palladium. It is also significantly less toxic compared to palladium or nickel,[28] though typically the ligand is the most costly and toxic component of iron catalyzed systems. Moreover, iron-based catalysts often demonstrate faster reaction kinetics than analogous palladium- or nickel-based reactions[29] and they can access reaction pathways distinct from palladium-catalyzed processes.[29] This reactivity has led to the development of a variety of iron-based catalysts for cross-coupling of sp^2 and sp^3 containing organohalides (including secondary alkyl halides) with alkyl, aryl, vinyl, or alkynyl Grignard reagents.[30]

Despite significant advances for these Kumada-type cross-coupling reactions, there is a dearth of iron-based catalysts used for Suzuki-Miyaura cross-coupling reactions. The few known examples rely on highly activated borate species generated from the addition of alkyl lithium reagents to boronic esters, and they require the use of $MgBr_2$ as an additive to achieve high yields (Scheme 2.1).[31-32] Due to iron being less electronegative than boron, it is possible that the Schlenk equilibrium would no longer favor transmetalation to iron as would be the case with magnesium.[33] Based on our experience and the experience of other groups,[34] however, the base additives typically used in palladium-catalyzed cross-coupling reactions lead to iron aggregates, which we

hypothesize may not be competent catalysts for the cross-coupling of alkyl electrophiles with aryl boronic ester nucleophiles.

Scheme 2.1. Previously developed Suzuki-Miyaura cross-coupling reactions mediated by an iron-based catalyst.
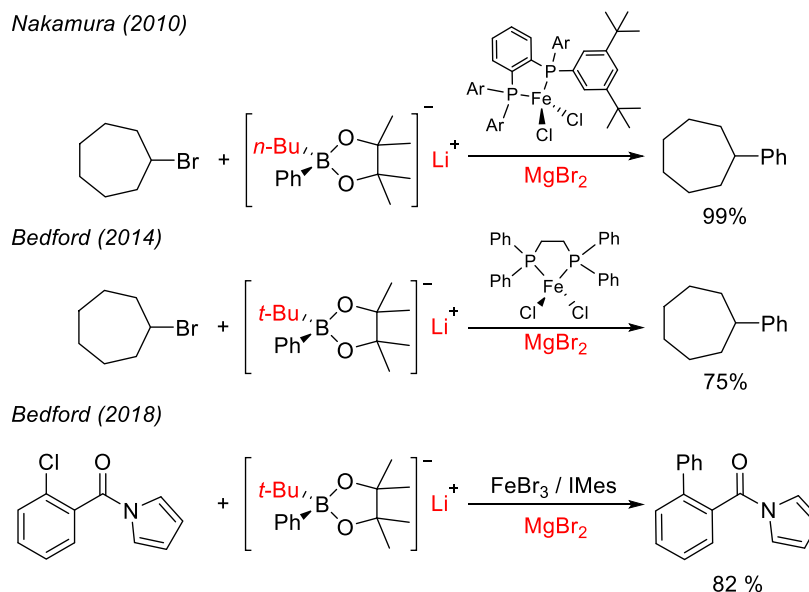
2.2 The Aggregation Hypothesis

Considering the efficiency of iron-catalyzed cross-coupling reactions between alkyl halides and Grignard reagents,[21] and the sluggishness of corresponding Suzuki-Miyaura cross-coupling reactions, we reasoned that the key step in an iron-catalyzed Suzuki-Miyaura cross-coupling reaction is the transmetalation event. Extensive studies have been carried out for the transmetalation event in palladium-catalyzed systems, which are relevant because transmetalation in iron-catalyzed cross-coupling reactions is believed to be mechanistically similar to palladium-catalyzed reactions (Figure 2.1a).[35] Investigations involving palladium-catalyzed systems have centered on the role that the base additives play in aiding transmetalation. Two viable pathways have emerged from these studies: either the base interacts with the boronic acid to form a more nucleophillic organoborate species **2.2** *in situ* or the base converts the palladium halide species

2.1, formed after oxidative addition, to a palladium hydroxide intermediate **2.3** that is better suited

for transmetalation with boronic acids (Figure 2.1b).[36]

Figure 2.1. (**a**) Mechanistic comparison between palladium-catalyzed and iron-catalyzed Suzuki-Miyaura cross coupling of alkyl halides and aryl boronic esters. (**b**) Proposed pathways for transmetallation in palladium-catalyzed Suzuki-Miyaura reactions and a spectroscopically identified intermediate likely involved in transmetalation.
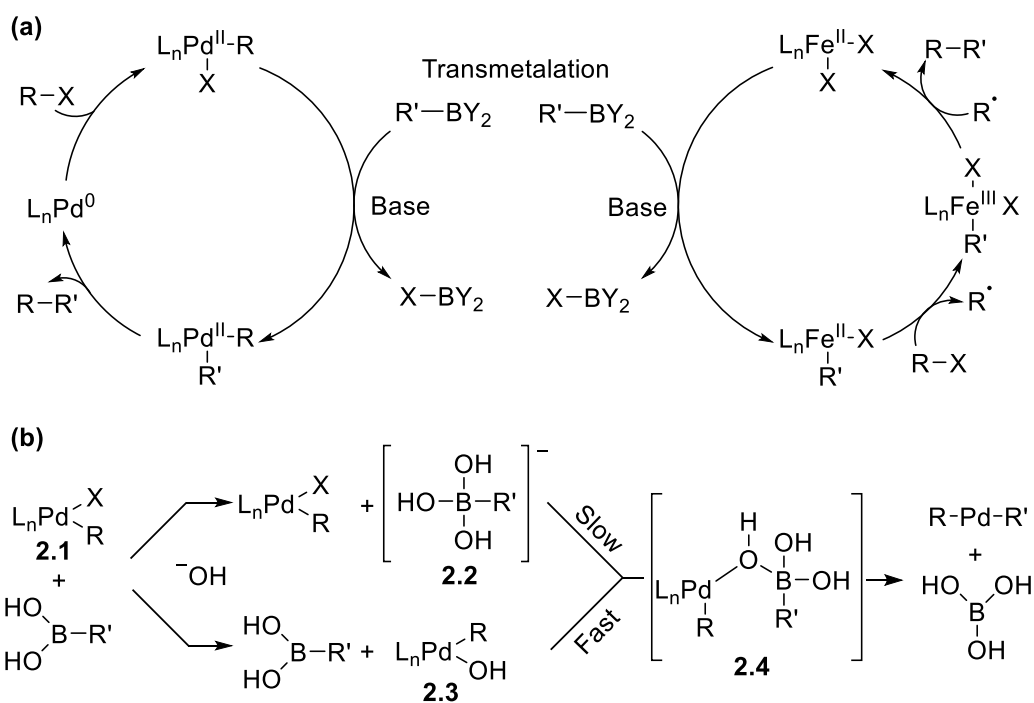
Recently, significant insight has been obtained for key intermediates involved in the

transmetalation step in palladium-catalyzed Suzuki-Miyaura couplings.[37-38] Hartwig and

coworkers synthesized a palladium hydroxide species and demonstrated that it was a competent

and kinetically more relevant transmetalation partner compared to a borate intermediate that

resulted from base activation of a boronic acid (Figure 2.1b).[37] Consistent with palladium

hydroxides being involved in boron-to-palladium transmetalation reactions, Denmark and

coworkers[38] characterized an intermediate (**2.4**) along the reaction coordinate that brings the

palladium species in close proximity with the boronic acid prior to transmetalation (Figure 2.1b).

While neither of these studies definitively rule out a transmetalation pathway that involves a borate

intermediate, both implicate the formation of palladium hydroxides that occurs during catalytic cross-coupling reactions. Unlike palladium hydroxides and alkoxides, which can exist as mononuclear complexes in solution (or as monomer-dimer equilibrium mixtures),[39] iron alkoxides and especially iron hydroxides are prone to irreversible aggregation.[40-42] We had previously observed this tendency[43] and hypothesized that the irreversible formation of higher-ordered iron aggregates would be detrimental to Suzuki-Miyaura reactions.

An alternative hypothesis for the slow transmetalation reactions is unfavorable thermodynamics for transmetalation from boron to iron. Slower transmetalation may be expected because iron is less electronegative than boron, and the position of Schlenk equilibria involved in the transmetalation process are often governed by electronegativity differences between the elements involved.[44] To investigate this possibility, we developed a computational model for the transmetalation reaction from phenyl boronic acid pinacol ester (PhB(pin)) to diphenylphosphinoethane (dppe) iron(II) complexes containing various anionic ligands that may be intermediates in transmetalation reactions (Figure 2.2). It should be noted at the onset that the mechanistic framework we are following throughout this paper involves an iron(II)/iron(III) cycle proposed by Nakamura (Figure 2.1a),[19] but we cannot definitively rule out other viable mechanisms such as an iron(I)/iron(II)/iron(III) cycle proposed by Bedford and Norrby (Figure 2.3).[45-46] As can be seen from Figure 2.2, transmetalation reactions from PhB(pin) to (dppe)FeCl$_2$ and (dppe)FePhCl are highly unfavorable thermodynamically (black trace Fig. 2.2), which has also been reported for similar calculations carried out using palladium-based complexes.[47] It is important to note that all of these calculations were carried out using the ΔH values. There is a significant deviation in the ΔG values when looking at the transition states in particular. The difficulty in estimating the entropic contribution of reactions computationally is a known limitation

25

Figure 2.2. DFT (B3LYP/6-31G*) computed energies for transmetalation from boron to iron in reactions between PhB(pin) and (dppe)FeX$_2$ (X = anionic ligand). The y-axis was truncated to conserve space.
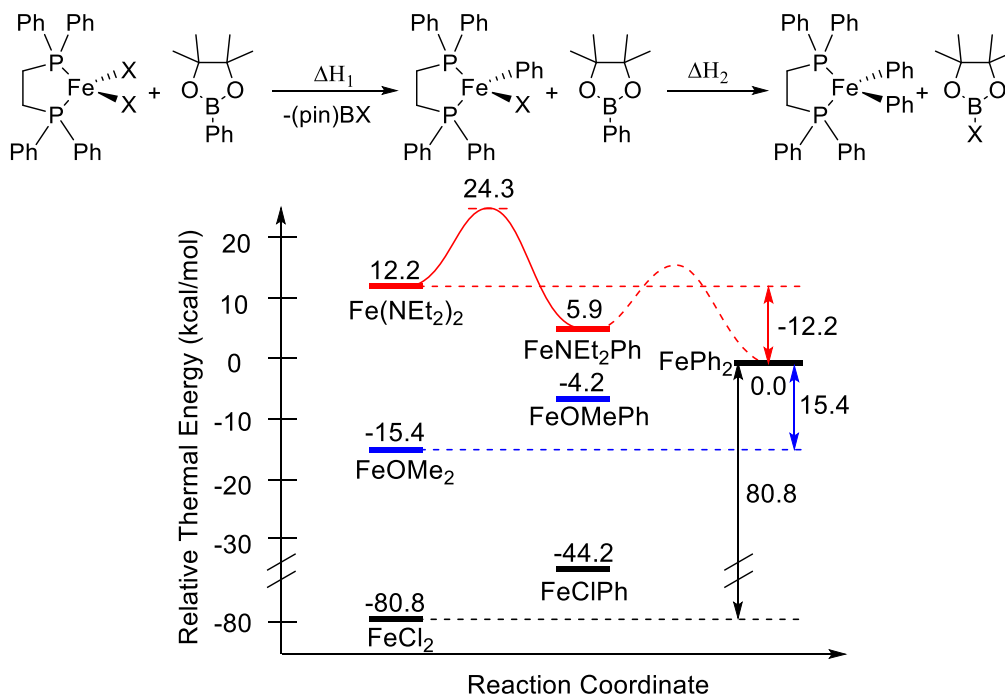
of some computational methods.[48] In contrast, transmetalation reactions from (dppe)Fe(OMe)$_2$ are significantly less uphill than those from iron halides (blue trace Fig. 2.2). When compared to analogous palladium catalyzed systems these values are nearly 10 kcal/mol further uphill, which reflects the electronegativity differences between palladium and iron.[47] However, these barriers are not large and energetically feasible to scale for cross-coupling reactions that occur at room temperature.

Given the insight that the calculations provided, we were compelled to investigate the possibility of a boron-to-iron transmetalation proceeding through the intermediacy of an iron alkoxide complex that contained the dppe ligand by pursuing the synthesis of such intermediates (Figure 2.4). Initially, salt metathesis routes were explored for the synthesis of iron alkoxides by treating (dppe)FeCl$_2$ (**2.5**) with aromatic or aliphatic alkoxide bases. Regardless to the identity of the alkali cations, however, green insoluble material was formed that was inactive for cross-

Figure 2.3. Iron(I)/iron(II)/iron(III) cycle proposed by Bedford and Norrby[45-46]
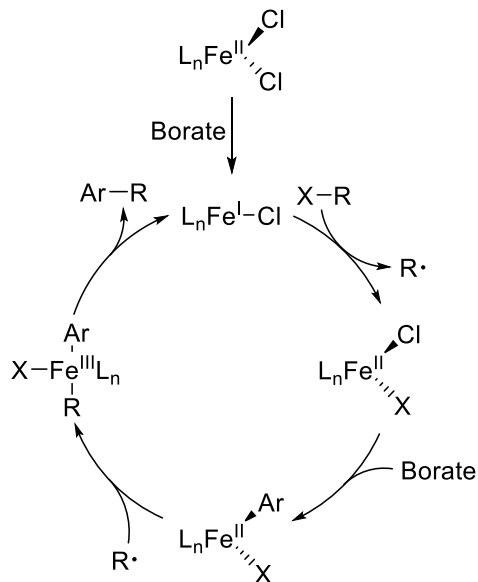
coupling when exposed to PhB(pin) and cycloheptyl bromide even when heated to 80 °C. Likewise, when (dppe)Fe(CH$_2$SiMe$_3$)$_2$[49] (**2.6**) was exposed to alcohols, a similar insoluble material was formed that was catalytically incompetent for cross-coupling reactions. The results from the protonolysis reaction were particularly surprising because Ashley Biernesser in our group had previously shown that alcoholysis reactions involving bis(imino)pyridine iron alkyls are a reliable and general way to form mononuclear iron alkoxides.[43] However, in this case similar reactions resulted in an intractable and insoluble precipitate, which was presumed to be higher ordered iron aggregates. Interestingly, when using the 5 coordinate iron alkoxide complex prepared by my coworkers we were unsuccessful in observing any boron intermediates that would be consistent with transmetallation. More recently, the Chirik group has reported that the reduced form of the bis(immino)pyridine iron alkoxide complexes are competent for transmetallation with neutral boronic esters.[50] Considering the propensity for aggregation among iron alkoxides[51], we next explored the possibility that intermediates other than alkoxides would be better suited to facilitate boron-to-iron transmetalation reactions. A computational survey of different anionic ligands

revealed that iron amides would undergo transmetalation with PhB(pin) that was thermodynamically downhill (Figure 2.2). For example, transmetalation between PhB(pin) and (dppe)Fe(NEt$_2$)$_2$ was 6 kcal/mol downhill to form (dppe)FePhNEt$_2$, which in turn is thermodynamically favorable to undergo a second transmetalation by another 6 kcal/mol to form (dppe)FePh$_2$ (red trace Fig. 2.2). Moreover, a transition state was also found for the transmetalation between PhB(pin) and (dppe)Fe(NEt$_2$)$_2$, which revealed a thermal barrier of 12.1 kcal/mol, well within the range of being kinetically feasible for a reaction occurring at room temperature. For the

Figure 2.4. (a) Salt metathesis route to iron alkoxides and their activity in alkyl-aryl Suzuki-Miyaura cross-coupling. (b) Protonolysis route to iron alkoxides and their activity in alkyl-aryl Suzuki-Miyaura cross-coupling. (c) Salt metathesis route to iron amides and their activity in alkyl-aryl Suzuki-Miyaura cross-coupling.
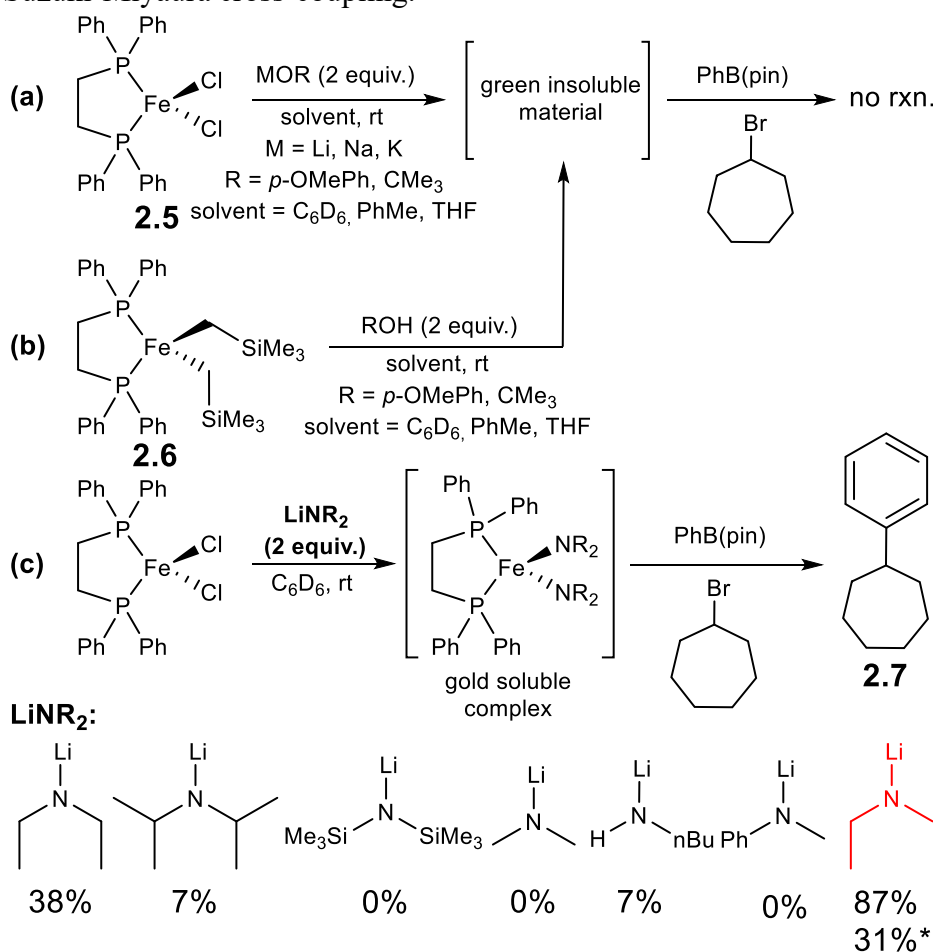
* Reaction run with 10% mol% (dppe)FeCl$_2$

28

sake of completeness, the ΔG value for this reaction was over 50 kcal/mol. This value would be outlandish for an entropic contribution of a reaction involving two molecules and is the reason all the values have been in terms of ΔH. The transition state found for transmetalation was similar to the analogous intermediate proposed by Denmark for palladium alkoxide systems:[38] there is significant interaction between the nitrogen of the iron amide with the boron of the boronic ester, which we propose leads to enhanced nucleophilicity of the complexed amide during transmetalation. This hypothesis is supported by the calculated Milliken charge in the transition state (Figure 2.5).

Considering this finding, we next pursued reactions that would result in the formation of iron amides. Unlike attempts to synthesize iron alkoxides, insoluble products were not formed when (dppe)FeCl$_2$ was treated with lithium diethylamide (Figure 2.3c). Instead, a golden homogeneous solution resulted, which demonstrated evidence for a single paramagnetic iron species being

Figure 2.5. – Plots of the Mulliken charge distribution obtained from DFT (B3LYP/631G*) calculations for the transition state obtained for transmetalation reaction between (dppe)Fe(NEt$_2$)$_2$ and PhB(pin). Mulliken charge distribution for PhB(pin) is also shown for reference.
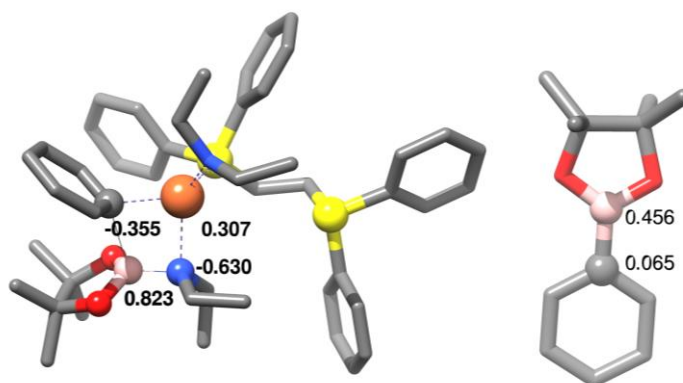
formed by ^{1}H NMR spectroscopy (Figure 2.6). The paramagnetic nature of the complex makes the absolute structural assignment impossible by NMR. Furthermore, the complex is unstable which has made it difficult to isolate for further characterization. We hypothesize that the expected

(dppe)Fe(NEt$_2$)$_2$ complex was being formed because the NMR is consistent with a single iron-containing species. Furthermore, the cross-coupled product **2.7** was formed in 38% yield when PhB(pin) and cycloheptyl bromide were added to the reaction mixture (Figure 2.3c).

Iron amides are attractive for further optimization because their electronic and steric properties can be readily tuned by altering the identity and number of substituents attached to nitrogen. Therefore, various lithium amides were evaluated as additives in the stoichiometric cross-coupling reaction (Figure 2.3c). This screen revealed an optimal size for the lithium amide reagent that was necessary to achieve high yields of the cross-coupled products. Sterically encumbered lithium amides, such as lithium diisopropylamide (LDA) or lithium hexamethyldisilazide (LiHMDS), led to poor yields of the desired cross-coupling products. On the other hand, small lithium amides,

Figure 2.6. ^{1}H NMR(C$_6$D$_6$, 400MHz) spectrum of reaction between (dppe)FeCl$_2$ and 2 equivalents of lithium dimethyl amide.

30
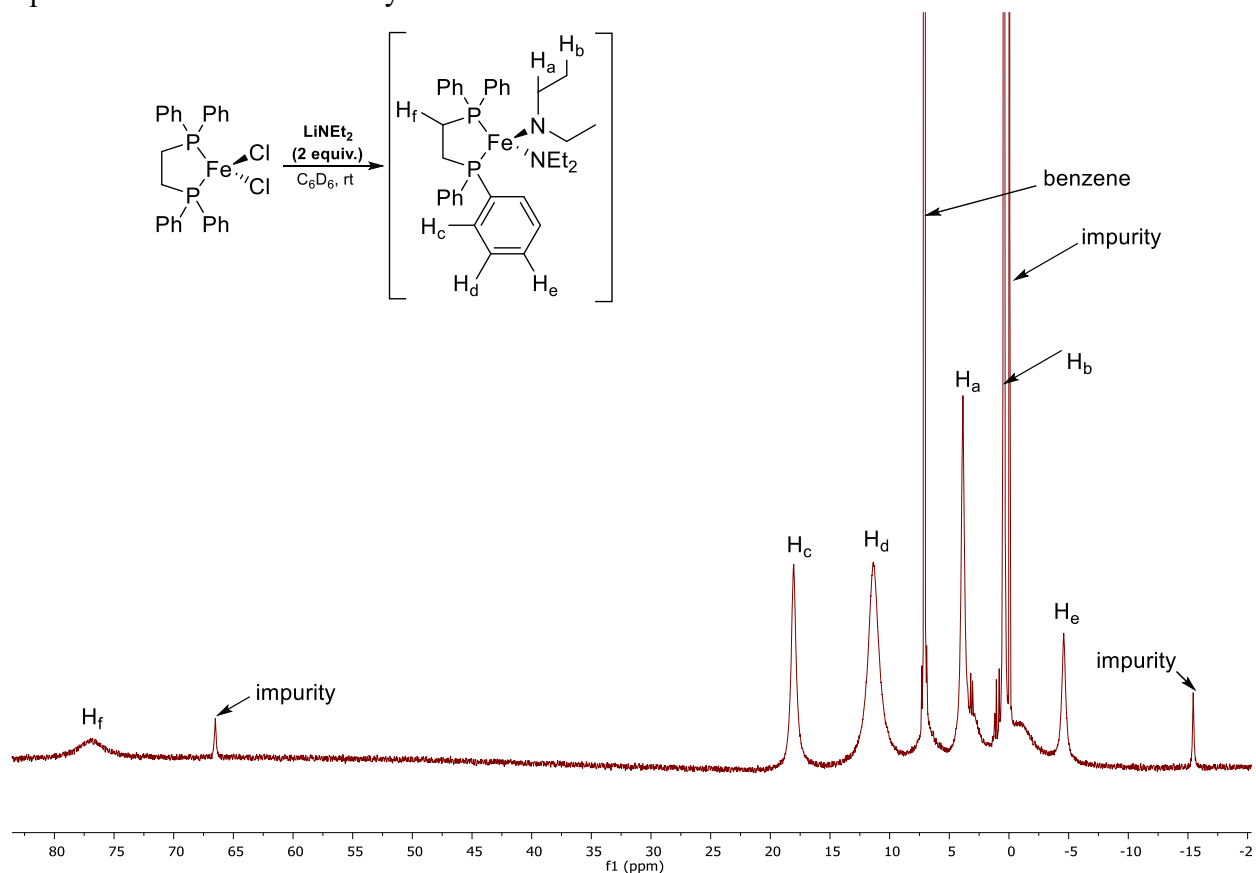
such as lithium dimethylamide or lithium butylamide, led to no product at all. A significant increase in yield was observed when lithium ethylmethylamide was used as the additive, forming the desired cross-coupled product **2.7** in 87% yield with the only byproducts being cycloheptane (**2.8**) and cycloheptene (**2.9**). Satisfyingly, the iron complex could be used in catalytic quantities when using this amide to give cross-coupled products in low chemical yields (31%) but with catalytic turnover (TON = 3).

2.3   Development of the catalytic transformation

To optimize the catalytic reaction, a variety of ligands were screened for the iron-catalyzed coupling between cycloheptyl bromide and PhB(pin) in the presence of lithium ethylmethylamide as the base. Chet Tyrol helped to collect approximately 70% of the data for the ligands studied and the major trends resulting from this process appear in Table 2.1. To provide a baseline for these studies, a reaction was run without any ligand. This reaction resulted in only slightly lower yields than when (dppe)FeCl$_2$ was used as a catalyst precursor (entry 1). Phosphines were promising candidates as ancillary ligands since bisphosphines are known to stabilize iron(II) centers in a variety of cross-coupling reactions between aryl nucleophiles and alkyl electrophiles.[4,5] Therefore, an extensive investigation of phosphine ligands including monodentate and bidentate phosphines with various electronic and steric constraints was undertaken (Table 2.1 entries 2-13). Monodentate phosphines typically gave only marginally better yields than when no ligand was used regardless to their steric and electronic properties (entries 2-4). Similarly, the chelate size of bidentate phosphines and more electron-rich phosphines related to dppe did not lead to any improvements (entries 5-8). Other bidentate phosphines including dppf (entry 9), (*rac*)-BINAP (entry 10), and Xantphos (entry 11) also did not improve yields significantly above levels obtained when no ligand was used in the reaction. The sterically restricted dppbz ligand gave yields slightly

higher than those with dppe (entry 12), and the more sterically encumbered SciOPP ligand afforded the desired product in the highest yield of any of the bisphosphines studied (entry 13). This ligand was the same ligand that Nakamura had found to be optimal for Kumada-type cross-coupling reactions between aryl Grignards and alkyl halides.[4] As Nakamura has alluded to, we hypothesize that the sterically encumbered SciOPP ligand is beneficial because it favors monomeric iron centers that are less prone to ligand disociation.[4]

Since phosphine ligands appeared to be labile in these reactions, we next investigated bidentate and tridentate ligands containing nitrogenous heterocycles. Whereas bipyridine ligands and pyridine bisoxazoline ligands (pyBox) resulted in similar yields as observed with simple bisphosphines (Table 2.2 entries 1 and 2), exploration of C_2-symmetric bisoxazoline ligands (Box) led to some improvement in yields (entries 3-6). These ligands have shown great utility for many cross-coupling applications, especially for reactions catalyzed by first row transition metals.[52] They are also attractive ligands because their steric and electronic properties can be modified by varying the substituents on either or both of the oxazoline rings or through modifications to the methylene backbone.[53-54] We found that yields in the cross-coupling reactions were particularly sensitive to the latter modification. While PhBox ligands with a methylene bridge give slightly higher yields than phosphines (entry 3) and isopropylidene linkers led to reduced yields of cross-coupled products (entry 4 and 6), the commercially available phenylcyano-Box ligand gave yields of the cross-coupled product that were superior to any other ligand that was screened (entry 7). Yields were significantly improved when an additional equivalent of phenylcyano-Box ligand relative to iron was added (entry 8). Higher yields in this reaction were likely obtained due to reduced amounts of cycloheptane and cycloheptene side products.

Table 2.1. Effect of phosphorous-based ancillary ligands on iron-catalyzed Suzuki-Miyaura cross-coupling reactions.

Reaction scheme: (bromocycloheptane) 1.0 equiv. + PhB(pin) 1.3 equiv. → FeCl₂ (10 mol%), Ligand (**X** mol%), LiNMeEt (120 mol%), C₆H₆, rt, 16 hr → phenylcycloheptane **2.7** + cycloheptane **2.8** + cycloheptene **2.9**
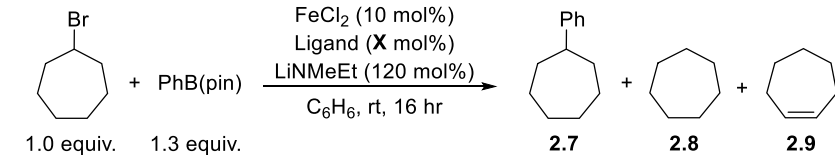
entry	ligand		X	2.7	2.8	2.9
1	No ligand		0	25	15	48
2	PPh₃		20	25	23	28
3	PCy₃		20	29	20	36
4	(Cy₂P-biphenyl, i-Pr substituted)		20	28	18	38
5	R₂P(CH₂)ₙPR₂	n = 2, R = Ph	10	31	20	28
6		n = 3, R = Ph	10	35	22	27
7		n = 4, R = Ph	10	36	20	28
8		n = 2, R = Me	10	31	41	6
9	(Fe ferrocene with PCy₂, PCy₂)		10	31	28	20
10	(rac) BINAP (PPh₂, PPh₂)		10	32	24	29
11	Xantphos (Ph₂P, PPh₂)		10	28	25	35
12	(Ar₂P–Ar₂P), R = H		10	37	23	27
13	R = t-Bu		10	43	28	12
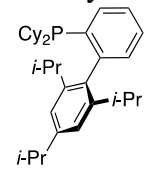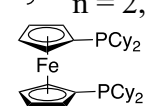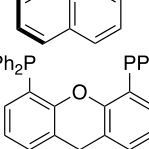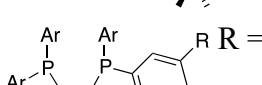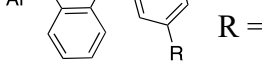
We hypothesized that reactions using *in situ* formed catalysts would result in a diverse speciation of iron complexes that might be detrimental to the yields of the reaction. We reasoned that the cyanoBox (**2.10**) ligands were superior to the unsubstituted and isopropylidene Box ligands due to their higher acidity. This property would make them more prone to undergo deprotonation under the basic conditions employed in the cross-coupling reactions. In order to investigate the iron speciation that is formed in situ, we synthesized iron complexes containing a

Table 2.2. Effect of nitrogen-based ancillary ligands on iron-catalyzed Suzuki-Miyaura cross-coupling reactions.
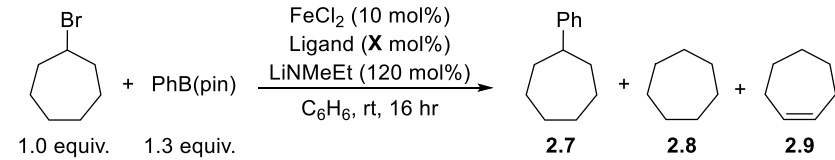
Reaction scheme: Cycloheptyl bromide (Br, 1.0 equiv.) + PhB(pin) (1.3 equiv.) → FeCl$_2$ (10 mol%), Ligand (**X** mol%), LiNMeEt (120 mol%), C$_6$H$_6$, rt, 16 hr → Ph-cycloheptane (**2.7**) + cycloheptane (**2.8**) + cycloheptene (**2.9**)
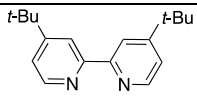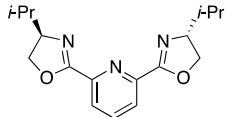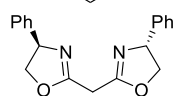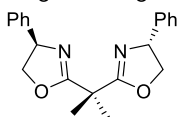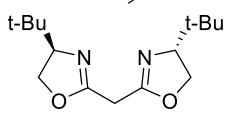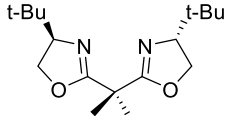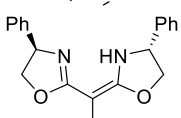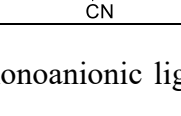
entry	ligand	X	2.7	2.8	2.9
1	4,4'-di-t-Bu-2,2'-bipyridine	10	30	20	26
2	2,6-bis(4-i-Pr-oxazoline)pyridine	10	34	27	13
3	bis(4-Ph-oxazoline)methane	10	36	14	16
4	2,2-bis(4-Ph-oxazoline)propane	10	25	16	26
5	bis(4-t-Bu-oxazoline)methane	10	7	13	8
6	2,2-bis(4-t-Bu-oxazoline)propane	10	27	16	35
7	cyanoBox (4-Ph), CN	10	58	14	10
8	cyanoBox (4-Ph), CN	20	72	6	6

neutral Box ligand (**2.11**), a monoanionic ligand Box ligand (**2.12**), and a homoleptic complex containing two equivalents of the monoanionic Box ligands (**2.13**). This last complex was synthesized in response to our observation that two equivalents of the cyanoBox ligand relative to iron led to better performance compared to analogous reactions with one equivalent of ligand.

As a baseline for comparison, the *in situ* generated catalyst was used under optimized conditions (table 2.3, entry 1). This produced the product in 68% yield after 24 hours. By comparison, when the premade complexes were subjected to the cross-coupling reaction conditions, all three were found to be catalytically active and produced the cross coupled products

in similar yields (Table 2.3, entries 2-4). These results suggest that the three precatalysts can be converted to a similar catalytically active species during the reaction. Although the yields obtained from all of the iron complexes was similar, complex **2.12** was found to be slightly more effective, producing 74% of the product and completely shutting down formation of the cycloheptane (**2.8**) byproduct after 24 hours. Adding an additional 10% of the ligand **2.10** to a reaction catalyzed by complex **2.12** led to slightly lower yields (71% vs 74%) but significantly less cycloheptene (**2.9**) byproduct was formed (entry 5). The remainder of the mass balance in this reaction was recovered starting material, leading to yields based on recovered starting materials that exceeded 90%. The lower isolated yields in the reaction were attributed to sluggish reaction kinetics observed in the presence of exogenous ligand. Supporting this notion, a reaction carried out for 48 hours led to nearly full conversion of cycloheptyl bromide and 82% yield of the desired product (entry 6).

Table 2.3. Dependency of iron-catalyzed cross-coupling reaction on the identity of the iron precursor.

entry	Fe complex	X (mol%)	2.7 (%)	2.8 (%)	2.9 (%)
1	FeCl$_2$	20	68	2	6
2	**2.11**	0	70	2	13
3	**2.12**	0	74	0	10
4	**2.13**	0	67	1	12
5	**2.12**	10	71	1	6
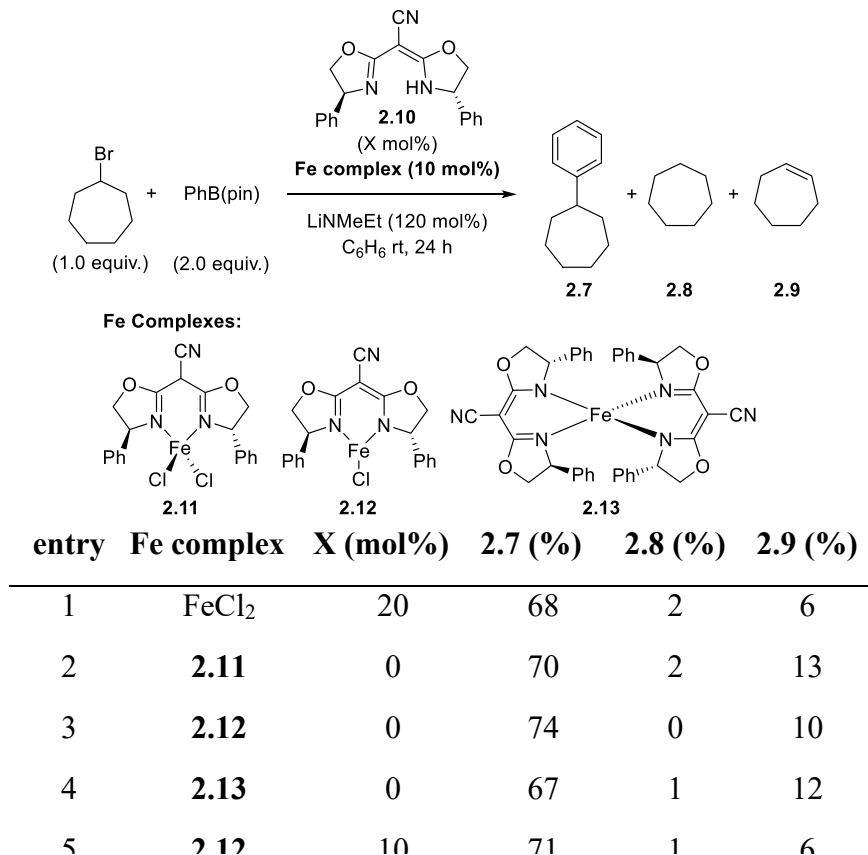
Alternatively, full conversion of the alkyl halide and nearly 90% yield was obtainable if an additional 10 mol% of **2.12** and 0.6 equivalents of lithium ethylmethylamide were added to the reaction after allowing the reaction to occur for six hours (entry 7).

2.4 Synthetic applicability of the iron-catalyzed Suzuki-Miyaura cross-coupling reaction.

The scope of the reaction was explored by varying the alkyl halide and boronic ester substrates (Figures 2.7 and 2.8). Primary and secondary alkyl bromides were well tolerated under the reaction conditions, although primary alkyl halides were less reactive than similar secondary alkyl halides. Primary alkyl halides **2.13a-2.13c** typically required heating to achieve high yields compared to secondary alkyl halides **2.7** and **2.14a-2.14c**. There was a marked difference in reactivity that was observed for activated and unactivated alkyl halides (e.g. **2.13** vs **2.15**). When unactivated alkyl halides **2.13** were employed, alkyl bromide **2.13b** was superior to alkyl iodide

Figure 2.7. Alkyl halide substrate scope using **2.12** as a catalyst. All yields are reported as isolated with the yields based on recovered starting material in parenthesis.
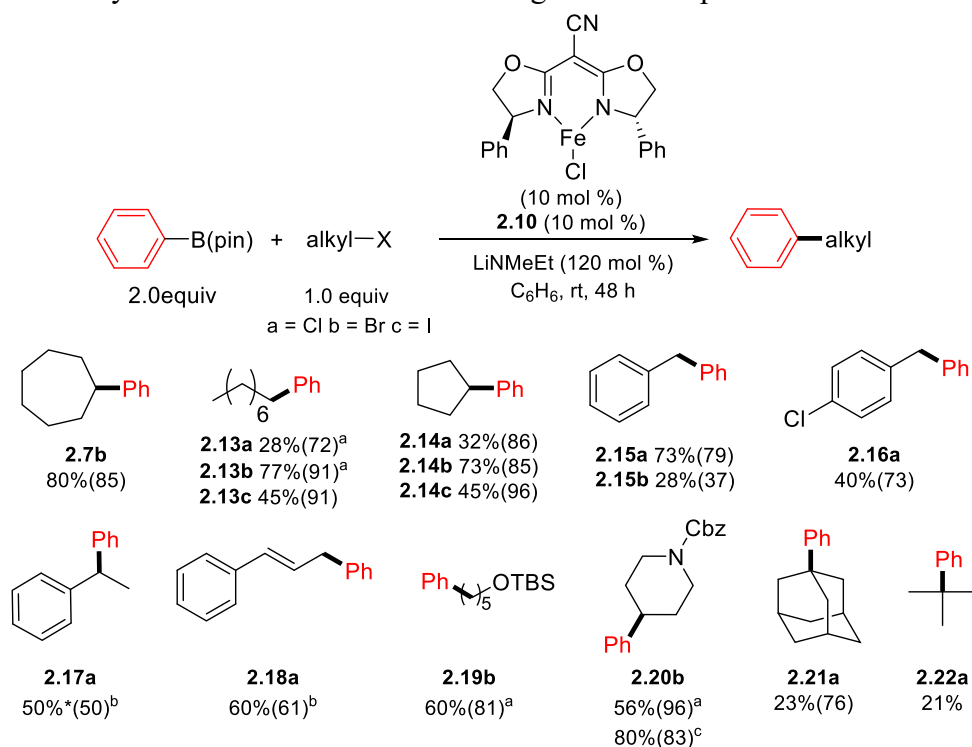
^{a} 50 °C. ^{b} **10** (0.1 mmol) and LiNMeEt (0.6 mmol) added after 24 h. ^{c} solvent was toluene.

2.13c, which in turn was superior to alkyl chloride **2.13a**. This trend was true regardless to whether the substrate was a primary alkyl halide **2.13** or secondary alkyl halide **2.14**. Tertiary alkyl halides **2.21** and **2.22** showed minimal amounts of the desired cross-coupled products regardless of the identity of the halide. In contrast, for activated alkyl halides **2.15**, higher yields were obtained for benzyl chloride (**2.15a**) compared to benzyl bromide (**2.15b**) due to the propensity for benzyllic substrates to undergo homocoupling.[55] This competing reaction was not observed for unactivated alkyl halides. Competing homocoupling of the alkyl halide was also observed for secondary benzyl chloride **2.17** and allylic halide **2.18**. Functionalized alkyl halides including a protected alcohol (**2.19**) and a protected amine (**2.20**) were tolerated leading to clean reactions whose major product was the desired cross-coupling product. The only other major species isolated from the functionalized alkyl halides was unreacted starting material as evidenced by the high yields based on recovered starting material. Unfortunately, functional groups with acidic protons were not tolerated under these conditions. These substrates include ketones, esters, nitriles, and amides. It seems likely that these substrates are not tolerant of the base that is being used in these reactions.

The reaction was also tolerant of different boronic esters (Figure 2.8). Cross coupling of napthyl boronic ester **2.23** proceeded similarly as PhB(pin). Electron-rich aryl boronic esters **2.24** and **2.25** demonstrated reduced efficiency, which is likely due to slower transmetalation rates being observed for these substrates.[56] Electron-deficient substrates **2.26** and **2.27** are also tolerated but these substrates also demonstrated sluggish reactivity and typically required heating to achieve high yields. We attribute the lower reactivity of the electron deficient boronic esters to the stability of borates that form between the amide base and the boronic ester. Heating reactions containing these borates liberates the amide base, which is important for the catalytic cross-coupling to occur (*vide infra*). Alkenyl boronic esters such as **2.28** provided some of the desired product but yields

were low. Reactions involving alkenyl boronic esters produced many other byproducts which have

been challenging to identify. Unfortunately, products derived from heteroaromatic substrates such

as **2.29** could not be obtained through this method. We believe the likely cause to be related to

heteroatom binding or the substantially modulated electronics of the aromatic system. This

challenged is addressed by the work presented in chapter 3.

Figure 2.8. Boronic ester substrate scope using **2.12** as a catalyst. All yields are reported as
isolated with the yields based on recovered starting material in parenthesis.
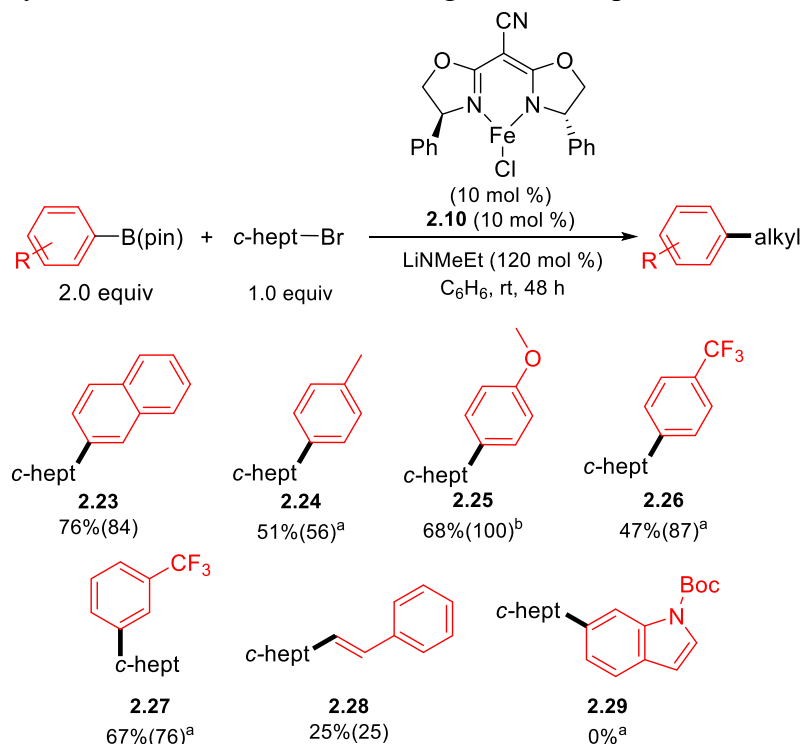
^{a} 50 °C. ^{b} **10** (0.1 mmol) and LiNMeEt (0.6 mmol) added after 24 h.

2.5   Mechanistic probes into cross-coupling

Our mechanistic understanding of the iron-catalyzed Suzuki-Miyaura cross-coupling

reaction promoted by lithium amides has been guided by the mechanistic framework proposed by

Nakamura[19] and supported with extensive studies by Neidig and coworkers[57-58] for the similar

iron-catalyzed Suzuki-Miyaura cross-coupling reaction between alkyl electrophiles and pre-

activated borate esters. In the mechanism proposed by Nakamura, the boronate serves only to transmetallate to the iron complex. Subsequently, the iron-aryl complex can reduce the alkyl halide to liberate a carbon-centered radical. This carbon-centered radical recombines with the metal in a poorly understood step to generate the cross-coupled products. Unlike palladium-catalyzed cross-coupling reactions, iron-catalyzed cross-coupling reactions often involve radical intermediates, which is likely the case here because ring-opened products (**2.31'**) are exclusively produced when cyclopropyl bromide (**2.30**) is used as a substrate and mixtures of direct cross-coupling (**2.33**) and cross-coupling that occurs after ring closing (**2.33'**) were observed when 6-bromohexene (**2.32**) was used as the substrate (Figure 2.9). These outcomes suggest the intermediacy of a carbon-based radical with lifetimes that are roughly 10^5 s^{-1}. Similar results were obtained by Nakamura,[19] which supports our working hypothesis that the cross-coupling mechanism follows a similar route as illustrated in Figure 2.10. While these results are not conclusive for the presence of radical intermediates, they also do not rule out a radical intermediate. A more sophisticated probe will be required to distinguish these products from the metal-mediated migratory insertion pathway that would furnish identical products using the substrate **2.32**.[59]

Two key differences between the system discussed here and those reported by Nakamura and Bedford are the identity of the ligand and the involvement of the amide base. We believe the

Figure 2.9. Radical clock substrates used to probe the intermediacy of organic radicals.
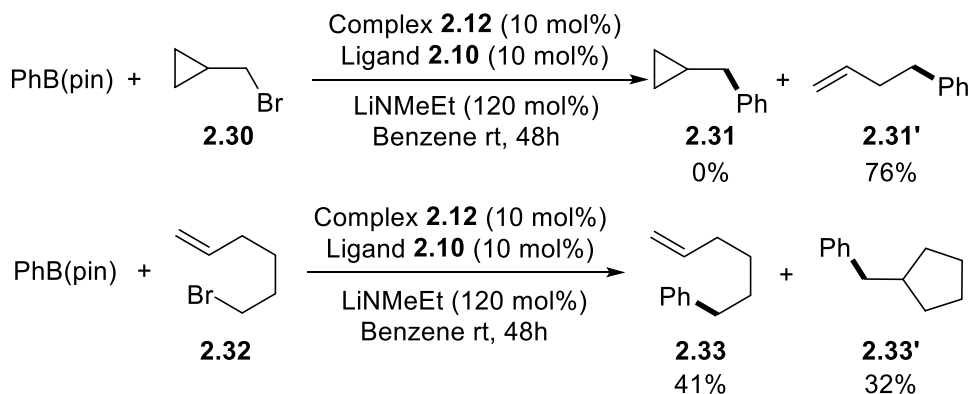
function of the lithium amide is twofold. Firstly, it can serve to deprotonate the cyano-Box ligand to convert a coordination complex between the Box ligand and iron dichloride (**2.11**) into an iron complex that contains an anionic Box ligand (**2.12**).[60] We hypothesize that this coordination environment strengthens the metal-ligand interaction and prevents deleterious aggregation that pervades with ligands, such as phosphines, that have weaker interactions with iron. The second role of the lithium amide is to convert the putative iron halide **2.12** into an iron amide species (**2.34**), which is the precursor to transmetalation that furnishes iron phenyl species **2.35**. This supposition was formulated based on our computational studies, which show that boron-to-iron transmetalation is made thermodynamically downhill and kinetically fast from an iron amide intermediate (*vide supra*). We have repeated these calculations with the cyano-Box iron complexes and found that the thermodynamics for transmetalation are similar to those reported in Figure 2.2, but the kinetic barriers for transmetalation are even lower than the barrier calculated for

Figure 2.10. Working mechanistic hypothesis for the cross-coupling of alkyl electrophiles with unactivated aryl boronic esters.
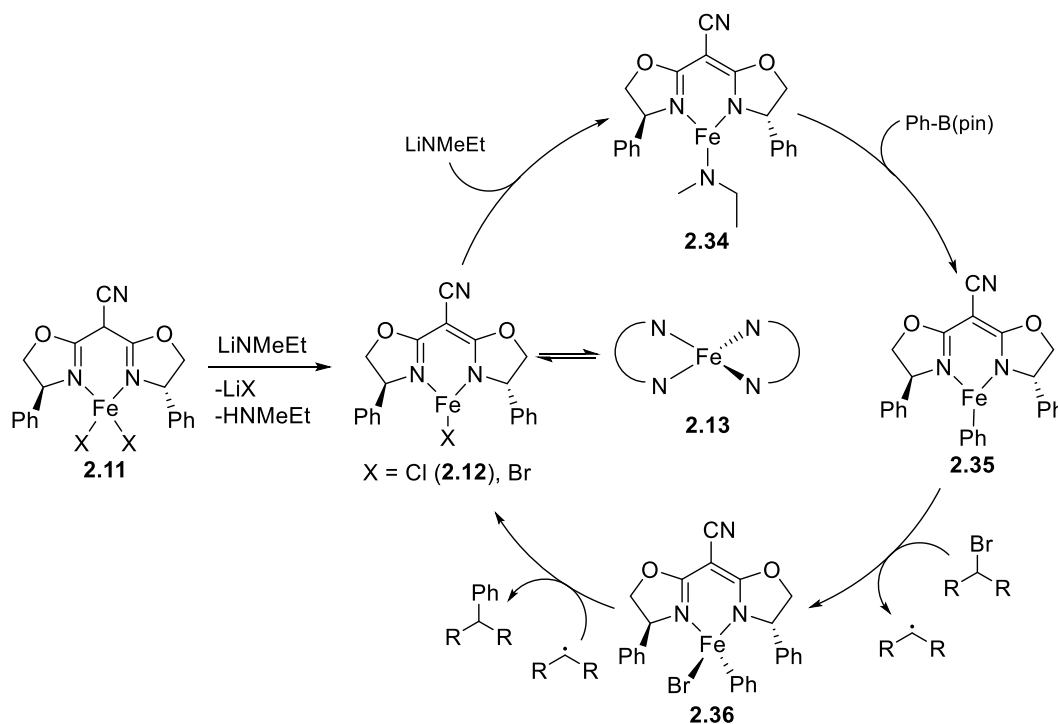
transmetalation involving (dppe)Fe(NEt$_2$)$_2$ (Figure 2.11). This difference is likely due to the reduced steric requirements of this ligand framework. Previously, the bisphosphine had to undergo a partial dissociation to allow the boronic ester in close enough proximity for transmetalation. This dissociation is very likely endergonic. With the bis(oxazoline) ligands, that dissociation is no longer required as it is already a three-coordinate metal complex. Several of the trends that we

Figure 2.11. (a) DFT (B3LYP/6-31G*) computed energies for transmetalation from boron to iron in reactions between PhB(pin) and CNBox^{Ph}FeX (X = anionic ligand). (b) Calculated transition state structures.
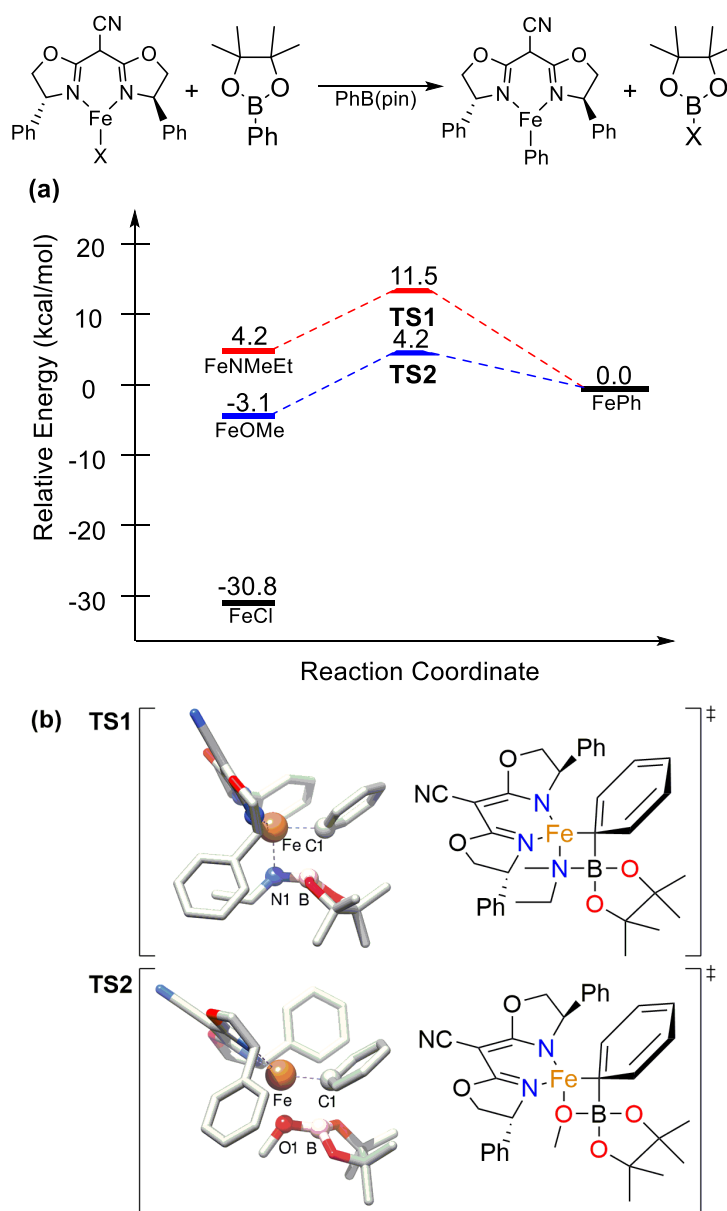
Figure 2.12. – ^{11}B NMR (128MHz) in THF of reaction between lithium ethylmethylamide and PhB(pin). Broad resonance centered at -3 ppm is from the borosilicate glass NMR tube. ^{11}B shift of PhB(pin) is 31 ppm.
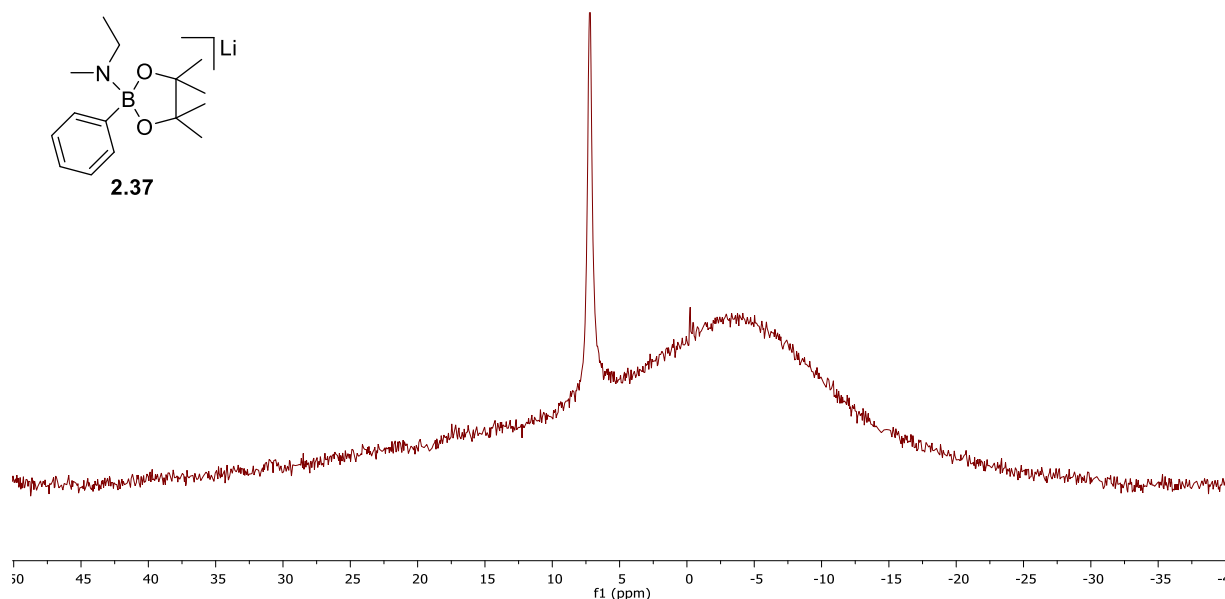
observed during the catalyst optimization process are more consistent with the notion that an iron

amide is involved in the transmetalation reaction as opposed to transmetalation proceeding through

Figure 2.13. Effect of adding independently prepared borate species [Ph(NMeEt)B(pin)]$^-$ resulting from addition of amide to boronic ester.
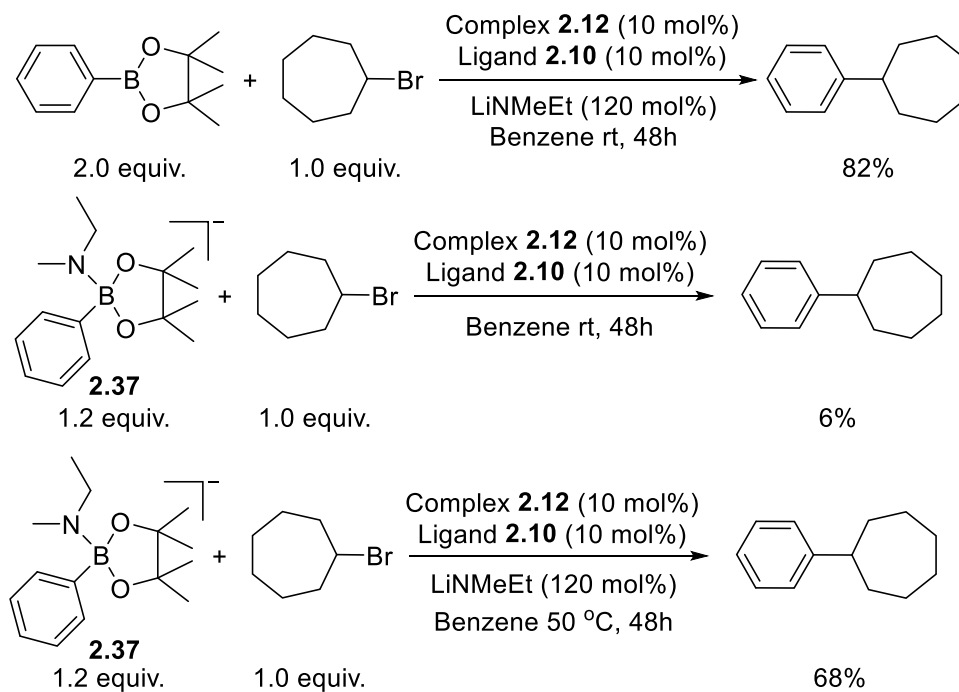
Figure 2.14. a) Reaction using phenyl boronic acid neopentyl glycol ester. b) cross-over reactions from borate intermediates.

a)

b)
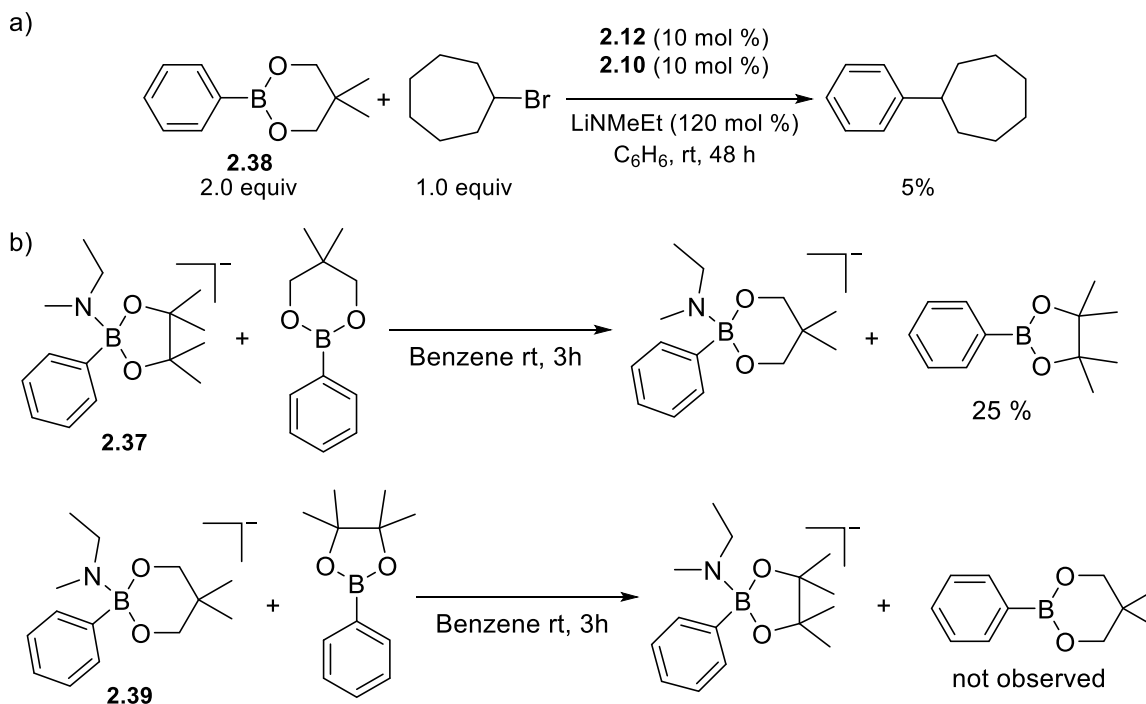
a borate species that forms from reaction with the boronic ester and the amide base. It is certainly true that PhB(pin) reacts immediately with lithium ethylmethylamide to make a borate species, which we have detected by ^{11}B NMR spectroscopy (Figure 2.12). However, boronic esters that are expected to more readily form borate species result in sluggish reactions (e.g. electron deficient boronic acid esters). Moreover, when the borate species, formed between PhB(pin) and lithium ethylmethylamide, is synthesized independently and purposely added to the cross-coupling reaction, we observe greatly diminished yields (6%) compared to when the lithium amide and boronic ester are added to the reaction separately (82%) (Figure 2.12). When a reaction containing the preformed borate is heated, the cross-coupling product is formed in higher yields (68%) but these yields are not near the levels observed when PhB(pin) and lithium amide are added separately at room temperature (Figure 2.13). While these finding do not necessarily rule out the intermediacy of a borate species, the inhibitory nature observed when such species predominate lead us to favor

43

a pathway that involves iron amide intermediates as a necessary precursor for transmetalation. It seems likely that the borate would be formed immediately under catalytic conditions but neither the borate or the lithium amide are particularly soluble in benzene. Furthermore, boronic esters that would give rise to very stable borates (i.e. **2.38**) were nearly incompetent for the reaction at all (Figure 2.14a). Furthermore, when the borate **2.37** was combined with the phenyl boronic acid neopentyl glycol ester **2.38** it was observed that the amide was transferred to **2.38** (Figure 2.14b). The converse reaction where the borate is first made using **2.38** revealed that none of the amide was transferred. This would further indicate that borates are more stable when they are generated from less sterically encumbered boronic esters.

Another notable observation that led to higher yields and less byproducts in the Suzuki-Miyaura cross-coupling reaction was the benefit of adding a second equivalent of ligand to the

Figure 2.15. a) Plot of products versus time for the cross-coupling of bromocycloheptane in the presence of extra ligand. Lines connecting data points are a guide for the eye and are not meant to be mathematical fits to the data.
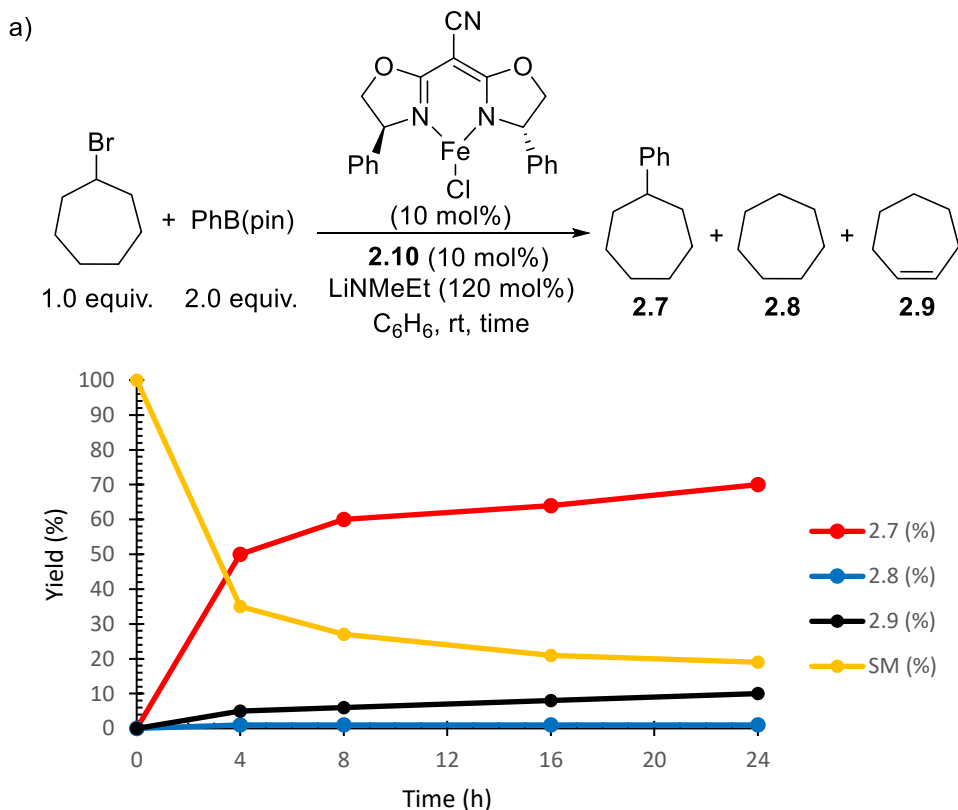
reaction. We hypothesize that the role of the second equivalent of ligand is to protect the catalyst from aggregation by forming homoleptic complexes akin to **2.13**. By monitoring the reaction in situ, we have observed that reactions carried out with an excess of ligand proceed at a slower rate but provide the product in greater selectivity for a longer period of time (Figure 2.15 vs 2.16). A reaction mechanism in which **2.12** is in equilibrium with **2.13** is consistent with these observations because it provides a resting state for the iron complexes that is off of the catalytic cycle (Figure 2.9). We hypothesize that the coordinatively saturated and sterically encumbered **2.13** protects the iron complex from unwanted decomposition pathways, such as aggregation, that may lead to the cycloheptane and cycloheptene side products. Since this species is not on the catalytic cycle,

Figure 2.16. Plot of products versus time for the cross-coupling of bromocycloheptane in the absence of extra ligand. Lines connecting data points are a guide for the eye and are not meant to be mathematical fits to the data.
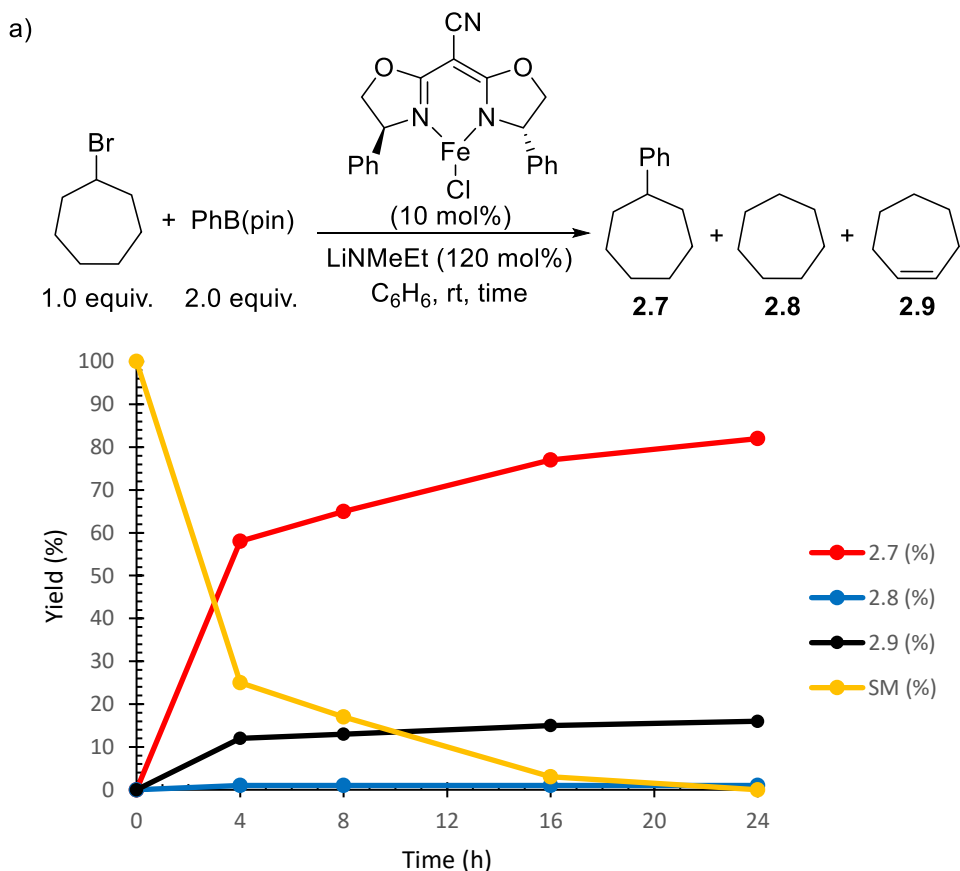
however, reaction rates are retarded under conditions where **2.13** is formed. This mechanism

explains how **2.11-2.13** are competent precatalysts for the cross-coupling reactions. That the

cyanoBox ligands are superior to either the methylene or isopropilidene versions of the Box

ligands is also consistent with this mechanism because the equilibration of **2.11-2.13** as well as

equilibration with other species that are on the catalytic cycle requires a ligand that can be

deprotonated by the lithium amide base and that can undergo reversible reaction with the various

iron species present during catalysis. Furthermore, a time course of the reaction in the absence of

ligand revealed that the starting material was consumed rapidly but the product was not formed

with any selectivity (Figure 2.17).

Figure 2.17. Plot of products versus time for the cross-coupling of bromocycloheptane in the absence of any ligand. Lines connecting data points are a guide for the eye and are not meant to be mathematical fits to the data.
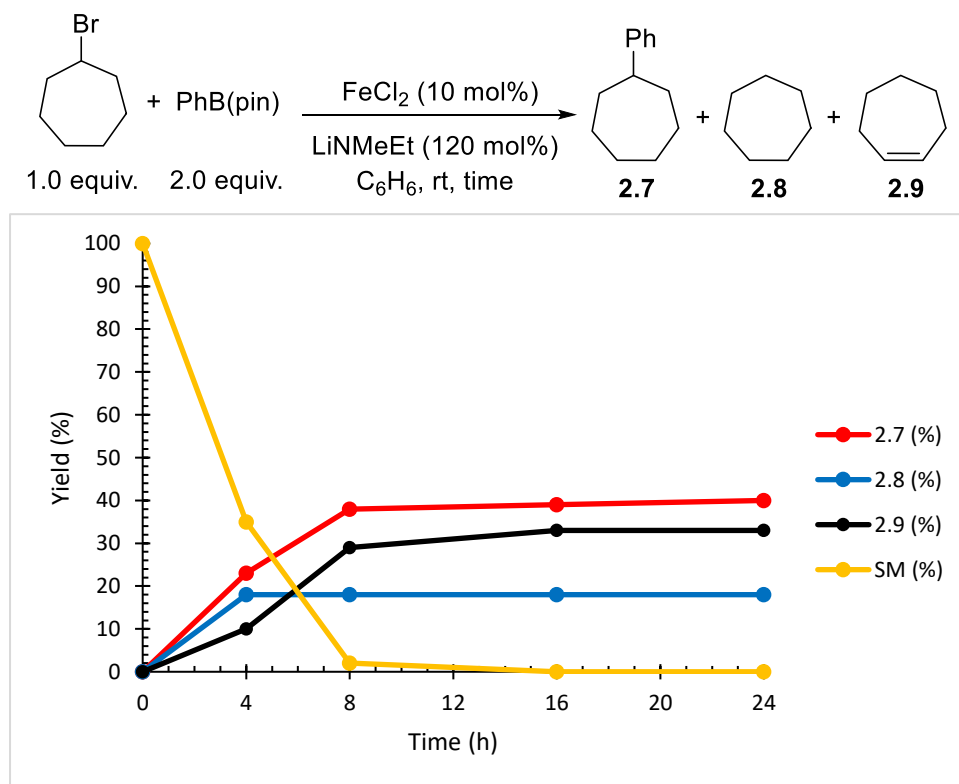
2.6   Application to a pharmaceutical target

Finally, to demonstrate the utility of the new cross-coupling method, the pharmaceutical agent Cinacalcet[61] was synthesized. Cinacalcet is a calcimimetic that activates calcium-sensing receptors through allosteric interactions with G protein-coupled receptors. It is used to treat secondary hyperparathyroidism, and in 2014 it was the 76th top selling drug on the market. Most currently used methods for the synthesis of Cinacalcet rely on noble metal catalysts for its construction (e.g. Figure 2.18a).[62-66] The Amgen patent published for the synthesis of Cinacalcet (trade name Sensipar[©]) contains many routes for the formation of the pharmaceutical agent, and among the most efficient routes are those that involves palladium-catalyzed cross-coupling reactions to make C_3-C_4 followed by hydrogenation of the resulting alkene (**2.40**) to form Cinacalcet.[64] Tewri and coworkers reported a three step procedure for the synthesis of Cinacalcet that utilized an iron-catalyzed cross-coupling reaction for the first time.[63] This reaction was a Kumada type cross-coupling reaction between an aryl Grignard and a vinyl halide to form C_3-C_4. As was the case with the palladium-catalyzed route, subsequent reduction of an unsaturated version of Cincalcet was required. We envisioned that the reduction step involved in most reported syntheses of Cinacalcet could be avoided if C_3-C_4 was formed using our newly developed iron-catalyzed Suzuki-Miyaura reaction, which would provide access to the pharmaceutical agent in two steps. Figure 2.18b contains the new synthesis, which takes advantage of the difference in reactivity between alkyl chlorides and bromides leading to an efficient coupling reaction between commercially available 1-bromo-3-chloropropane (**2.41**) and aryl boronic acid (**2.42**). The reaction proceeded in 55% yield with only 10% of bisarylated product being formed. The alkyl halide **2.43** formed could be efficiently elaborated to Cinacalcet by using it to alkylate the commercially available amine **2.44** in the presence of a catalytic amount of potassium iodide. This route

constitutes a very high yielding synthesis of Cinacalcet (41% overall) in less steps reported in the

Amgen patent and without the use of noble metal catalysts. This synthesis would not have been

Figure 2.18. Synthesis of Cinacalcet: (a) three-step syntheses previously reported. (b) two-step
synthesis using iron-catalyzed alkyl-aryl Suzuki-Miyaura cross-coupling reaction
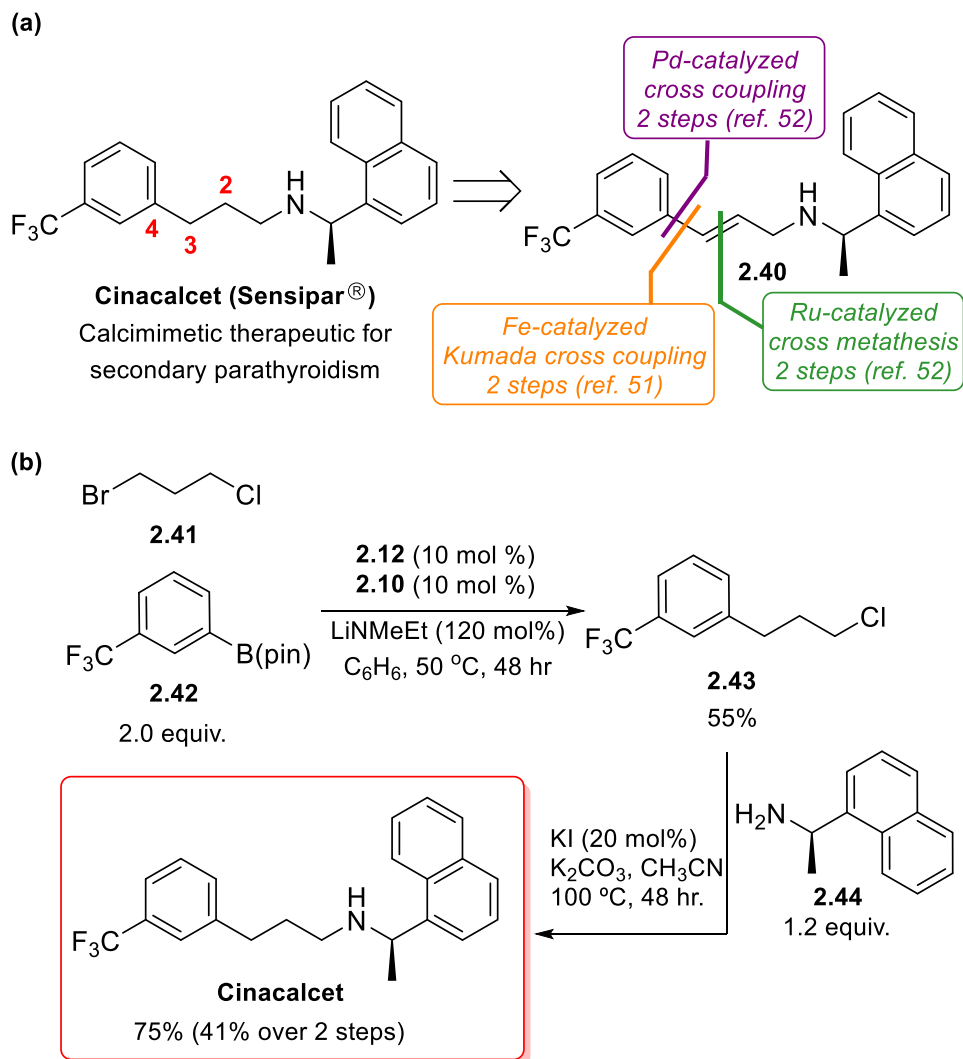
possible without the help of Chet Tyrol and Alexander Wong. The final synthesis was carried out

by Chet but there were several other routes the three of us had devised that did not play out as

successfully as this synthesis. In one route we attempted to do the S_N2 reaction first followed by

cross-coupling. Unfortunately, we were unable to maintain the protecting group on the amine and

still achieve selective alkylation.

48

2.7   Conclusions

In summary, an iron-catalyzed Suzuki-Miyaura cross-coupling reaction between alkyl halides and unactivated aryl boronic esters was developed that did not require activation of the boronic ester nor the addition of magnesium additives. These results reveal that the key limitation that had previously limited iron-catalyzed Suzuki-Miyaura systems was the irreversible formation of iron alkoxides and hydroxides aggregates that would be formed under conditions typically used for palladium-catalyzed Suzuki-Miyaura reactions. Computational studies revealed the viability of amide bases to mediate transmetalation so that it is thermodynamically and kinetically accessible. Stoichiometric experiments suggested that putative iron amides prevent irreversible aggregation, which allows the cross-coupling to proceed under catalytic conditions with good to excellent yields. The usefulness of the catalytic cross-coupling reaction in chemical synthesis was demonstrated with the synthesis for Cinacalcet, an active pharmaceutical ingredient currently used for the treatment of secondary hyperparathyroidism. The synthesis was the shortest ever reported and avoided the use of non-noble metals, which may be beneficial for economic and environmental reasons. Future efforts will be directed towards increasing our mechanistic understanding of the reaction, expanding the substrate scope available for the cross-coupling reactions, and developing protocols for enantioselective and analogous alkyl-alkyl Suzuki-Miyaura cross-coupling reactions.

2.8   Experimental

General Considerations. Unless stated otherwise, all reactions were carried out in oven-dried glassware in a nitrogen-filled glovebox or using standard Schlenk-line techniques.[67] Solvents including dichloromethane, pentane, toluene, diethyl ether, and tetrahydrofuran were purified by passage through two activated alumina columns under a blanket of argon[68] and then degassed by brief exposure to vacuum. Phenylboronic acid, 2-naphthaleneboronic acid, 4-

methoxyphenylboronic acid, *p*-tolylboronic acid, 4-trifluoromethylphenylboronic acid, 3-trifluoromethylphenylboronic acid pinacol ester were bought from Oakwood Chemicals and dried over P_2O_5 followed by passage through an alumina plug in the glovebox before use. All prepared boronic pinacol esters were used after passage through alumina under a nitrogen atmosphere. Methylethyl amine was purchased from TCI America; diisopropylamine and lithium dimethylamide were purchased from Alfa Aesar, butylamine and diethylamine were purchased from Sigma-Aldrich and (R)-(+)-1-(1-Naphthyl)ethylamine was purchased from Oakwood Chemicals. All amines that were liquids at room temperature were dried over calcium hydride for at least 24 hours before being vacuum-distilled. 2,3-dimethyl-2,3-butanediol and 2,2-dimethylpropane-1,3-diol were purchased from Alfa and used without further purification. Anhydrous iron (II) chloride was purchased from Sigma Aldrich and used without further purification. All bisphosphines were purchased from Sigma-Aldrich, Fisher Scientific, TCI America, Oakwood, or Strem Chemicals and dried over P_2O_5 before use in the glovebox. All bis(oxazoline) ligands including (4*S*)-(+)-Phenyl-α-[(4*S*)-phenyloxazolidin-2-ylidene]-2-oxazoline-2-acetonitrile (**2.10**) were purchased from Sigma-Aldrich and dried over P_2O_5 before use in the glovebox. Purchased alkyl halides were dried over calcium hydride for at least 24 hours before being vacuum-distilled, while all solids were dried over P_2O_5 before use in the glovebox. All alkyl halides were purchased from Sigma-Aldrich, Oakwood Chemicals and Fisher Scientific.

^{1}H, ^{11}B, {^{1}H}^{13}C, and ^{19}F nuclear magnetic resonance (NMR) spectra were recorded at ambient temperature on Varian VNMRS operating at 400 MHz, 500 MHz, or 600 MHz for ^{1}H NMR at 160 MHz for ^{11}B NMR, 125 MHz for {^{1}H}^{13}C or 470 MHz for ^{19}F NMR. All {^{1}H}^{13}C NMR was collected while broad-band decoupling was applied to the ^{1}H region. The residual protio solvent impurity was used as an internal reference for ^{1}H NMR spectra and {^{1}H}^{13}C NMR spectra. Boron

trifluoride diethyl etherate was used as an external standard ($BF_3 \cdot O(C_2H_5)_2$: 0.0 ppm) for ^{11}B NMR and ^{19}F NMR ($BF_3 \cdot O(C_2H_5)_2$: -153.0 ppm). The line listing for NMR spectra of diamagnetic compounds are reported as follows: chemical shift (multiplicity, coupling constant, integration) while paramagnetic compounds are reported as chemical shift (peak width at half height, number of protons). Solvent suppressed spectra were collected for paramagnetic compounds in THF using the PRESAT macro on the VNMR software. Infrared (IR) spectra were recorded on a Bruker Alpha attenuated total reflectance infrared spectrometer. High-resolution mass spectra were obtained at the Boston College Mass Spectrometry Facility on a JEOL AccuTOF DART instrument. Single crystal X-ray Intensity data were measured on a Bruker Kappa Apex Duo diffractometer using a high brightness IμS copper source with multi-layer mirrors. The low temperature device used is an Oxford 700 series Cryostream system with temperature range of 80-400 K. An Olympus SZ1145 stereo zoom microscope is used to view and mount crystals. The crystal structure was solved using ShellX.

Computational Procedures. All computations were carried out using Density Functional Theory (DFT) methodology employing the hybrid B3LYP functional (composed of Becke's 1988 exchange functional[69] and Lee, Yang, and Parr's correlation functional[70]) in conjunction with the 6-31G* basis set.[71] All calculations with phospine ligands were carried out in a tetrahydrofuran (THF) solvent simulated by Tomasi's Polarizable Continuum Model (PCM).[72] Stationary-point characterization of all optimized geometries were carried out by means of frequency calculations utilizing the same level of theory as was used in the geometry optimizations. Gibbs free energies and enthalpies (computed at 298 K and 1 atm) and zero-point corrected energies were calculated using the computed normal mode frequencies (not scaled). All calculations were carried out using Gaussian 09 program[73] All iron complexes were calculated in the quintet state. In all cases for

minima, the intermediate (triplet) and low (singlet) spin states were higher in energy between 15 and 40 kcal/mol.

Synthesis of (2,2-bis((S)-4-phenyl-4,5-dihydrooxazol-2-yl)acetonitrile)*FeCl₂* (2.11). To a 20 mL scintillation vial equipped with a stir-bar was added iron dichloride (0.3 g, 0.9 mmol) and THF (10 mL). After stirring for one hour, 2,2-bis((S)-4-phenyl-4,5-dihydrooxazol-2-yl)acetonitrile (0.115 g, 0.9 mmol) was added. The solution became clear and slightly yellow almost immediately. After stirring for 12 hours the solvent was removed *en vacuo* and the oil was triturated with pentane. This yielded an off-white solid (0.285 g, 69%). ^{1}H NMR (500 MHz, THF) δ -30 ($w_{1/2}$ = 307 Hz, 4H), -4.2 ($w_{1/2}$ = 59 Hz, 2H), -3.8 ($w_{1/2}$ = 33 Hz, 4H), -1.1 ($w_{1/2}$ = 21 Hz, 2H), 10.8 ($w_{1/2}$ = 76 Hz, 2H) , 56.8 ($w_{1/2}$ = 512 Hz, 1H) ppm. IR: 2201, 1595, 1533, 1493, 1452, 1067, 697 cm⁻¹.
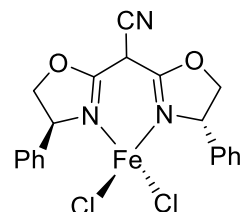
Synthesis of (2,2-bis((S)-4-phenyl-4,5-dihydrooxazol-2-yl)aceto nitrile*)FeCl*, (CNBoxᴾʰ)FeCl (2.12). In the glovebox, to a 7 mL scintillation vial equipped with stir bar was added 2,2-bis((S)-4-phenyl-4,5-dihydrooxazol-2-yl)acetonitrile (0.81 g, 2.5 mmol). This was then dissolved in THF (3 mL) and sodium hydride (0.065 g, 2.7 mmol) was added using THF (2 mL) to transfer it. This mixture was stirred for 12 hours before being filtered through celite. The celite and vial were rinsed with THF (5 mL). To a 20 mL scintillation vial equipped with a stir-bar was added iron dichloride (0.31 g, 2.5 mmol) and THF (5 mL). After stirring for one hour, the Na{2,2-bis((S)-4-phenyl-4,5-dihydrooxazol-2-yl)acetonitrile} solution was added. The solution went from pale yellow-brown to a white suspension almost immediately. After stirring for 12 hours the solvent was removed *en vaccuo* and the solid washed with THF and redried. This yielded an off-

white solid (0.95 g, 81%). To generate X-ray quality crystals, a soxhlet extraction in refluxing CH$_3$CN was carried out for two days to remove residual sodium chloride. Concentration of the filtrate gave a white solid, and crystals suitable for X-ray diffraction were grown from a cold CH$_3$CN/toluene solution. The crystal structure contained two molecules of **10** in the asymmetric unit. Each iron was tetrahedral by virtue of coordinating to the nitrile moiety of the nearest neighbor iron complex. This interaction is presumed to be replaced by solvent during the cross coupling reaction (See S18-S33). ^{1}H NMR (500 MHz, THF) δ -30 ($w_{1/2}$ = 307 Hz, 4H), -4.2 ($w_{1/2}$ = 59 Hz, 2H), -3.8 ($w_{1/2}$ = 33 Hz, 4H), -1.1 ($w_{1/2}$ = 21 Hz, 2H), 10.8 ($w_{1/2}$ = 76 Hz, 2H) , 56.8 ($w_{1/2}$ = 512 Hz, 1H) ppm. IR: 2203, 1606, 1533, 1440, 1067, 694 cm^{-1}.

Synthesis of (2,2-bis((S)-4-phenyl-4,5-dihydrooxazol-2-yl)acetonitrile)$_2$Fe (2.13): To a 20 mL scintillation vial equipped with a stir-bar was added iron dichloride (0.032 g, 0.25 mmol) and THF (10 mL). After stirring for one hour Li-2,2-bis((S)-4-phenyl-4,5-dihydrooxazol-2-yl)acetonitrile (0.170 g, 0.5 mmol) was added. The solution became clear and brown almost immediately. After stirring for 12 hours the solvent was removed *en vaccuo* to yield a light tan solid (0.110 g, 63%). ^{1}H NMR (500 MHz, THF) broad resonances, δ -27.3 ($w_{1/2}$ = 406 Hz, 2H), -6.0 ($w_{1/2}$ = 86 Hz, 4H),   -0.4 ($w_{1/2}$ = 49 Hz, 2H), 7.3 ($w_{1/2}$ = 31 Hz, 1H), 18.8 ($w_{1/2}$ = 150 Hz, 2H), 78.4 ($w_{1/2}$ = 604 Hz, 1H) ppm. IR: 2204, 1595, 1510, 1425, 1068, 697 cm^{-1}.
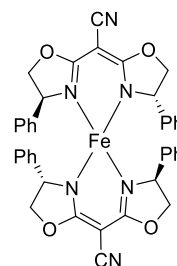
General procedure for the synthesis of boronic esters All boronic esters were prepared according to a procedure adapted from previous syntheses.[74]

Synthesis of *5,5-Dimethyl-2-phenyl-1,3,2-dioxaborinane (2.37)*. On the Schlenk line under a nitrogen atmosphere, phenyl-boronic acid (1.00 g, 8.20 mmol) and anhydrous pentane (22 mL) were added to an oven-dried two-neck flask containing a
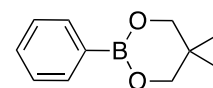
53

stir bar. The flask was brought to 0 °C and neopentanol glycol (0.94 g, 9.02 mmol) was added neat and stirred at room temperature for 24 hours. Sodium sulfate was added to the solution and then filtered with diethyl ether. The solvent was removed under reduced pressure to give a crude white solid that was filtered through a plug of silica eluting with dichloromethane to yield the product that was analytically pure by ^{1}H NMR spectroscopy (1.40 g, 90% yield). ^{1}H NMR (500 MHz, CDCl$_3$) δ 1.03 (s, 6H), 3.77 (s, 4H), 7.37-7.33 (m, 2H), 7.40-7.45 (m, 1H), 7.78-7.82 (d, 2H) ppm. ^{11}B NMR (128 MHz, CDCl$_3$) δ 26.9 ppm.

Synthesis of *4,4,5,5-Tetramethyl-2-phenyl-1,3,2-dioxaborolane.* On the Schlenk line under a nitrogen atmosphere, phenyl-boronic acid (5.00 g, 41.0 mmol) and anhydrous pentane (110 mL) were added to an oven-dried two-neck flask containing a stir bar. The flask was brought to 0 °C and pinacol (5.08 g, 43 mmol) was added neat and stirred at room temperature for 24 hours. Sodium sulfate was added to the solution and then filtered with diethyl ether. The solvent was removed under reduced pressure to give a crude white solid that was filtered through a plug of silica eluting with dichloromethane to yield the product that was analytically pure by ^{1}H NMR spectroscopy (7.50 g, 90% yield). ^{1}H NMR (500 MHz, CDCl$_3$) δ 1.35 (s, 6H), 7.35-7.39 (m, 2H), 7.43-7.48 (m, 1H), 7.79-7.83 (m, 2H) ppm. ^{11}B NMR (128 MHz, CDCl$_3$) δ 31.0 ppm.
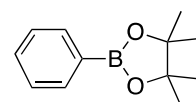
General procedure for ligand screening. In a nitrogen-filled glovebox, iron dichloride (3 mg, 0.024 mmol) was combined in a 7 mL scintillation vial with lithium ethylmethylamide (18.5 mg, 0.28 mmol) and ligand (0.024 mmol or 0.048 mmol) based on the amount relative to the metal described in the table. A stirbar was then added to the vial followed by a 0.5 mL stock solution of bromocycloheptane (43 mg, 32 µL, 0.240 mmol), phenyl boronic acid pinacol ester (63 mg, 0.300 mmol) and tetradecane (12 mg, 15.4 µL, 0.060 mmol). The resulting solution was diluted to a total

54

volume of around 7 mL. The vial was then seal with a Teflon lined cap and the mixture was stirred for 16 hours. The reaction was then removed from the glovebox and quenched by the addition of 1 drop of water. The reaction was then dried over sodium sulfate and filtered through celite. 0.200 mL of this reaction was then diluted with dichloromethane and analyzed by quantitative GC.

General procedure for stoichiometric experiments involving deprotonated alcohols and amines.
In a nitrogen-filled glovebox, complex **2.5** (10 mg, 0.020 mmol) was weighed out into a 4 mL scintillation vial. To this was added the alkoxide or amide solid (0.040 mmol). These solids were then dissolved in C_6D_6 (0.600 mL). The solution, and solids, were transferred to a J. Young tube for characterization. ^{1}H NMR was collected and monitored for changes over time. In the alkoxide cases no signals were observed except for those associated with the free ligand. After 30 minutes bromocyclophetpane (0.020 mmol) and phenylboronic acid pinacol ester (0.020 mmol) were added to the J. Young tube and mixed in by shaking. The reaction was monitored by ^{1}H NMR and after 24 hours the reaction was analyzed by quantitative GC to determine if any minor species were formed.

General procedure for stoichiometric experiments involving protonolysis of an iron-alkyl complex. In a nitrogen-filled glovebox, complex **2.6** (20 mg, 0.032 mmol) was weighed into a 4 mL scintillation vial. This complex was dissolved in C_6D_6 (0.600 mL) and an alcohol (0.064 mmol) was added. The solution was then transferred to a J. Young tube and analyzed by ^{1}H NMR. In all cases, this resulted in a precipitate forming in the J. young tube and no signals being observed in the NMR. After 30 minutes bromocyclophetpane (0.032 mmol) and phenylboronic acid pinacol ester (0.032 mmol) were added to the J. Young tube and mixed in by shaking. The reaction was monitored by ^{1}H NMR and after 24 hours the reaction was analyzed by quantitative GC to determine if any minor species were formed.

General procedure for precatalyst screening. In a nitrogen-filled glovebox, iron complex (0.025 mmol) was combined in a 7 mL scintillation vial with lithium ethylmethylamide (18.5 mg, 0.30 mmol) and ligand (0.025 mmol or 0.0 mmol) based on the amount relative to the metal described in the table. A stirbar was then added to the vial followed by a 0.5 mL stock solution of bromocycloheptane (46 mg, 34 µL, 0.250 mmol), phenyl boronic acid pinacol ester (102 mg, 0.500 mmol) and tetradecane (13 mg, 16.1 µL, 0.060 mmol). The resulting solution was diluted to a total volume of around 7 mL. The vial was then seal with a Teflon lined cap and the mixture was stirred for 24 hours. The reaction was then removed from the glovebox and quenched by the addition of 1 drop of water. The reaction was then dried over sodium sulfate and filtered through celite. 0.200 mL of this reaction was then diluted with dichloromethane and analyzed by quantitative GC.

General procedure for iron-catalyzed Suzuki-Miyaura cross-coupling, Procedure A: In a nitrogen-filled glovebox complex **2.12** (21 mg, 0.05 mmol), 2,2-bis((S)-4-phenyl-4,5-dihydrooxazol-2-yl)acetonitrile ligand (16.5 mg, 0.05 mmol) and lithium-ethylmethyl amide (38.5 mg, 0.6 mmol) were added to a 7 mL vial containing a stir bar. Benzene (5 mL) was added to the stirring vial followed immediately by a 1 mL benzene solution of phenylboronic acid pinacol ester (204 mg, 1.0 mmol) and alkyl halide (0.5 mmol). The reaction was stirred vigorously and after 15 minutes, a precipitate formed. After 48 hours of stirring, the reaction was brought out of the glovebox and quenched with a saturated aqueous solution of ammonium chloride (10 mL). The aqueous phase was washed with dichloromethane (3 x 40 mL) and the combined organic phases were dried over sodium sulfate and filtered. Trimethoxybenzene (42 mg, 0.25 mmol) was added as an internal standard before evaporating the solvent. A spectroscopic yield was determined by ^{1}H NMR spectroscopy before the crude product was purified by silica column chromatography.

General procedure for iron-catalyzed Suzuki-Miyaura cross-coupling, Procedure B: In a nitrogen filled glovebox, complex **2.12** (21 mg, 0.05 mmol), 2,2-bis((S)-4-phenyl-4,5-dihydrooxazol-2-yl)acetonitrile ligand (16.5 mg, 0.05 mmol) and lithium-ethylmethyl amide (38.5 mg, 0.6 mmol) were added to a 7 mL vial containing a stir bar. Benzene (5 mL) was added to the stirring vial followed immediately by a 1 mL benzene solution of phenylboronic acid pinacol ester (204 mg, 1.0 mmol) and alkyl halide (0.5 mmol). The reaction was sealed with a teflon cap and electrical tape. It was then removed from the glovebox and stirred vigorously at 50 °C. A precipitate forms on the vial wall after 10 minutes of stirring. After 48 hours, the reaction was quenched with a saturated aqueous solution of ammonium chloride (10 mL) and the aqueous phase was washed with dichloromethane (3 x 40 mL). The combined organic phases were dried over sodium sulfate and filtered. Trimethoxybenzene (42 mg, 0.25 mmol) was added as an internal standard before evaporating the solvent. A spectroscopic yield was determined by ^{1}H NMR spectroscopy before the crude product was purified by silica column chromatography.

General procedure for iron-catalyzed Suzuki-Miyaura cross-coupling, Procedure C: In a nitrogen filled glovebox, complex **2.12** (21 mg, 0.05 mmol), 2,2-bis((S)-4-phenyl-4,5-dihydrooxazol-2-yl)acetonitrile ligand (16.5 mg, 0.05 mmol) and lithium-ethylmethyl amide phenylboronic acid pinacol ester borate (161 mg, 0.6 mmol) were added to a 7 mL vial with a stir bar. Benzene (5 mL) was added to the stirring vial followed immediately by a 1 mL benzene solution of phenylboronic acid pinacol ester (82 mg, 0.4 mmol) and alkyl halide (0.5 mmol). The reaction was stirred vigorously at room temperature. After 15 minutes, a precipitate formed. After stirring 24 hours, an additional aliquot of complex **2.12** (10.5 mg, 0.025 mmol) and lithium ethylmethylamide (19.25 mg, 0.3 mmol) were added to the reaction mixture. The reaction was sealed and stirred for another 24 hours. After this time, the reaction was brought out of the

glovebox and quenched with a saturated aqueous solution of ammonium chloride (10 mL) and the aqueous phase was washed with dichloromethane (3 x 40 mL). The combined organic phases were dried over sodium sulfate and filtered. Trimethoxybenzene (42 mg, 0.25 mmol) was added as an internal standard before evaporating the solvent. A spectroscopic NMR yield was taken before the crude was purified by silica column chromatography to afford pure product. Specific column conditions are provided below for each substrate.

Cross-coupling reaction between PhB(pin) and cyclopropylmethylbromide (2.30) radical clock substrate In a nitrogen-filled glovebox complex **2.12** (21 mg, 0.05 mmol), 2,2-bis((S)-4-phenyl-4,5-dihydrooxazol-2-yl)acetonitrile ligand **2.10** (16.5 mg, 0.05 mmol) and lithium-ethylmethyl amide (38.5 mg, 0.6 mmol) were added to a 7 mL vial containing a stir bar. Benzene (5 mL) was added to the stirring vial followed immediately by a 1 mL benzene solution of phenylboronic acid pinacol ester (204 mg, 1.0 mmol) and cyclopropylmethylbromide (67 mg, 48 μL, 0.5 mmol). The reaction was stirred vigorously and after 15 minutes, a precipitate formed. After 48 hours of stirring, the reaction was brought out of the glovebox and quenched with a saturated aqueous solution of ammonium chloride (10 mL). The aqueous phase was washed with dichloromethane (3 x 40 mL) and the combined organic phases were dried over sodium sulfate and filtered. Trimethoxybenzene (42 mg, 0.25 mmol) was added as an internal standard before evaporating the solvent. A spectroscopic yield was determined by ^{1}H NMR spectroscopy before the crude product was further purified. This product was purified by silica gel flash column chromatography, eluting with 100% hexanes to afford purified product as a colorless oil (76% spectroscopic yield / 76% brsm, 55% isolated yield). $R_f = 0.80$ (100% hexane), ^{1}H NMR (500 MHz, CDCl$_3$) δ 2.36 (q, J = 7.3Hz, 2H), 2.69 (t, J = 8.2Hz, 2H), 4.99 (dd, J = 13.7, 26 Hz, 2H), 5.84 (m, 1H), 7.17 (m, 2H), 7.25 (m, 2H), 7.44 (m, 1H) ppm.

Cross-coupling reaction between PhB(pin) and 6-bromohex-1-ene (2.32) radical clock

substrate In a nitrogen-filled glovebox complex **2.12** (21 mg, 0.05 mmol), 2,2-bis((S)-4-phenyl-4,5-dihydrooxazol-2-yl)acetonitrile ligand **2.10** (16.5 mg, 0.05 mmol) and lithium-ethylmethyl amide (38.5 mg, 0.6 mmol) were added to a 7 mL vial containing a stir bar. Benzene (5 mL) was added to the stirring vial followed immediately by a 1 mL benzene solution of phenylboronic acid pinacol ester (204 mg, 1.0 mmol) and 6-bromohex-1-ene (81 mg, 67 μL, 0.5 mmol). The reaction was stirred vigorously and after 15 minutes, a precipitate formed. After 48 hours of stirring, the reaction was brought out of the glovebox and quenched with a saturated aqueous solution of ammonium chloride (10 mL). The aqueous phase was washed with dichloromethane (3 x 40 mL) and the combined organic phases were dried over sodium sulfate and filtered. Trimethoxybenzene (42 mg, 0.25 mmol) was added as an internal standard before evaporating the solvent. This reaction produced a mixture of the cyclized and uncyclized products. To verify the ratio the mixture was also analyzed by gas chromatography. R_f = 0.80 (100% hexane), ^{1}H NMR (500 MHz, CDCl$_3$) δ 2.36 (q, J = 7.3Hz, 2H), 2.69 (t, J = 8.2Hz, 2H), 4.99 (dd, J = 13.7, 26 Hz, 2H), 5.84 (m, 1H), 7.17 (m, 2H), 7.25 (m, 2H), 7.44 (m, 1H) ppm.

Procedure for borate cross-over experiments. In a nitrogen filled glovebox, a borate (0.25 mmol) was weighed out into a 7 mL scintillation vial equipped with a stirbar. To this was added a solution of the opposing boronic ester (0.250 mmol). The borate was nearly completely insoluble in both cases. To determine conversion an aliquot was taken into a J. Young tube and analyzed by boron NMR. The conversion was determined by integrating the boronic ester signals relative to one another.

Procedure for the preparation of borates. In a nitrogen filled glovebox, a solution of boronic ester (1 mmol) in THF (10 mL) was prepared. To this solution was added lithium ethyl methylamide

59

(68 mg, 1 mmol). The solvent was then removed under vacuum and the solid was used without further purification. Borate signals we in the range of 0-5 ppm by boron NMR.

Procedure for timecourse experiments. In a nitrogen-filled glovebox an iron complex (0.05 mmol), ligand (0.05 mmol) and lithium-ethylmethyl amide (19.2 mg, 0.3 mmol) were added to a 7 mL vial containing a stir bar. Benzene (5 mL) was added to the stirring vial followed immediately by a 1 mL benzene solution of phenylboronic acid pinacol ester (102 mg, 0.5 mmol), tetradecane (12.4 mg, 0.063 mmol), and bromocycloheptane (44 mg, 0.25 mmol). The reaction was stirred vigorously and after 15 minutes, a precipitate formed. Aliquots were removed at 0, 4, 8, 16, and 24 hour time points. Each aliquot was 0.5 mL and was diluted with dichloromethane before being analyzed by quantitative GC.

Substrate Scope:

Phenylcycloheptane **(2.7).** Phenylcycloheptane was synthesized from bromocycloheptane by Procedure A and purified by silica gel flash column chromatography, eluting with 100% hexanes to afford product as a colorless oil (68 mg, 85% spectroscopic yield / 85% brsm, 80% isolated yield). ^{1}H-NMR matched previously reported values.[32] R_f = 0.60 (100% hexane) ^{1}H NMR (500 MHz, CDCl$_3$): δ 1.46 – 1.78 (m, 8H), 1.80 (ddd, J = 13.4, 6.6, 3.4 Hz, 2H), 1.92 (ddt, J = 13.5, 6.6, 3.3 Hz, 2H), 2.66 (tt, J = 10.7, 3.7 Hz, 1H), 7.08 – 7.23 (m, 2H), 7.23 – 7.33 (m, 2H) ppm.
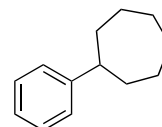
Phenyloctane **(2.13).** Phenyloctane was synthesized from octylbromide by Procedure B and purified by silica gel flash column chromatography, eluting with 100% hexanes to afford product as a colorless oil (73 mg, 85% spectroscopic yield / 91% brsm, 77% isolated yield). ^{1}H-NMR matched previously reported
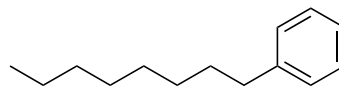
values.[32] R_f = 0.60 (100% hexane) ^{1}H NMR (500MHz, CDCl$_3$) δ 0.86 – 0.91 (m, 3H), 1.25 – 1.33 (m, 10H), 1.59 – 1.64 (m, 2H), 2.60 (t, J = 7.8 Hz, 2H), 7.18 (d, J = 7.6 Hz, 3H), 7.27 (t, J = 7.4 Hz, 2H) ppm. Phenyloctane was also synthesized from octyl chloride by Procedure B (28% spectroscopic yield / 72% brsm, 28% isolated yield) and octyl iodide by Procedure A (47% spectroscopic yield, / 91% brsm, 45% isolated yield).

Phenylcyclopentane (**2.14**). Phenylcyclopentane was synthesized from bromocyclopentane by Procedure A and purified by silica gel flash column chromatography, eluting with 100% Hexanes to afford product as a colorless oil (53 mg, 80% spectroscopic yield / 85% brsm, 73% isolated yield). ^{1}H-NMR matched previously reported values.[32] R_f = 0.60 (100% hexane) ^{1}H NMR (500MHz, CDCl$_3$) δ 1.53 – 1.74 (m, 4H), 1.75 – 1.87 (m, 2H), 1.99 – 2.14 (m, 2H), 2.99 (tt, J = 9.5, 7.4 Hz, 1H), 7.09 – 7.39 (m, 5H) ppm. Phenylcyclopentane was also synthesized from chlorocyclopentane by Procedure A (32% spectroscopic yield / 86% brsm, 32% isolated yield) and iodocyclopentane by Procedure A (45% spectroscopic yield, / 96% brsm, 45% isolated yield).
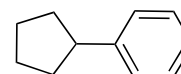
Diphenylmethane (**2.15**). Diphenylmethane was synthesized from benzyl chloride by Procedure A and purified by silica gel flash column chromatography, eluting with 100% hexanes to afford product as a colorless oil (61 mg, 79% spectroscopic yield / 79% brsm, 73% isolated yield). ^{1}H-NMR matched previously reported values.[32] R_f = 0.50 (100% hexane) ^{1}H NMR (500MHz, CDCl$_3$) δ 4.01 (s, 2H), 7.20 (s, 2H), 7.19 – 7.28 (m, 6H), 7.27 – 7.36 (m, 4H) ppm. Diphenylmethane was also synthesized from benzyl bromide (28% spectroscopic yield / 37% brsm).
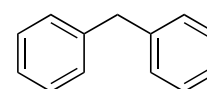
1-benzyl-4-chlorobenzene (**2.16**). 1-benzyl-4-chlorobenzene was synthesized from 4-Chlorobenzyl chloride by Procedure A and purified by
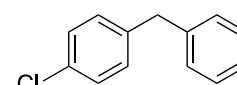
61

silica gel flash column chromatography, eluting with 100% Hexanes to afford product as a colorless oil (40 mg, 54% spectroscopic yield / 73% brsm, 40% isolated yield).^{1}H-NMR matched previously reported values.[75] R_f = 0.50 (100% hexane) ^{1}H NMR (500MHz, CDCl$_3$) δ 3.95 (s, 2H), 7.17 – 7.39 (m, 9H) ppm.

1,1-diphenylethane **(2.17).** 1,1-diphenylethane was synthesized from 1-chloroethylbenzene by Procedure C and purified by silica gel flash column chromatography, eluting with 100% Hexanes to afford product as a colorless oil (50% spectroscopic yield / 50% brsm, product isolated as a mixture with the dimer of the alkyl halide). ^{1}H-NMR matched previously reported values.[75] R_f = 0.50 (100% hexane) ^{1}H NMR (500MHz, CDCl$_3$) δ 1.66 (d, J = 7.2 Hz, 3H), 4.17 (q, J = 7.3 Hz, 1H), 7.19 (t, J = 7.2 Hz, 2H), 7.22 – 7.25 (m, 4H), 7.29 (t, J = 7.6 Hz, 4H) ppm.
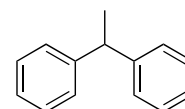
1,3-diphenylpropene **(2.18).** 1,3-diphenylpropene was synthesized from 3-chloropropenylbenzene by Procedure A and purified by silica gel flash column chromatography, eluting with 100% Hexanes to afford product as a colorless oil (58 mg, 61% spectroscopic yield / 61% brsm, 60% isolated yield). ^{1}H-NMR matched previously reported values.[32] R_f = 0.20 (100% hexane) ^{1}H NMR (500MHz, CDCl$_3$) δ 3.56 (d, J = 6.7 Hz, 2H), 6.36 (dt, J = 15.8, 6.9 Hz, 1H), 6.46 (d, J = 15.8 Hz, 1H), 7.15 – 7.39 (m, 10H) ppm.
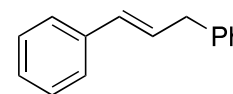
3-Phenylpropoxy-tert-butyldimethylsilane **(2.19).** 3-Phenylprop oxy-tert-butyldimethylsilane was synthesized from 3-bromopropoxy-tert-butyldimethylsilane by Procedure B and purified by silica gel flash column chromatography, eluting with 100% Hexanes to afford product as a colorless oil (75 mg, 65% spectroscopic yield / 81% brsm, 60% isolated yield). ^{1}H-NMR matched previously reported values.[76] R_f = 0.15 (100%
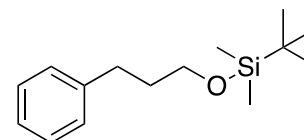
pentane) [^1]H NMR (500MHz, CDCl$_3$) δ 0.5 (s, 6H), 0.91 (s, 9H), 1.79 – 1.89 (m, 2H), 2.64 – 2.71 (m, 2H), 3.64 (t, J = 6.3 Hz, 2H), 3.64 (t, J = 5.7 Hz, 2H), 7.14 – 7.22 (m, 3H), 7.27 (m, 2H) ppm.

4-phenylpiperidine-1-carboxylic acid benzyl ester **(2.20).** 4-phenylpiperidine-1-carboxylic acid benzyl ester was synthesized from 4-bromopiperidine-1-carboxylic acid benzyl ester by Procedure B and purified by silica gel flash column chromatography, eluting with 1:5 EtOAc/Hexanes to afford product as a colorless oil (83 mg, 70% spectroscopic yield / 96% brsm, 56% isolated yield). [^1]H-NMR matched previously reported values.[77] R$_f$ = 0.20 (1:5 EtOAc/hexane) [^1]H NMR (500MHz, CDCl$_3$) δ 1.56 – 1.72 (m, 2H), 1.85 (d, J = 12.7 Hz, 2H), 2.67 (tt, J = 12.2, 3.6 Hz, 1H), 2.89 (t, J = 12.9 Hz, 2H), 4.32 (s, 2H), 5.16 (s, 2H), 7.17 – 7.25 (m, 3H), 7.26 – 7.42 (m, 7H) ppm.
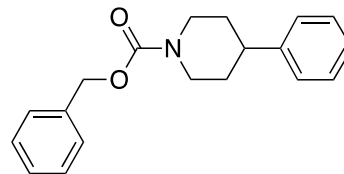
Adamantylbenzene **(2.21).** Adamantylbenzene was synthesized from chloroadamantane by Procedure A, using phenylboronic acid pinacol ester. The yield of this compound was determined by GC because it is formed as a mixture with chloroadamantane which coelutes with from silica gel (23% spectroscopic yield).
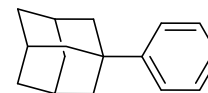
tert-butylbenzene **(2.22).** Tert-butylbenzene was synthesized from 2-chloro-2-methyl- propane by Procedure A, using phenylboronic acid pinacol ester. Product was purified by silica gel flash column chromatography, eluting with 100% Hexanes to afford purified product as a colorless oil (14 mg, 23% spectroscopic yield /21% isolated yield). [^1]H-NMR matched previously reported values.[78] R$_f$ = 0.60 (100% hexane) [^1]H NMR (400 MHz, CDCl$_3$) δ 7.84 – 7.79 (m, 2H), 7.49 – 7.44 (m, 1H), 7.40 – 7.34 (m, 2H), 1.35 (s, 9H).
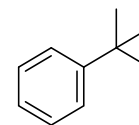
63

2-cycloheptylnaphthalene **(2.23).** 2-cycloheptylnaphthalene was synthesized from bromocycloheptane by Procedure A, using naphthalene-2-boronic acid pinacol ester in place of phenylboronic acid pinacol ester. Product was purified by silica gel flash column chromatography, eluting with 100% Hexanes to afford purified product as a white crystalline (85 mg, 84% spectroscopic yield /84% brsm**,** 76% isolated yield). ^{1}H-NMR matched previously reported values.[79] R_f= 0.45 (100% hexane) ^{1}H NMR (500 MHz, CDCl$_3$) δ = 1.85-1.58 (m, 10H), 2.01-1.98, (m, 2H), 2.86-2.81 (m, 1H), 7.44-7.45 (m, 3H), 7.61 (s, 1H), 7.79-7.75(m, 3H) ppm.
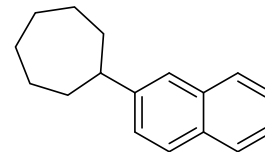
p-tolylcycloheptane **(2.24).** *p*-tolylcycloheptane was synthesized from bromocycloheptane by Procedure B using *p*-tolylboronic acid pinacol ester in place of phenylboronic acid pinacol ester. Product was purified by silica gel flash column chromatography, eluting with 30% EtOAc in Hexane to afford purified product as a colorless oil (48 mg, 51% spectroscopic yield / 56% brsm**,** 51% isolated yield). ^{1}H-NMR matched previously reported values.[80] R_f= 0.70 (100% hexane) ^{1}H NMR (400 MHz, CDCl$_3$) δ = 1.67-1.55 (m, 8H),1.82-1.73 (2H), 1.93-1.84 (m, 2H), 2.31 (s, 3H), 2.66-2.58 (m, 1H), 7.08 (s, 4H) ppm.
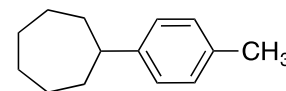
(4-methoxyphenyl)cycloheptane **(2.25)**. (4-methoxyphenyl)cyclo heptane was synthesized from bromocycloheptane by Procedure C using (4-methoxyphenyl) boronic acid pinacol ester in place of phenylboronic acid pinacol ester. Product was purified by silica gel flash column chromatography, eluting with 30% EtOAc in Hexane to afford purified product as a colorless oil (69 mg, 68% spectroscopic yield / 100% brsm, 68% isolated yield). ^{1}H-NMR matched previously reported values.[32] R_f= 0.60 (10% EtOAc in hexane) ^{1}H NMR (500 MHz, CDCl$_3$) δ = 1.65-1.49 (m, 6H), 1.72-1.65 (m, 2H), 1.82-1.73 (m, 2H), 1.93-1.83 (m, 2H), 2.66-2.57 (m, 1H), 3.78 (s, 3H), 6.83-6.81 (m, 2H), 7.12-7.10 (m, 2H) ppm.
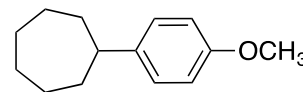
64

(4-trifluoromethyl)phenyl)cycloheptane **(2.26).** (4-trifluoromethyl) phenyl)cycloheptane was synthesized from bromocycloheptane by Procedure B, using (4-trifluoromethyl)phenyl) boronic acid pinacol ester in place of phenylboronic acid pinacol ester. Product was purified by silica gel flash column chromatography, eluting with 100% hexanes to afford purified product as a white crystalline solid (57 mg, 47% spectroscopic yield / 87% brsm, 47% isolated yield). ^{1}H-NMR matched previously reported values.[32] R_f = 0.50 (100% hexane), ^{1}H NMR (500 MHz, CDCl$_3$) δ 1.64 (m, 8H), 1.82 (s, 2H), 1.94 – 1.86 (m, 2H), 2.72 (tt, 1H), 7.52 (d, J = 8.0 Hz, 2H) ppm.
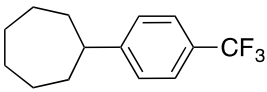
(3-trifluoromethyl)phenyl)cycloheptane **(2.27)** (3-trifluoromethyl) phenyl)cycloheptane was synthesized from bromocycloheptane by Procedure B, using (3-trifluoromethyl)phenyl) boronic acid pinacol ester in place of phenylboronic acid pinacol ester. Product was purified by silica gel flash column chromatography, eluting with 100% hexanes to afford purified product as a white crystalline solid (81 mg, 67% spectroscopic yield / 76% brsm, 67% isolated yield). R_f = 0.80 (100% hexane), ^{1}H NMR (500 MHz, CDCl$_3$) δ 1.75 – 1.62, 1.82 (s, 2H), 1.90 (d, J = 15.6 Hz, 2H), 2.74 (m, 1H), 7.48 (t, J = 7.7 Hz, 2H), 7.70 (d, J = 7.9 Hz, 1H), 7.97 (d, J = 7.5 Hz, 1H) ppm. {^{1}H}^{13}C NMR (125 MHz, CDCl$_3$) δ 27.1 (s), 27.8 (s), 36.7 (s), 46.9 (s), 122.4 (q, J = 3.9 Hz), 123.4 (q, J = 3.8 Hz), 124.3 (q, J = 270.6 Hz), 128.6 (s), 130.1 (q, J = 1.4 Hz), 130.5 (q, J = 31.4 Hz), 150.7 (s) ppm. ^{19}F NMR (470 MHz, CDCl$_3$) δ -62.1 (s) ppm. IR: 2922, 1446, 1327, 1158, 1121, 1073, 796, 702, 664 cm^{-1}. HRMS (ESI) *m/z* [M]$^+$ calcd. For C$_{14}$H17F$_3$ 242.12769; found 242.12858.
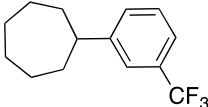
(E)-styrenylcycloheptane **(2.28).** (E)-styrenylcycloheptane was synthesized from bromocycloheptane by Procedure A using (E)-styrenyl boronic acid pinacol ester in place of phenylboronic acid pinacol ester.

65
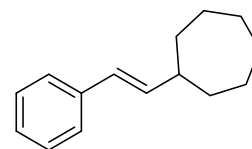
Product was purified by silica gel flash column chromatography, eluting with pure Hexane to afford purified product as a colorless oil (25 mg, 27% spectroscopic yield / 25% brsm, 25% isolated yield). ^{1}H-NMR matched previously reported values.[81] R_f = 0.80 (100% hexane), ^{1}H NMR (400 MHz, CDCl$_3$) δ 1.39-1.75 (m, 10H), 1.79-1.86 (m, 2H), 2.33 (m, 1H), 6.22 (dd, J = 15.9, 7.6 Hz, 1H), 6.32 (d, J = 15.9 Hz, 1H), 7.18 (t, J = 7.2 Hz, 1H), 7.28 (t, J = 7.6 Hz, 2H), 7.34 (d, J = 7.6 Hz, 2H).

Cross-coupling reaction between PhB(pin) and cyclopropylmethylbromide (2.30). In a nitrogen-filled glovebox complex **2.12** (21 mg, 0.05 mmol), 2,2-bis((S)-4-phenyl-4,5-dihydrooxazol-2-yl)acetonitrile ligand (16.5 mg, 0.05 mmol) and lithium-ethylmethyl amide (38.5 mg, 0.6 mmol) were added to a 7 mL vial containing a stir bar. Benzene (5 mL) was added to the stirring vial followed immediately by a 1 mL benzene solution of phenylboronic acid pinacol ester (204 mg, 1.0 mmol) and cyclopropylmethylbromide (67 mg, 48 µL, 0.5 mmol). The reaction was stirred vigorously and after 15 minutes, a precipitate formed. After 48 hours of stirring, the reaction was brought out of the glovebox and quenched with a saturated aqueous solution of ammonium chloride (10 mL). The aqueous phase was washed with dichloromethane (3 x 40 mL) and the combined organic phases were dried over sodium sulfate and filtered. Trimethoxybenzene (42 mg, 0.25 mmol) was added as an internal standard before evaporating the solvent. A spectroscopic yield was determined by ^{1}H NMR spectroscopy using trimethoxy benzene as an internal standard. (76% spectroscopic yield)[32] The product was volatile which complicated isolation. ^{1}H NMR (500 MHz, CDCl$_3$) δ 2.36 (q, J = 7.3 Hz, 2H), 2.69 (t, J = 8.2 Hz, 2H), 4.99 (dd, J = 13.7, 26 Hz, 2H), 5.84 (m, 1H), 7.17 (m, 2H), 7.25 (m, 2H), 7.44 (m, 1H) ppm.

Cross-coupling reaction between PhB(pin) and 6-bromohex-1-ene (2.32). In a nitrogen-filled glovebox complex **2.12** (21 mg, 0.05 mmol), 2,2-bis((S)-4-phenyl-4,5-dihydrooxazol-2-

66

yl)acetonitrile ligand (16.5 mg, 0.05 mmol) and lithium-ethylmethyl amide (38.5 mg, 0.6 mmol) were added to a 7 mL vial containing a stir bar. Benzene (5 mL) was added to the stirring vial followed immediately by a 1 mL benzene solution of phenylboronic acid pinacol ester (204 mg, 1.0 mmol) and 6-bromohex-1-ene (81 mg, 67 µL, 0.5 mmol). The reaction was stirred vigorously and after 15 minutes, a precipitate formed. After 48 hours of stirring, the reaction was brought out of the glovebox and quenched with a saturated aqueous solution of ammonium chloride (10 mL). The aqueous phase was washed with dichloromethane (3 x 40 mL) and the combined organic phases were dried over sodium sulfate and filtered. Trimethoxybenzene (42 mg, 0.25 mmol) was added as an internal standard before evaporating the solvent. This reaction produced a mixture of the cyclized and uncyclized products. To verify the ratio the mixture was also analyzed by gas chromatography as well as the relative integration of the alkene peaks to the overlapping benzylic peaks by NMR. The ratio is between 1.25:1 (GC) and 1.56:1 (NMR) for cyclized to uncyclized products. Hex-5-enylbenzene(**2.33**)[82] - R_f = 0.60 (100% hexane). ^{1}H NMR (500 MHz, CDCl$_3$) δ 1.45 (m, 2H), 1.65 (m, 2H), 2.10 (m, 2H), 2.62 (t, J = 7.5 Hz, 2H), 5.00 (dd, J = 13.7, 26 Hz, 2H), 5.81 (ddt, J = 16.9, 10.1, 6.7 Hz, 1H), 7.18 (m, 3H), 7.26 (m, 2H) ppm. Cyclopentylmethylbenzene(**2.33'**)[83] R_f = 0.60 (100% hexane). ^{1}H NMR (500 MHz, CDCl$_3$) δ 1.21 (m, 2H), 1.53 (m, 2H), 1.65 (m, 2H) 1.71 (m, 2H) 2.10 (m, 1H) 2.6 (d, J = 7.5 Hz, 2H), 7.18 (m, 3H), 7.26 (m, 2H) ppm.

Cross-coupling reaction between Phenyl boronic acid neopentyl glycol ester (2.37) and cycloheptyl bromide. In a nitrogen-filled glovebox complex **2.12** (21 mg, 0.05 mmol), 2,2-bis((S)-4-phenyl-4,5-dihydrooxazol-2-yl)acetonitrile ligand (16.5 mg, 0.05 mmol) and lithium-ethylmethyl amide (38.5 mg, 0.6 mmol) were added to a 7 mL vial containing a stir bar. Benzene (5 mL) was added to the stirring vial followed immediately by a 1 mL benzene solution of

67

phenylboronic acid neopentyl glycol ester (190 mg, 1.0 mmol), tetradecane (25 mg, 32 μL, 0.125 mmol) and bromocycloheptane (88 mg, 68 μL, 0.5 mmol). The reaction was stirred vigorously and after 5 minutes, a precipitate formed. After 48 hours of stirring, the reaction was brought out of the glovebox and quenched with a drop of water, dried with sodium sulfate, and filtered through celite. The mixture was then analyzed by GC using an achiral column with tetradecane as the internal standard. Phenylcycloheptane was formed in 5% yield.

Synthesis of 1-(3-chloropropyl)-3-(trifluoromethyl)benzene (2.43). In a nitrogen filled glovebox, complex **2.12** (84 mg, 0.20 mmol), cyano-phenyl-bisoxazoline ligand (66 mg, 0.20 mmol) and lithium-ethylmethyl amide (156 mg, 2.40 mmol) were added to a 20 mL vial containing a stir bar. Benzene (15 mL) was added to the stirring vial followed immediately by a 5 mL benzene solution of *m*-trifluoromethylboronic acid pinacol ester (**2.42**, 1.09 g, 4.00 mmol) and 1-bromo-3-chloropropane (**2.41**, 197 μL, 314 mg, 2.00 mmol). The vial was sealed using electrical tape before being brought outside the glovebox. The reaction was stirred vigorously at 50 °C. A precipitate formed on the vial wall after 10 minutes of stirring. After 48 hours, the reaction was quenched with a saturated aqueous solution of ammonium chloride (10 mL) and the aqueous phase was washed with dichloromethane (3 x 40 mL). The combined organic phases were dried over sodium sulfate and filtered. Trimethoxybenzene (42 mg, 0.25 mmol) was added as an internal standard before evaporating the solvent. A spectroscopic yield of 60% was determined by ^{1}H NMR spectroscopy before the crude product was purified by silica gel flash column chromatography, eluting with hexanes to afford the product (R_f = 0.50), which was then further isolated from the bisarylated product (although it doesn't affect the subsequent reaction) through distillation (R_f = 0.50). The product was obtained as a colorless oil (244.9 mg, 55%). IR (neat): 2958, 2866, 2360, 1449, 1325, 1161, 1095, 1072, 900, 799, 701, 658

cm^{-1}; ^{1}H NMR (400 MHz, CDCl$_3$): δ 2.04 – 2.14 (m, 2H), 2.85 (t, J = 7.5 Hz, 2H), 3.53 (t, J = 6.3 Hz, 2H), 7.37 – 7.49 (m, 4H); {^{1}H}^{13}C NMR (125 MHz, CDCl$_3$): δ 32.55, 33.71, 43.88, 123.08 (q, ^3J = 3.9 Hz), 124.10 (q, ^1J = 272.43 Hz), 125.17 (q, ^3J = 3.9 Hz), 128.9, 130.81 (q, ^2J =32.41 Hz), 131.93, 141.59. ^{19}F NMR (470 MHz, CDCl$_3$): δ -62.56 ppm. HRMS (ESI) m/z [M]$^+$ calcd. For C$_{10}$H$_{10}$F$_3$Cl 222.64; found 222.04.

Synthesis of Cinacalcet. To a 20 mL Schlenk tube was added alkyl chloride (240 mg, 1.08 mmol), present as a mixture of **2.43** and bisarylated product, potassium iodide (40 mg, 0.24 mmol) and potassium carbonate (331 mg, 2.40 mmol). On a Schlenk line, the Schlenk tube was evacuated and backfilled with nitrogen and then (*R*)-(+)-1-(1-naphthyl)ethylamine (**2.44**, 231 μL, 246 mg, 1.44 mmol) was added by syringe after addition of anhydrous acetonitrile (4 mL). The flask was sealed and then heated to 100 °C for 48 hours. At this time, the reaction was cooled, the insoluble material was filtered, and the solvent evaporated to yield a brown oil. The crude product was dissolved in dichloromethane (20 mL), washed with 5% aqueous hydrochloric acid (25 mL), saturated sodium bicarbonate solution (25 mL), and deionized water (25 mL). The combined organic phases were dried over sodium sulfate, filtered, and the solvent was removed under reduced pressure. The product was isolated as a pure colorless oil[84] (270 mg, 70%). ^{1}H-NMR matched previously reported values.[15] R$_f$ = 0.30 (1:1 EtOAc/hexane), ^{1}H NMR (400 MHz, CDCl$_3$): δ 1.36 (bs, 1H), 1.49 (d, J = 6.6 Hz, 3H), 1.84 (tt, J = 7.4 Hz, 2H), 2.55 – 2.79 (m, 4H), 4.62 (q, J = 6.6 Hz, 1H), 7.28 – 7.38 (m, 2H), 7.39 – 7.55 (m, 5H), 7.61 – 7.67 (m, 1H), 7.75 (d, J = 8.1 Hz, 1H), 7.88 (dd, J = 7.6, 1.7 Hz, 1H), 8.17 – 8.22 (m, 1H). ^{13}C NMR (500 MHz, CDCl$_3$) δ 23.56, 31.83, 33.37, 47.23, 53.73, 122.58 (q, ^3J = 4.3 Hz), 122.62, 122.88, 124.24 (q, ^1J = 274.33 Hz), 124.99 (q, ^3J = 3.7 Hz), 125.27, 125.64,
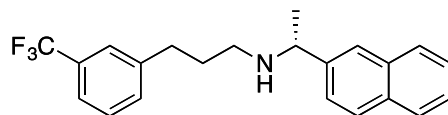
125.72, 127.15, 128.6, 128.94, 130.52 (q, ^2J = 31.9 Hz), 131.3, 131.72, 133.95, 141.17, 143.04.

HRMS (ESI) m/z [M]$^+$ calcd. For $C_{22}H_{22}F_3N$ 357.41; found 357.18. α_{589}^{24} (c = 1.0, CHCl$_3$) = +21.8$^°$

2.9 References

1.   Jana, R.; Pathak, T. P.; Sigman, M. S., Advances in Transition Metal (Pd,Ni,Fe)-Catalyzed Cross-Coupling Reactions Using Alkyl-organometallics as Reaction Partners. *Chemical Reviews* **2011,** *111* (3), 1417-1492.
2.   Brown, D. G.; Boström, J., Analysis of Past and Present Synthetic Methodologies on Medicinal Chemistry: Where Have All the New Reactions Gone? *Journal of Medicinal Chemistry* **2016,** *59* (10), 4443-4458.
3.   Miyaura, N.; Yamada, K.; Suzuki, A., A new stereospecific cross-coupling by the palladium-catalyzed reaction of 1-alkenylboranes with 1-alkenyl or 1-alkynyl halides. *Tetrahedron Letters* **1979,** *20* (36), 3437-3440.
4.   Miyaura, N.; Yamamoto, Y., 9.05 - Boron. In *Comprehensive Organometallic Chemistry III*, Mingos, D. M. P.; Crabtree, R. H., Eds. Elsevier: Oxford, 2007; pp 145-244.
5.   Martin, R.; Buchwald, S. L., Palladium-Catalyzed Suzuki−Miyaura Cross-Coupling Reactions Employing Dialkylbiaryl Phosphine Ligands. *Accounts of Chemical Research* **2008,** *41* (11), 1461-1473.
6.   Hall, D. G., Structure, Properties, and Preparation of Boronic Acid Derivatives. In *Boronic Acids*, Wiley-VCH Verlag GmbH & Co. KGaA: 2011; pp 1-133.
7.   Liu, T. Z.; Lee, S. D.; Bhatnagar, R. S., Toxicity of palladium. *Toxicology Letters* **1979,** *4* (6), 469-473.
8.   Netherton, M. R.; Fu, G. C., Suzuki Cross-Coupling of Alkyl Tosylates that Posess b Hydrogen Atoms: Synthetic and Mechanistic Studies. *Angewandte Chemie International Edition* **2002,** *41* (20), 3910-3912.
9.   Han, C.; Buchwald, S. L., Negishi Coupling of Secondary Alkylzinc Halides with Aryl Bromides and Chlorides. *Journal of the American Chemical Society* **2009,** *131*, 7532-7533.
10.   Netherton, M. R.; Dai, C.; Neuschutz, K.; Fu, G. C., Room-Temperature Alkyl-Alkyl Suzuki Cross-Coupling of Alkyl Bromides that Possess b-Hydrogens. *Journal of the American Chemical Society* **2001,** *123*, 10099-10100.
11.   Kirchhoff, J. H.; Dai, C.; Fu, G. C., A Method for Palladium-Catalyzed Cross-Coupling of Simple Alkyl Chlorides: Suzuki Reactions Catalyzed by [Pd2(dba)3]/PCy3. *Angewandte Chemie International Edition* **2002,** *41* (11), 1945-1947.
12.   Tang, H.; Menzel, K.; Fu, G. C., Ligands for Palladium-Catalyzed Cross-Couplings of Alkyl Halides: Use of an Alkyldiaminophosphane Expands the Scope of the Stille Reaction. *Angewandte Chemie International Edition 2003*, 5079-5082.
13.   Choi, J.; Fu, G. C., Transition metal-catalyzed alkyl-alkyl bond formation: Another dimension in cross-coupling chemistry. *Science* **2017,** *356*, eaaf7230.
14.   Lundin, P. M.; Fu, G. C., Asymmetric Suzuki Cross-Couplings of Activated Secondary Alkyl Electrophiles: Arylations of Racemic α-Chloroamides. *Journal of the American Chemical Society* **2010,** *132* (32), 11027-11029.

15.   Owston, N. A.; Fu, G. C., Asymmetric Alkyl-Alkyl Cross-Couplings of Unactivated Secondary Alkyl

Electrophiles: Stereoconvergent Suzuki Reactions of Racemic Acylated Halohydrins. *Journal of American Chemical Society* **2010,** *132*, 11908-11909.

16.   Mako, T. L.; Byers, J. A., Recent advances in iron-catalysed cross coupling reactions and their mechanistic underpinning. *Inorganic Chemistry Frontiers* **2016,** *3*, 766-790.

17.   Martin, R.; Furstner, A., Cross-Coupling of Alkyl Halides with Allyl Grignard Reagents catalyzed by a Low-Valent Iron Complex. *Angewandte Chemie, International Edition in English* **2004,** *43*, 3955-3957.

18.   Hashimoto, T.; Hatakeyama, T.; Nakamura, M., Stereospecific Cross-Coupling between Alkenylboronates and Alkyl Halides Catalyzed by Iron−Bisphosphine Complexes. *Journal of Organic Chemistry* **2012,** *77*, 1168-1173.

19.   Hatakeyama, T.; Hashimoto, T.; Kondo, Y.; Fujiwara, Y.; Seike, H.; Takaya, H.; Tamada, Y.; Ono, T.; Nakamura, M., Iron-Catalyzed Suzuki-Miyaura Coupling of Alkyl Halides. *Journal of the American Chemical Society* **2010,** *132*, 10674-10676.

20.   Ghorai, S. K.; Jin, M.; Hatakeyama, T.; Nakamura, M., Cross-Coupling of Non-activated Chloroalkanes with Aryl Grignard Reagents in the Presence of Iron/N-Heterocyclic Carbene Catalysts. *Organic Letters* **2012,** *14* (4), 1066-1069.

21.   Nakamura, M.; Matsuo, K.; Ito, S.; Nakamura, E., Iron-Catalyzed Cross-Coupling of Primary and Secondary Alkyl Halides with Aryl Grignard Reagents. *Journal of the American Chemical Society* **2004,** *126*, 3686-3687.

22.   Hatakeyama, T.; Fujiwara, Y.; Okada, Y.; Itoh, T.; Hashimoto, T.; Kawamura, S.; Ogata, K.; Takaya, H.; Nakamura, M., KumadaTamaoCorriu Coupling of Alkyl Halides Catalyzed by an IronBisphosphine Complex. *Chemistry Letters* **2011,** *40*, 1030-1032.

23.   Bedford, R. B.; Hall, M. A.; Hodges, G. R.; Huwe, M.; Wilkinson, M. C., Simple mixed Fe–Zn catalysts for the Suzuki couplings of tetraarylborates with benzyl halides and 2-halopyridinesw. *Chemical Communication* **2009**, 6430-6432.

24.   Bedford, R. B.; Carter, E.; Cogswell, P. M.; Gower, N. J.; Haddow, M. F.; Harvey, J. N.; Murphy, D. M.; Neeve, E. C.; Nunn, J., Simplifying Iron-Phosphine Catalysts for Cross-Coupling Reactions. *Angewandte Chemie, International Edition* **2013,** *52*, 1285-1288.

25.   Hedström, A.; Izakian, Z.; Vreto, I.; Wallentin, C.-J.; Norrby, P.-O., On the Radical Nature of Iron-Catalyzed Cross-Coupling Reactions. *Chemistry – A European Journal* **2015,** *21* (15), 5946-5953.

26.   Guisan-Ceinos, M.; Tato, F.; Bunuel, E.; Calle, P.; Cardenas, D. J., Fe-catalysed Kumada-type alkyl-alkyl cross-coupling. Evidence for the intermediacy of Fe(i) complexes. *Chemical Science* **2013,** *4* (3), 1098-1104.

27.   Gärtner, D.; Stein, A. L.; Grupe, S.; Arp, J.; Jacobi von Wangelin, A., Iron-Catalyzed Cross-Coupling of Alkenyl Acetates. *Angewandte Chemie International Edition* **2015,** *54* (36), 10545-10549.

28.   Ysart, G.; Miller, P.; Crews, H.; Robb, P.; Baxter, M.; L'Argy, C. D.; Lofthouse, S.; Sargent, C.; Harrison, N., Dietary exposure estimates of 30 elements from the UK Total Diet Study. *Food Additives & Contaminants* **1999,** *16* (9), 391-403.

29.   Fürstner, A.; Leitner, A.; Méndez, M.; Krause, H., Iron-Catalyzed Cross-Coupling Reactions. *Journal of the American Chemical Society* **2002,** *124* (46), 13856-13863.

30.   Mako, T. L.; Byers, J. A., Recent advances in iron-catalysed cross coupling reactions and their mechanistic underpinning. *Inorganic Chemistry Frontiers* **2016,** *3* (6), 766-790.

31.   Hatakeyama, T.; Hashimoto, T.; Kondo, Y.; Fujiwara, Y.; Seike, H.; Takaya, H.; Tamada, Y.; Ono, T.; Nakamura, M., Iron-Catalyzed Suzuki−Miyaura Coupling of Alkyl Halides. *Journal of the American Chemical Society* **2010,** *132* (31), 10674-10676.

32.   Bedford, R. B.; Brenner, P. B.; Carter, E.; Carvell, T. W.; Cogswell, P. M.; Gallagher, T.; Harvey, J. N.; Murphy, D. M.; Neeve, E. C.; Nunn, J.; Pye, D. R., Expedient Iron-Catalyzed Coupling of Alkyl, Benzyl and Allyl Halides with Arylboronic Esters. *Chemistry – A European Journal* **2014,** *20* (26), 7935-7938.

33.   Smith, M. B.; Becker, W. E., The constitution of the grignard reagent—II: The reaction between R2Mg and MgX2 in ether. *Tetrahedron* **1966,** *22* (9), 3027-3036.

34.   Dunsford, J. J.; Clark, E. R.; Ingleson, M. J., Highly nucleophilic dipropanolamine chelated boron reagents for aryl-transmetallation to iron complexes. *Dalton Transactions* **2015,** *44* (47), 20577-20583.

35.   This mechanism is only one of several that have been proposed in the literature. All proposed mechanisms have similar transmetalation steps.

36.   Miyaura, N., Cross-coupling reaction of organoboron compounds via base-assisted transmetalation to palladium(II) complexes. *Journal of Organometallic Chemistry* **2002,** *653* (1), 54-57.

37.   Carrow, B. P.; Hartwig, J. F., Distinguishing Between Pathways for Transmetalation in Suzuki−Miyaura Reactions. *Journal of the American Chemical Society* **2011,** *133* (7), 2116-2119.

38.   Thomas, A. A.; Denmark, S. E., Pre-transmetalation intermediates in the Suzuki-Miyaura reaction revealed: The missing link. *Science* **2016,** *352* (6283), 329-332.

39.   Driver, M. S.; Hartwig, J. F., Energetics and Mechanism of Alkylamine N−H Bond Cleavage by Palladium Hydroxides: N−H Activation by Unusual Acid−Base Chemistry. *Organometallics* **1997,** *16* (26), 5706-5715.

40.   Schmidbaur, H.; Schmidt, M., Ferrosiloxanes and Ferrosiliconate Anions. *Journal of the American Chemical Society* **1962,** *84* (18), 3600-3601.

41.   Adams, R.; Martin, R.; Winter, G., Magnetism, electronic spectra, and structure of transition metal alkoxides. II. The preparation and magnetism of iron(III) alkoxides. *Australian Journal of Chemistry* **1966,** *19* (3), 363-371.

42.   Bochmann, M.; Wilkinson, G.; Young, G. B.; Hursthouse, M. B.; Malik, K. M. A., Preparation and properties of 1-adamantoxides, 2-adamantoxides, and 1-adamantylmethoxides of Ti, V, Nb, Nb, Cr, Cr, Mo, Mn, Fe, and Co. The crystal and molecular structure of tetrakis(1-adamantoxo)dimethylaminemolybdenum(IV). *Journal of the Chemical Society, Dalton Transactions* **1980,** (6), 901-910.

43.   Biernesser, A. B.; Li, B.; Byers, J. A., Redox controlled polymerization of lactide catalyzed by bis(imino)pyridine iron bis(alkoxide) complexes. *Journal of the American Chemical Society* **2013,** *135* (135), 16553-16560.

44.   Schlenk, W.; Schlenk, W., Über die Konstitution der Grignardschen Magnesiumverbindungen. *Berichte der deutschen chemischen Gesellschaft (A and B Series)* **1929,** *62* (4), 920-924.

45.   Hedstrom, A.; Izakian, Z.; Vreto, I.; Wallentin, C.-J.; Norrby, O., On the Radical Nature of Iron-Catalyzed Cross-Coupling Reactions. *Chemistry, A European Journal* **2015,** *21*, 5946-5953.

46.   Bedford, R. B.; Brenner, P. B.; Carter, E.; Carvell, T. W.; Cogswell, P. M.; Gallagher, T.; Harvey, J. N.; Murphy, D. M.; Neeve, E. C.; Nunn, J.; Pye, D., Expedient Iron-Catalyzed

Coupling of Alkyl, Benzyl and Allyl Halides with Arylboronic Esters. *Chemistry, A European Journal* **2014**, *20*, 7935-7938.

47.   Audran, G.; Brémond, P.; Marque, S. R. A.; Siri, D.; Santelli, M., Calculated linear free energy relationships in the course of the Suzuki–Miyaura coupling reaction. *Tetrahedron* **2014**, *70* (13), 2272-2279.

48.   Yuriev, E.; Agostino, M.; Ramsland, P. A., Challenges and advances in computational docking: 2009 in review. *Journal of Molecular Recognition* **2011**, *24* (2), 149-164.

49.   Hoyt, J. M.; Shevlin, M.; Margulieux, G. W.; Krska, S. W.; Tudge, M. T.; Chirik, P. J., Synthesis and Hydrogenation Activity of Iron Dialkyl Complexes with Chiral Bidentate Phosphines. *Organometallics* **2014**, *33* (20), 5781-5790.

50.   Peterson, P. O.; Rummelt, S. M.; Wile, B. M.; Stieber, S. C. E.; Zhong, H.; Chirik, P. J., Direct Observation of Transmetalation from a Neutral Boronate Ester to a Pyridine(diimine) Iron Alkoxide. *Organometallics* **2020**, *39* (1), 201-205.

51.   Eckert, N. A.; Smith, J. M.; Lachicotte, R. J.; Holland, P. L., Low-Coordinate Iron(II) Amido Complexes of β-Diketiminates: Synthesis, Structure, and Reactivity. *Inorganic Chemistry* **2004**, *43* (10), 3306-3321.

52.   Ghosh, A. K.; Mathivanan, P.; Cappiello, J., C2-Symmetric chiral bis(oxazoline)–metal complexes in catalytic asymmetric synthesis1Dedicated to Professor E. J. Corey with deep respect and sincere appreciation.1. *Tetrahedron: Asymmetry* **1998**, *9* (1), 1-45.

53.   Lou, S.; Fu, G. C., Nickel/Bis(oxazoline)-Catalyzed Asymmetric Kumada Reactions of Alkyl Electrophiles: Cross-Couplings of Racemic α-Bromoketones. *Journal of the American Chemical Society* **2010**, *132* (4), 1264-1266.

54.   Neely, J. M.; Bezdek, M. J.; Chirik, P. J., Insight into Transmetalation Enables Cobalt-Catalyzed Suzuki–Miyaura Cross Coupling. *ACS Central Science* **2016**, *2* (12), 935-942.

55.   Ackerman, L. K. G.; Anka-Lufford, L. L.; Naodovic, M.; Weix, D. J., Cobalt co-catalysis for cross-electrophile coupling: diarylmethanes from benzyl mesylates and aryl halides. *Chemical Science* **2015**, *6* (2), 1115-1119.

56.   Miyaura, N.; Suzuki, A., Palladium-Catalyzed Cross-Coupling Reactions of Organoboron Compounds. *Chem. Rev.* **1995**, *95* (7), 2457-2483.

57.   Diafuku, S. L.; Al-Afyouni, M. H.; Snyder, B. E. R.; Kneebone, J. L.; Neidig, M. L., A Combined Mössbauer, Magnetic Circular Dichroism, and Density Functional Theory Approach for Iron Cross-Coupling Catalysis: Electronic Structure, In Situ Formation, and Reactivity of Iron-Mesityl-Bisphosphines. *Journal of the American Chemical Society* **2014**, *136*, 9132-9143.

58.   Daifuku, S. L.; Kneebone, J. L.; Snyder, B. E. R.; Neidig, M. L., Iron(II) Active Species in Iron−Bisphosphine Catalyzed Kumada and Suzuki−Miyaura Cross-Couplings of Phenyl Nucleophiles and Secondary Alkyl Halides. *Journal of the American Chemical Society* **2015**, *137*, 11432-11444.

59.   Creutz, S. E.; Lotito, K. J.; Fu, G. C.; Peters, J. C., Photoinduced Ullmann C–N Coupling: Demonstrating the Viability of a Radical Pathway. *Science* **2012**, *338* (6107), 647-651.

60.   Nolin, K. A.; Ahn, R. W.; Kobayashi, Y.; Kennedy-Smith, J. J.; Toste, F. D., Enantioselective Reduction of Ketones and Imines Catalyzed by (CN-Box)ReV–Oxo Complexes. *Chemistry – A European Journal* **2010**, *16* (31), 9555-9562.

61.   Torres, P. U., Cinacalcet HCl: A Novel Treatment for Secondary Hyperparathyroidism Caused by Chronic Kidney Disease. *Journal of Renal Nutrition* **2006**, *16* (3), 253-258.

62.   Lei, F.; Qu, B.; Li, X.; Guo, L.; Guan, M.; Hai, L.; Jin, H.; Wu, Y., Efficient Synthesis of Substances Related to Cinacalcet Hydrochloride via Heck Coupling. *Synthetic Communications* **2014,** *44* (19), 2879-2885.

63.   Tewari, N.; Maheshwari, N.; Medhane, R.; Nizar, H.; Prasad, M., A Novel Method for the Large Scale Synthesis of Cinacalcet Hydrochloride Using Iron Catalyzed C–C Coupling. *Organic Process Research & Development* **2012,** *16* (9), 1566-1568.

64.   Theil, O. Methods of Synthesizing Cinacalcet and salts therof. 2012.

65.   Lifshitz-Liron, R. Process for Preparing Cinacalcet Hydrochloride. 2006.

66.   Srinivasan, C. Process for preparation of 3-halopropylbenzene derivatives as intermediates for calcimimetic agents. 2010.

67.   Burger, B. J.; Bercaw, J. E., *New Developments in the Synthesis, Manipulation and Characterization of Organometallic Compounds*. American Chemical Society: Washington D.C., 1987.

68.   Pangborn, A. B.; Giardello, M. A.; Grubbs, R. H.; Rosen, R. K.; Timmers, F. J., Safe and Convenient Procedure for Solvent Purification. *Organometallics* **1996,** *15* (5), 1518-1520.

69.   Becke, A. D., Density-functional exchange-energy approximation with correct asymptotic behavior. *Physical Review A* **1988,** *38* (6), 3098-3100.

70.   Lee, C.; Yang, W.; Parr, R. G., Development of the Colle-Salvetti correlation-energy formula into a functional of the electron density. *Physical Review B* **1988,** *37* (2), 785-789.

71.   Rassolov, V. A.; Pople, J. A.; Ratner, M. A.; Windus, T. L., 6-31G* basis set for atoms K through Zn. *The Journal of Chemical Physics* **1998,** *109* (4), 1223-1229.

72.   Miertuš, S.; Scrocco, E.; Tomasi, J., Electrostatic interaction of a solute with a continuum. A direct utilizaion of AB initio molecular potentials for the prevision of solvent effects. *Chemical Physics* **1981,** *55* (1), 117-129.

73.   Gaussian 09, Revision A.02, M. J. Frisch, G. W. Trucks, H. B. Schlegel, G. E. Scuseria, M. A. Robb, J. R. Cheeseman, G. Scalmani, V. Barone, G. A. Petersson, H. Nakatsuji, X. Li, M. Caricato, A. Marenich, J. Bloino, B. G. Janesko, R. Gomperts, B. Mennucci, H. P. Hratchian, J. V. Ortiz, A. F. Izmaylov, J. L. Sonnenberg, D. Williams-Young, F. Ding, F. Lipparini, F. Egidi, J. Goings, B. Peng, A. Petrone, T. Henderson, D. Ranasinghe, V. G. Zakrzewski, J. Gao, N. Rega, G. Zheng, W. Liang, M. Hada, M. Ehara, K. Toyota, R. Fukuda, J. Hasegawa, M. Ishida, T. Nakajima, Y. Honda, O. Kitao, H. Nakai, T. Vreven, K. Throssell, J. A. Montgomery, Jr., J. E. Peralta, F. Ogliaro, M. Bearpark, J. J. Heyd, E. Brothers, K. N. Kudin, V. N. Staroverov, T. Keith, R. Kobayashi, J. Normand, K. Raghavachari, A. Rendell, J. C. Burant, S. S. Iyengar, J. Tomasi, M. Cossi, J. M. Millam, M. Klene, C. Adamo, R. Cammi, J. W. Ochterski, R. L. Martin, K. Morokuma, O. Farkas, J. B. Foresman, and D. J. Fox, Gaussian, Inc., Wallingford CT, 2016.

74.   Potter, B.; Edelstein, E. K.; Morken, J. P., Modular, Catalytic Enantioselective Construction of Quaternary Carbon Stereocenters by Sequential Cross-Coupling Reactions. *Organic Letters* **2016,** *18* (13), 3286-3289.

75.   Vasilopoulos, A.; Zultanski, S. L.; Stahl, S. S., Feedstocks to Pharmacophores: Cu-Catalyzed Oxidative Arylation of Inexpensive Alkylarenes Enabling Direct Access to Diarylalkanes. *Journal of the American Chemical Society* **2017,** *139* (23), 7705-7708.

76.   Ichikawa, T.; Netsu, M.; Mizuno, M.; Mizusaki, T.; Takagi, Y.; Sawama, Y.; Monguchi, Y.; Sajiki, H., Development of a Unique Heterogeneous Palladium Catalyst for the Suzuki–Miyaura Reaction using (Hetero)aryl Chlorides and Chemoselective Hydrogenation. *Advanced Synthesis & Catalysis* **2017,** *359* (13), 2269-2279.

74

77. Huihui, K. M. M.; Caputo, J. A.; Melchor, Z.; Olivares, A. M.; Spiewak, A. M.; Johnson, K. A.; DiBenedetto, T. A.; Kim, S.; Ackerman, L. K. G.; Weix, D. J., Decarboxylative Cross-Electrophile Coupling of N-Hydroxyphthalimide Esters with Aryl Iodides. *Journal of the American Chemical Society* **2016,** *138* (15), 5016-5019.

78. Terao, J.; Nakamura, M.; Kambe, N., Non-catalytic conversion of C–F bonds of benzotrifluorides to C–C bonds using organoaluminium reagents. *Chem. Commun.* **2009,** (40), 6011-6013.

79. Tobisu, M.; Takahira, T.; Chatani, N., Nickel-Catalyzed Cross-Coupling of Anisoles with Alkyl Grignard Reagents via C–O Bond Cleavage. *Organic Letters* **2015,** *17* (17), 4352-4355.

80. Xia, C.-L.; Xie, C.-F.; Wu, Y.-F.; Sun, H.-M.; Shen, Q.; Zhang, Y., Efficient cross-coupling of aryl Grignard reagents with alkyl halides by recyclable ionic iron(iii) complexes bearing a bis(phenol)-functionalized benzimidazolium cation. *Organic & Biomolecular Chemistry* **2013,** *11* (46), 8135-8144.

81. Yang, F.; Fu, S. Y.; Chu, W.; Li, C.; Tong, D. G., Monodisperse amorphous CuB23 alloy short nanotubes: novel efficient catalysts for Heck coupling of inactivated alkyl halides and alkenes. *RSC Advances* **2014,** *4* (86), 45838-45843.

82. Graham, T. J. A.; Poole, T. H.; Reese, C. N.; Goess, B. C., Regioselective Semihydrogenation of Dienes. *The Journal of Organic Chemistry* **2011,** *76* (10), 4132-4138.

83. Yus, M.; Ortiz, R., Tandem Intramolecular Carbolithiation-Lithium/Zinc Transmetallation and Applications to Carbon−Carbon Bond-Forming Reactions. *European Journal of Organic Chemistry* **2004,** *2004* (18), 3833-3841.

84. Guérin, C.; Bellosta, V.; Guillamot, G.; Cossy, J., Synthesis of Amines from Alcohols in a Nonepimerizing One-Pot Sequence – Synthesis of Bioactive Compounds: Cinacalcet and Dexoxadrol. *European Journal of Organic Chemistry* **2012,** *2012* (15), 2990-3000.

Chapter 3. Rational Design of an Iron-Based Catalyst for Suzuki-Miyaura Coupling of Heteroaromatic Boronic Esters and Tertiary Alkyl Electrophiles

3.1. Introduction

Due in part to nearly 40 years of ligand design and catalyst development, the Suzuki-Miyaura cross-coupling reaction now accounts for the formation of nearly 40% of all C–C bonds in the pharmaceutical industry.[1] As discussed in chapter 2, despite the utility, applicability[2], and generality[3-5] of the Suzuki-Miyaura reaction, there remain underexplored classes of substrates that require further catalyst development. One alternative way to identify existing gaps in the synthetic methodology is by evaluating the number of articles that have been published for various types of electrophiles used in Suzuki-Miyaura cross-coupling reactions (Figure 3.1a). The vast majority of reported Suzuki-Miyaura reactions involve the cross-coupling of two sp^2-hybridized substrates. This limitation is a probable contributor to the historic exploration of mostly flat molecules as potential drug candidates in the pharmaceutical industry. Recently, there has been a growing interest to "escape from flatland," and move towards the construction of saturated molecules containing stereogenic centers.[6] However, there are far fewer Suzuki-Miyaura reactions that involve at least one sp^3-hybridized substrate. Fewer still are examples that use heteroaromatic coupling partners in alkyl-aryl cross-coupling reactions (Figure 3.1b).[7] The dearth of published examples for this class of substrates is particularly notable considering that nearly 70% of all pharmaceutical molecules contain heterocycles.[8] The system reported in chapter 2 for example could not tolerate heteroaromatic boronic esters. Further analysis of the literature also reveals that among reported examples of alkyl-aryl Suzuki-Miyaura cross-coupling reactions, most common are reactions involving primary alkyl fragments (Figure 3.1b). Reports of successful cross-coupling with secondary and tertiary alkyl coupling partners are rare, particularly when the alkyl fragment is the electrophilic partner. There exist only four examples in the literature where tertiary

Figure 3.1. Number of journal articles published* that describe Suzuki-Miyaura cross-coupling reactions for: a) various hybridization of nucleophiles and electrophiles involved and the types of nucleophiles and electrophiles involved in sp^2-sp^3 cross coupling reactions (inset), and b) types of nucleophiles and electrophiles used in sp^2-sp^3 cross coupling reactions for primary, secondary, and tertiary sp^3-hybridized substrates. *Dataset generated using SciFinder®. Full details available in the experimental section.

a)

b
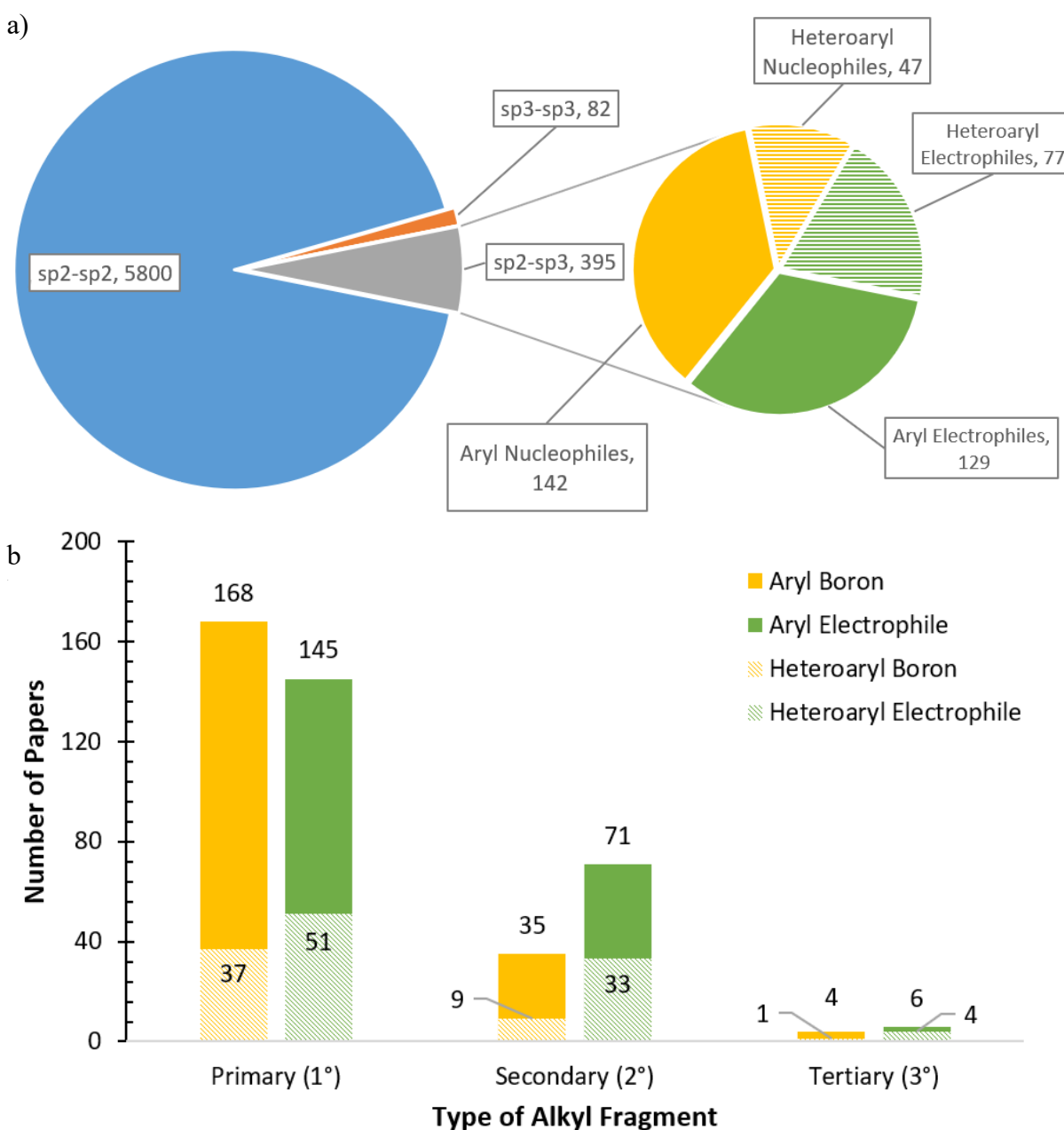
substrates are used,[9-12] and only one system was shown to tolerate a wide variety of heteroaromatic

nucleophiles, albeit with a very limited tertiary electrophile scope.[10]

Another consideration is that most coupling reactions involving primary electrophiles are carried out using palladium-based catalysts,[13] which are toxic[14] and costly.[15] Nearly all reported Suzuki-Miyaura reactions involving secondary and tertiary electrophiles employ nickel-based catalysts, which have similar toxicity[16] and long-term viability[17] concerns as palladium-based catalysts. Moreover, the reported nickel-based catalysts rarely include heteroaromatic substrates in the disclosed substrate scope.[9, 18-19] Abundant and potentially less toxic iron-based catalysts have been developed for alkyl-aryl cross-coupling reactions, but most are limited to reactions involving basic Grignard (i.e. Kumada-type) or difficult-to-handle alkyl zinc (i.e. Negishi-type) transmetalating reagents.[20-30] Iron-based catalysts used for the Suzuki-Miyaura cross-coupling reaction are exceedingly rare[22, 31-33] with many remaining substrate limitations.

To expand the scope of available substrates for Suzuki-Miyaura cross-coupling and to improve the system reported in chapter 2, the development of new catalysts is required. To accomplish this goal a better understanding of the mechanistic framework underlying these cross-coupling reactions is required. The goal of the work in this chapter was to expand the understanding of the mechanism and transition this knowledge into better catalysts for Suzuki-Miyaura cross-coupling reactions.

3.2 Working Mechanistic Hypothesis and Stoichiometric Studies

Our initial studies resulted in the working mechanistic hypothesis presented in Figure 3.2a.[34-35] Iron amide intermediate **II** is formed from reaction of an iron chloride precursor **I** with the lithium amide base, which could subsequently undergo transmetalation with the aryl boronic ester to give an iron aryl intermediate **III.** Following halogen atom abstraction from the alkyl halide substrate, subsequent C-C bond formation by either radical recombination with **IV** followed by reductive elimination or radical rebound leads to product formation and regeneration of the iron

Figure 3.2. Working mechanistic hypothesis and ligand design features for catalysts used in Suzuki-Miyaura cross-coupling reactions catalyzed by iron-based complexes.
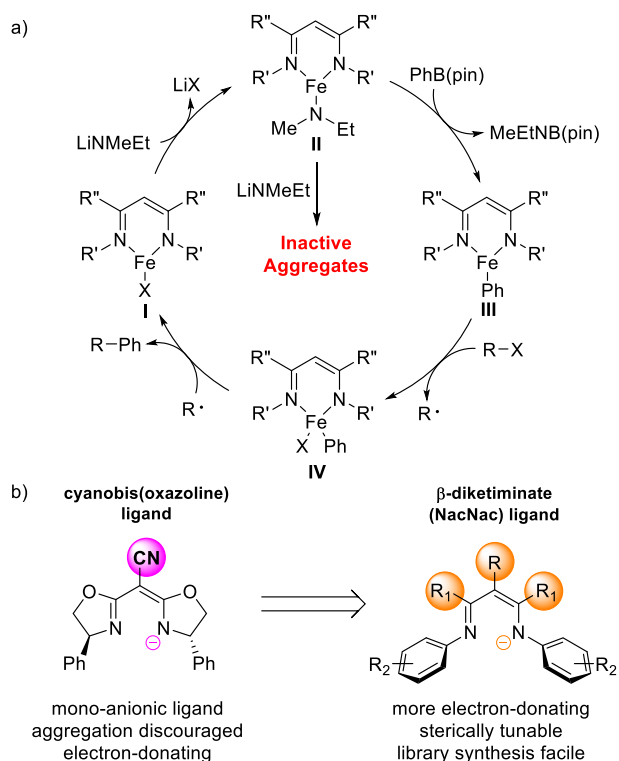
halide precursor. This working mechanistic hypothesis suggested two ligand design principles that would be suitable for further catalyst development:[33] 1) To prevent deleterious iron aggregation, bidentate anionic ligands and ligands with tunable steric bulk positioned proximal to the metal center were targeted; 2) to facilitate the key transmetalation step, electron-donating ligands and ligands that supported low coordination numbers were also desirable.

A class of ligands that adhered to both design principles is the β-diketiminate ligands (Figure 3.2b). These ligands are better σ-donors than the less basic cyanobis(oxazoline) ligands. Moreover, the Holland group[36-39] and others[40-42] have demonstrated that these ligands are exceptional for stabilizing low-coordinate iron species, including 3-coordinate iron alkoxide[37] and amide complexes.[37] In accordance with the mechanistic framework presented in Figure 3.2, discrete iron complexes **3.3** and **3.4** were synthesized within the β-diketiminate framework to

Scheme 3.1. Stoichiometric reactions relevant to Suzuki-Miyaura cross-coupling reactions involving iron complexes supported by β-diketiminate ligands.
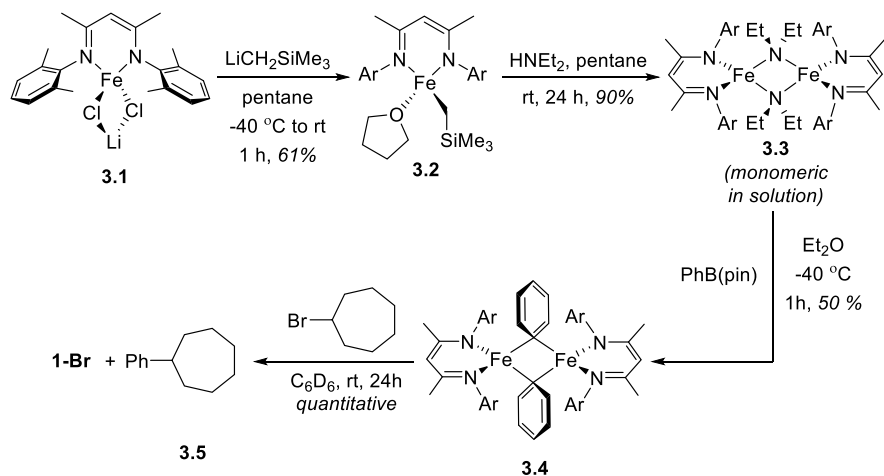
determine if this class of ligands would allow for the isolation of these highly reactive intermediates (Scheme 3.1). While direct reaction between lithium amides and **3.1** led to a complex mixture of products, synthesis of **3.3** was achieved through the protonolysis of iron alkyl complex **3.2** with diethylamine in a route similar to one previously published for the synthesis of iron alkoxides (Scheme 3.1).[43] The structure of this compound as determined by X-ray crystallography confirmed the formation of an iron amide species (Figure 3.3a). In the solid state, **3.3** was dimeric and roughly D_{2d} symmetric by virtue of two μ^2-diethylamide ligands, a common feature for many

Figure 3.3. X-ray crystal structures of **3.3** and **3.4**. Thermal ellipsoids drawn at the 50% probability. See experimental for a complete list of bond distances and angles.

a) Complex **3.3**
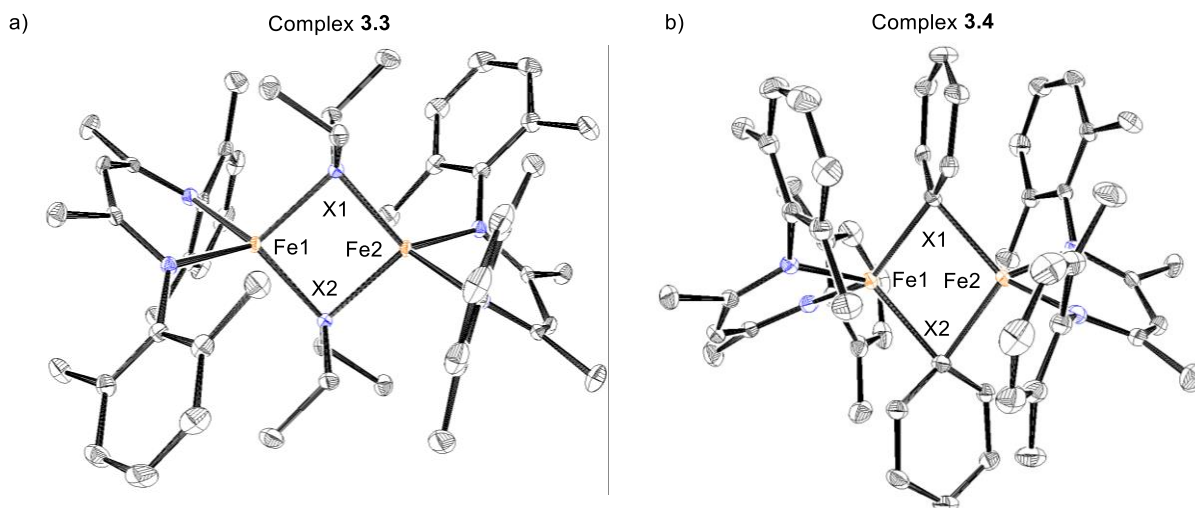
b) Complex **3.4**

Figure 3.4. ^{1}H NMR of 2,4-bis[(2,6-dimethylphenyl)imino]pentane iron *N,N*-diethylamide complex (**3.3**).
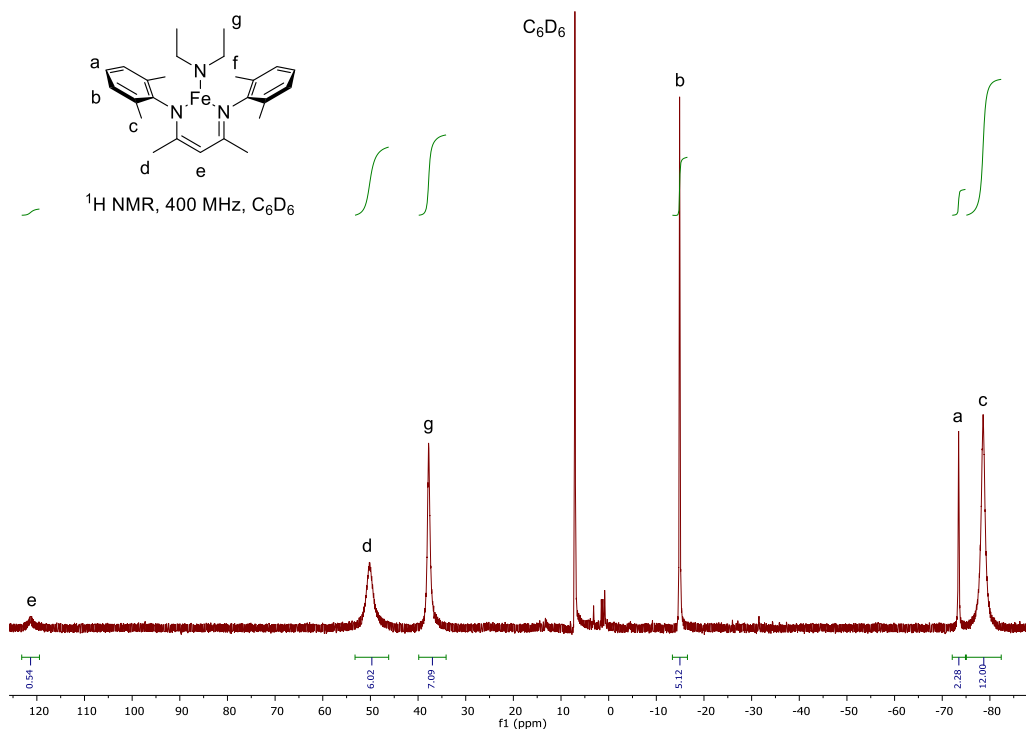
iron complexes containing 2,6-dimethylphenylimine β-diketiminate ligands.[37] In solution, all protons except those closest to the metal center could be identified in the ^{1}H NMR spectrum (Figure 3.4). However, in contrast to the solid-state structure, diffusion-ordered NMR spectroscopy (DOSY) of the complex is more consistent with the major species in solution being mononuclear (Figure 3.5). For the development of the method we use for paramagnetic DOSY please refer to appendix A. The DOSY spectrum in figure 3.5 clearly shows a signle diffusion coefficient for the paramagnetic species. This diffusion coefficient is smaller than that of the solvent but is still larger than what would be expected for a dimeric molecule (D = 5-7 x 10^{-6} cm/m^2). When **3.3** was treated with 1 equivalent of phenylboronic acid pinacol ester (B(pin)) in benzene, an immediate color change occurred that coincided with changes in the ^{1}H and ^{11}B NMR spectra consistent with the formation of an iron phenyl complex **3.4**. The structure of the iron phenyl complex also appeared dimeric in the solid state using X-ray crystallography (Figure 3.4b). Finally, upon treating complex

82

3.4 with bromocycloheptane, the cross-coupled product was obtained in nearly quantitative yields with the concomitant formation of iron halide complex **3.1** (Scheme 3.1).

Taken together, the results from the stoichiometric experiments are consistent with the mechanistic framework presented in Figure 3.2. Although we were unable to demonstrate that aggregation was the critical failure of the Box ligands these experiments also support the notion that the β-diketiminate iron complexes undergo more reversible aggregation events than the cyanobis(oxazoline) iron complexes described in chapter 2. Moreover, the rapid conversion (seconds at room temperature) of the iron amide **3.3** to the iron phenyl **3.4** highlights the efficient transmetalation reaction afforded by the electron-releasing and sterically accommodating β-diketiminate ligands. Finally, efficient transmetalation occurs even in the absence of a borate intermediate. This outcome is consistent with transmetalation proceeding predominantly through an iron amide intermediate, and is in agreement with similar alkoxide intermediates proposed to be involved in Suzuki-Miyaura reactions catalyzed by palladium-based complexes.[44] Interestingly,

Figure 3.5. DOSY NMR of 2,4-bis[(2,6-dimethylphenyl)imino]pentane iron *N,N*-diethylamide complex (**3.3**).
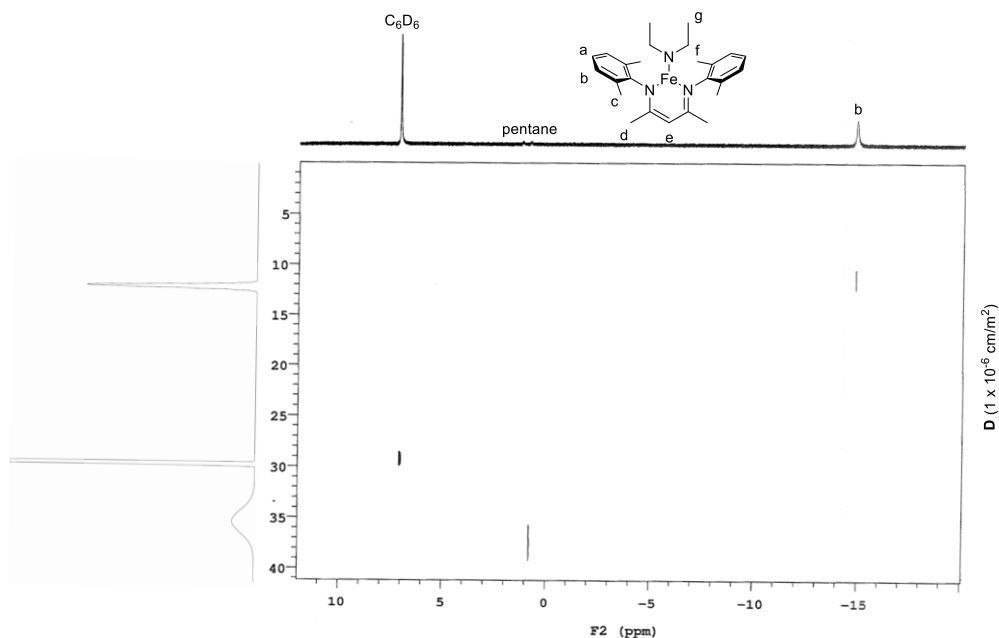
the stoichiometric reaction between the iron phenyl complex **3.4** and bromocycloheptane took nearly 24 hours to go to completion which is significantly slower than one would expect based on the catalytic reactions disclosed in chapter 2.

3.3 Catalyst Optimization

Despite the slow kinetics of the stoichiometric experiemnts, iron(II) halide complexes supported by these ligands are suitable precatalysts for a cross-coupling reaction between PhB(pin) and bromocycloheptane (Table 3.1). Importantly, the discrete iron complex must be made prior to cross-coupling; much lower yields were obtained if the ligand was combined with iron dichloride (Table 3.1, entry 2). The rate of the reaction was found to be sensitive to the substitution pattern installed on the aryl imines. In general, the reaction rate increased with decreasing steric bulk: complexes containing 2-aryl imine ligands (**3.7-3.10**) were superior compared to complexes containing 2,6-disubstituted aryl imine ligands (**3.1, 3.6, 3.11-3.14**) (Table 3.1). Presumably, this trend is due to the accessibility of a less crowded transmetalation pathway. Despite this trend, there appears to be an optimal steric size for the complexes containing 2-substituted aryl imine ligands because 2-methylphenyl imine complex **3.10** was less efficient than 2-ethylphenyl imine complex **3.9** and unsubstituted phenyl imine complex **3.15** was highly inefficient for cross-coupling. It is likely that the optimal ligand steric size is a consequence of the propensity for less substituted aryl imine β-diketiminate ligands to undergo irreversible dimerization reactions, which hinder productive cross-coupling reactions. In comparison to the notable steric influence of the ligand, the electronic effects of the ligand minimally impact the overall rate of the reaction. For example, 2,6-dimethyl-4-methoxyphenyl imine complex **3.13** and complex **3.6** containing a 2,6-dimethylphenyl imine ligand with CF_3 substituents in the β-diketiminate backbone led to nearly the same reaction rate as the 2,6-dimethylphenyl imine complex **3.1**. All complexes studied, except

those with very little steric bulk (**3.15**) or excessive steric bulk (**3.14**), were highly selective in generating the desired cross-coupling products.

Table 3.1. Iron(II) β-diketiminate complexes used as precatalysts for Suzuki-Miyaura cross-coupling of PhB(pin) and bromocycloheptane.
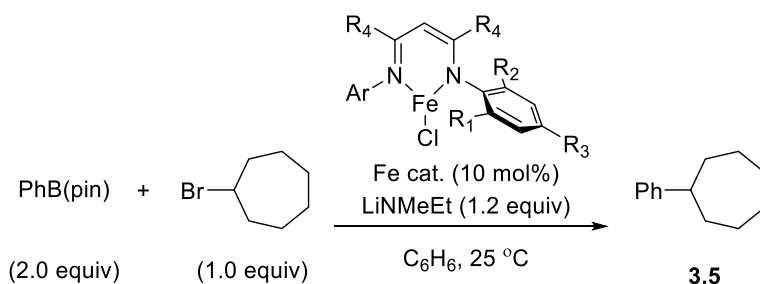
Fe complex	R_1	R_2	R_3	R_4	k_{app} (x 10^{-5} s^{-1})[a]	k_{rel}	Yield of 3.5 (%)
3.1	Me	Me	H	Me	2.43	1.0	91
3.1[b]	Me	Me	H	Me	N/A	N/A	57
3.6	Me	Me	H	CF$_3$	2.34	1.0	99
3.7	tBu	H	H	Me	7.95	3.3	96
3.8	iPr	H	H	Me	44.0	18.1	95
3.9	Et	H	H	Me	45.4	18.7	99
3.10	Me	H	H	Me	29.9	12.3	85
3.11	Me	Me	Me	Me	3.38	1.4	99
3.12	Me	Me	Br	Me	0.63	0.3	53
3.13	Me	Me	OMe	Me	3.47	1.4	99
3.14	iPr	iPr	H	Me	2.31	1.0	1
3.15	H	H	H	Me	N/A	N/A	28

[a] k_{app} based on the conversion of bromocycloheptane and only uses values up to 50% conversion. [b]**3.1** generated *in situ* by reaction of the free ligand with iron dichloride.

Unlike the system reported in chapter 2 using cyanobis(oxazoline) ligands,[33] early catalyst decomposition in the reaction was not observed when using complexes supported by β-diketiminate ligands (Figure 3.6). The extended catalyst lifetime obviated the need for the addition of exogenous ligand employed previously. Instead, additional equivalents of exogenous ligand now led to diminished reaction efficiency, with no benefit to overall yield (Table 3.2, entry 6). This likely indicates that an iron species with two ligands on it is no longer able to participate in the

Figure 3.6. Plots of Conversion vs. time for representative β-diketiminate iron complexes.

PhB(pin) + Br—⟨cycloheptane⟩ →[Fe cat. (10 mol%), LiNMeEt (1.2 equiv), C$_6$H$_6$, 25 °C] Ph—⟨cycloheptane⟩

(2.0 equiv)   (1.0 equiv)   **3.5**

Conversion of Bromocycloheptane vs Time

Legend: 3.1, 3.6, 3.7, 3.9, CNBoxPhFeCl

Y-axis: Converstion (%)
X-axis: Time (h)
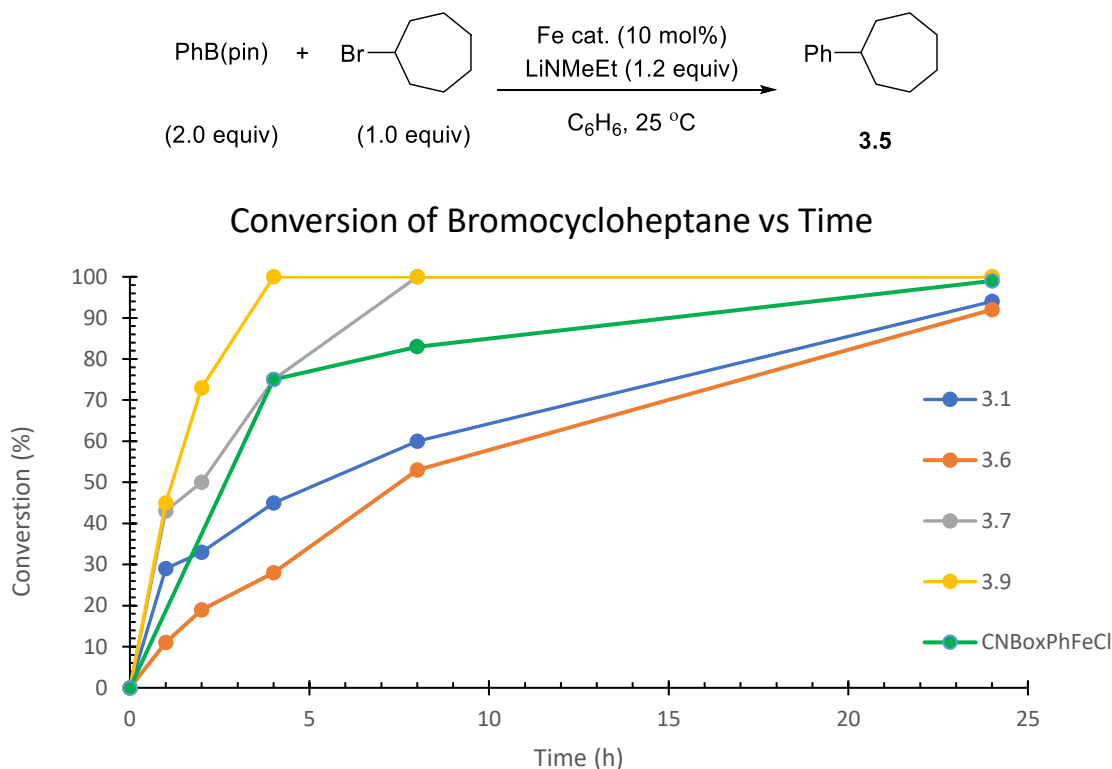
catalytic reaction. More definitive studies with a discrete complex with two ligands on it should be prepared to further test this hypothesis. In addition to this practical advantage, an excess of boronic ester substrate is no longer required to extend catalyst lifetime. An excess of boronic ester substrate does accelerate the reaction and make it slightly more selective, which may indicate that the relative rate of transmetalation is important for the overall reaction kinetics (Table 3.2, entries 1-5). The catalyst loading could not be lowered without dramatic loss in activity (Table 3.2, entries 3, 7, and 8).

After optimizing the catalytic reactions, it only became more clear that the kinetics of the stoichiometric reactions are inconsistent with the catalytic reaction. One possibility for this discrepancy is that the iron phenyl complex **3.4** is not sufficiently reducing to perform the halogen abstraction. Based on this assumption, the iron amide is the only other species in the catalytic reaction that could serve as a reducing agent. As a means to test this hypothesis a CV was collected

86

Table 3.2. Equivalency and catalyst loading evaulation.

Entry	X (equiv.)	Y mol%	Yield (%)
1	1.3	10	80
2	1.5	10	90
3	2.0	10	95
4	2.2	10	96
5	2.5	10	97

of the iron amide **3.3** which determined that it had a reducing potential of -1.7 V vs Fc/Fc$^+$ (Figure 3.7). It was not possible to collect a clean CV of complex **3.4** due to the instability of the compund. Furthermore, when a mixture of **3.3** and **3.4** was prepared and treated with bormocycloheptane the cross coupled product was formed immediately upon mixing (Figure 3.8a). This result could

Figure 3.7. Cyclic voltammogram for complex **3.3** carried out at a scan rate of 0.1V/s using 1M N(n-Bu)$_4$PF$_6$ in THF as the electrolyte. The potential was referenced to Fc/Fc$^+$.

implicate that a mechanism that involves two different metal centers is operative under the catalytic

conditions. An idea of what this mechanism could potential be is presented in Figure 3.8b. In this

mechanism, the iron amide **3.3** could perform the halogen abstraction reaction (Right cycle). This

would generate an oxidize iron complex. The carbon-centered radical that is generated from this

reaction could then combine with an iron-aryl complex **3.4** to generate an intermediate that is

primed for reductive elimination. The least likely intermediate here is the putatively generated

two-coordinate iron(I) intermediate after reductive elimination. This intermediate, or one like it,

could then conproportionate with the oxidized iron amide complex to regenerate the starting amide

complex and an equivalent of the iron halide. Further studies into this mechanism are underway in

collaboration with Mike Neidig's group at the University of Rochester. An exciting possibility with

Figure 3.8. a) Stoichiometric reaction between **3.3**, **3.4**, and bromocycloheptane. b) Proposed mechanism that utilizes two different metal centers.

this system is that the two different iron-centers do not necessarily require the same ligand. One could envision a system where two catalysts that are each more refined for their specific role. For example, an even more reducing iron complex could be used in place of the iron amide. Increasing the reducing power further may even allow access to substrates that are more difficult to activate such as alkyl fluorides.

3.4 Substrate Scope

The generality of the cross-coupling reaction for a variety of heteroaromatic boronic ester substrates was tested next (Figure 3.9). Catalyst **3.7** was selected for this purpose because a cursory exploration of boronic ester substrates demonstrated that **3.7** led to higher yields than catalyst precursors that were faster in the reaction between PhB(pin) and bromocycloheptane (e.g., **3.8-3.10**). The sterically more encumbered ligand in **3.7** likely provides the optimal steric environment to overcome irreversible substrate binding while maintaining the accessibility needed for transmetalation. With this system, my coworker Alex Wong was able to demonstrate good reactivety with several heteroaromatic boronic ester substrates. These compounds produced the desired products in good to excellent yields (Figure 3.9). 2-thiophenyl-B(pin) and 3-thiophenyl-B(pin) produced the desired cross-coupling products **3.16-3.19** involving primary and secondary alkyl halides in moderate to good yields. These results demonstrate complementary reactivity with electrophilic aromatic substitution of thiophene rings, which selectively functionalize at the 2-position, and are prone to rearrangement when primary alkyl halides are used.[45-46] In addition to thiophenes, furans were compatible (**3.20**) and several nitrogen-containing heteroaromatic boronic esters resulted in moderate to good yields (e.g., **3.22**, **3.23**, **3.26** and **3.28**). The latter substrates often required the reaction to be carried out at 50 °C or an excess of boronic ester. Quinolines, Boc-protected indoles, and sterically encumbered pyridines were all tolerated (**3.22**, **3.23** and

89

3.25). Such substrates were completely inactive when cyanobis(oxazoline) complexes were used. It is possible that nitrogen-based heterocycles are problematic for iron-based cross-coupling reactions because they undergo substrate inhibition. This limitation was overcome by using the β-diketiminate ligands, which have a larger steric demand proximal to the metal center compared to the cyanobis(oxazoline) ligands (Figure 3.2). This larger steric demand is primarily created by the orientation of the substituents on the aromatic rings being directly over the metal center. Nevertheless, substrates more likely to bind to iron, such as sterically unencumbered pyridines or heterocycles containing multiple heteroatoms (e.g. **3.21**, **3.24** or **3.27**), did not undergo efficient cross-coupling using the β-diketiminate ligands.

Figure 3.9. Substrate scope with respect to the boronic ester coupling partner. Yields in parenthesis are based on recovered starting material.
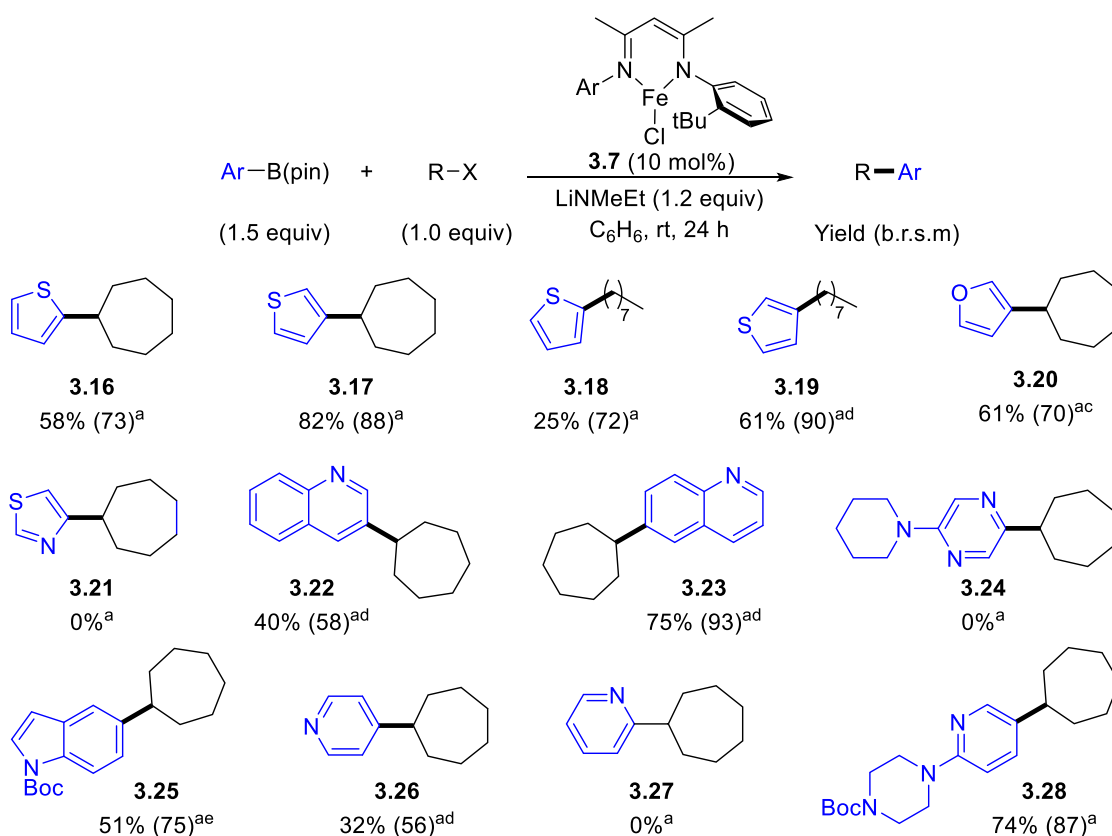
^{a}X = Br. ^{b}X = Cl. ^{c}0.1 mmol of electrophile. ^{d}at 50 °C. ^{e}2.0 equiv. of B(pin).

In addition to the boronic ester scope, the previously reported alkyl halide substrate scope was maintained to a high degree, with generally faster and cleaner reactions being observed using β-diketiminate complexes (e.g., **3.29-3.34**, Figure 3.10). Primary and secondary alkyl halides were well tolerated with alkyl bromides being superior to alkyl chlorides and alkyl iodides. It was additionally found that suitable protected alcohols were tolerated under these conditions (e.g., **3.35,** Figure 3.10). One notable exception were benzylic halide substrates (**3.32**), which did not perform as well as with the cyanobis(oxazoline) complexes. Presumably, the higher reducing ability of the β-diketiminate iron complexes leads to unproductive side reactions (Figure 3.7). Finally, tertiary alkyl halides proved to be excellent substrates for the cross-coupling reaction (Figure 3.10). Previously, the cyanobis(oxazoline) iron complexes led to low yields of cross-coupled product with 1-chloroadamantane,[33] but the reaction was not general for a variety of tertiary alkyl halides. In contrast, cross-coupling using **3.7** resulted in a near quantitative yield of **3.37** when 1-chloroadamantane was used as a substrate. Despite this result, the fluorinated catalyst **3.36** was more general for cross-coupling of a variety of tertiary alkyl chlorides. It is possible that the greatest challenge with the coupling of tertiary electrophiles is the reductive elimination step. If this is the case, a ligand that generates a more electron deficient metal center should be better able to promote this reactivity. Using this catalyst, reactions between *tert*-butyl chloride and a variety of electronically diverse boronic esters led to good to excellent yields of cross-coupled products (e.g., **3.38-3.41**). Bulkier RMe₂Cl substrates led to good yields of cross-coupled product and near quantitative yields based on recovered starting material (e.g., **3.42**). The limitation of the current

system appears to be with tertiary alkyl halides of the general formula R_2MeCl and larger, which were completely unreactive under the reaction conditions (e.g., **3.43-3.44**).

To the best of our knowledge, there are no previous reports of Suzuki-Miyaura reactions that utilize an iron-based catalyst for cross-coupling of a variety of tertiary electrophiles. Nickel-based catalysts are more commonly used for this type of cross-coupling reaction,[47-48] but often lead to mixtures of regioisomers[49] containing the desired cross-coupling product with a newly formed quaternary center and a less sterically encumbered product that results from chain-walking prior

Figure 3.10. Substrate scope with respect to the electrophile.
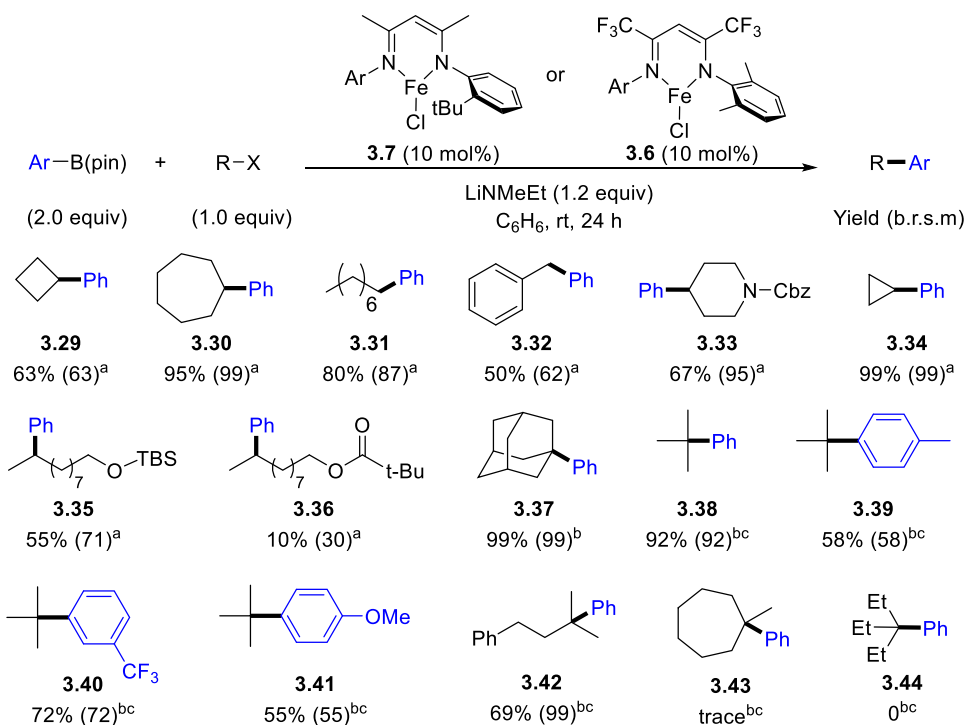
^aX = Br. ^bX = Cl. ^cComplex **3.6** was used as the catalyst.

to product formation. These isomeric products can be difficult to separate. Unlike the nickel-based catalysts, products resulting from isomerization by chain-walking were not observed using the iron-based catalyst (e.g., **3.42** vs Figure 3.11). This outcome could be due to the lower stability of of earlier transition metal alkene complexes which are intermediates during the β-hydride elimination/reinsertion process required for chain-walking.[50]

Figure 3.11. Gong's reported system for the reductive coupling of tertiary electrophiles.[48]
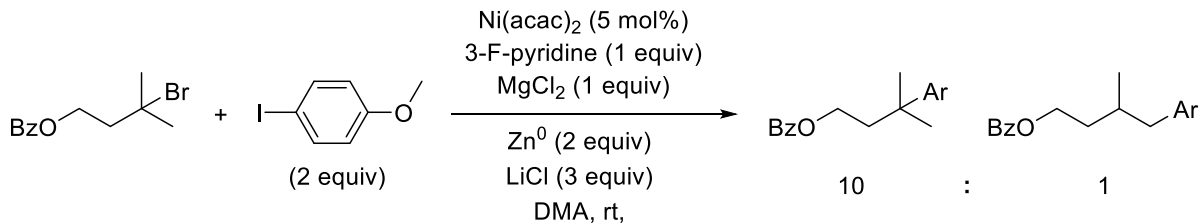
3.5 Conclusions

In this chapter, an iron-based catalyst system was designed for the efficient cross-coupling of unactivated boronic ester nucleophiles and alkyl halide electrophiles. Key to the design in question was stoichiometric experments which informed further reactivty. High reaction rates could be attributed to the use of electronically releasing β-diketiminate ligands that favor reactive intermediates with low coordination numbers, are less likely to dissociate, and are less likely to undergo irreversible aggregation so as to form unproductive iron aggregates. The highly active catalyst system proved to be efficient for cross-coupling reactions involving heteroaromatic boronic ester nucleophiles and tertiary alkyl halide electrophiles. Both classes of substrates are underrepresented in the field of cross-coupling catalysis. Finally, methodology development will be coupled with mechanistic studies focused on better understanding the key C-C bond forming step, which remains poorly understood in catalytic cross-coupling reactions involving iron complexes.[51-52] Other members of the group are currently attempting to get detailed kinetic information to further improve the catalysts presented here. Additionally, the idea that two catalysts could be devised to work in tandem for these processes is currently being explored.

3.6 Experimental Procedures

General Considerations. Unless stated otherwise, all reactions were carried out in oven-dried glassware in a nitrogen-filled glovebox or using standard Schlenk-line techniques.[1] Solvents

including dichloromethane, pentane, toluene, diethyl ether, and tetrahydrofuran were purified by passage through two activated alumina columns under a blanket of argon[2] and then degassed by brief exposure to vacuum. All prepared boronic acid pinacol esters were used after passage through alumina under a nitrogen atmosphere. Methylethyl amine was purchased from TCI America; diisopropylamine and lithium dimethylamide were purchased from Alfa Aesar; butylamine and diethylamine were purchased from Sigma-Aldrich. All amines that were liquids at room temperature were dried over calcium hydride for at least 24 hours before being vacuum-distilled. 2,3-dimethyl-2,3-butanediol and 2,2-dimethylpropane-1,3-diol were purchased from Alfa and used without further purification. Anhydrous iron (II) chloride was purchased from Sigma-Aldrich and used without further purification. Purchased alkyl halides were dried over calcium hydride for at least 24 hours before being vacuum-distilled, while all solids were dried over P_2O_5 before use in the glovebox. All alkyl halides were purchased from Sigma-Aldrich, Oakwood Chemicals and Fisher Scientific. Many of the heteroaromatic boronic esters were graciously provided by Amgen. These compounds were then dried over P_2O_5, brought into a nitrogen glovebox, and passed through basic alumina before use.

^{1}H, ^{11}B, {^{1}H}^{13}C, and ^{19}F nuclear magnetic resonance (NMR) spectra were recorded at ambient temperature on Varian VNMRs operating at 400 MHz, 500 MHz, or 600 MHz for ^{1}H NMR at 160 MHz for ^{11}B NMR, 125 MHz for {^{1}H}^{13}C or 470 MHz for ^{19}F NMR. All {^{1}H}^{13}C NMR spectra were collected while broad-band decoupling was applied to the ^{1}H region. The residual protio solvent impurity was used as an internal reference for ^{1}H NMR spectra and {^{1}H}^{13}C NMR spectra. Boron trifluoride diethyl etherate was used as an external standard for ^{11}B NMR (BF$_3$·O(**6**H$_5$)$_2$: 0.0 ppm) and for ^{19}F NMR (BF$_3$·O(**6**H$_5$)$_2$: -153.0 ppm). The line listing for NMR spectra of diamagnetic compounds are reported as follows: chemical shift (multiplicity, coupling

constant, integration) while paramagnetic compounds are reported as: chemical shift (peak width at half height, number of protons). All paramagnetic spectra were collected at 25 °C. Solvent suppressed spectra were collected for paramagnetic precatalysts in THF using the PRESAT macro on the VNMR software. DOSY NMR are not usually collected for paramagnetic compounds due to complications with fast relaxation times. The DOSY spectra collected here were collected on a 600 MHz Agilent NMR spectrometer using the Doneshot macro. The diffusion delay was set to 8 ms and the gradients were arrayed between 1000 and 25000. Samples were typically collected with 4 scans per gradient. Infrared (IR) spectra were recorded on a Bruker Alpha attenuated total reflectance infrared spectrometer. High-resolution mass spectra were obtained at the Boston College Mass Spectrometry Facility on a JEOL AccuTOF DART instrument. Single crystal X-ray Intensity data were measured on a Bruker Kappa Apex Duo diffractometer using a high brightness IμS copper source with multi-layer mirrors. The low temperature device used is an Oxford 700 series Cryostream system with temperature range of 80-400 K. An Olympus SZ1145 stereo zoom microscope was used to view and mount crystals. The crystal structure was solved using ShellX.

General procedure for literature survey featured in Figure 3.1. The data set was generated using the Substances: Chemical Structure search function on Scifinder®. In the reaction editor, a boron fragment and an electrophile fragment were drawn to match the desired functionality. The initial search set was first refined by the number of steps. We chose a step count of one to maximize the methodology papers included in the data set while eliminating some of the papers that simply use already known reactions in a broader synthesis. From the data set of single-step reactions, the Get References tool was used to consolidate reactions by document. The set of manuscripts was then refined by document type to only include journal articles. Finally, the data

set was refined by research topic using the keyword "cross coupling" to generate the final data set used for the graphs. This procedure was repeated for every disconnection.

General procedure for NacNac ligand evaluation and conversion versus time plots. In a nitrogen-filled glovebox, iron complex (0.025 mmol) was combined in a 7 mL scintillation vial with lithium ethylmethylamide (18.5 mg, 0.30 mmol). A stirbar was then added to the vial followed by a 0.5 mL stock solution of bromocycloheptane (46 mg, 34 µL, 0.250 mmol), phenyl boronic acid pinacol ester (102 mg, 0.500 mmol) and tetradecane (13 mg, 16.1 µL, 0.060 mmol). The resulting solution was diluted to a total volume of around 7 mL. The vial was then seal with a Teflon lined cap and the mixture was stirred for 24 hours. 100 µL aliquots were taken at several timepoints to determine converstion and yield of the reaction by GC. After 24 hours the reaction was removed from the glovebox and quenched by the addition of 1 drop of water. The reaction was then dried over sodium sulfate and filtered through celite. 200 µL of this reaction was then diluted with dichloromethane and analyzed by quantitative GC for the final timepoint.

General procedure for equivalency screen. In a nitrogen-filled glovebox, iron complex **3.7** (0.025 mmol 0.0125 mmol or 0.0025 mmol) was combined in a 7 mL scintillation vial with lithium ethylmethylamide (18.5 mg, 0.30 mmol). A stirbar was then added to the vial followed by a 0.5 mL solution of bromocycloheptane (46 mg, 34 µL, 0.250 mmol), phenyl boronic acid pinacol ester (X equivalents) and tetradecane (13 mg, 16.1 µL, 0.060 mmol). The resulting solution was diluted to a total volume of around 7 mL. The vial was then seal with a Teflon lined cap and the mixture was stirred for 24 hours. After 24 hours the reaction was removed from the glovebox and quenched by the addition of 1 drop of water. The reaction was then dried over sodium sulfate and filtered through celite. 200 µL of this reaction was then diluted with dichloromethane and analyzed by quantitative GC for the final timepoint.

96

General procedure for for CV collection. In a nitrogen filled glovebox, to a 20 mL scintillation vial was added 0.1 M NBu$_4$PF$_6$ in THF (1.5 mL). A background spectrum was collected of this electrolyte from -1.0 V to 1.0 V. This background had little to no signal. Complex **3.3** (1.5 mg) was then added to this solution and a spectrum was taken again. No signals were observed so the potential was scanned down to -2.4 V where a small feature was observed. Shrinking the voltage window around this feature gave a more clear redox pair that was further refined by reducing the scan rate to 0.02 V/s. A separate vial of the electrolyte was used to determine the potential of the Fc/Fc$^+$ redox couple as addition of Fc to complex **3.3** caused all electrochemical signal to disapear.

General procedure for synthesis of β-diketiminate ligands. To one-necked 250 mL round-bottom flask equipped with stir bar was added aniline (2.2 equiv), 2,4-pentanedione (1.0 equiv), and ethanol (50 mL). 12 M hydrochloric acid (1.2 equiv) was added dropwise to the stirring reaction mixture. A reflux condenser was attached to the reaction vessel, and the reaction mixture heated to reflux under nitrogen on the Schlenk line for 3 days. The reaction mixture was removed from heat and allowed to cool to room temperature before evaporation *in vacuo*. The resulting tan solid was suspended in hexane, then further washed with hexane through a Büchner funnel. The collected hydrochloride salts were dissolved in dichloromethane and washed with saturated NaHCO$_3$ (aq) (5 x 20 mL). The collected aqueous layers were extracted with dichloromethane, and the combined organic layers were dried over sodium sulfate, filtered, and concentrated *in vacuo*. In some cases, the collected residue was distilled to remove excess aniline before it was dissolved in hot isopropanol or methanol and subsequently cooled to -40 °C overnight for crystallization. The crystals were collected by filtration and the mother liquor   was concentrated

and resubjected to recrystallization. Yields reported are the combined yields obtained from the initial crop of crystals and the second crop of crystals obtained from the mother liquor.

General procedure for synthesis of β-diketiminate iron chloride complexes.[53] To an oven-dried round-bottom flask equipped with stirbar was added β-diketiminate ligand (9.8 mmol, 1.0 equiv) and pentane (40 mL, 0.244 M). On the Schlenk line, the mixture was cooled to -78 °C and degassed by placing the solution under vacuum for at least 5 minutes. A solution of butyl lithium in hexanes (4.21 mL, 2.3 M, 9.75 mmol) was added dropwise while stirring. In most cases, a white precipitate formed rapidly. The reaction mixture was warmed to room temperature while stirring before the solvent was removed under vacuum. The sealed reaction vessel was transferred into a glovebox, where the solid was collected on a frit and washed with cold pentane (5 mL at -40 °C). The solid was dried and weighed to determine stoichiometry for the next step. No characterization of the lithium salts of the ligand were carried out. The collected deprotonated ligand (9.8 mmol) was then dissolved in THF (10 mL) in a 20 mL scintillation vial. This solution was added dropwise to a slurry of iron dichloride (9.8 mmol) in THF (10 mL) prepared in a separate scintillation vial equipped with stir bar. This mixture was allowed to stir overnight. The resulting solution was cooled and passed through celite which was washed with additional THF (~20 mL), then concentrated under vacuum. The resulting semi-solid was then washed with pentane, dried, and collected. Spectra of the 2,4-bis(2,6-diethylphenylimido)pentane[3] and 2,4-bis(2,6-diisopropylphenylimido)pentane[4] complexes matched literature line listings.

Elemental analysis of the following iron complexes revealed samples with C, H, and N ratios that match what would be expected for the desired complexes containing variable amounts of THF (typically 2 or 3 equivalents). We have also independently identified that there appears to be exactly 1 equivalent of lithium chloride in the 2,4-bis(2,6-dimethylphenylimido)pentane iron

chloride complex by ICP-OES, which is likely true for all examined complexes. Discrepancies in the elemental analysis are an unidentified inorganic impurity that is not lithium chloride, which accounts for ~5-15 % of the mass. This difficulty has been observed previously in the purification of similar complexes.[5]

Synthesis of 2,4-bis[(2,6-dimethylphenyl)imino]pentane iron chloride complex (3.1). Synthesized according to general procedure using 2,4-bis[(2,6-dimethylphenyl)imino]pentane (3.0 g, 9.8 mmol) **(1a)** as the ligand which resulted in the formation of a yellow crystalline solid (3.3 g, 58% yield). ^{1}H NMR (400 MHz, THF) δ -68.7 ($w_{1/2}$ = 180 Hz, 6H), -52.0 ($w_{1/2}$ = 100 Hz, 2H), -39.7 ($w_{1/2}$ = 264 Hz, 1H), 6.2 ($w_{1/2}$ = 254 Hz, 12H), 16.1 ($w_{1/2}$ = 82 Hz, 4H) ppm. IR: 2916, 1519, 1373, 1038, 760 cm^{-1}. Elemental analysis for $C_{21}H_{25}Cl_2FeLiN_2(C_4H_8O)_{0.1}$ calc'd C 66.09% H 6.69% N 7.20% Found C 55.71% H 5.69% N 6.06%.
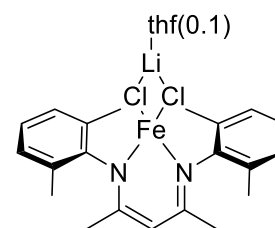
Synthesis of 2,4-bis[(2,6-dimethylphenyl)imino]pentane (3.1a). Synthesized from 2,6-dimethylaniline (9.1 g, 75 mmol) and 2,4-pentanedione (3.0 g, 30 mmol) according to the general procedure which afforded a white crystalline solid (6.0 g, 65% yield). ^{1}H NMR (400 MHz, CDCl$_3$) δ 12.19 (br s, 1H), 7.03 (d, J = 8.0 Hz, 4H), 6.95 (t, J = 7.5 Hz. 2H), 4.88 (s, 1H), 2.17 (s, 12H), 1.70 (s, 6H). NMR spectrum is in agreement with literature precedence.[6]
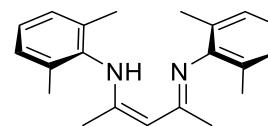
Synthesis of 3-cyano-2,4-bis[(2,6-dimethylphenyl)imino]pentane iron chloride complex (3.1b). Synthesized according to general procedure using 3-cyano-2,4-bis[(2,6-dimethylphenyl)imino]pentane (340 mg, 1.0 mmol) **(1a)** as the ligand which resulted in the formation of a tan crystalline solid (300 mg, 48% yield). ^{1}H NMR (400 MHz,

99
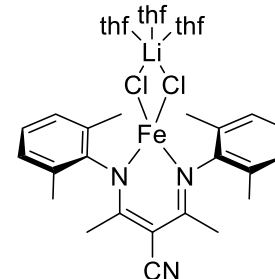
THF) δ -51.6 ($w_{1/2}$ = 78 Hz, 2H), -37.7 ($w_{1/2}$ = 294 Hz, 6H), 9.1 ($w_{1/2}$ = 52 Hz, 4H) ppm. IR: 2953, 2194, 1559, 1387, 1044, 848, 765 cm^{-1}. Elemental analysis for $C_{22}H_{24}Cl_2FeLiN_3(C_4H_8O)_3$ calc'd C 70.82% H 8.39% N 7.29% Found C 58.81% H 6.86% N 6.04%.

Synthesis of 3-cyano-2,4-bis[(2,6-dimethylphenyl)imino]pentane (3.1c). Synthesized according to an adapted literature procedure[7] from 2,4-bis[(2,6-dimethylphenyl)imino]pentane (500 mg, 1.63 mmol) and afforded a white crystalline solid (360 mg, 67% yield) after recrystallization from methanol. ^{1}H NMR (500 MHz, CDCl$_3$) δ 14.19 (s, 1H), 7.15 – 6.92 (m, 6H), 2.12 (s, 12H), 2.03 (s, 6H) ppm. HRMS (ESI) *m/z* [M]$^+$ calculated for $C_{22}H_{26}N_3$ 332.21212; found 332.21157. NMR spectrum is in agreement with literature precedence.[7]
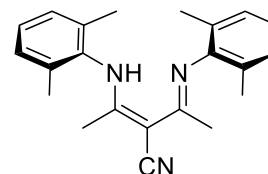
Synthesis of 2,4-bis[(2,6-dimethylphenyl)imino]pentane iron CH$_2$TMS tetrahydrofuran adduct (3.2). In the glovebox, to a 7 mL scintillation vial equipped with magnetic stir bar was added 2,4-bis[(2-methylphenyl)imino]pentane iron chloride complex (**3.1**) (800 mg, 1.37 mmol) and pentane (2 mL). This mixture was allowed to cool to -40 °C in the freezer. A solution of LiCH$_2$TMS (129 mg, 1.0 equiv) in pentane (1 mL) was added to the stirring reaction mixture. The reaction vessel was sealed and a dark yellow precipitate formed immediately. The reaction was allowed to stir for 1 hour, at which point the precipitate was filtered off through celite and the filtrate concentrated *in vacuo*. The residue was dissolved in pentane and transferred to a vial to recrystallize in the freezer overnight. The mother liquor was decanted to afford the product as a yellow solid (434 mg, 61% yield). ^{1}H NMR (400 MHz, C$_6$D$_6$) δ 81.30 ($w_{1/2}$ = 294 Hz, 6H), 34.65 ($w_{1/2}$ = 303 Hz, 9H), 3.31 ($w_{1/2}$ = 37 Hz, 4H), 1.58 ($w_{1/2}$ = 12 Hz, 4H), -4.97 ($w_{1/2}$ = 42 Hz, 4H), -61.48 ($w_{1/2}$ = 406 Hz, 12H), -69.12 ($w_{1/2}$ = 68 Hz, 2H). NMR spectrum is in agreement with literature precedence.[8]
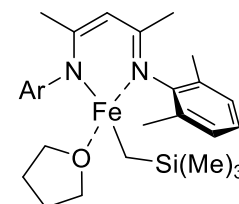
100

Synthesis of 2,4-bis[(2,6-dimethylphenyl)imino]pentane iron *N,N*-diethylamide (3.3). In the glovebox, to a 20 mL scintillation vial equipped with magnetic stir bar was added 2,4-bis[(2,6-dimethylphenyl)imino]pentane iron CH$_2$TMS tetrahydrofuran adduct (**3.2**) (200 mg, 390 umol) and pentane (5 mL). To this mixture was added diethylamine (40 uL, 1.0 equiv). The resulting mixture was allowed to stir overnight, turning from yellow to red-orange. The reaction vessel was transferred to the freezer to recrystallize overnight. The pentane was decanted and the resultant red-orange solid washed with fresh cold pentane, and residual pentane removed *in vacuo* to afford the product as a red-orange solid (150 mg, 90% yield). δ 121.30 ($w_{1/2}$ = 780 Hz, 1H), 50.20 ($w_{1/2}$ = 961 Hz, 6H), 37.77 ($w_{1/2}$ = 355 Hz, 6H), -14.89 ($w_{1/2}$ = 97 Hz, 4H), -73.44 ($w_{1/2}$ = 110 Hz, 2H), -78.58 ($w_{1/2}$ = 530 Hz, 12H). IR: 1506, 1378, 1173, 1096, 765 cm^{-1}. Elemental analysis for C$_{25}$H$_{35}$FeN$_3$ calc'd C 69.28% H 8.14% N 9.70% Found C 68.6% H 7.65% N 9.45%.
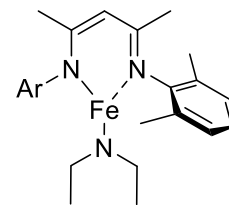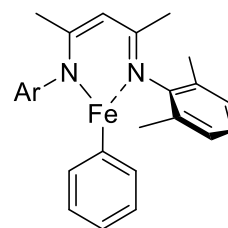
Synthesis of 2,4-bis[(2,6-dimethylphenyl)imino]pentane iron phenyl (3.4). In the glovebox, to a 7 mL scintillation vial was added 2,4-bis[(2,6-dimethylphenyl)imino]pentane iron *N,N*-diethylamide (**3.3**) (100 mg, 190 μmol) and diethyl ether (1 mL). To this mixture was added phenylboronic acid pinacol ester (42 mg, 200 μmol). The resulting mixture was cooled in a glovebox freezer to -40 °C, turning from red-orange to yellow-black. After approximately one hour, the product precipitated as black metallic crystals that were of X-ray quality. The diethyl ether was decanted and the resultant solid was washed with fresh cold pentane (3 x 1 mL) to remove residual boron-containing compounds. Residual pentane was removed *in vacuo* to afford the product as a pure black solid (42 mg, 50% yield). ^{1}H NMR (600 MHz, C$_6$D$_6$) δ 158.37 ($w_{1/2}$ = 585 Hz, 1H), 116.81 ($w_{1/2}$ = 832 Hz, 1H), 71.76 ($w_{1/2}$ = 635 Hz, 6H), 23.39 ($w_{1/2}$ = 410 Hz, 2H), -6.76 ($w_{1/2}$ = 383 Hz,

4H), -72.87 ($w_{1/2}$ = 709 Hz, 12H), -78.37 ($w_{1/2}$ = 365 Hz, 2H). IR: 1518, 1377, 1180, 757, 709 cm^{-1}. Elemental analysis for $C_{27}H_{30}FeN_2$ calc'd C 73.97% H 6.90% N 6.39% Found C % H % N %.

Procedure for the stoichiometric reaction of complex 3.4 with bromocycloheptane. In a nitrogen-filled glovebox, complex **3.3** (12 mg, 0.03 mmol) was dissolved in C_6D_6 (0.5 mL) and transferred into a J. Young tube. A solution of phenylboronic acid pinacol ester (5.6 mg, 0.03 mmol) in C_6D_6 (0.1 mL) was then added. The reaction was checked by ^1H NMR to verify that complex **3.3** had fully converted to **3.4**. Bromocycloheptane (4.9 mg, 3.8 μL, 0.03 mmol) was added to the tube, it was sealed and then shaken to fully mix. Over the course of the next 24 hours, the reaction was checked periodically by ^1H NMR until complex **3.4** was fully consumed to generate **3.5**.

Synthesis of 1,1,1,5,5,5-hexafluoro-2,4-bis[(2,6-dimethylphenyl)imino]pentane iron chloride complex (3.6). Synthesized according to general procedure using 1,1,1,5,5,5-hexafluoro-2,4-bis[(2,6-dimethylphenyl)imino]pentane (0.95 g, 2.3 mmol) **(3.6a)** as the ligand which resulted in the formation of a dark red-purple crystalline solid (1.44 g, 90% yield). ^1H NMR (400 MHz, THF) δ -53.9 ($w_{1/2}$ = 89 Hz, 1H), 15.5 ($w_{1/2}$ = 356 Hz, 12H), 18.7 ($w_{1/2}$ = 760 Hz, 4H ppm. IR: 1564, 1173, 1136, 769 cm^{-1}. Elemental analysis for $C_{21}H_{19}Cl_2F_6FeLiN_2(C_4H_8O)_{2.08}$ calc'd C 57.92% H 5.91% N 4.61% Found C 49.27% H 5.03% N 3.88%.
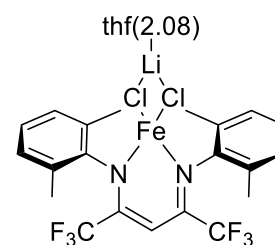
Synthesis of 1,1,1,5,5,5-hexafluoro-2,4-bis[(2,6-dimethylphenyl)imino]pentane (3.6a). Synthesized according to an alternate literature procedure[9] using 2,6-dimethylaniline (10.5 g, 86.5

102
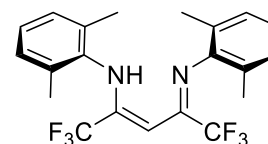
mmol) and 1,1,1,5,5,5-hexafluoro-2,4-pentanedione (3 g, 14.4 mmol) and afforded the product as a yellow crystalline solid (2.2 g, 37% yield). ^{1}H NMR (500 MHz, CDCl$_3$) δ 11.87 (s, 1H), 7.08 – 7.00 (m, 6H), 5.89 (s, 1H), 2.16 (s, 12H) ppm. ^{19}F NMR (470 MHz, CDCl$_3$) δ -67.7 ppm. NMR spectrum is in agreement with literature precedence.[9]

Synthesis of 2,4-bis[(2-*tert*-butylphenyl)imino]pentane iron chloride complex (3.7). Synthesized according to general procedure using 2,4-bis[(2-*tert*-butylphenyl)imino]pentane (860 mg, 2.4 mmol) **(6a)** as the ligand which resulted in the formation of a yellow crystalline
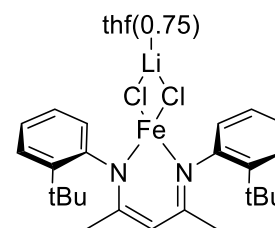
solid (1.25 g, 82% yield). ^{1}H NMR (of the major rotameric species) (400 MHz, THF) δ -62.3 ($w_{1/2}$ = 137 Hz, 6H), -48.1 ($w_{1/2}$ = 69 Hz, 2H), -46.5 ($w_{1/2}$ = 206 Hz, 1H), -5.1 ($w_{1/2}$ = 210 Hz, 18H), 14.3 ($w_{1/2}$ = 60 Hz, 2H) 16.7 (three overlapping peaks, 4H) ppm. IR: 2914, 1377, 1187, 1037, 754 cm^{-1}. Elemental analysis for C$_{25}$H$_{33}$Cl$_2$FeLiN$_2$(C$_4$H$_8$O)$_{0.75}$ calc'd C 62.46% H 8.07% N 3.94% Found C 54.29% H 6.44% N 4.61%.

Synthesis of 2,4-bis[(2-*tert*-butylphenyl)imino]pentane (3.7a). Synthesized from 2-*tert*-butylaniline (8.67 g, 58 mmol) and 2,4-pentanedione (2.53 g, 25 mmol) according to the general procedure
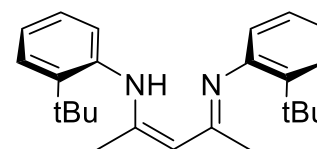
which afforded light yellow needles (6.2 g, 67% yield). ^{1}H NMR (500 MHz, CDCl$_3$) δ 12.52 (s, 1H), 7.34 (d, J = 7.9 Hz, 2H), 7.13 (t, J = 7.7 Hz, 2H), 7.04 (t, J = 7.5 Hz, 2H), 6.80 (d, J = 7.7 Hz, 2H), 4.92 (s, 1H), 1.83 (s, 6H), 1.29 (s, 18H). ^{13}C NMR (126 MHz, CDCl$_3$) δ 159.39, 144.72, 143.17, 126.31, 126.24, 126.04, 123.94, 96.73, 35.03, 30.36, 21.13. NMR spectra are in agreement with literature precedence.[10]

103

Synthesis of 2,4-bis[(2-isopropylphenyl)imino]pentane iron chloride complex (3.8). Synthesized according to the general procedure using 2,4-bis[(2-isopropylphenyl)imino]pentane (1.35 g, 4.0 mmol) **(3.8a)** as the ligand which resulted in the formation of a yellow-orange crystalline solid (1.0 g, 40% yield). ^{1}H NMR (400 MHz, THF) δ -67.2 ($w_{1/2}$ = 161 Hz, 6H), -50.2 ($w_{1/2}$ = 68 Hz, 1H), -49.5 ($w_{1/2}$ = 61 Hz, 1H), -22.7 ($w_{1/2}$ = 116 Hz, 3H), -21.0 ($w_{1/2}$ = 186 Hz, 3H), -1.6 ($w_{1/2}$ = 59 Hz, 3H), 15.2 ($w_{1/2}$ = 42 Hz, 1H), 15.7 ($w_{1/2}$ = 32 Hz, 1H), 16.2 ($w_{1/2}$ = 50 Hz, 1H) ppm. IR: 3100, 1594, 1378, 1030, 751, 697 cm^{-1}. Elemental analysis for $C_{23}H_{29}Cl_2FeLiN_2(C_4H_8O)_1$ calc'd C 69.37% H 7.98% N 5.99% Found C 52.29% H 6.14% N 4.66%.
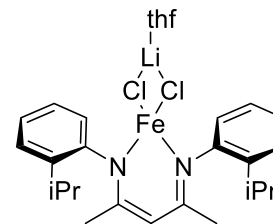
Synthesis of 2,4-bis[(2-isopropylphenyl)imino]pentane (3.8a). Synthesized from 2-isopropylaniline (6.76 g, 50 mmol) and 2,4-pentanedione (2.38 g, 23.8 mmol) according to the general procedure with distillation of residual aniline required to obtain the light yellow crystalline product (1.3 g, 16% yield). ^{1}H NMR (400 MHz, CDCl$_3$) δ 12.45 (br s, 1H), 7.25 (m, 2H), 7.10 (m, 4H), 6.88 (m, 2H), 4.90 (s, 1H), 3.18 (p, J = 6.9 Hz, 2H), 1.88 (s, 6H), 1.15 (d, J = 6.9 Hz, 12H). NMR spectrum is in agreement with literature precedence.[11]
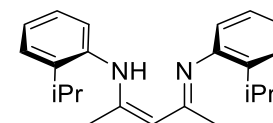
Synthesis of 2,4-bis[(2-ethylphenyl)imino]pentane iron chloride complex (3.9). Synthesized according to the general procedure using 2,4-bis[(2-ethylphenyl)imino]pentane (1.45 g, 4.7 mmol) **(3.9a)** as the ligand which resulted in the formation of a yellow-orange crystalline solid (0.90 g, 33% yield). ^{1}H NMR (400 MHz, THF) δ -67.2 ($w_{1/2}$ = 162 Hz, 6H), -52.1 ($w_{1/2}$ = 187
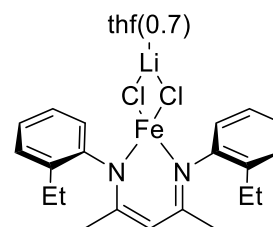
Hz, 2H), -14.2 ($w_{1/2}$ = 103 Hz, 3H), -11.3 ($w_{1/2}$ = 132 Hz, 3H), 15.9 ($w_{1/2}$ = 289 Hz, 4H) ppm. IR: 2963, 1518, 1373, 1021, 740 cm^{-1}. Elemental analysis for $C_{21}H_{25}Cl_2FeLiN_2(C_4H_8O)_{0.7}$ calc'd C 67.64% H 7.30% N 6.63% Found C 53.35% H 5.87% N 5.35%.

Synthesis of 2,4-bis[(2-ethylphenyl)imino]pentane (3.9a). Synthesized from 2-ethylaniline (7.99 g, 66 mmol) and 2,4-pentanedione (3 g, 30 mmol) according to the general procedure with distillation of residual aniline required to obtain the light yellow crystalline product (1.45 g, 16% yield). ^{1}H NMR (400 MHz, CDCl$_3$) δ 12.50 (s, 1H), 7.22 – 7.09 (m, 4H), 7.03 (t, J = 7.4 Hz, 2H), 6.89 (d, J = 7.7 Hz, 2H), 4.89 (s, 1H), 2.57 (q, J = 7.5 Hz, 4H), 1.89 (s, 6H), 1.12 (t, J = 7.5 Hz, 6H). NMR spectrum is in agreement with literature precedence.[10]
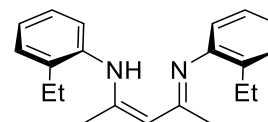
Synthesis of 2,4-bis[(2-methylphenyl)imino]pentane iron chloride complex (3.10). Synthesized according to the general procedure using 2,4-bis[(2-methylphenyl)imino]pentane (2.8 g, 9.9 mmol) **(3.10a)** as the ligand which resulted in a yellow-orange crystalline solid (1.1 g, 20% yield). A bisligated iron species is very difficult to remove from this compound and was done by sequential recrystallization from pentane at -40 °C. ^{1}H NMR (400 MHz, THF) δ -20.6 ($w_{1/2}$ = 427 Hz, 4H), -15.1 ($w_{1/2}$ = 169 Hz, 2H), -10.4 ($w_{1/2}$ = 180 Hz, 1H), 12.4 ($w_{1/2}$ = 180 Hz, 6H), 98.2 ($w_{1/2}$ = 437 Hz, 4H) ppm. IR: 3301, 1665, 1539, 1320, 752, 691 cm^{-1}. Elemental analysis for $C_{19}H_{21}Cl_2FeLiN_2(C_4H_8O)_{0.05}$ calc'd C 64.40% H 6.02% N 7.82% Found C 68.77% H 6.49% N 8.28%.
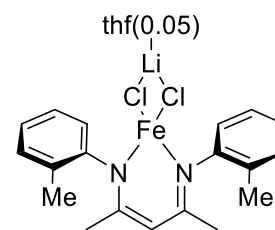
Synthesis of 2,4-bis[(2-methylphenyl)imino]pentane (3.10a).
Synthesized from 2-methylaniline (10 g, 93 mmol) and 2,4-pentanedione (4.45g, 44 mmol) according to the general procedure with distillation of residual aniline required to obtain the light yellow crystalline product (2.76 g, 22% yield). ^{1}H NMR (400 MHz, CDCl$_3$) δ 12.52 (br s, 1H), 7.20 – 7.10 (m, 4H), 7.02 – 6.88 (m, 4H), 4.90 (s, 1H), 2.19 (s, 6H), 1.90 (s, 6H) ppm. NMR spectrum is in agreement with literature precedence.[12]
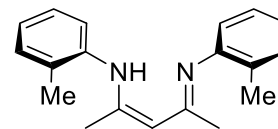
Synthesis of 2,4-bis[(2,4,6-trimethylphenyl)imino]pentane iron chloride complex (3.11). Synthesized according to general procedure using 2,4-bis[(2,4,6-trimethylphenyl)imino]pentane (2.0 g, 6 mmol) **(3.11a)** as the ligand which resulted in the formation of a bright yellow crystalline solid (1.9 g, 52% yield). ^{1}H NMR (400 MHz, THF) δ -71.6 ($w_{1/2}$ = 145 Hz, 6H), -41.3 ($w_{1/2}$ = 227 Hz, 1H), 6.7 ($w_{1/2}$ = 238 Hz, 12H), 16.6 ($w_{1/2}$ = 71 Hz, 4H), 45.1 ($w_{1/2}$ = 41 Hz, 6H) ppm. IR: 2883, 1524, 1375, 1198, 1038, 759 cm^{-1}. Elemental analysis for C$_{23}$H$_{29}$Cl$_2$FeLiN$_2$(C$_4$H$_8$O)$_2$ calc'd C 71.11% H 8.66% N 5.35% Found C 58.63% H 7.15% N 4.35%.
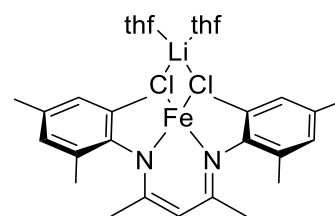
Synthesis of 2,4-bis[(2,4,6-trimethylphenyl)imino]pentane (3.11a). Synthesized from 2,4,6-trimethylaniline (10.9 g, 80.4 mmol) and 2,4-pentanedione (3.5 g, 35 mmol) according to the general procedure which afforded a tan crystalline solid (6 g, 51% yield). ^{1}H NMR (400 MHz, CDCl$_3$) δ 12.13 (s, 1H), 6.84 (s, 4H), 4.84 (s, 1H), 2.24 (s, 6H), 2.10 (s, 12H), 1.67 (s, 6H). NMR spectrum is in agreement with literature precedence.[13]
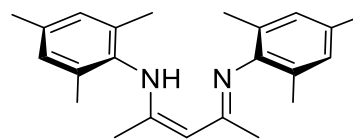
106

Synthesis of 2,4-bis[(4-bromo-2,6-dimethylphenyl)imino]pentane iron chloride complex (3.12). Synthesized according to general procedure using 2,4-bis[(4-bromo-2,6-dimethylphenyl)imino]pentane (2.1 g, 4.5 mmol) (3.12a) as the ligand which resulted in the formation of a brown solid (2.1 g, 62% yield). ^{1}H NMR (500 MHz, THF) δ -64.5 ($w_{1/2}$ = 133 Hz, 6H), -35.5 ($w_{1/2}$ = 196 Hz, 1H), 6.1 ($w_{1/2}$ = 231 Hz, 12H), 16.1 ($w_{1/2}$ = 56 Hz, 4H) ppm. IR: 2974, 1573, 1375, 1180, 1039, 851 cm^{-1}. Elemental analysis for $C_{21}H_{23}Br_2Cl_2FeLiN_2(C_4H_8O)_{1.6}$ calc'd C 52.16% H 5.72% N 4.44% Found C 43.30% H 4.75% N 3.70%.
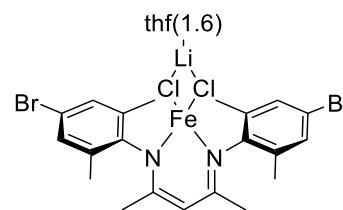
Synthesis of 2,4-bis[(4-bromo-2,6-dimethylphenyl)imino]pentane (3.12a). Synthesized from 4-bromo-2,6-dimethylaniline (10 g, 50 mmol) and 2,4-pentanedione (2.38 g, 23.8 mmol) according to the general procedure which afforded a brown solid (2.5 g, 23% yield). ^{1}H NMR (400 MHz, CDCl$_3$) δ 11.96 (s, 1H), 7.18 (s, 4H), 4.89 (s, 1H), 2.12 (s, 12H), 1.67 (s, 6H). ^{13}C NMR (101 MHz, CDCl$_3$) δ 161.23, 142.88, 134.46, 130.63, 117.36, 94.28, 20.49, 18.30, 17.03, 14.35. IR: 2917, 1618, 1546, 1462, 1432, 1374, 1280, 1177, 1025, 990, 861, 846, 731 cm^{-1}. HRMS (ESI) m/z [M]$^+$ calculated for $C_{21}H_{25}N_2Br_2$ 463.03790; found 463.03720.
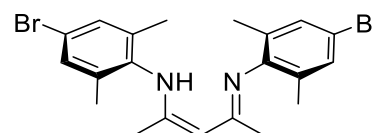
Synthesis of 2,4-bis[(4-methoxy-2,6-dimethylphenyl)imino]pentane iron chloride complex (3.13). Synthesized according to general procedure using 2,4-bis[(4-methoxy-2,6-dimethylphenyl)imino]pentane (400
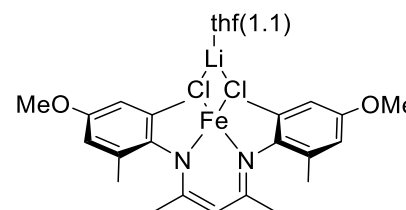
mg, 1.1 mmol) **(3.13a)** as the ligand which resulted in the formation of a yellow crystalline solid (400 mg, 56% yield). ^{1}H NMR (400 MHz, THF) δ -74.3 ($w_{1/2}$ = 197 Hz, 6H), -42.3 ($w_{1/2}$ = 310 Hz, 1H), 2.7 ($w_{1/2}$ = 82 Hz, 6H), 6.2 ($w_{1/2}$ = 244 Hz, 12H), 15.4 ($w_{1/2}$ = 74 Hz, 4H) ppm. IR: 2914, 1600, 1376, 1187, 1037, 892 cm^{-1}. Elemental analysis for $C_{23}H_{29}Cl_2FeLiN_2O_2(C_4H_8O)_{1.1}$ calc'd C 65.16% H 7.54% N 5.55% Found C 50.80% H 5.90% N 4.32%.

Synthesis of 2,4-bis[(4-methoxy-2,6-dimethylphenyl)imino]pentane (3.13a). Synthesized from 4-methoxy-2,6-dimethylaniline (1.93 g, 12.8 mmol) and 2,4-pentanedione (580 mg, 5.8 mmol) according to the general procedure which afforded a tan solid (410 mg, 19% yield). ^{1}H NMR (600 MHz, CDCl$_3$) δ 12.09 (s, 1H), 6.59 (s, 4H), 4.83 (s, 1H), 3.75 (s, 6H), 2.12 (s, 12H), 1.66 (s, 6H). ^{13}C NMR (101 MHz, CDCl$_3$) δ 161.67, 156.26, 137.22, 133.26, 113.10, 93.51, 55.48, 20.39, 18.77. IR: 3274, 2918, 2834, 1619, 1550, 1475, 1435, 1317, 1272, 1180, 1147, 1062, 850, 835, 727, 708 cm^{-1}. HRMS (ESI) m/z [M]$^+$ calculated for $C_{23}H_{31}N_2O_2$ 367.23800; found 367.23763.
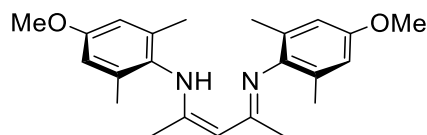
Synthesis of 2,4-bis[(2,6-diisopropylphenyl)imino]pentane iron chloride complex (3.14). Synthesized according to general procedure using 2,4-bis[(2,6-diisopropylphenyl)imino]pentane (5.0 g, 11.9 mmol) **(3.14a)** as the ligand which resulted in the formation of a yellow crystalline solid (4.0 g, 48% yield). ^{1}H NMR (400 MHz, THF) δ 15.28 ($w_{1/2}$ = 40 Hz, 4H), 2.23 ($w_{1/2}$ = 51 Hz, 12H), -16.55 ($w_{1/2}$ = 115 Hz, 12H), -42.97 ($w_{1/2}$ = 56 Hz, 2H), -63.88 ($w_{1/2}$ = 116 Hz, 6H). NMR spectrum is in agreement with literature precedence.[4]
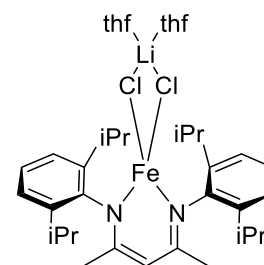
Synthesis of 2,4-bis[(2,6-diisopropylphenyl)imino]pentane (3.14a). Synthesized from 2,6-diisopropylaniline (29.8 g, 168 mmol) and 2,4-pentanedione (8.0 g, 80 mmol) according to the general procedure which afforded a white crystalline solid (21 g, 63% yield). ^{1}H NMR (500 MHz, CDCl$_3$) δ 12.11 (s, 1H), 7.12 (m, 6H), 4.87 (s, 1H), 3.11 (septet, J = 6.9 Hz, 4H), 1.72 (s, 6H), 1.21 (d, J = 6.9 Hz, 12H), 1.12 (d, J = 6.9 Hz, 12H). NMR spectrum is in agreement with literature precedence.[14]
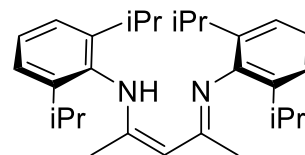
Synthesis of 2,4-bis(phenyl)imino]pentane iron chloride complex (3.15). Synthesized according to general procedure using 2,4-bis[(phenyl)imino]pentane (0.308 g, 1.2 mmol) **(3.15a)** as the ligand which resulted in the formation of a brown-white tacky solid (0.25 g, 39% yield). ^{1}H NMR (400 MHz, THF) δ 98.01 ($w_{1/2}$ = 428 Hz, 4H), 12.37 ($w_{1/2}$ = 179 Hz, 6H), -13.47 ($w_{1/2}$ = 75 Hz, 1H), -15.05 ($w_{1/2}$ = 163 Hz, 2H), -20.53 ($w_{1/2}$ = 363 Hz, 4H) ppm. NMR spectrum is in agreement with literature precedence.[15]
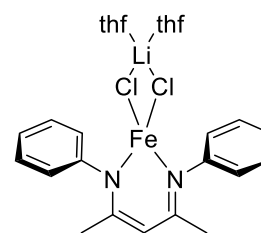
Synthesis of 2,4-bis[(2,6-diisopropylphenyl)imino]pentane (3.15a). Synthesized from aniline (9.52 g, 102 mmol) and 2,4-pentanedione (4.45 g, 44.5 mmol) according to the general procedure which afforded a colorless crystalline solid (1.1 g, 10% yield). ^{1}H NMR (500 MHz, CDCl$_3$) δ 12.61 (s, 1H), 7.44 (d, J = 7.4 Hz, 4H), 7.13 (m, 4H), 6.88 (m, 2H), 4.87 (s, 1H), 1.90 (s, 6H) ppm. NMR spectrum is in agreement with literature precedence.[16]
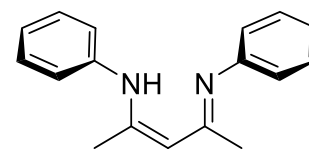
General procedure A for cross-coupling reaction of alkyl halides and aryl boronic esters. In a nitrogen-filled glovebox, iron complex (0.05 mmol) and lithium ethylmethyl amide (0.60 mmol)

109

were added to a 7 mL vial containing a stir bar. A 1 mL benzene solution of boronic acid pinacol ester (1.0 mmol) and alkyl halide (0.50 mmol) was added to the stirring vial followed immediately by benzene (5 mL). The reaction was allowed to stir vigorously and quickly became homogenous. Typically, the reaction turns a dark red-black, though in the case of certain heteroaromatic boronic esters exotic colors have been observed. After 24 hours of stirring, the reaction was brought out of the glovebox and quenched with a saturated aqueous solution of ammonium chloride (10 mL). The aqueous phase was washed with dichloromethane (3 x 40 mL) and the combined organic phases were dried over sodium sulfate and filtered. Trimethoxybenzene (42 mg, 0.25 mmol) was added as an internal standard before evaporating the solvent *in vacuo*. An estimated yield was determined by analyzing the ^{1}H NMR spectrum of the crude reaction mixture, and yields based on recovered starting material were calculated from this spectrum. The product was then purified by silica gel flash column chromatography.

General procedure B for cross-coupling reaction of alkyl halides and aryl boronic esters. In a nitrogen-filled glovebox, iron complex (0.05 mmol) and lithium ethylmethyl amide (0.60 mmol) were added to a 7 mL vial containing a stir bar. A 1 mL benzene solution of boronic acid pinacol ester (0.75 mmol) and alkyl halide (0.50 mmol) was added to the stirring vial followed immediately by benzene (5 mL) and sealing of the reaction vessel. In some cases, the sealed reaction was removed from the glovebox and heated to 50 °C. The reaction was allowed to stir vigorously and quickly became homogenous. Typically, the reaction turns a dark red-black, though in the case of certain heteroaromatic boronic esters exotic colors have been observed After 24 hours of stirring, the reaction was quenched with a saturated aqueous solution of ammonium chloride (10 mL). The aqueous phase was washed with dichloromethane (3 x 40 mL) and the combined organic phases were dried over sodium sulfate and filtered. Trimethoxybenzene (42 mg, 0.25 mmol) was added

as an internal standard before evaporating the solvent *in vacuo*. An estimated yield was determined by analyzing the ^{1}H NMR spectrum of the crude reaction mixture, and yields based on recovered starting material were calculated from this spectrum. The product was then purified by silica gel flash column chromatography.

Synthesis of 2-cycloheptyl thiophene (3.16). 2-cycloheptyl thiophene was synthesized from bromocycloheptane and 2-thiophene boronic acid pinacol ester according to general procedure B using the 2-*tert*-butylphenyl catalyst **5** and purified by silica gel flash column chromatography, eluting with 100% hexanes (R_f = 0.75) to afford the product as a colorless oil (26 mg, 67% spectroscopic yield, 73% based on recovered starting material, 58% isolated yield). ^{1}H NMR (500 MHz, CDCl$_3$) δ 7.09 (dd, J = 5.1, 1.2 Hz, 1H), 6.90 (dd, J = 5.1, 3.4 Hz, 1H), 6.78 (d, 1H), 3.03 (septet, J = 4.6 Hz, 1H), 2.12 – 2.03 (m, 1H), 1.81 – 1.64 (m, 4H), 1.57 – 1.48 (m, 5H). ^{13}C NMR (126 MHz, CDCl$_3$) δ 153.65, 126.32, 122.00, 121.69, 41.61, 37.53, 28.13, 26.32. IR: 2923, 2853, 1459, 1442, 1234, 850, 815, 689 cm^{-1}. HRMS-DART (*m/z*): [M+H]$^+$ calculated for C$_{11}$H$_{16}$S, 180.31; found, 181.10.
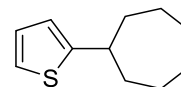
Synthesis of 3-cycloheptyl thiophene (3.17). 3-cycloheptyl thiophene was synthesized from bromocycloheptane and 3-thiophene boronic acid pinacol ester according to general procedure B using the 2-*tert*-butylphenyl catalyst 5 and purified by silica gel flash column chromatography, eluting with 100% hexanes (R_f = 0.75) to afford the product as a yellow oil (37 mg, 88% spectroscopic yield, 88% based on recovered starting material, 82% isolated yield). ^{1}H NMR (500 MHz, CDCl$_3$) δ 7.22 (t, J = 3.9 Hz, 1H), 6.97 (d, J = 5.0 Hz, 1H), 6.91 (s, 1H), 2.83 (septet, J = 9.9, 4.0 Hz, 1H), 1.98 (m, 2H), 1.80 – 1.72 (m, 2H), 1.71 – 1.47 (m, 8H). [13]C
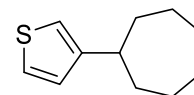
111

NMR (126 MHz, CDCl$_3$) δ 150.46, 127.34, 125.09, 118.10, 41.93, 36.39, 28.26, 26.80. IR: 2921, 2853, 1459, 771, 645 cm^{-1}. HRMS-DART (*m/z*): [M+H]$^+$ calculated for C$_{11}$H$_{16}$S, 180.31; found, 181.10.

Synthesis of 2-octylthiophene (3.18). 2-octylthiophene was synthesized from 1-bromooctane and 2-thiophene boronic acid pinacol ester according to general procedure B using the 2-*tert*-butylphenyl catalyst 5 and purified by silica gel flash column chromatography, eluting with 100% hexanes (R$_f$ = 0.65) to afford the product as a colorless oil (12 mg, 28% spectroscopic yield, 72% based on recovered starting material, 25% isolated yield). ^{1}H NMR (400 MHz, CDCl$_3$) δ 7.10 (d, J = 5.1 Hz, 1H), 6.91 (dd, J = 5.1, 3.4 Hz, 1H), 6.77 (d, J = 3.4 Hz, 1H), 2.82 (t, J = 7.7 Hz, 2H), 1.67 (p, J = 7.5 Hz, 2H), 1.40 – 1.23 (m, 10H), 0.88 (t, J = 6.7 Hz, 3H). ^{13}C NMR (101 MHz, CDCl3) δ 146.05, 126.77, 124.02, 122.84, 32.01, 31.96, 30.07, 29.48, 29.37, 29.29, 22.81, 14.25. IR: 2925, 2854, 1464, 907, 733, 690 cm^{-1}. HRMS-DART (*m/z*): [M+H]$^+$ calculated for C$_{12}$H$_{20}$S, 196.35; found, 197.14.
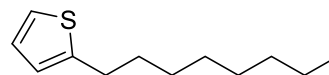
Synthesis of 3-octylthiophene (3.19). 3-octylthiophene was synthesized from 1-bromooctane and 3-thiophene boronic acid pinacol ester according to general procedure B using the 2-*tert*-butylphenyl catalyst 5 and heated to 50 °C, then purified by silica gel flash column chromatography, eluting with 100% hexanes (R$_f$ = 0.65) to afford the product as a colorless oil (30 mg, 64% spectroscopic yield, 90% based on recovered starting material, 61% isolated yield). ^{1}H NMR (400 MHz, CDCl$_3$) δ 7.23 (m, 1H), 6.96 – 6.89 (m, 2H), 2.62 (t, J = 7.7 Hz, 2H), 1.62 (p, J = 7.3 Hz, 2H), 1.37 – 1.25 (m, 10H), 0.88 (t, J = 6.5 Hz, 3H). ^{13}C NMR (101 MHz, CDCl$_3$) δ 143.44, 128.45, 125.16, 119.89, 32.04, 30.72, 30.44, 29.59, 29.50, 29.41, 22.82,
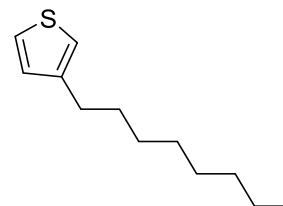
14.26. IR: 2925, 2854, 1465, 907, 773, 733 cm^{-1}. HRMS-DART (*m/z*): [M+H]$^+$ calculated for C$_{12}$H$_{20}$S, 196.35; found, 197.14.

Synthesis of 3-cycloheptyl furan (3.20). 3-cycloheptyl furan was synthesized from bromocycloheptane and 3-furyl boronic acid pinacol ester according to general procedure B using the 2-*tert*-butylphenyl catalyst 5 and purified by silica gel flash column chromatography, eluting with 100% hexanes (R$_f$ = 0.95) to afford the product as a colorless oil (10 mg, 70% spectroscopic yield, 70% based on recovered starting material, 61% isolated yield). ^{1}H NMR (500 MHz, CDCl$_3$) δ 7.33 (s, 1H), 7.19 (s, 1H), 6.28 (s, 1H), 2.63 (septet, 1H), 1.94 (m, 2H), 1.71 (m, 2H), 1.68 – 1.62 (m, 2H), 1.57 – 1.48 (m, 6H). ^{13}C NMR (126 MHz, CDCl$_3$) δ 142.64, 137.53, 132.61, 110.10, 36.88, 35.77, 28.34, 26.50. IR: 2925, 2855, 1752, 1448, 1346, 1073, 1014 cm^{-1}. HRMS-DART (*m/z*): [M+H]$^+$ calculated for C$_{11}$H$_{16}$O, 164.25; found, 165.13.
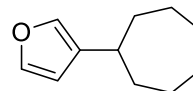
Synthesis of 3-cycloheptyl quinoline (3.22). 3-cycloheptyl quinoline was synthesized from bromocycloheptane and 3-quinolyl boronic acid pinacol ester according to general procedure B using the 2-*tert*-butylphenyl catalyst 5 and heated to 50 °C, then purified by silica gel flash column chromatography, eluting with 30% ethyl acetate in hexanes (R$_f$ = 0.65) to afford the product as a colorless oil (23 mg, 45% spectroscopic yield, 58% based on recovered starting material, 40% isolated yield). ^{1}H NMR (500 MHz, CDCl$_3$) δ 8.81 (s, 1H), 8.08 (s, 1H), 7.92 (s, 1H), 7.78 (d, J = 8.2 Hz, 1H), 7.65 (s, 1H), 7.52 (s, 1H), 2.90 (septet, 1H), 2.03 – 2.00 (m, 2H), 1.90 – 1.83 (m, 2H), 1.82 – 1.70 (m, 4H), 1.70 – 1.57 (m, 4H). ^{13}C NMR (151 MHz, CDCl$_3$) δ 151.50, 146.88, 142.35, 132.20, 129.19, 128.57, 128.45, 127.59, 126.60, 44.61, 36.69, 28.03,
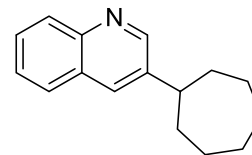
27.29. IR: 2922, 2853, 1493, 1460, 787, 750 cm^{-1}. HRMS-DART (*m/z*): [M+H]$^+$ calculated for C$_{16}$H$_{19}$N, 225.34; found, 226.16.

Synthesis of 6-cycloheptyl quinoline (3.23). 6-cycloheptyl quinoline was synthesized from bromocycloheptane and 6-quinolyl boronic acid pinacol ester according to general procedure B using the 2-*tert*-butylphenyl catalyst 5 and heated to 50 °C, then purified by silica gel flash column chromatography, eluting with 30% ethyl acetate in hexanes (R$_f$ = 0.45) to afford the product as a colorless oil (42 mg, 80% spectroscopic yield, 93% based on recovered starting material, 75% isolated yield). ^{1}H NMR (500 MHz, CDCl$_3$) δ 8.85 (d, J = 4.2 Hz, 1H), 8.10 (d, J = 8.4 Hz, 1H), 8.03 (d, J = 8.6 Hz, 1H), 7.63 – 7.55 (m, 2H), 7.36 (dd, J = 8.3, 4.2 Hz, 1H), 2.87 (septet, 1H), 2.05 – 1.96 (m, 2H), 1.89 – 1.81 (m, 2H), 1.81 – 1.68 (m, 4H), 1.68 – 1.57 (m, 4H). ^{13}C NMR (101 MHz, CDCl$_3$) δ 149.59, 148.41, 147.16, 135.90, 129.98, 129.39, 128.52, 124.16, 121.11, 47.04, 36.84, 28.10, 27.41. IR: 2921, 2853, 1593, 1498, 1459, 827 cm^{-1}. HRMS-DART (*m/z*): [M+H]$^+$ calculated for C$_{16}$H$_{19}$N, 225.34; found, 226.16.
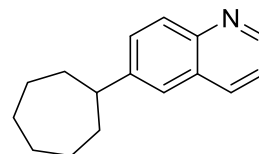
Synthesis of 5-cycloheptyl-1-*N*-Boc-indole (3.25). 5-cycloheptyl-1-*N*-Boc-indole was synthesized from bromocycloheptane and 1-Boc-indole-5-boronic acid pinacol ester according to general procedure A using the 2-*tert*-butylphenyl catalyst 5 and heated to 50 °C, then purified by silica gel flash column chromatography, eluting with 10% ethyl acetate in hexanes (R$_f$ = 0.30) to afford the product as a colorless oil (40 mg, 61% spectroscopic yield, 51% based on recovered starting material, 75% isolated yield). ^{1}H NMR (500 MHz, CDCl$_3$) δ 8.06 – 7.98 (m, 1H), 7.62 – 7.54 (m, 1H), 7.37 (d, *J* = 1.8 Hz, 1H), 7.16 (dd, *J* = 8.6, 1.8 Hz, 1H), 6.51 (dd, *J* = 3.7, 0.8 Hz, 1H), 2.76 (tt, *J* = 10.6, 3.6 Hz, 1H), 2.00
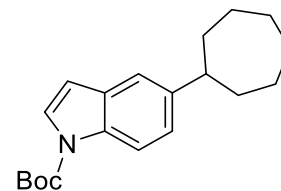
– 1.91 (m, 2H), 1.91 – 1.78 (m, 1H), 1.80 – 1.65 (m, 12H), 1.67 (s, 9H), 1.65 – 1.58 (m, 1H), 1.61 – 1.50 (m, 1H). ^{13}C NMR (126 MHz, CDCl$_3$) δ 144.63, 130.68, 125.87, 123.44, 118.35, 114.87, 107.26, 83.36, 46.98, 37.28, 31.58, 28.20, 27.98, 27.26, 22.64, 14.10. IR: 2925, 2854, 1733, 1469, 1369, 1253, 1161 cm^{-1}. HRMS-DART (*m/z*): [M+H]$^+$ calculated for C$_{20}$H$_{27}$NO$_2$, 313.44; found, 314.21.

Synthesis of 6-(4-Boc-piperazin-1-yl)-3-cycloheptyl pyridine

(3.28). 6-(4-Boc-piperazin-1-yl)-3-cycloheptylpyridine was synthesized from bromocycloheptane and 6-(4-Boc-piperazin-1-yl)pyridine-3-boronic acid pinacol ester according to general
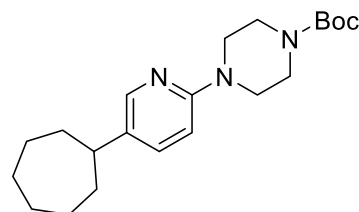
procedure B using the 2-*tert*-butylphenyl catalyst 5 and purified by silica gel flash column chromatography, eluting with 30% ethyl acetate in hexanes (R$_f$ = 0.75) to afford the product as a white solid (66 mg, 81% spectroscopic yield, 87% based on recovered starting material, 74% isolated yield). ^{1}H NMR (500 MHz, CDCl$_3$) δ 8.04 (s, 1H), 7.35 (d, J = 8.7 Hz, 1H), 6.60 (d, J = 8.7 Hz, 1H), 3.54 (m, 4H), 3.46 (m, 4H), 2.58 (septet, 1H), 1.85 (m, 2H), 1.77 (m, 2H), 1.68 (m, 2H), 1.64 – 1.50 (m, 6H), 1.48 (s, 9H). ^{13}C NMR (151 MHz, CDCl$_3$) δ 154.96, 146.04, 136.40, 135.11, 107.59, 80.12, 45.87, 43.57, 36.82, 29.85, 28.58, 28.02, 27.12. IR: 2923, 2855, 1697, 1604, 1408, 1365, 1238, 1168 cm^{-1}. HRMS-DART (*m/z*): [M+H]$^+$ calculated for C$_{21}$H$_{33}$N$_3$O$_2$, 359.51; found, 360.30.

Synthesis of phenylcyclobutane (3.29). Phenylcyclobutane was synthesized from bromocyclobutane and phenyl boronic acid pinacol ester according to
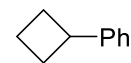
general procedure A using the 2-tert-butylphenyl catalyst 5 and purified by silica gel flash column chromatography, eluting with 100% hexanes to afford product as a colorless oil (20 mg, 63% spectroscopic yield, 63% based on recovered starting material, 61% isolated

yield). Rf = 0.70 (100% hexanes) 1H NMR (400 MHz, CDCl3): δ 7.15 – 7.33 (m, 5H), 3.56 (p, J = 8.8, 8.1 Hz, 1H), 1.81 – 2.40 (m, 6H) ppm. NMR spectrum is in agreement with literature precedence.18

Synthesis of phenylcycloheptane (3.30). Phenylcycloheptane was synthesized from bromocycloheptane and phenyl boronic acid pinacol ester according to general procedure A using the 2-tert-butylphenyl catalyst 5 and purified by silica gel flash column chromatography, eluting with 100% hexanes to afford product as a colorless oil (42 mg, 99% spectroscopic yield, 99% based on recovered starting material, 95% isolated yield). Rf = 0.60 (100% hexanes) 1H NMR (500 MHz, CDCl3): δ 7.23 – 7.33 (m, 2H), 7.08 – 7.23 (m, 2H), 2.66 (tt, J = 10.7, 3.7 Hz, 1H), 1.92 (ddt, J = 13.5, 6.6, 3.3 Hz, 2H), 1.80 (ddd, J = 13.4, 6.6, 3.4 Hz, 2H), 1.46 – 1.78 (m, 8H) ppm. NMR spectrum is in agreement with literature precedence.19
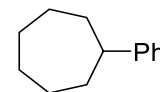
Synthesis of phenyloctane (3.31). Phenyloctane was synthesized from octylbromide and phenyl boronic acid pinacol ester according to general procedure A using the 2-tert-butylphenyl catalyst 5 and purified by silica gel flash column chromatography, eluting with 100% hexanes to afford product as a colorless oil (36 mg, 82% spectroscopic yield, 87% based on recovered starting material, 80% isolated yield). Rf = 0.60 (100% hexanes) 1H NMR (500 MHz, CDCl3) δ 7.27 (t, J = 7.4 Hz, 2H), 7.18 (d, J = 7.6 Hz, 3H), 2.60 (t, J = 7.8 Hz, 2H), 1.59 – 1.64 (m, 2H), 1.25 – 1.33 (m, 10H), 0.86 – 0.91 (t, J = 6.9 Hz, 3H) ppm. NMR spectrum is in agreement with literature precedence.19
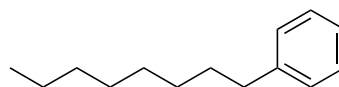
Synthesis of diphenylmethane (3.32). Diphenylmethane was synthesized from benzyl chloride and phenyl boronic acid pinacol ester according to
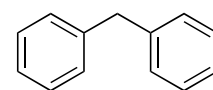
116

general procedure A using the fluorinated catalyst 9, and purified by silica gel flash column chromatography, eluting with 100% hexanes to afford product as a colorless oil (21 mg, 54% spectroscopic yield, 62% based on recovered starting material, 50% isolated yield). Rf = 0.55 (100% hexanes) 1H NMR (500 MHz, CDCl3) δ 7.27 – 7.36 (m, 4H), 7.19 – 7.28 (m, 6H), 7.20 (s, 2H), 4.01 (s, 2H) ppm. NMR spectrum is in agreement with literature precedence.[19]

Synthesis of 4-phenylpiperidine-1-carboxylic acid benzyl ester (3.33). 4-phenylpiperidine-1-carboxylic acid benzyl ester was synthesized from 4-bromopiperidine-1-carboxylic acid benzyl ester and phenyl boronic acid pinacol ester according to general procedure A using the 2-tert-butylphenyl catalyst and purified by silica gel flash column chromatography, eluting with 1:5 EtOAc/hexanes to afford product as a colorless oil (49 mg, 70% spectroscopic yield, 95% based on recovered starting material, 67% isolated yield). Rf = 0.20 (1:5 EtOAc/hexanes) 1H NMR (500 MHz, CDCl3) δ 7.26 – 7.42 (m, 7H), 7.17 – 7.25 (m, 3H), 5.16 (s, 2H), 4.32 (br s, 2H), 2.89 (t, J = 12.9 Hz, 2H), 2.67 (tt, J = 12.2, 3.6 Hz, 1H), 1.85 (d, J = 12.7 Hz, 2H), 1.56 – 1.72 (m, 2H) ppm. NMR spectrum is in agreement with literature precedence.[19]
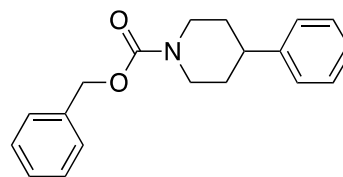
Synthesis of phenylcyclobutane (3.34). Phenylcyclobutane was synthesized from bromocyclobutane and phenyl boronic acid pinacol ester according to general procedure A using the 2-tert-butylphenyl catalyst 5 and purified by silica gel flash column chromatography, eluting with 100% hexanes to afford product as a colorless oil (28 mg, 99% spectroscopic yield, 99% based on recovered starting material, 95% isolated yield). 1H NMR (500 MHz, CDCl3) δ 7.47 (d, J = 7.4 Hz, 2H), 7.15 (t, J = 7.5 Hz, 1H), 7.09 (d, J = 7.8 Hz, 2H),
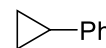
117

1.91 (tt, J = 8.7, 5.1 Hz, 1H), 0.97 (q, J = 8.4 Hz, 2H), 0.71 (q, J = 4.6 Hz, 2H) ppm. NMR spectrum is in agreement with literature precedence..20

Synthesis of tert-butyldimethyl((9-phenyldecyl)oxy)silane (3.35). tert-butyldimethyl((9-phenyldecyl)oxy)silane was synthesized from tert-butyldimethyl((9-bromodecyl)oxy)silane and phenyl boronic acid pinacol ester according to general procedure A using the 2-tert-butylphenyl catalyst 5 and purified by silica gel flash column chromatography, eluting with 100% hexanes to afford product as a colorless oil (48 mg, 71% spectroscopic yield, 71% based on recovered starting material, 55% isolated yield). Slight decomposition was observed on silica. Rf = 0.45 (100% hexanes) 1H NMR (600 MHz, CDCl3) δ 7.31 – 7.26 (m, 2H), 7.21 – 7.12 (m, 3H), 3.59 (t, J = 6.7 Hz, 2H), 2.67 (q, J = 7.1 Hz, 1H), 1.56 – 1.51 (m, 2H), 1.51 – 1.44 (m, 2H), 1.35 – 1.19 (m, 13H), 1.18 – 1.12 (m, 2H), 0.90 (s, 9H), 0.05 (s, 6H). 13C NMR (151 MHz, CDCl3) δ 150.61, 130.88, 129.62, 128.36, 65.98, 42.59, 41.09, 35.52, 32.32, 32.19, 32.07, 30.35, 28.65, 28.43, 24.97, 21.03, -2.59. HRMS-DART (m/z): [M+H]+ calculated for C22H41OSi, 349.29054; found, 349.29212.
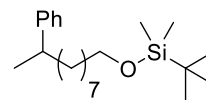
Synthesis of adamantylbenzene (3.37). Adamantylbenzene was synthesized from chloroadamantane and phenyl boronic acid pinacol ester according to general procedure A using the 2-tert-butylphenyl catalyst 5 and purified by silica gel flash column chromatography, eluting with 100% hexanes to afford product as a white solid (52 mg, 99% spectroscopic yield, 99% based on recovered starting material, 98% isolated yield). 1H NMR (500 MHz, CDCl3) δ 7.2–7.4 (m, 5 H), 2.10 (m, 3 H), 1.92 (m, 6 H), 1.77 (m, 6 H) ppm. NMR spectrum is in agreement with literature precedence.21
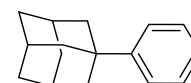
Synthesis of tert-butylbenzene (3.38). Tert-butylbenzene was synthesized from 2-chloro-2-methyl-propane and phenyl boronic acid pinacol ester according to general procedure A using the fluorinated catalyst 9 and purified by silica gel flash column chromatography, eluting with 100% hexanes to afford purified product as a colorless oil (28 mg, 92% spectroscopic yield, 85% isolated yield). Rf = 0.60 (100% hexanes) 1H NMR (400 MHz, CDCl3) δ 7.84 – 7.79 (m, 2H), 7.49 – 7.44 (m, 1H), 7.40 – 7.34 (m, 2H), 1.35 (s, 9H). NMR spectrum is in agreement with literature precedence.[22]
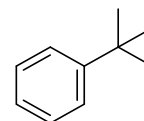
Synthesis of 1-tert-butyl-4-methylbenzene (3.39). 1-tert-butyl-4-methylbenzene was synthesized from 2-chloro-2-methylpropane and 4-tolyl boronic acid pinacol ester according to general procedure A using the fluorinated catalyst 9 and purified by silica gel flash column chromatography, eluting with 100% hexanes to afford purified product as a colorless oil (21 mg, 58% spectroscopic yield, 56% isolated yield). 1H NMR (500 MHz, CDCl3) δ 7.31 (d, J = 7.9 Hz, 2H), 7.14 (d, J = 7.9 Hz, 2H), 2.34 (s, 3H), 1.33 (s, 9H). NMR spectrum is in agreement with literature precedence.[23]
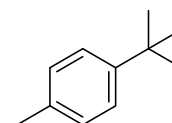
Synthesis of 1-tert-butyl-3-trifluoromethylbenzene (3.40). 1-tert-butyl-3-trifluoromethylbenzene was synthesized from 2-chloro-2-methylpropane and (meta-trifluoromethyl)phenyl boronic acid pinacol ester according to general procedure A using the fluorinated catalyst 9 and purified by silica gel flash column chromatography, eluting with 100% hexanes to afford purified product as a colorless oil (35 mg, 72% spectroscopic yield, 69% isolated yield). 1H NMR (500 MHz, CDCl3) δ 7.05 (m, 5H), 1.27 (s, 9H). NMR spectrum is in agreement with literature precedence.[24]
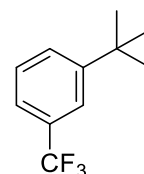
Synthesis of 1-tert-butyl-4-methoxybenzene (3.41). 1-tert-butyl-4-methoxybenzene was synthesized from 2-chloro-2-methylpropane and 4-anisolyl boronic acid pinacol ester according to general procedure A using the fluorinated catalyst 9 and purified by silica gel flash column chromatography, eluting with 100% hexanes to afford purified product as a colorless oil (21 mg, 55% spectroscopic yield, 51% isolated yield). 1H NMR (500 MHz, CDCl3) δ 7.33 (d, J = 8.3 Hz, 2H), 6.87 (d, J = 8.3 Hz, 2H), 3.81 (s, 3H), 1.32 (s, 9H). NMR spectrum is in agreement with literature precedence.[25]
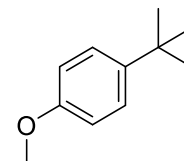
Synthesis of 1,1-dimethyl-1,3-diphenylpropane (3.42). 1,1-dimethyl-1,3-diphenylpropane was synthesized from 3-chloro-1,1-dimethyl-1-phenylpropane and phenyl boronic acid pinacol ester according to general procedure A using the fluorinated catalyst 9 and purified by silica gel flash column chromatography, eluting with 100% hexanes to afford product as a colorless oil (38 mg, 69% spectroscopic yield, 99% based on recovered starting material, 65% isolated yield). 1H NMR (500 MHz, CDCl3) δ 7.47 – 7.08 (m, 10H), 2.36 (t, J = 7.3 Hz, 2H), 1.94 (t, J = 8.6 Hz, 2H), 1.39 (s, 6H). NMR spectrum is in agreement with literature precedence.[26]
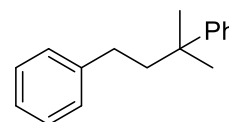
3.7 References

1.   Brown, D. G.; Boström, J., Analysis of Past and Present Synthetic Methodologies on Medicinal Chemistry: Where Have All the New Reactions Gone? *J. Med. Chem.* **2016,** *59* (10), 4443-4458.
2.   Lundgren, R. J.; Stradiotto, M., Addressing Challenges in Palladium-Catalyzed Cross-Coupling Reactions Through Ligand Design. *Chemistry - A European Journal* **2012,** *18* (32), 9758-9769.
3.   Wolfe, J. P.; Singer, R. A.; Yang, B. H.; Buchwald, S. L., Highly Active Palladium Catalysts for Suzuki Coupling Reactions. *J. Am. Chem. Soc.* **1999,** *121* (41), 9550-9561.
4.   Izquierdo, F.; Zinser, C.; Minenkov, Y.; Cordes, D. B.; Slawin, A. M. Z.; Cavallo, L.; Nahra, F.; Cazin, C. S. J.; Nolan, S. P., Insights into the Catalytic Activity of [Pd(NHC)(cin)Cl] (NHC=IPr, IPrCl, IPrBr) Complexes in the Suzuki–Miyaura Reaction. *ChemCatChem* **2018,** *10* (3), 601-611.
5.   Fihri, A.; Luart, D.; Len, C.; Solhy, A.; Chevrin, C.; Polshettiwar, V., Suzuki–Miyaura cross-coupling coupling reactions with low catalyst loading: a green and sustainable protocol in pure water. *Dalton Transactions* **2011,** *40* (13), 3116-3121.
6.   Lovering, F.; Bikker, J.; Humblet, C., Escape from Flatland: Increasing Saturation as an Approach to Improving Clinical Success. *J. Med. Chem.* **2009,** *52* (21), 6752-6756.
7.   Schäfer, P.; Palacin, T.; Sidera, M.; Fletcher, S. P., Asymmetric Suzuki-Miyaura coupling of heterocycles via Rhodium-catalysed allylic arylation of racemates. *Nature Communications* **2017,** *8*, 15762.
8.   Lamberth, C.; Dinges, J.; Dinges, J. r., *Bioactive Heterocyclic Compound Classes : Pharmaceuticals*. John Wiley & Sons, Incorporated: Weinheim, GERMANY, 2012.
9.   Zultanski, S. L.; Fu, G. C., Nickel-Catalyzed Carbon–Carbon Bond-Forming Reactions of Unactivated Tertiary Alkyl Halides: Suzuki Arylations. *J. Am. Chem. Soc.* **2013,** *135* (2), 624-627.
10.   Yotsuji, K.; Hoshiya, N.; Kobayashi, T.; Fukuda, H.; Abe, H.; Arisawa, M.; Shuto, S., Nickel-Catalyzed Suzuki–Miyaura Coupling of a Tertiary Iodocyclopropane with Wide Boronic Acid Substrate Scope: Coupling Reaction Outcome Depends on Radical Species Stability. *Adv. Synth. Catal.* **2015,** *357* (5), 1022-1028.
11.   Zhou, Q.; Cobb, K. M.; Tan, T.; Watson, M. P., Stereospecific Cross Couplings To Set Benzylic, All-Carbon Quaternary Stereocenters in High Enantiopurity. *J. Am. Chem. Soc.* **2016,** *138* (37), 12057-12060.
12.   Ariki, Z. T.; Maekawa, Y.; Nambo, M.; Crudden, C. M., Preparation of Quaternary Centers via Nickel-Catalyzed Suzuki–Miyaura Cross-Coupling of Tertiary Sulfones. *J. Am. Chem. Soc.* **2018,** *140* (1), 78-81.
13.   Hills, I. D.; Netherton, M. R.; Fu, G. C., Toward an Improved Understanding of the Unusual Reactivity of Pd0/Trialkylphosphane Catalysts in Cross-Couplings of Alkyl Electrophiles: Quantifying the Factors That Determine the Rate of Oxidative Addition. *Angew. Chem. Int. Ed.* **2003,** *42* (46), 5749-5752.
14.   Liu, T. Z.; Lee, S. D.; Bhatnagar, R. S., Toxicity of palladium. *Toxicol. Lett.* **1979,** *4* (6), 469-473.
15.   Wang, L.; Green, L.; Li, Z.; McCabe Dunn, J.; Bu, X.; Welch, C. J.; Li, C.; Wang, T.; Tu, Q.; Bekos, E.; Richardson, D.; Eckert, J.; Cui, J., Screening Binary Systems of Chelating Agents Combined with Carbon or Silica Gel Adsorbents: The Development of a Cost-Effective Method

to Remove Palladium from Pharmaceutical Intermediates and APIs. *Organic Process Research & Development* **2011,** *15* (6), 1371-1376.

16.   Guideline on the Specification Limits for Residues of Metal Catalysts. Agency, E. M., Ed. London, UK, 2007.

17.   Hunt, A. J.; Matharu, A. S.; King, A. H.; Clark, J. H., The importance of elemental sustainability and critical element recovery. *Green Chemistry* **2015,** *17* (4), 1949-1950.

18.   Choi, J.; Fu, G. C., Transition metal–catalyzed alkyl-alkyl bond formation: Another dimension in cross-coupling chemistry. *Science* **2017,** *356* (6334), eaaf7230.

19.   González-Bobes, F.; Fu, G. C., Amino Alcohols as Ligands for Nickel-Catalyzed Suzuki Reactions of Unactivated Alkyl Halides, Including Secondary Alkyl Chlorides, with Arylboronic Acids. *J. Am. Chem. Soc.* **2006,** *128* (16), 5360-5361.

20.   Martin, R.; Fürstner, A., Cross-Coupling of Alkyl Halides with Allyl Grignard Reagents catalyzed by a Low-Valent Iron Complex. *Angew. Chem. Int. Ed.* **2004,** *43*, 3955-3957.

21.   Hashimoto, T.; Hatakeyama, T.; Nakamura, M., Stereospecific Cross-Coupling between Alkenylboronates and Alkyl Halides Catalyzed by Iron−Bisphosphine Complexes. *J. Org. Chem.* **2012,** *77*, 1168-1173.

22.   Hatakeyama, T.; Hashimoto, T.; Kondo, Y.; Fujiwara, Y.; Seike, H.; Takaya, H.; Tamada, Y.; Ono, T.; Nakamura, M., Iron-Catalyzed Suzuki-Miyaura Coupling of Alkyl Halides. *J. Am. Chem. Soc.* **2010,** *132*, 10674-10676.

23.   Ghorai, S. K.; Jin, M.; Hatakeyama, T.; Nakamura, M., Cross-Coupling of Non-activated Chloroalkanes with Aryl Grignard Reagents in the Presence of Iron/*N*-Heterocyclic Carbene Catalysts. *Org. Lett.* **2012,** *14* (4), 1066-1069.

24.   Nakamura, M.; Matsuo, K.; Ito, S.; Nakamura, E., Iron-Catalyzed Cross-Coupling of Primary and Secondary Alkyl Halides with Aryl Grignard Reagents. *J. Am. Chem. Soc.* **2004,** *126*, 3686-3687.

25.   Hatakeyama, T.; Fujiwara, Y.; Okada, Y.; Itoh, T.; Hashimoto, T.; Kawamura, S.; Ogata, K.; Takaya, H.; Nakamura, M., Kumada-Tamao-Corriu Coupling of Alkyl Halides Catalyzed by an Iron-Bisphosphine Complex. *Chem. Lett.* **2011,** *40*, 1030-1032.

26.   Bedford, R. B.; Hall, M. A.; Hodges, G. R.; Huwe, M.; Wilkinson, M. C., Simple mixed Fe–Zn catalysts for the Suzuki couplings of tetraarylborates with benzyl halides and 2-halopyridinesw. *Chem. Commun.* **2009**, 6430-6432.

27.   Bedford, R. B.; Carter, E.; Cogswell, P. M.; Gower, N. J.; Haddow, M. F.; Harvey, J. N.; Murphy, D. M.; Neeve, E. C.; Nunn, J., Simplifying Iron-Phosphine Catalysts for Cross-Coupling Reactions. *Angew. Chem. Int. Ed.* **2013,** *52*, 1285-1288.

28.   Guisan-Ceinos, M.; Tato, F.; Bunuel, E.; Calle, P.; Cardenas, D. J., Fe-catalysed Kumada-type alkyl-alkyl cross-coupling. Evidence for the intermediacy of Fe(I) complexes. *Chemical Science* **2013,** *4* (3), 1098-1104.

29.   Gärtner, D.; Stein, A. L.; Grupe, S.; Arp, J.; Jacobi von Wangelin, A., Iron-Catalyzed Cross-Coupling of Alkenyl Acetates. *Angew. Chem. Int. Ed.* **2015,** *54* (36), 10545-10549.

30.   Hedström, A.; Izakian, Z.; Vreto, I.; Wallentin, C.-J.; Norrby, O., On the Radical Nature of Iron-Catalyzed Cross-Coupling Reactions. *Chem. Eur. J.* **2015,** *21*, 5946-5953.

31.   Bedford, R. B.; Brenner, P. B.; Carter, E.; Carvell, T. W.; Cogswell, P. M.; Gallagher, T.; Harvey, J. N.; Murphy, D. M.; Neeve, E. C.; Nunn, J.; Pye, D., Expedient Iron-Catalyzed Coupling of Alkyl, Benzyl and Allyl Halides with Arylboronic Esters. *Chem. Eur. J.* **2014,** *20*, 7935-7938.

32.   O'Brien, H. M.; Manzotti, M.; Abrams, R. D.; Elorriaga, D.; Sparkes, H. A.; Davis, S. A.; Bedford, R. B., Iron-catalysed substrate-directed Suzuki biaryl cross-coupling. *Nature Catalysis* **2018,** *1* (6), 429-437.

33.   Crockett, M. P.; Tyrol, C. C.; Wong, A. S.; Li, B.; Byers, J. A., Iron-Catalyzed Suzuki–Miyaura Cross-Coupling Reactions between Alkyl Halides and Unactivated Arylboronic Esters. *Org. Lett.* **2018,** *20* (17), 5233-5237.

34.   Daifuku, S. L.; Kneebone, J. L.; Snyder, B. E. R.; Neidig, M. L., Iron(II) Active Species in Iron–Bisphosphine Catalyzed Kumada and Suzuki–Miyaura Cross-Couplings of Phenyl Nucleophiles and Secondary Alkyl Halides. *J. Am. Chem. Soc.* **2015,** *137* (35), 11432-11444.

35.   Sears, J. D.; Neate, P. G. N.; Neidig, M. L., Intermediates and Mechanism in Iron-Catalyzed Cross-Coupling. *J. Am. Chem. Soc.* **2018,** *140* (38), 11872-11883.

36.   Smith, J. M.; Lachicotte, R. J.; Holland, P. L., Tuning metal coordination number by ancillary ligand steric effects: synthesis of a three-coordinate iron() complex. *Chem. Commun.* **2001,** (17), 1542-1543.

37.   Eckert, N. A.; Smith, J. M.; Lachicotte, R. J.; Holland, P. L., Low-Coordinate Iron(II) Amido Complexes of β-Diketiminates: Synthesis, Structure, and Reactivity. *Inorg. Chem.* **2004,** *43* (10), 3306-3321.

38.   Vela, J.; Smith, J. M.; Yu, Y.; Ketterer, N. A.; Flaschenriem, C. J.; Lachicotte, R. J.; Holland, P. L., Synthesis and Reactivity of Low-Coordinate Iron(II) Fluoride Complexes and Their Use in the Catalytic Hydrodefluorination of Fluorocarbons. *J. Am. Chem. Soc.* **2005,** *127* (21), 7857-7870.

39.   Holland, P. L., Electronic Structure and Reactivity of Three-Coordinate Iron Complexes. *Acc. Chem. Res.* **2008,** *41* (8), 905-914.

40.   Bart, S. C.; Hawrelak, E. J.; Lobkovsky, E.; Chirik, P. J., Low-Valent α-Diimine Iron Complexes for Catalytic Olefin Hydrogenation. *Organometallics* **2005,** *24* (23), 5518-5527.

41.   Hennessy, E. T.; Betley, T. A., Complex N-Heterocycle Synthesis via Iron-Catalyzed, Direct C–H Bond Amination. *Science* **2013,** *340* (6132), 591-595.

42.   Lee, W.-T.; Jeon, I.-R.; Xu, S.; Dickie, D. A.; Smith, J. M., Low-Coordinate Iron(II) Complexes of a Bulky Bis(carbene)borate Ligand. *Organometallics* **2014,** *33* (20), 5654-5659.

43.   Biernesser, A. B.; Li, B.; Byers, J. A., Redox-Controlled Polymerization of Lactide Catalyzed by Bis(imino)pyridine Iron Bis(alkoxide) Complexes. *J. Am. Chem. Soc.* **2013,** *135* (44), 16553-16560.

44.   Carrow, B. P.; Hartwig, J. F., Distinguishing Between Pathways for Transmetalation in Suzuki−Miyaura Reactions. *J. Am. Chem. Soc.* **2011,** *133* (7), 2116-2119.

45.   Kamitori, Y.; Hojo, M.; Masuda, R.; Izumi, T.; Tsukamoto, S., Silica gel as an effective catalyst for the alkylation of phenols and some heterocyclic aromatic compounds. *J. Org. Chem* **1984,** *49* (22), 4161-4165.

46.   Huang, Z.; Zhang, J.; Zhou, Y.; Wang, N.-X., Enantioselective Friedel–Crafts Alkylation of Thiophenes with Ethyl Glyoxylate: Easy Access to Chiral Secondary Alcohols. *Eur. J. Org. Chem.* **2011,** *2011* (5), 843-847.

47.   Wang, X.; Wang, S.; Xue, W.; Gong, H., Nickel-Catalyzed Reductive Coupling of Aryl Bromides with Tertiary Alkyl Halides. *J. Am. Chem. Soc.* **2015,** *137* (36), 11562-11565.

48.   Wang, X.; Ma, G.; Peng, Y.; Pitsch, C. E.; Moll, B. J.; Ly, T. D.; Wang, X.; Gong, H., Ni-Catalyzed Reductive Coupling of Electron-Rich Aryl Iodides with Tertiary Alkyl Halides. *J. Am. Chem. Soc.* **2018,** *140* (43), 14490-14497.

49.   Cherney, A. H.; Hedley, S. J.; Mennen, S. M.; Tedrow, J. S., Xantphos as a Branch-Selective Ligand for the Acyclic sec-Alkyl Negishi Cross-Coupling of Heteroaryl Halides. *Organometallics* **2019,** *38* (1), 97-102.

50.   Hartwig, J. F., *Organotransition metal chemistry : from bonding to catalysis*. University Science Books: Mill Valley, Calif. ;, 2010.

51.   Lee, W.; Zhou, J.; Gutierrez, O., Mechanism of Nakamura's Bisphosphine-Iron-Catalyzed Asymmetric C(sp2)–C(sp3) Cross-Coupling Reaction: The Role of Spin in Controlling Arylation Pathways. *J. Am. Chem. Soc.* **2017,** *139* (45), 16126-16133.

52.   Sharma, A. K.; Sameera, W. M. C.; Jin, M.; Adak, L.; Okuzono, C.; Iwamoto, T.; Kato, M.; Nakamura, M.; Morokuma, K., DFT and AFIR Study on the Mechanism and the Origin of Enantioselectivity in Iron-Catalyzed Cross-Coupling Reactions. *J. Am. Chem. Soc.* **2017,** *139* (45), 16117-16125.

53.   Feldman, J.; McLain, S. J.; Parthasarathy, A.; Marshall, W. J.; Calabrese, J. C.; Arthur, S. D., Electrophilic Metal Precursors and a β-Diimine Ligand for Nickel(II)- and Palladium(II)-Catalyzed Ethylene Polymerization. *Organometallics* **1997,** *16* (8), 1514-1516.

124

Chapter 4. C-H activation promoted by iron-based complexes and the discovery of a three-component reaction based on this reactivity

4.1. Introduction

Metal catalyzed C-H activation reactions are becoming a mainstay of chemical synthesis.[1] The primary reason that C-H activation reactions are becoming more widely used is because they provide access to products that could be accessed through cross-coupling type reactions without needing to preinstall functional groups required for cross-coupling reactions.[2] This shift in reaction design has tremendous potential in the late stage functionalization of pharmaceuticals where installing functional groups can be challenging.[3] To this end, monumental efforts have been explored by many groups and significant progress has been made with respect to sp^2 C-H activation and more recently sp^3 C-H activation.[4] Particularly useful are methods such as those developed by MacMillan and coworkers that allow for the functionalization of weak α-amino C-H bonds as well

Figure 4.1. Overview of methods for C-H activation.

MacMillan et al. 2016
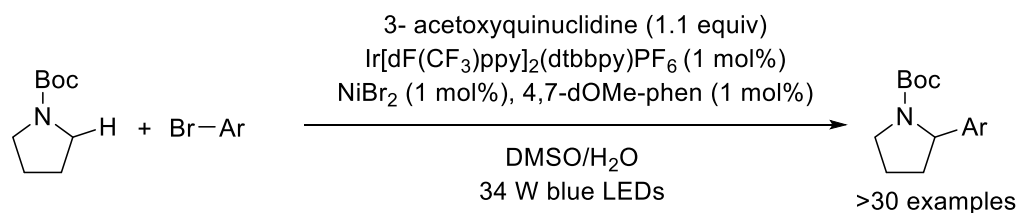
Alexanian et al. 2015
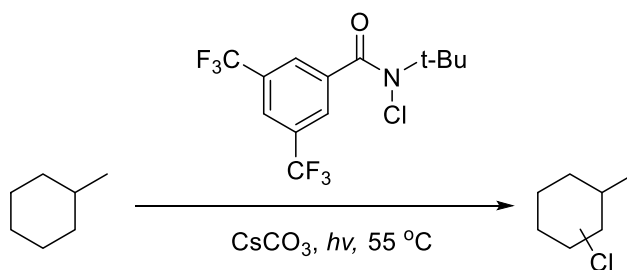
This Work
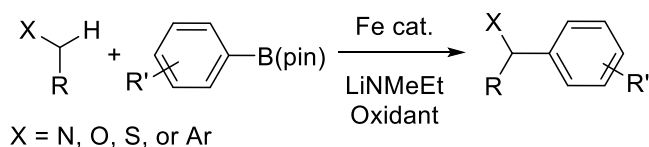
as other weak C-H bonds (Figure 4.1).[5] Recently, the Alexanian group has also developed non-transition metal catalyzed C-H halogenation reactions (Figure 4.1).[6] There have also been many recent examples of copper catalyzed reactions that are capable of functionalizing benzylic C-H bonds.[7] Follow-up work on these studies reports the use of peroxides[8] or NFSI[9] for the arylation of benzylic C-H bonds. While these methods have primarily been developed using copper catalysts, there is also precedence in the literature for the use of iron catalysts in similar transformations.[10] Typically, these reactions utilize an ill-defined metal source, such as iron oxide, as well as superstoichiometric amounts of Grignard reagents (greater than 4 equivalents). These reactions also typically do not utilize ligands, and as such, have limited opportunities for enhancements in scope, regioselectivity, or enantioselectivity.

4.2. Discovery and Optimization of C-H Activation

In solvent screenings for the initially explored cross-coupling reaction, unexplained peaks were observed in GC traces of reactions run in solvents with weak C-H bonds, such as THF and toluene. Ultimately, it was determined that these peaks corresponded to products resulting from C-H arylation at the site with the weakest C-H bonds. Based on these results, we wanted to evaluate if this reaction could be pursued intentionally to produce high yields for a wide range of substrates. To accomplish this, it was first necessary to determine the best way to promote the C-H activation side reaction over the original cross-coupling reaction. We hypothesized that the addition of an alkyl halide that does not undergo cross-coupling could serve as a sufficient oxidant for the reaction. Sterically unencumbered halides such as octyl bromide lead to almost exclussive cross coupling (table 4.1, entry 1). More sterically encumbered electrophiles such as bromocycloheptane lead to a mixture of cross-coupling and C-H activation (table 4.1, entry 2). Tert-butyl bromide provided the desired C-H activation product with complete selectivity over the cross-coupling

127

product (Table 4.1, entry 3). After this was established, a preliminary ligand screen was carried out. The results from this screen (Table 4.2 and Table 4.3) demonstrated similar results to our previous studies in that most phosphines provided only minor improvements over ligandless conditions (Table 4.2, entry 1). Notably, small electron-rich phosphines such as trimethyl phosphine did improve the yields by a small margin (entry 7). Other monodentate phosphines provided no improvements over ligandless conditions (entries 2-9). Likewise, bidentate phosphines also demonstrated no improvements over ligandless conditions, regardless of the bite angles or electronic properties of the ligands (Table 4.3, entries 1-9). Slightly more success was found when nitrogen based ligands were used in this reaction (Table 4.4). Ligands that are typically used for iron catalysis, such as pyridine, resulted in small boosts in yield (entry 2). Small bidentate nitrogen based ligands such as bypridine or quinoline ligands almost completely shut down the reactivity (entries 3 and 4). Other bipyridine derivatives resulted in either moderate improvements (entry 6) or almost no difference in yields (entries 5 and 7). Diamine ligands that have been successful with nickel based systems[11] were totally ineffective for this C-H activation reaction (entries 8-9). Bisoxazoline ligands (entries 10-14) were also largely ineffective for improving this

Table 4.1. Alkyl halide evaluation

Entry	RX	4.1	4.2
1	CH₃(CH₂)₅CH₂Br	5	58
2	cycloheptyl–Br	22	45
3	tert-butyl–Br	33	0
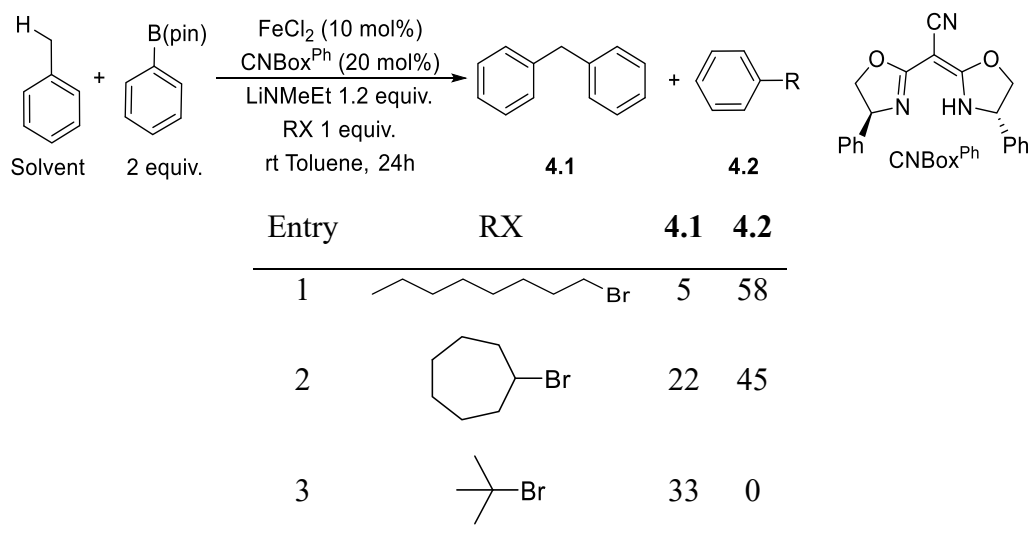
Table 4.2. Evaluation of monodentate phosphine ligands for C-H arylation

Entry	Ligand	X %	**4.1** (%)
1	None	0	16
2	PPh₃	20	23
3	P(2-furyl)₃	20	12
4	P(o-tolyl)₃	20	15
5	P(o-anisyl)₃	20	18
6	PCy₃	20	15
7	PMe₃	20	31
8	(XPhos structure)	10	16
9	(cyclopropane phosphine structure)	10	19
10	Dmpe	10	14

reaction, with the exception of the cyanated ligand (entry 12). Additionally, tridentate ligands either of the pybox class or the bis(imino)pyridine class were also ineffective in providing the product in higher yields (entries 15-17). Interestingly, the much more sterically encumbered bis(imino)pyridine ligand was more effective for this C-H activation reaction (entry 17). Based on the results from both ligand evaluations, the best ligands for promoting this reaction were the cyanated bis-oxazoline ligands which gave 25% yield under the screening conditions and 33% under the more optimal conditions for the originally developed cross-coupling reaction. Based on the still low yields, this project was put on hold temporarily to pursue the project reported in

chapter 3. As a result, the NacNac ligands have not be evaluated under the conditions reported in these initial screens. The NacNac ligands were however evaluated moving forward with the project.

Table 4.3. Evaluation of bidentate phosphine ligands for C-H arylation
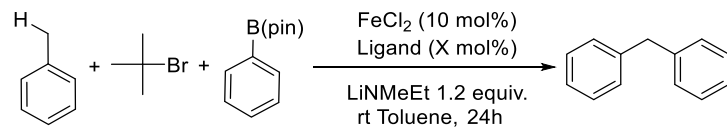
Entry	Ligand		X %	4.1 (%)
1	Dmpe		10	14
2		n = 0	10	15
3		n = 1	10	15
4		n = 2	10	18
5			10	20
6			10	21
7			10	18
8			10	18
9			10	14

130
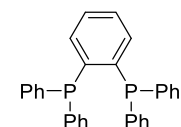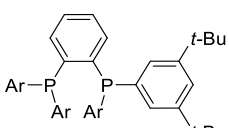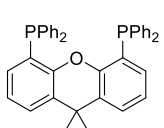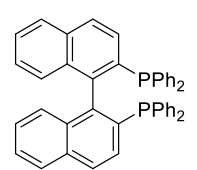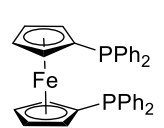
Table 4.4. Evaluation of nitrogen based ligands for C-H arylation
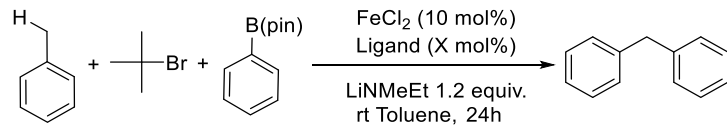
Entry	Ligand		X %	4.1 (%)
1	None		0	16
2	pyridine		20	23
3			10	3
4			10	2
5			10	17
6			10	24
7			10	10
8			10	10
9			10	14
10		R = H	10	18
11		R = Me$_2$	10	9
12		R = CN	10	25
13			10	15
14			10	7
15			10	16
16		R = 2,6MePh	10	10
17		R = 2,6iPrPh	10	22
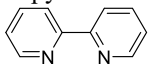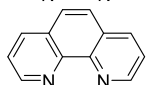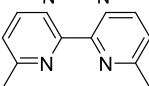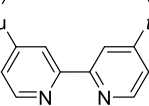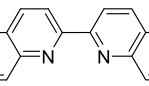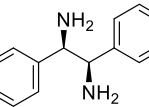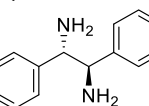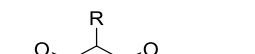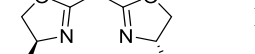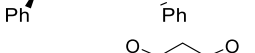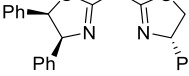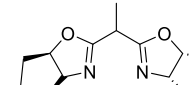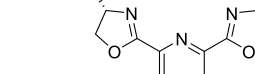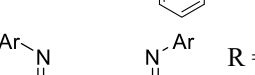
4.3.   Mechanistic insights into C-H activation

Based on the inability to improve the reaction dramatically by catalyst screening, the next step is to try and garner some mechanistic insight for further improvements. We hypothesize that the C-H arylation products are being formed through a radical abstraction/recombination event like the one presented in Figure 4.2. Based on our other experiences in the cross-coupling of alkyl electrophiles and aryl boronic ester, we hypothesize that the transmetallation and carbon-carbon bond forming reactions proceed through a similar mechanism to that reported in chapter 3 (Figure 4.2 left cycle). The key difference in the reactivity that leads to C-H functionalization is in the step after halogen abstraction (Figure 4.2, right cycle). The radical that, under normal circumstances, would recombine to generate cross-coupling product can now engage the solvent to do a hydrogen atom abstraction. In this scenario, the substrate could be tuned to have weaker C-H bonds that further favor the abstraction process. Additionally, the hypothetical hydrogen atom abstractor R could be tuned to favor the abstraction process over the direct recombination event. In line with this, it was determined that when a reaction was run in ethyl benzene instead of toluene, the

Figure 4.2. Proposed mechanism for the formation of C-H arylation products.
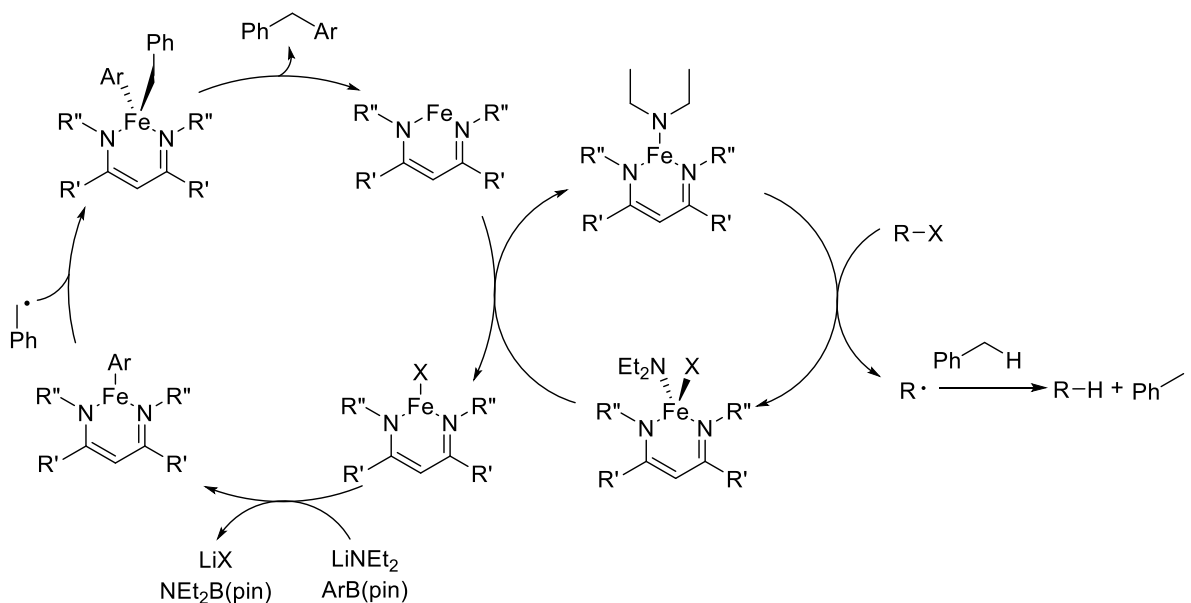
Scheme 4.1. C-H activation carried out in a solvent with weaker C-H bonds.
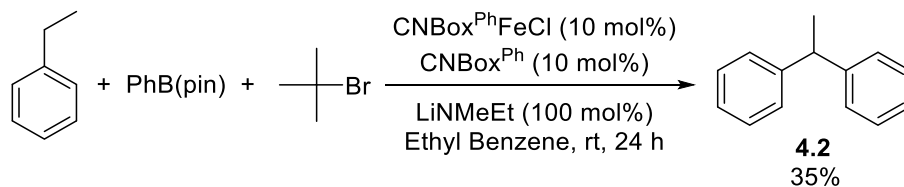
reaction efficiency indeed improved (Scheme 4.1). The improved yield is likely due to the fact that

ethylbenzene has weaker benzylic C-H bonds than toluene.[12] However, the yields of **4.2** still leave

significant room for improvement. As a result, a screen of hydrogen atom abstractors was carried

out. The ideal candidate for a H-atom abstractor would be a radical species that generates a very

strong X-H bond as well as actively dicourages direct recombination with the metal center. These

two considerations are likely the reason for the empirical observation that more sterically

encumbered alkyl halides lead to increased yields of C-H activated products. Unfortunately,

tertiary alkyl halides also have the weakest product C-H bonds among alkyl electrophiles (Table

4.5, entries 1-2). In order to better study the effects of specific changes in the ligand and

electrophile, the decision was made to move to the more modular β-diketiminate (NacNac) ligand

framework. Various electrophiles were then examined using the conditions that had been most

optimal for the reactions conducted with the bisoxazoline frameworks (Table 4.5). In contrast to

the bisoxazoline ligands, the NacNac ligand provides a large amount of direct cross-coupling in

reactions with tertiary electrophiles (entries 1 and 2). Likewise, similarly encumbered neopentyl

electrophiles failed to significantly bias the reaction toward selective C-H functionalization

(entries 3 and 4). Furthermore, substrates that would generate an even more potent H-atom

abstractor failed to provide any useful reactivity (entry 5).

Table 4.5. Alternate oxidant screen.

H—(toluene, benzylic CH) + B(pin)—Ph (2 equiv.) → 2,6MePhNacNacFeCl (10 mol%), LiNMeEt 1.0 equiv., RX 1 equiv., rt Toluene, 24h → Ph-CH₂-Ph (**4.1**) + Ph—R (**4.2**)

Solvent (2 equiv.)
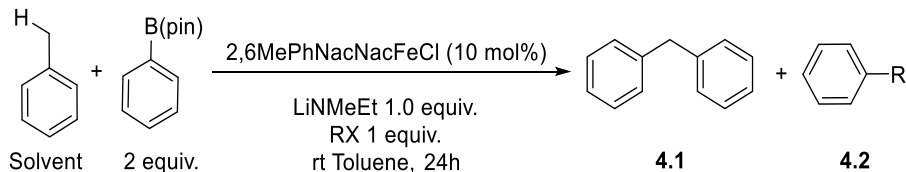
Entry	RX	BDE of R-H (kcal/mol)	**4.1** (%)	**4.2** (%)
1	(CH₃)₃C–Cl	~95	0	48
2	(CH₃)₃C–Br	~95	5	trace
3	neopentyl chloride (Cl-CH₂-C(CH₃)₃)	~100	0	0
4	neopentyl bromide (Br-CH₂-C(CH₃)₃)	~100	4	5
5	3,5-(CF₃)₂-C₆H₃-C(O)-N(Cl)(t-Bu)	~110	0	0

As an alternative probe for this reaction, a substrate containing a tertiary alkyl halide (**4.3**) that was in position to do a 1,5 H atom abstraction was subjected to the reaction conditions. This substrate could in theory, if the abstraction from solvent pathway is operative, generate exclusively the arylated oxidant at the benzylic position. If alternative pathways are operative, it would be expected that arylation of the solvent would still be the only observed product. Interestingly, this reaction resulted in the formation of both possible products in a ratio of 1.74 to one for arylation of the oxidant to arylation of the solvent (Scheme 4.2). This result, while not conclusive, still indicates that hydrogen atom abstraction from the solvent is likely the operative pathway as it has been able to compete with the intramolecular reaction.
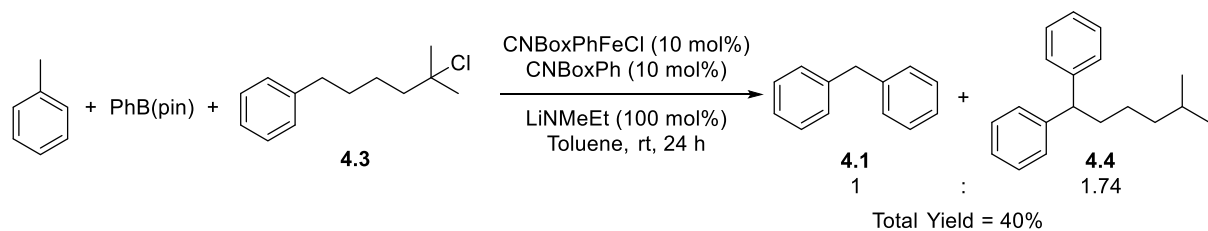
Scheme 4.2. Substrate capable of a 1,5 H-atom transfer to a more stable location.

Since screening various electrophiles did not increase the productivity of the C-H activation reaction, a screen of various NacNac ligated iron complexes was evaluated to see if any could bias the reaction toward exclusive C-H functionalization (Figure 4.3). While the NacNac complexes had not been previously utilized in these reactions, the high modularity of the framework was appealing for the logical optimization of the C-H activation reactivity. However, the initial screen resulted in nearly no C-H arylation for a variety of ligands with drastically different steric and electronic properties. The only complex that was able to provide the C-H arylation product with any selectivity was complex **4.13**, which produced only 7% of the arylation product while almost completely suppressing the direct coupling product. The sterically more

Figure 4.3. Screen of NacNac-based complexes for the C-H arylation of toluene with PhB(pin).
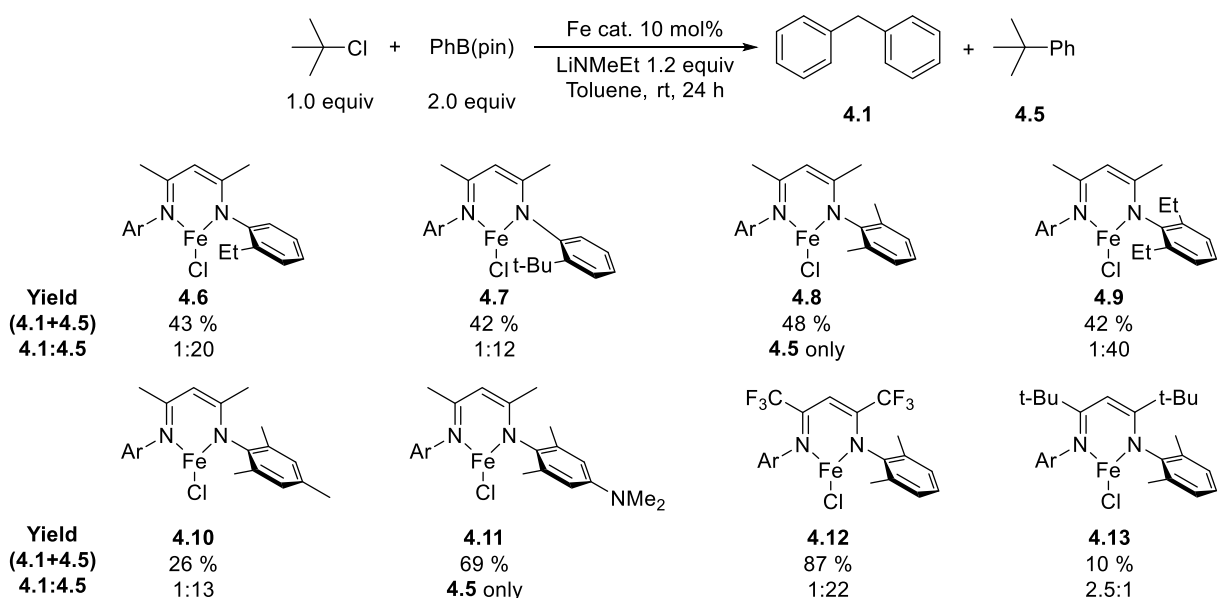
encumbered 2,6-diisoproylaryl ligand was not screened in these reactions because it previously

did not show any productive coupling.

To better probe the difference in radical lifetimes that were accessible using the different

NacNac based complexes, a series of reactions were carried out using radical clock substrates that

undergo partial ring-closing reactions under the standard conditions (Figure 4.4). In this case, the

free radical generated from 6-bromo-1-hexene cylizes with a rate constant around 1 x 10^5.[13]

Therefore, since a longer lived radical intermediate is desired here, a reaction that favors the

cyclized product should be ideal. That assumption does rely on the rate of the cross-coupling

reaction not being dependent on that radical recombination step. Unsurprisingly, the complex

(**4.13**) that was found to be the best for selective C-H functionalization also promoted reactivity

consistent with a longer lived radical intermediate. This is consistent with this complex being

sterically demanding around the metal center and having a significantly different bite angle than

the other NacNac complexes.[14] Sterically unencumbered complexes such as the 2-tertbutylphenyl

complex (**4.7**) resulted in almost exclusively direct coupling products. This is once again consistent

Figure 4.4. Screen of NacNac-based complexes for the coupling of a substrate prone to radical cyclization.
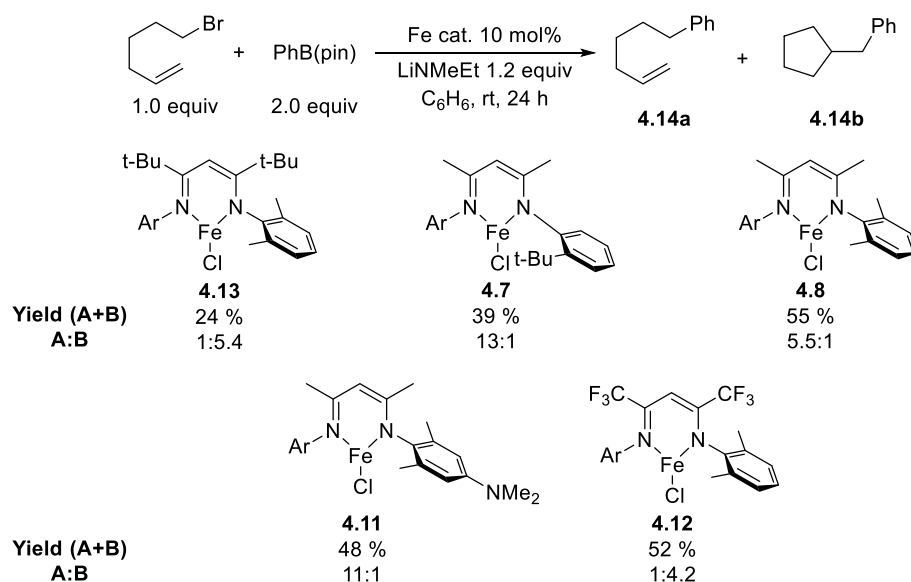
with a more open metal center that the radical intermediate can intercept. Interestingly, the electron-deficient fluorinated complex (**4.12**) also demonstrated results consistent with longer radical lifetimes. This is inconsistent with prior observations, where this complex is highly efficient for the coupling of tertiary electrophiles.[15] The screening of catalysts and conditions to this point has not lead to significantly increased yields in these reactions. In combination with the fact that during the course of these studies similar works were published by the Liu[9] and Stahl[8] groups, it was determined that further studies should focus on new directions for this chemistry.

4.4. The discovery of a three-component coupling reaction

In the course of optimization for the direct C-H functionalization reaction, it was serendipitously discovered that using catalyst **4.13** with lithium dimethyl amide, phenyl boronic acid pinacol ester, and tert-butyl chloride formed a new product (Table 4.6, entry 1). After separation on silica gel, this unknown appears to be *N*-methyl-*N*-neopentylaniline. This

Table 4.6. Base screening for C-H arylation of toluene using the tBu backbone NacNac complex.
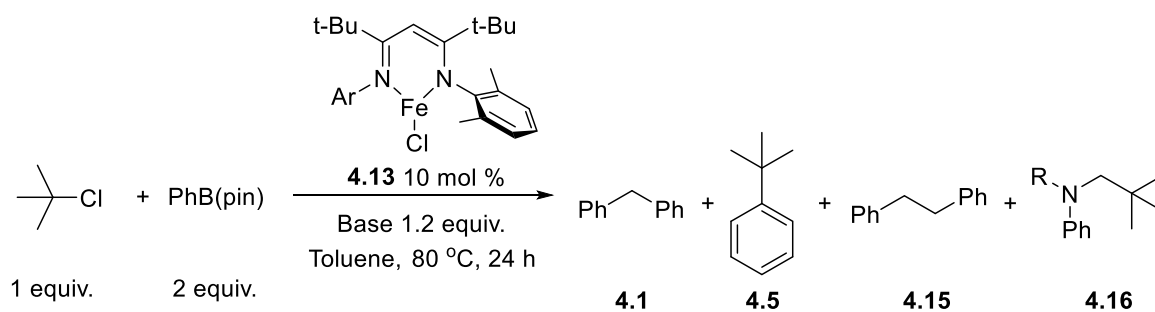
Entry	Base	4.1 (%)	4.5 (%)	4.15 (%)	4.16 (%)
1	LiNMe$_2$	10	2	0	~10
2	LiNMeEt	12	0	0	~1*
3	LiNEt$_2$	42	0	0	trace
4	LiNiPr$_2$	4	4	~8	0

*similar to entry 1 but hard to identify as it is in such low concentration.

unexpected product is the result of a three-component coupling of the lithium amide, the boronic

ester, and the alkyl halide. Effectively, it is a tandem C-N coupling and C-H alkylation which

would constitute the first reaction of this type in the literature. It was also determined that if any

component of the reactions presented in Table 4.6 is left out, this new product is not observed. It

is likely that the minor peaks observed in the GC spectra of entries 2 and 3 are also associated with

a similar product. This three-component coupling could provide an alternative method of

synthesizing tertiary amines, which are important motifs in pharmaceutical products.[16] As a

preliminary attempt at optimizing this unique reaction, equivalencies of every component in the

reaction were varied (Table 4.7). Increasing concentrations of both the alkyl halide and lithium

amide resulted in an increase in the three-component coupling product (entries 3 and 4) while

Table 4.7. Equivalency screening of three component coupling reaction.

Entry	X	Y	Z	4.16 (%)	4.5 (%)	4.17 (%)
1	1	1	1	9	trace	trace
2	2	1	1	4	0	0
3	1	2	1	15	2	4
4	1	1	2	13	trace	trace
5	1	1	3	5	0	3
6	2	1	2	21	trace	trace
7	2	1	3	1	0	0
8	1	3	3	27	5	4

increasing the equivalencies of the halide was counterproductive to the reaction (entries 2 and 6). Further increasing the amide concentration also resulted in lower yield unless the boronic ester concentration was also increased (entries 5 and 8). Simultaneous increases in the halide and amide led to improved product yields relative to increasing one of the components (entry 6), however, further increasing the amide once again shut down the reaction. These initial results are promising for further optimization, though the current trends are difficult to understand.

As a next step in optimization, the concentration and catalyst loading were evaluated (Table 4.8). As can be seen from entries 1-4 the reaction has reached completion by 4 hours with minimal increase in product afterward. Conversion of the alkyl chloride is difficult to track as it is volatile.

Table 4.8. Concentration and catalyst loading evaluation.

Entry	Time (h)	**X** mM	**Y** mol%	4.16	4.5	4.17
1	2	36	10	8	trace	0
2	4	36	10	10	trace	trace
3	20	36	10	10	trace	trace
4	40	36	10	11	trace	trace
5	20	63	10	9	trace	trace
6	20	125	10	8	trace	trace
7	20	36	5	18	trace	trace
8	20	36	2	15	trace	0
9	20	36	20	4	trace	trace

Since we believe bimetallic mechanisms can be operative under standard cross-coupling conditions, the concentration was increased to see if it made an impact on these reactions. Increasing the concentration appeared to only reduce product formation, possibly indicating catalyst decomposition through aggregation (entries 3, 5-6). By contrast reducing the catalyst loading, and thus the catalyst concentration, led to much higher yields (entries 7 and 8) while increasing catalyst loading dramatically lowered yield (Entry 9).

The next step for optimization of this reaction was the evaluation of various solvents (Table 4.9). Other aromatic solvents such as anisole and difluorobenzene demonstrated similar yields of three-component coupling product as benzene (entry 1 vs 3 and 6). Toluene reduced the yields of

Table 4.9 Solvent evaluation for three-component coupling..
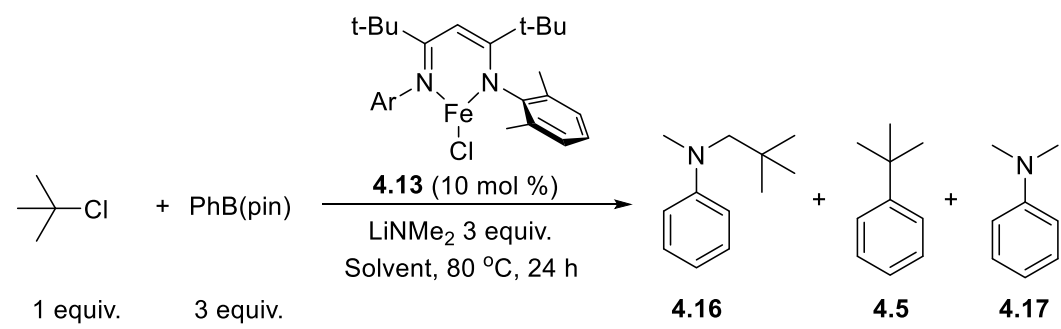
Entry	Solvent	**4.16** (%)	**4.5** (%)	**4.17** (%)
1	Benzene	28	5	4
2	Toluene	22	2	1
3	Anisole	30	2	1
4	THF*	0	0	0
5	2-MeTHF	0	0	0
6	1,2-difluorobenzene	32	1	1
7	Diethyl ether*	8	8	4
8	Pentane*	9	30	0

*Reaction run at rt for 48 h

the three-component product significantly, possibly because of alternative C-H abstractions that are possible in a solvent with weak C-H bonds (entry 2). Etherial solvents other than anisole were either completely ineffective in providing the three-component product (entries 4 and 5) or provided the product in significantly reduced yields (Entry 7). Finally, alkane solvents also proved ineffective for the production of three-component products (Entry 8). Interestingly, pentane did provide the direct cross-coupling product in substantial yields. This observation may be important for the further optimization of the cross-coupling of tertiary electrophiles.

Based on these results, it seems likely that catalyst death is the main limiting factor for improving the yields of this reaction. Based on this assumption, methods for suppressing the catalyst decomposition were explored. One possible mechanism for catalyst decomposition is the over-oxidation of the catalyst by the alkyl halide substrate. We hypothesized that this is the reason that reactions run in excess of the alkyl halide are low yielding (entry 2, table 4.7). To probe if this was a possible decomposition pathway in this reaction, the alkyl halide substrate was added slowly to a set of reactions. The results of the slow addition are summarized in Table 4.10. Under conditions where the alkyl halide is in excess, the reaction is low yielding (entry 1). However, adding the electrophile in small batches over the course of 6 hours improved the yield (entry 2). Furthermore, addition via syringe pump seemed to give similar results (entry 3). However, increasing or decreasing the addition rate appeared to be detrimental to the reaction (entries 4 and 5). Further optimization of the addition time will likely lead to somewhat improved yields in these

Table 4.10. Slow addition of the alkyl halide.
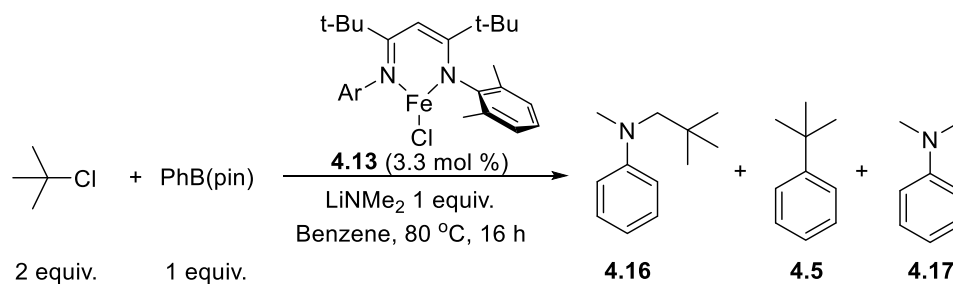
Entry	Deviation from standard conditions	Addn Time	**4.16** (%)	**4.5** (%)	**4.17** (%)
1	None		4	2	0
2	Batchwise addition of *t*BuCl 3 times	6 hours	23	2	1
3	Syringe pump addition of *t*BuCl	6 hours	22	2	1
4	Syringe pump addition of *t*BuCl	2 hours	9	1	1
5	Syringe pump addition of *t*BuCl	20 hours	2	1	1

reactions. It is unlikely however that the yields will be improved into the range of what could be considered synthetically useful by the optimization of this parameter alone. For this reason, we chose to approch the mechanism of this reaction to further improve yields.

4.5.   Mechanistic insights into the three-compenent coupling reaction

Based on the improvements associated with slow addition of the electrophile, several other substrates were screened to determine if there were any that were more amenable to this reaction (Figure 4.5). Based on these results, there is a lower limit on the steric demand of the electrophile substrate. In the cases where the carbon-centered radical is too accessible, direct cross-coupling dominates (i.e. cyclopropyl and adamantyl). Larger substrates all appeared to behave similarly to tert-butyl chloride in this reaction. Quite surprisingly, this included the extremely sterically bulky triethyl substituted substrate, which proceeded in similar yields to the tert-butyl chloride under

142

these conditions. After some further optimization, these substrates will be revisited to characterize their reactivity more completely.

Figure 4.5. Electrophile evaluation for three-component coupling reaction.
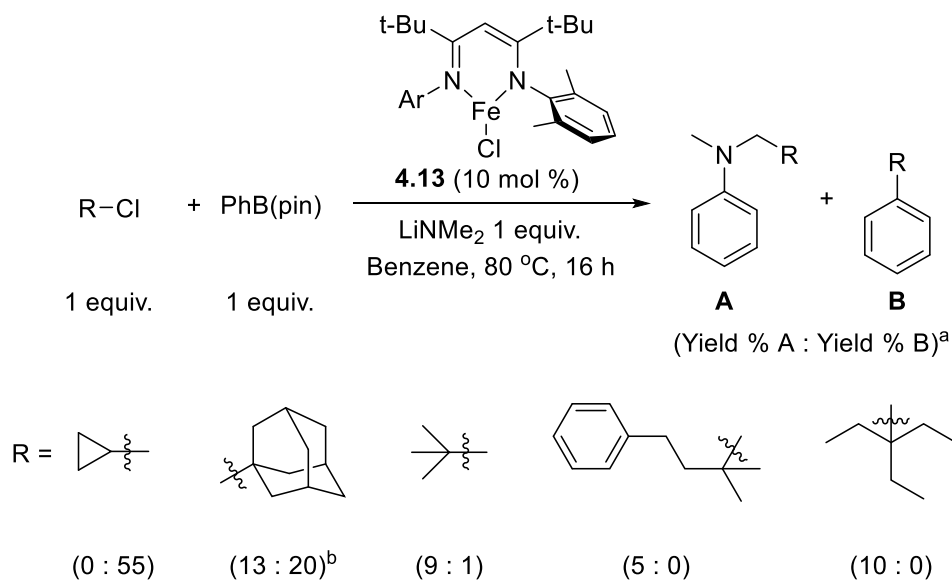
ªYields based on external standard. ᵇThe bromide was used in this reaction as the chloride was found to give the product B exclusively.

Due to the novel nature of the reactivity demonstrated here, there is very little known about how the product of this reaction is being generated. A trace amount of dimethyl aniline is observed in all three-component reactions that have been carried out. A reasonable mechanism could be that the dimethyl aniline is being formed and then is further functionalized to generate the product. If this is the case, a reaction where diemethyl aniline is added should produce this product regardless of whether or not phenyl boronic acide pinacol ester is added. Based on this idea, a crossover experiment was designed to determine if the C-C bond formation occurs before or after the C-N bond forming reaction (Figure 4.6). In this reaction, dimethyl aniline was added at the start of the reaction and *p*-methoxyphenylB(pin) was used. Under these conditions, no product that would be consistent with the functionalization of the dimethyl aniline was observed. Coupled with the observation that the other three-component product was formed in similar yields to a reaction run

143

without the dimethyl aniline suggests that the product is not being formed via a pathway in which C-N coupling occurs first.

Figure 4.6. Crossover experiment using dimethylaniline as an additive.
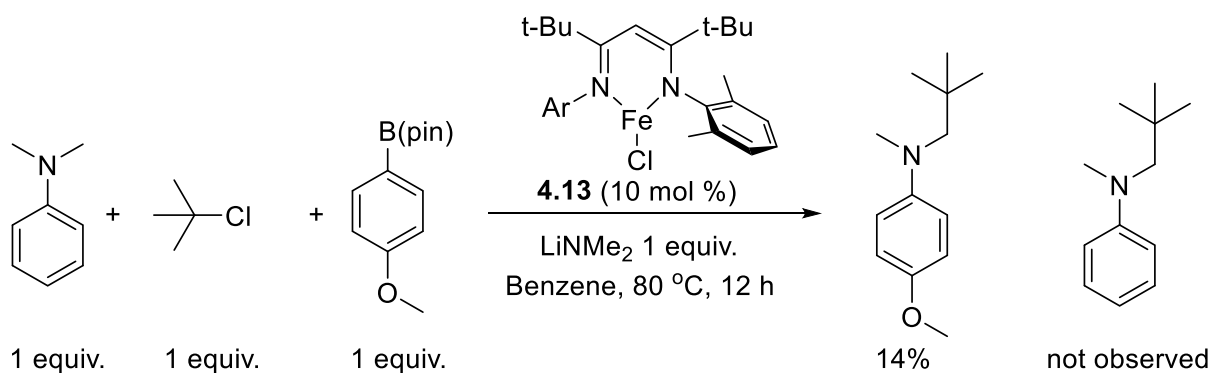
Based on this crossover experiment and the optimization data presented earlier, a possible mechanism can be proposed (Figure 4.7). In this mechanism, the first bond-forming reaction is likely the C-C bond formation followed by C-N bond formation. Starting from the iron halide precatalyst (**I**), the first step would likely be a salt metathesis with the lithium amide to form an iron amide (**II**). The next step would then be either a halogen abstraction or a transmetalation. Some preliminary calculations suggest that transmetalation from an iron(III) intermediate would be less favorable therefore transmetallation would occur first and furnish iron aryl species **III**. Subsequent halogen abstraction could then generate an oxidized iron aryl halide complex **IV**. Another salt metathesis reaction could then occur to generate an iron amide aryl complex (**V**). The exact mechanism of the C-C bond formation is hard to determine, but it seems likely that it goes through a H-atom abstraction from intermediate **V** followed by a radical recombination to generate the iron neopentyl methyl amide complex (**VII**). Subsequent reductive elimination ultimately furnishes the desired product. Interestingly, this reaction ties together a Chan-Lam coupling (a formally reductive process from the perspective of the metal) with an oxidative C-H functionalization to give a process that is overall redox neutral at the metal center. These types of

144

multi-step redox processes are rare in the chemical literature, with each step typically being performed with an external oxidant or reductant. This mechanism is also consistent with some of the products being formed from the reaction. For example, dimethylaniline could be formed from reductive elimination from complex **V**. Likewise, if intermediate **III** is intercepted by a carbon-centered radical it could produce the direct cross-coupling product. The main limitation of this mechanistic framework is that a second equivalent of the tert-butyl radical is required before the halogen abstraction can take place. This could indicated a mechanism that once again makes use of two different metal centers to make the bonds required. These mechanistic experiments when

Figure 4.7. Working mechanistic hypothesis.
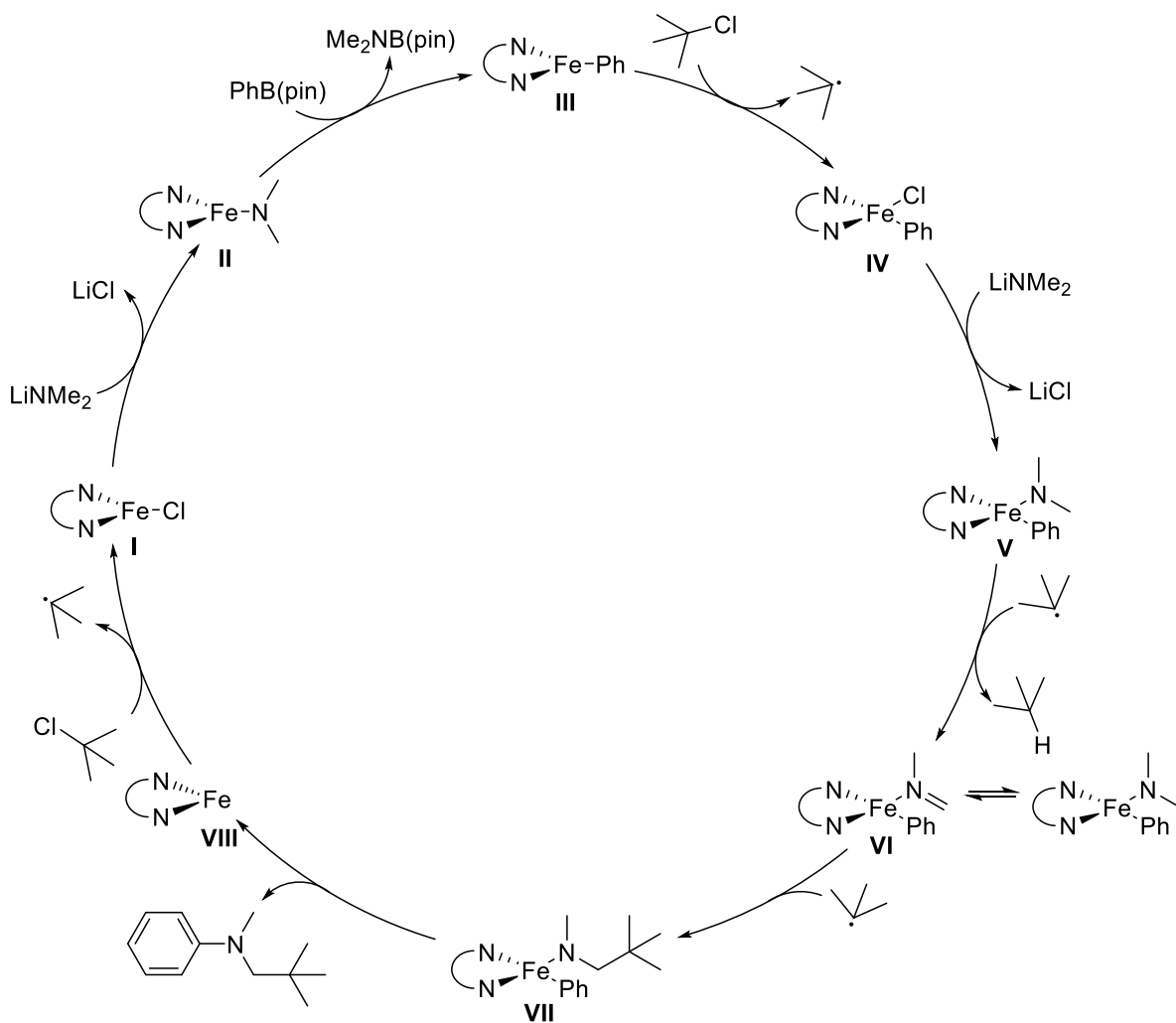
taken together seem to indicate that catalyst death is likely still the main limiting factor. As a result, future studies will need to focus on further catalyst development for these reactions.

4.6.   Conclusions and Outlook

While these studies have not yet resulted in a synthetically viable method for the production of tertiary amines, they have demonstrated that this reactivty is worth continuing to explore. It is worth noting that at this point in the studies, a significant disruption occurred due to the Covid-19 epidemic. Due to these highly unusual circumstances, a few of the directions that were being explored will be discussed for the purposes of informing future students that may participate in these projects. A key focus that has helped with may of the previous projects in the group has been ligand design. Based on this idea, the synthesis of several new ligands was underway at the start of the laboratory shutdown. Of particular interest are NacNac ligands that have alternate steric and electronic properties. The only ligands that we have so far observed the three-component coupling reactivity with are those with tert-butyl substitutions in the backbone of the ligand. In theory it should be possible to substitute the tert-butyl groups with other substituents that impart similar steric encumberance. Furthermore, NacNac ligands in the class with electronic properties have been underexplored for all transformations. Finally, a substrate that contains both a boronic ester and an alkyl halide was designed as another probe into the mechanism of this reaction. Some of these experiments may still be possible to carry out as we look toward reopening the chemistry building but the majorty of them will like have to be carried out by future students. One thing is certain however, none of the reactivity discovered in this chapter would have been discovered without the explorations detailed in chapters two and three.

4.7. Experimental

General Considerations. Unless stated otherwise, all reactions were carried out in oven-dried glassware in a nitrogen-filled glovebox or using standard Schlenk-line techniques.[17] Solvents including dichloromethane, pentane, toluene, diethyl ether, and tetrahydrofuran were purified by passage through two activated alumina columns under a blanket of argon[18] and then degassed by brief exposure to vacuum. Other solvents were dried over calcium hydride for a minimum of 2 days, degassed, and distilled prior to use. Phenyl boronic acid was purchased from Oakwood Chemicals. All prepared boronic pinacol esters were used after passage through alumina under a nitrogen atmosphere. Methylethyl amine was purchased from TCI America; diisopropylamine and lithium dimethylamide were purchased from Alfa Aesar, diethylamine was purchased from Sigma-Aldrich. All amines that were liquids at room temperature were dried over calcium hydride for at least 24 hours before being vacuum-distilled. 2,3-dimethyl-2,3-butanediol was purchased from Alfa and used without further purification. Anhydrous iron (II) chloride was purchased from Strem Chemicals and used without further purification. Purchased alkyl halides were dried over calcium hydride for at least 24 hours before being vacuum-distilled, while all solids were dried over P_2O_5 before use in the glovebox. All alkyl halides were purchased from Sigma-Aldrich, Oakwood Chemicals and Fisher Scientific.

^{1}H, ^{11}B, and {^{1}H}^{13}C nuclear magnetic resonance (NMR) spectra were recorded at ambient temperature on Varian VNMRS operating at 400 MHz, 500 MHz, or 600 MHz for ^{1}H NMR at 160 MHz for ^{11}B NMR, 125 MHz for {^{1}H}^{13}C NMR. All {^{1}H}^{13}C NMR was collected while broadband decoupling was applied to the ^{1}H region. The residual protio solvent impurity was used as an internal reference for ^{1}H NMR spectra and {^{1}H}^{13}C NMR spectra. Boron trifluoride diethyl etherate was used as an external standard ($BF_3 \cdot O(C_2H_5)_2$: 0.0 ppm) for ^{11}B NMR. The line listing

for NMR spectra of diamagnetic compounds are reported as follows: chemical shift (multiplicity, coupling constant, integration) while paramagnetic compounds are reported as chemical shift (peak width at half height, number of protons). Solvent suppressed spectra were collected for paramagnetic compounds in THF using the PRESAT macro on the VNMR software. Gas chromatography was performed on a Shimadzu GC-2014 gas chromatograph using a Rxi-5ms Column and tetradecane as an internal standard. Infrared (IR) spectra were recorded on a Bruker Alpha attenuated total reflectance infrared spectrometer. High-resolution mass spectra were obtained at the Boston College Mass Spectrometry Facility on a JEOL AccuTOF DART instrument.

General procedure for screening of conditions for iron-catalyzed C-H activation reactions: In a nitrogen-filled glovebox iron dichloride (3.1 mg, 0.025 mmol), ligand (0.025 mmol or 0.05 mmol) and lithium amide (0.300 mmol) were added to a 7 mL vial containing a stir bar. Toluene (5 mL) was added to the stirring vial followed immediately by a 1 mL toluene solution of phenylboronic acid pinacol ester (51 mg, 0.250 mmol), tetradecane (16.2 µL, 0.075 mmol), and *tert*-butyl chloride (27 µL, 0.250 mmol). The reaction was then sealed and removed from the glovebox. The reaction was heated to 80 ºC for the specified time. After the specified amount of time, the reaction was quenched with a drop of water. The reaction was then dried over sodium sulfate and filtered. Yield was determined by quantitative gas chromatography.

Procedure for the C-H activation of ethyl benzene. In a nitrogen-filled glovebox iron complex (0.025 mmol) and lithium amide (0.30 mmol) were added to a 7 mL vial containing a stir bar. Ethyl benzene (5 mL) was added to the stirring vial followed immediately by a 1 mL ethyl benzene solution of phenylboronic acid pinacol ester (51 mg, 0.250 mmol), tetradecane (16.2 µL, 0.075 mmol), and *tert*-butyl chloride (27 µL, 0.250 mmol). The reaction was then sealed and stirred

for 24 hours. After the specified amount of time, the reaction was quenched with a drop of water. The reaction was then dried over sodium sulfate and filtered. Yield was determined by NMR using trimethoxybenzene as an external standard.

Procedure for the competition experiment between toluene and compound 4.3. In a nitrogen-filled glovebox CNBox^{Ph}FeCl (12.0 mg, 0.025 mmol), CNBox^{Ph} ligand (8.3 mg, 0.025 mmol), and lithium amide (16.3 mg, 0.25 mmol) were added to a 7 mL vial containing a stir bar. Toluene (5 mL) was added to the stirring vial followed immediately by a 1 mL toluene solution of phenylboronic acid pinacol ester (51 mg, 0.250 mmol), and compound **4.3** (52.7 mg, 0.250 mmol). The reaction was then sealed and stirred for 24 hours. After the specified amount of time, the reaction was quenched with a drop of water. The reaction was then dried over sodium sulfate and filtered. Yield was determined by NMR using trimethoxybenzene as an external standard. The product ratios were determined by integrating the triplet at 3.90 ppm relative to the singlet at 3.99 ppm. The singlet is associated with compound **4.1** and the triplet is associated with compound **4.4**. The compounds could not be separated from one another as the R$_f$ values are nearliy identical and the reaction was run on too small of a scale.

General procedure for screening of alternative oxidants. In a nitrogen-filled glovebox iron complex (0.025 mmol) and lithium ethylmethyl amide (19.5 mg. 0.30 mmol) were added to a 7 mL vial containing a stir bar. Toluene (5 mL) was added to the stirring vial followed immediately by a 1 mL benzene solution of phenylboronic acid pinacol ester (102 mg, 0.500 mmol), Tetradecane (0.060 mmol) and oxidant (0.250 mmol). The reaction was then sealed and stirred for 24 hours. After this time, the reaction was quenched with a drop of water. The reaction was then dried over sodium sulfate and filtered. Yield and relative ratios of products was determined by quantitative GC.

149

General procedure for screening of NacNac complexes for iron-catalyzed C-H activation

reactions: In a nitrogen-filled glovebox iron complex (0.025 mmol) and lithium amide (0.30 mmol) were added to a 7 mL vial containing a stir bar. Toluene (5 mL) was added to the stirring vial followed immediately by a 1 mL toluene solution of phenylboronic acid pinacol ester (51 mg, 0.250 mmol), tetradecane (16.2 µL, 0.075 mmol), and *tert*-butyl chloride (27 µL, 0.250 mmol). The reaction was then sealed and removed from the glovebox. The reaction was heated to 80 ºC for the specified time. After the specified amount of time, the reaction was quenched with a drop of water. The reaction was then dried over sodium sulfate and filtered. Yield was determined by quantitative gas chromatography.

General procedure for screening of NacNac complexes for radical clock substrates: In a nitrogen-filled glovebox iron complex (0.025 mmol) and lithium ethylmethyl amide (19.5 mg. 0.30 mmol) were added to a 7 mL vial containing a stir bar. Benzene (5 mL) was added to the stirring vial followed immediately by a 1 mL benzene solution of phenylboronic acid pinacol ester (102 mg, 0.500 mmol), and 6-bromo-1-hexene (33.4 µL, 0.250 mmol). The reaction was then sealed and stirred for 24 hours. After this time, the reaction was quenched with a drop of water. The reaction was then dried over sodium sulfate and filtered. Yield and relative ratios of products was determined by ^{1}H NMR

General procedure for screening of conditions for iron-catalyzed three-component coupling reactions: In a nitrogen-filled glovebox iron complex (0.025 mmol), and lithium dimethyl amide (0.250 mmol) were added to a 7 mL vial containing a stir bar. Benzene (5 mL) was added to the stirring vial followed immediately by a 1 mL benzene solution of phenylboronic acid pinacol ester (51 mg, 0.250 mmol), tetradecane (16.2 µL, 0.075 mmol), and *tert*-butyl chloride (27 µL, 0.250 mmol). The reaction was then sealed and removed from the glovebox. The reaction

was heated to 80 °C for the specified time. After the specified amount of time, the reaction was quenched with a drop of water. The reaction was then dried over sodium sulfate and filtered. Yield was determined by quantitative gas chromatography.

Procedure for the three-component coupling reaction with a dimethyl aniline additive. In a nitrogen-filled glovebox iron complex **4.11** (16.7 mg, 0.025 mmol), and lithium dimethyl amide (12.8 mg, 0.250 mmol) were added to a 7 mL vial containing a stir bar. Benzene (5 mL) was added to the stirring vial followed immediately by a 1 mL benzene solution of paramethoxyphenylboronic acid pinacol ester (59 mg, 0.250 mmol), tetradecane (16.2 μL, 0.062 mmol), dimethyl aniline (30 mg, 0.250 mmol) and *tert*-butyl chloride (27 μL, 0.250 mmol). The reaction was then sealed and removed from the glovebox. The reaction was heated to 80 °C for the specified time. After the specified amount of time, the reaction was quenched with a drop of water. The reaction was then dried over sodium sulfate and filtered. Yield was determined by NMR using trimethoxybenzene as an external standard. The reaction was also analyzed by GC to determine if any minor products were present and none were found.

General procedure for synthesis of β-diketiminate ligands. See chapter 3 for detailed proceedure for the preparation of these ligands.

Synthesis of 2,2,6,6-tetramethyl-3,5-bis[(2,6-dimethylphenyl)imino]heptane. Synthesized according to a literature procedure.[19] NMR features broad peaks due to rapid tautomerization. ^{1}H NMR (400 MHz, CDCl$_3$) δ 7.05 – 6.86 (s, 4H), 6.84 – 6.74 (s, 2H), 3.29 (s, 2H), 2.04 – 1.78 (s, 12H), 1.43 – 1.21 (s, 9H), 1.02 – 0.85 (s, 9H). Shifts match literature values.
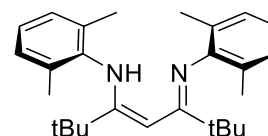
General procedure for synthesis of β-diketiminate iron chloride complexes. See chapter 3 for a detailed proceedure for the synthesis of these complexes.

151

Synthesis of 2,2,6,6-tetramethyl-3,5-bis[(2,6-dimethylphenyl)imino]heptane iron chloride complex (4.8). Synthesized according to general procedure using 2,2,6,6-tetramethyl-3,5-bis[(2,6-dimethylphenyl)imino]heptane as the ligand. ^{1}H NMR (400 MHz, THF) δ -75.0 ($w_{1/2}$ = 105 Hz, 2H), -51.4 ($w_{1/2}$ = 348 Hz, 1H), 12.8 ($w_{1/2}$ = 152 Hz, 36H), 21.7 ($w_{1/2}$ = 383 Hz, 12H), 22.9 ($w_{1/2}$ = 82 Hz, 4H) ppm. IR: 3301, 1665, 1539, 1320, 752, 691 cm^{-1}.
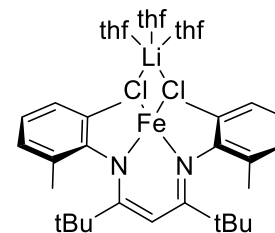
Synthesis of *(5-chloro-5-methylhexyl)benzene* (4.3) 2-methyl-6-phenyl-hexan-2-ol (1 g, 5.20 mmol) was placed into a 7mL vial. To it was added. hydrogen chloride (12 M, 2 mL). The vial was capped, and the mixture was shaken for 10 minutes. The organic phase was then separated, and the aqueous phase extracted with hexane (3x 2 mL). The organic phase was then dried with sodium sulfate and concentrated. It was then loaded onto a plug of silica and eluted with hexanes (200 mL). This was then collected, and the solvent removed under vacuum. To yield the pure product which matched literature values[20] (710 mg, 64 % yield). ^{1}H NMR (500 MHz, Chloroform-d) δ 7.31 – 7.25 (m, 2H), 7.18 (m, 3H), 2.64 (t, J = 7.7 Hz, 2H), 1.81 – 1.74 (m, 2H), 1.65 (m, =2H), 1.56 (s, 6H).
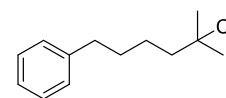
Synthesis of *N*-methyl-*N*-neopentylaniline. In a nitrogen-filled glovebox iron complex (0.025 mmol), and lithium amide (0.250 mmol) were added to a 7 mL vial containing a stir bar. Benzene (5 mL) was added to the stirring vial followed immediately by a 1 mL benzene solution of phenylboronic acid pinacol ester (51 mg, 0.250 mmol), tetradecane (16.2 µL, 0.075 mmol), and *tert*-butyl chloride (27 µL, 0.250 mmol). The reaction was then sealed and removed from the glovebox. The reaction was heated to 80 °C for 4 hours. The reaction was quenched with a drop of water. The reaction was then dried over sodium sulfate and

152
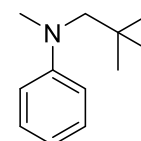
filtered. The product was purified by chromatography on silica gel (R_f = 0.65 in 100% hexanes). NMR shifts matched literature values.[21] ^{1}H NMR (600 MHz, CDCl$_3$) δ 7.46 (t, J = 7.5 Hz, 2H), 6.75 (d, J = 8.2 Hz, 2H), 6.65 (t, J = 7.2 Hz, 1H), 3.13 (s, 2H), 2.98 (s, 3H), 0.99 (s, 9H).

4.8. References

1.   Shang, R.; Ilies, L.; Nakamura, E., Iron-Catalyzed C–H Bond Activation. *Chemical Reviews* **2017,** *117* (13), 9086-9139.
2.   Wang, P.; Verma, P.; Xia, G.; Shi, J.; Qiao, J. X.; Tao, S.; Cheng, P. T. W.; Poss, M. A.; Farmer, M. E.; Yeung, K.-S.; Yu, J.-Q., Ligand-accelerated non-directed C–H functionalization of arenes. *Nature* **2017,** *551*, 489.
3.   Liu, T.; Qiao, J. X.; Poss, M. A.; Yu, J.-Q., Palladium(II)-Catalyzed Site-Selective C(sp3)−H Alkynylation of Oligopeptides: A Linchpin Approach for Oligopeptide–Drug Conjugation. *Angewandte Chemie International Edition* **2017,** *56* (36), 10924-10927.
4.   Davies, H. M. L.; Morton, D., Recent Advances in C–H Functionalization. *The Journal of Organic Chemistry* **2016,** *81* (2), 343-350.
5.   Le, C.; Liang, Y.; Evans, R. W.; Li, X.; MacMillan, D. W. C., Selective sp3 C–H alkylation via polarity-match-based cross-coupling. *Nature* **2017,** *547*, 79.
6.   Carestia, A. M.; Ravelli, D.; Alexanian, E. J., Reagent-dictated site selectivity in intermolecular aliphatic C–H functionalizations using nitrogen-centered radicals. *Chemical Science* **2018,** *9* (24), 5360-5365.
7.   Shaw, M. H.; Shurtleff, V. W.; Terrett, J. A.; Cuthbertson, J. D.; MacMillan, D. W. C., Native functionality in triple catalytic cross-coupling: sp[3] C–H bonds as latent nucleophiles. *Science* **2016,** *352* (6291), 1304-1308.
8.   Vasilopoulos, A.; Zultanski, S. L.; Stahl, S. S., Feedstocks to Pharmacophores: Cu-Catalyzed Oxidative Arylation of Inexpensive Alkylarenes Enabling Direct Access to Diarylalkanes. *Journal of the American Chemical Society* **2017,** *139* (23), 7705-7708.
9.   Zhang, W.; Chen, P.; Liu, G., Copper-Catalyzed Arylation of Benzylic C–H bonds with Alkylarenes as the Limiting Reagents. *Journal of the American Chemical Society* **2017,** *139* (23), 7709-7712.
10.   Singh, P. P.; Gudup, S.; Ambala, S.; Singh, U.; Dadhwal, S.; Singh, B.; Sawant, S. D.; Vishwakarma, R. A., Iron oxide mediated direct C-H arylation/alkylation at [small alpha]-position of cyclic aliphatic ethers. *Chemical Communications* **2011,** *47* (20), 5852-5854.
11.   Hu, X., Nickel-catalyzed cross coupling of non-activated alkyl halides: a mechanistic perspective. *Chemical Science* **2011,** *2* (10), 1867-1886.
12.   Anslyn, E. V.; Dougherty, D. A., *Modern physical organic chemistry*. University Science: Sausalito, CA, 2006.
13.   Griller, D.; Ingold, K. U., Free-radical clocks. *Accounts of Chemical Research* **1980,** *13* (9), 317-323.
14.   Holland, P. L., Electronic Structure and Reactivity of Three-Coordinate Iron Complexes. *Accounts of Chemical Research* **2008,** *41* (8), 905-914.
15.   Crockett, M. P.; Wong, A. S.; Li, B.; Byers, J. A., Rational Design of an Iron-Based Catalyst for Suzuki–Miyaura Cross-Couplings Involving Heteroaromatic Boronic Esters and

Tertiary Alkyl Electrophiles. *Angewandte Chemie International Edition* **2020,** *59* (13), 5392-5397.

16.   Vitaku, E.; Smith, D. T.; Njardarson, J. T., Analysis of the Structural Diversity, Substitution Patterns, and Frequency of Nitrogen Heterocycles among U.S. FDA Approved Pharmaceuticals. *Journal of Medicinal Chemistry* **2014,** *57* (24), 10257-10274.

17.   Burger, B. J.; Bercaw, J. E., *New Developments in the Synthesis, Manipulation and Characterization of Organometallic Compounds*. American Chemical Society: Washington D.C., 1987.

18.   Pangborn, A. B.; Giardello, M. A.; Grubbs, R. H.; Rosen, R. K.; Timmers, F. J., Safe and Convenient Procedure for Solvent Purification. *Organometallics* **1996,** *15* (5), 1518-1520.

19.   M. Budzelaar, P. H.; van Oort, A. B.; Orpen, A. G., β-Diiminato Complexes of VIII and TiIII – Formation and Structure of Stable Paramagnetic Dialkylmetal Compounds. *European Journal of Inorganic Chemistry* **1998,** *1998* (10), 1485-1494.

20.   Khalaf, A., Modern Friedel-Crafts chemistry. I. Cycloalkylations of some secondary and tertiary phenylalkyl chlorides in the presence of the mild aluminum trichloride/nitromethane and iron(III) chloride catalysts. *Rev. Roum. Chim.* **1973,** *18* (2), 297-304.

21.   LUBOSCH, W.; SEEBACH, D., ChemInform Abstract: NUCLEOPHILIC AMINOALKYLATION WITH THIOPIVALAMIDES. *Chemischer Informationsdienst* **1980,** *11* (20).

Appendix A: Adding Diffusion Ordered NMR Spectroscopy (DOSY) to the Arsenal for Characterizing Paramagnetic Complexes

A.1   Introduction

Catalysis involving first-row transition metal complexes has been increasing in popularity recently due to a trend toward using more sustainable and less toxic resources as well as the potential for exploiting complementary reactivity compared to noble metal complexes.[1] A challenging aspect of studying first-row transition metal complexes is that many are paramagnetic due to small ligand-field splittings that result from more contracted 3d valence orbitals. Unlike their diamagnetic counterparts, techniques such as ^{1}H NMR spectroscopy make structure determination of paramagnetic complexes difficult because resonances are paramagnetically shifted and broad.[2] These properties result in lost information that can normally be deduced from chemical shift and J-coupling. Moreover, some paramagnetic compounds have missing resonances that are a consequence of peak broadening and/or fast relaxation times. As a result, alternative tools to study paramagnetic compounds are employed. Some of the popular techniques include X-ray crystallography, mass spectrometry, XAS spectroscopy, EPR spectroscopy,[3] SQUID magnetometry,[4] and Mössbauer spectroscopy.[5] While all of these techniques provide valuable information, many require instrumentation that is not widely available or are solid-state measurements that may not be relevant in the solution state where most catalytic reactions occur.

Since the early 1990s, diffusion-ordered NMR spectroscopy (DOSY) has grown in popularity as a powerful method to deconvolute complicated one-dimensional ^{1}H NMR spectra.[6] Initially, this technique was used to characterize aggregates, such as micelles[7] or coordination polymers.[8] More recently, DOSY has seen widespread use as a method to

complement size exclusion chromatography for determining the molecular weight of polymers[9] and to distinguish copolymers from mixtures of homopolymers.[10-12] The technique has also been invaluable to demonstrate interactions between molecules in solution, such as those between frustrated Lewis acid-base pairs.[13]

Despite its successful implementation for the characterization of diamagnetic small molecules and macromolecules, there are no systematic reports that describe using DOSY for the characterization of paramagnetic systems involving first row transition elements; the technique has however recently been used to characterize some paramagnetic complexes containing lanthanide elements.[14] Herein, DOSY spectroscopy is used to characterize paramagnetic compounds containing first-row transition metal elements. This study includes qualitative characterization of several paramagnetic compounds, including those containing more than one metal, and quantitative molecular weight determination for some paramagnetic complexes. These findings illustrate the utility of this technique for parsing mixtures, investigating complex equilibria, and elucidating aggregation states of paramagnetic complexes containing first row transition metals in solution.

The use of DOSY as a standard method has benefited greatly from recent advances in pulse sequences, which facilitate more rapid collection of high resolution data.[15] Coupled with these advances has been the development of accurate methods for determining molecular weight of small molecules and aggregates in solution. To circumvent such difficulties with using internal calibration curves,[16] Stalke and coworkers developed a method to measure molecular weight using external calibration curves.[17] This method has been particularly useful in elucidating the solution structure of organolithium and Grignard reagents.[18-21]

A.2 The development of the technique

Paramagnetic compounds pose a unique challenge for their characterization by DOSY because protons in paramagnetic complexes have broad signals due to fast nuclear spin relaxation times (T_1 and T_2) and electronic relaxation.[22] Moreover, hyperfine coupling to the paramagnetic centers cause ^1H NMR signals to resonate in a chemical shift window spanning several hundred ppm.[23-24] It is with these reasons in mind that iron-based complex **A1** was initially chosen to probe the viability of using DOSY spectroscopy to characterize paramagnetic complexes involving first row transition metals. Being high spin iron(II), the electronic correlation time (τ_s) for this complex is suitably short so that a one dimensional ^1H NMR spectrum with good signal to noise can be acquired.[22] The NMR spectrum of this complex has peaks in a wide chemical shift range with a variety of spin lattice relaxation
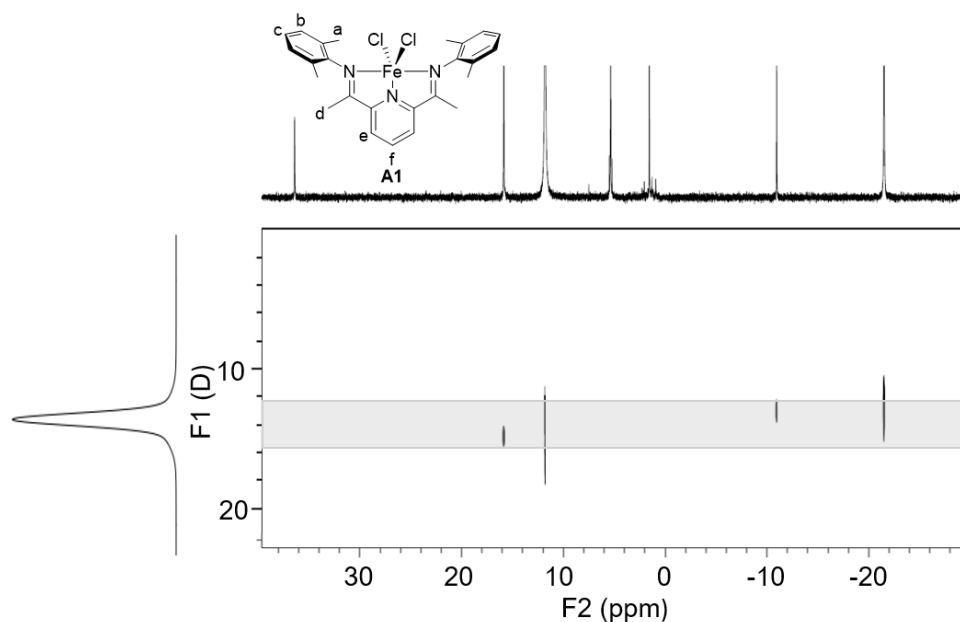
Figure A1 – DOSY Spectrum for **1** in CD_2Cl_2 at 25 °C. Peaks represented in the top spectrum are those with an observable diffusion peak in the DOSY spectrum. Weaker signals are not represented in the 2-D diffusion spectrum illustrated because the stronger signals would overwhelm the spectrum (note: The resonance observable at 82.9 ppm in the ^1H NMR spectrum did not result in an observable diffusion peak and is not included here so that the other resonances can be more clearly distinguished from one another).

Peak Assignment	δ (ppm)	$w_{1/2}$ (Hz)	T1 (ms)	DOSY Signal Observed
e	82.9	58	21.9	N
f	36.0	5	14.4	Y
b	15.9	147	56.5	Y
a	11.9	4	4.2	Y
c	-11.1	21	79.4	Y
d	-21.6	44	13.6	Y

Table A1 – Chemical shift (δ), peak width at half-width ($w_{1/2}$), and spin lattice relaxation times (T1) from ^{1}H NMR, and the observation of a DOSY signal for **A1** in CD_2Cl_2 at 25 ºC.

times (T_1) and peak widths ($w_{1/2}$), which make it amenable to study whether these factors play a role for observing a diffusion signal in the DOSY spectrum (Table A1). Satisfyingly, a single diffusion signal was observed in the DOSY spectrum for complex **A1**, and all resonances were observable except the resonance at 82.9 ppm (Figure A1).

The single diffusion peak observed in the DOSY spectrum combined with integration of the one-dimensional ^{1}H NMR spectrum confirmed that a single component existed in solution. Moreover, **A1** qualitatively had the diffusion properties expected, demonstrating a much lower diffusion coefficient measured for **A1** (D = 11.9x10^{-9}) than the solvent (D = 34.4x10^{-9}). However, when the complex was referenced to the calibration curve established by Stalke and coworkers,[25] the predicted molecular weight was 394 g/mol, which was 21% lower than the molecular weight of the complex (496 g/mol).

While these findings were promising for using DOSY to assess the purity of paramagnetic compounds and to provide a qualitative assessment of their molecular weight, we sought a more quantitative way to measure molecular weight. The inclusion of heavy metal elements is one difference between the compounds being studied here and those used previously to create the calibration curves needed for molecular weight measurements. Due to their higher density, complexes that contain transition metal elements are expected to result in diffusion coefficients that are much larger than organic molecules of similar

molecular weight. Thus, molecular weights of transition metal complexes will be underestimated when using a calibration curve comprised of compounds that do not contain a heavy element. This difficulty has been identified and addressed by Stalke and coworkers using correction factors based on molecular density.[26] Unfortunately, these correction factors have only been measured in C_6D_6 and THF-d_8 and the spectra acquired in this study were acquired in CD_2Cl_2. Therefore, to provide more quantitative information in diclhoromethane, the existing calibration curves were extended by using molecules containing heavier nuclei.
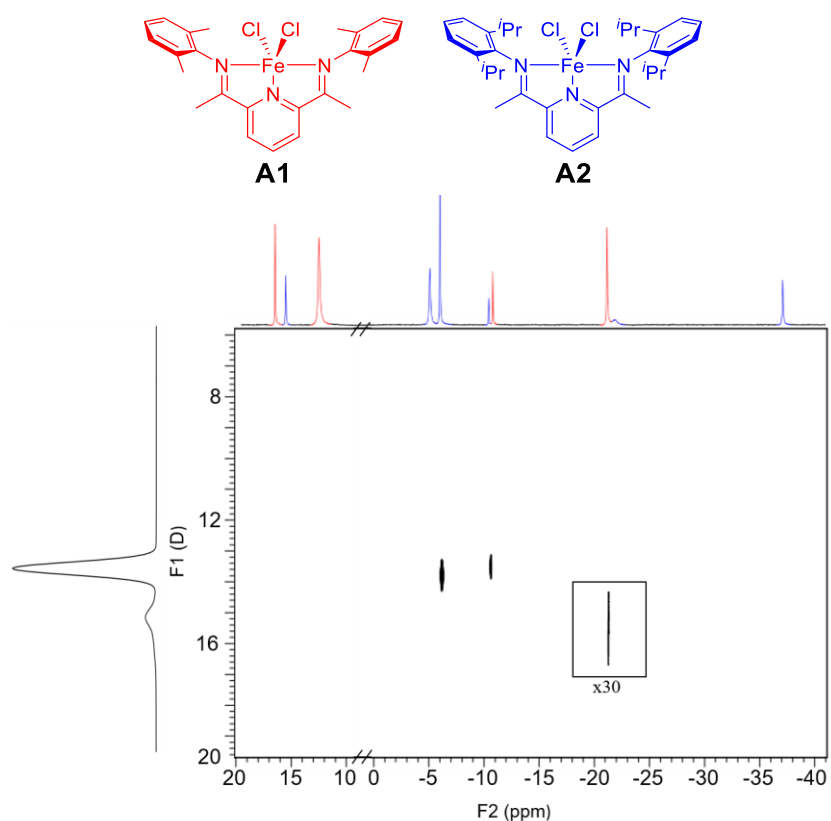
Figure A2 – DOSY Spectrum of a mixture of **A1** and **A2** in CD_2Cl_2 at 25 ºC. Peaks represented in the top spectrum are those with an observable diffusion peak in the DOSY spectrum. Weaker signals are not represented in the 2-D diffusion spectrum illustrated because the stronger signals would overwhelm the spectrum. (note: the portion of the spectrum between 0 and 10 ppm and above 17 ppm is not included as a space saving measure). Inset is pictured at 30x magnification

A.3 Calibration curve generation

To generate the new calibration curve, DOSY spectra were acquired in dichloromethane for eight compounds, comprised primarily of first row transition metal metallocene complexes (e.g., ferrocene, titanocene dichloride, etc.). As expected, a linear trend with a good fit was observed when molecular weight was plotted against the measured diffusion coefficient, but the slope and intercepts of the curve differed from the curve generated by Stalke and coworkers (See experimental section).[17, 25] This difference likely reflects the density differences of the compounds used for the two calibration curves. When the data obtained in Figure 1 for the characterization of **A1** was applied to the new calibration, a mass of 513 g/mol was obtained. This mass is in very good agreement with the molecular weight of the complex (496 g/mol), with an error of less than 5%.

A.4 Practical applications of the new method

To further highlight the practicality of the technique for parsing mixtures of paramagnetic complexes, a mixture of **A1** and a similar but larger bis(imino)pyridine iron dichloride complex (**A2**) was characterized by DOSY (Figure A2). The DOSY spectrum of the mixture could clearly be separated into two components, where the species with small diffusion coefficients (Figure A2, top) have predicted molecular weights consistent with complex **2** (603 g/mol as compared to predicted of 608 g/mol) and the species with large diffusion coefficients (Figure A2, bottom) have predicted molecular weights that are more consistent with the smaller complex **A1** (485 g/mol as compared to predicted of 496 g/mol).

Finally, to test the limitations of the developed method, DOSY spectra were acquired for two heterobimetallic compounds **A3** and **A4**, where one of the metals was a paramagnetic, first row transition-metal (Figure A3). Encouragingly, the DOSY spectra for both compounds demonstrated diffusion signals. Compound **A3** had a single, distinct peak in

160

the diffusion spectrum (Figure A3a), which was consistent with the complex being monomeric in solution.[27] In contrast, complex **A4** had a very sophisticated DOSY spectrum (Figure A3b). All structural information to date has suggested that **A4** is dimeric, but the reactivity of the complex suggests that the dimer is in equilibrium with a monomeric complex.[28-29] The diffusion coefficients determined for this complex in solution from the DOSY spectrum suggest that the complex exists as a mixture of compounds with the
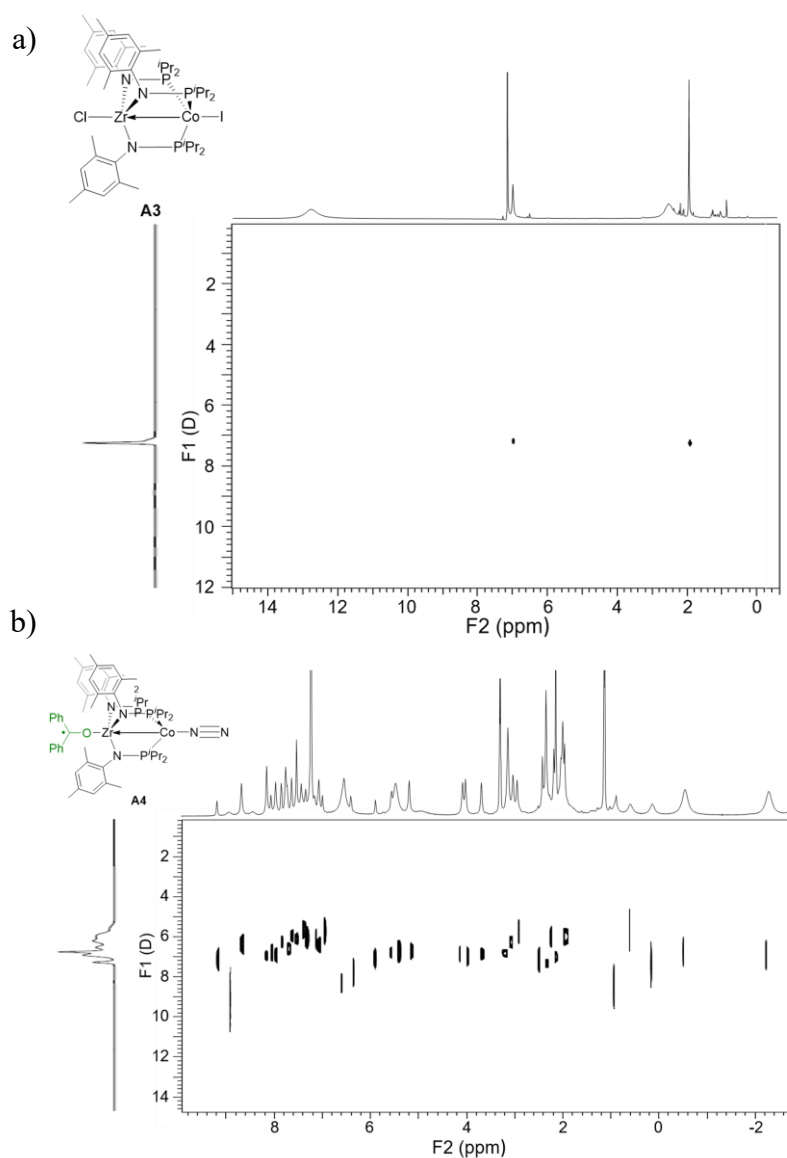
Figure A3 – DOSY spectra of a) complex **A3** and b) complex **A4** in C_6H_6 at 25 °C. Complex **A4** has been characterized as a dimer, but the DOSY spectrum is more consistent with a monomeric species as a major contributor in solution.

majority of the spectroscopically visible signals having similar molecular weights as **A3**. The mixture of compounds could be a variety of things, including various solvated species or species with hemilabile amidophosphine ligands. What is certain from the DOSY spectrum is that a major component of **A4** is monomeric in solution. This data provides direct evidence for existence of a monomer for **A4**, which had only been deduced indirectly from reactivity studies. Unfortunately, complex **A3** and **A4** did not fit calibration curves generated in C_6H_6 or to corrections provided by Stalke and coworkers.[26] The molecular weight correction provided by Stalke did get close for complex **A3,** predicting a molecular weight of 842 g/mol which is a 21% difference from the actual molecular weight (1067 g/mol). Regardless to the calibration curves used, the molecular weights for these bimetallic compounds were systematically underestimated. This limitation was attributed to the presence of multiple heavy-metal elements, which deviated significantly compared to the compounds used to generate the calibration curves used for molecular weight measurements. Moreover, the molecular weights of these dinuclear compounds were extremely large, which posed a problem for finding reference compounds of similar molecular weights needed to generate the calibration curves.

In order to provide some practical guidelines for users wanting to use DOSY to characterize paramagnetic complexes containing first row transition metal complexes, an
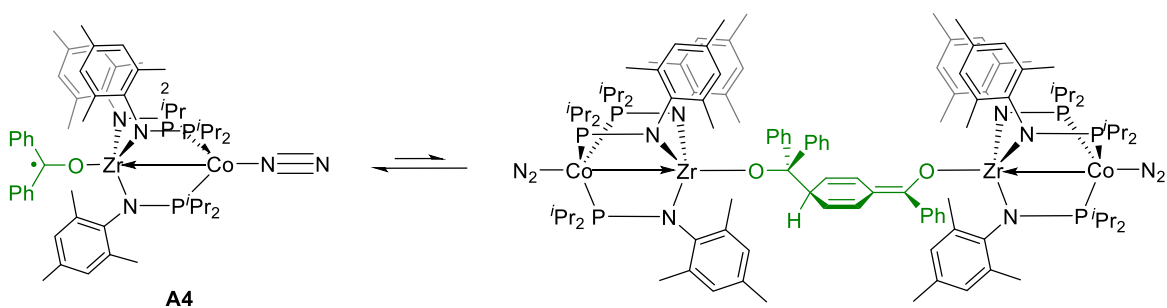
Scheme A1. Proposed disruption of the dimer of **A4** in the solution phase.

162

analysis of the peaks observable by DOSY from the paramagnetic compounds studied here was undertaken. Analysis of 34 peaks observed in the ^{1}H NMR spectra from five compounds revealed that T1 and $w_{1/2}$ had a significant effect on the ability to observe usable signals in the DOSY spectra. Resonances that were broad and with short T1 were less likely to be observable in the DOSY spectrum. Particularly predictive was the ratio between $w_{1/2}$ and T1, which can be obtained in short order from routine ^{1}H NMR spectra and T1 measurements. Resonances that had a $w_{1/2}$:T1 less than 100 were observable by DOSY 92% of the time, while those with $w_{1/2}$:T1 less than 1000 gave diffusion signals 71% of the time. On the other hand, resonances with $w_{1/2}$:T1 greater than 10,000 resulted in diffusion peaks only 12% of the time. Without exception, the ^{1}H NMR resonances that did not result in a diffusion peak in the DOSY spectrum were those that were significantly paramagnetically shifted. No DOSY signals could be observed for any resonances with chemical shifts greater than 40 ppm or less than -25 ppm. It should also be mentioned that no diffusion peaks could be observed in DOSY spectra for compounds that contained metals with short electronic relaxation times (e.g., Mn(Ac)$_2\cdot$ 4H$_2$O).

The findings presented here demonstrate that it is possible to collect quantitative diffusion spectra of paramagnetic molecules containing one paramagnetic first row transition metal center. Moreover, qualitative information can be obtained for bimetallic complexes that contain one paramagnetic transition metal center. While not experimentally verified, in principle, quantitative information about these complexes could also be obtained if suitable reference compounds of the appropriate molecular weight were available to generate a calibration curve. Overall, these results demonstrate the potential power of using DOSY spectroscopy for characterizing paramagnetic complexes by

163

ascertaining aggregation states, determining solution state molecular weights, and parsing complicated mixtures. Such information will be invaluable to researchers interested in studying the coordination chemistry of paramagnetic complexes and developing new catalysts that involve base metals.

Excitingly, some of these challenges were recently addressed using a cryoprobe in addition to the pulse sequence adaptations described here. While these results are preliminary, they indicate that some of the limitations detailed here will be lessened as the available NMR technologies continue to advance. Finally, the work presented in this appendix would have been significantly less powerful without the collaboration of Hongtu in Christine Thomas's lab. Their complexes proved invaluable as a point of study to further refine the technique.

A.5   Experimental

General Considerations

All reactions were carried out in oven-dried glassware using standard Schlenk[30] line techniques, unless otherwise stated. Dichloromethane, pentane, toluene, diethyl ether, and tetrahydrofuran were used after passage through alumina under a blanket of argon and then degassed briefly by exposure to vacuum. Iron salts, analines, 2,6-diacetylpyridine, tetrakis(trimethylsilyl)silane, and ammonium hexafluorophosphate were purchased from Sigma-Aldrich, Fischer Scientific, TCI America, Oakwood, or Strem Chemicals. Methylene chloride-d_2, THF-d_8, and benzene-d_6 were purchased from Cambridge isotopes and dried from ketyl radical solutions or calcium hydride. ^{1}H NMR spectra were recorded at ambient temperature on a Varian 600MHz spectrometer. All spectra were acquired in 7mm NMR tubes without spinning. All DOSY spectra were collected using the Doneshot pulsing sequence with a pulse length of 2ms and a diffusion time $\Delta = 8$ms.

164

The gradients were incremented into 25 levels from 1000 to 25000. Data are reported as follows: chemical shift (integration, multiplicity). All chemical shifts are reported in ppm from tetramethylsilane with the solvent as internal reference.

Calibration Curve Generation

To utilize the this technique for measuring the molecular weight of compounds containing first-row transition metals a new set of calibration curves had to be generated. This curve is displayed in Figure E1 and the data with which it was generated from is in Table E1.
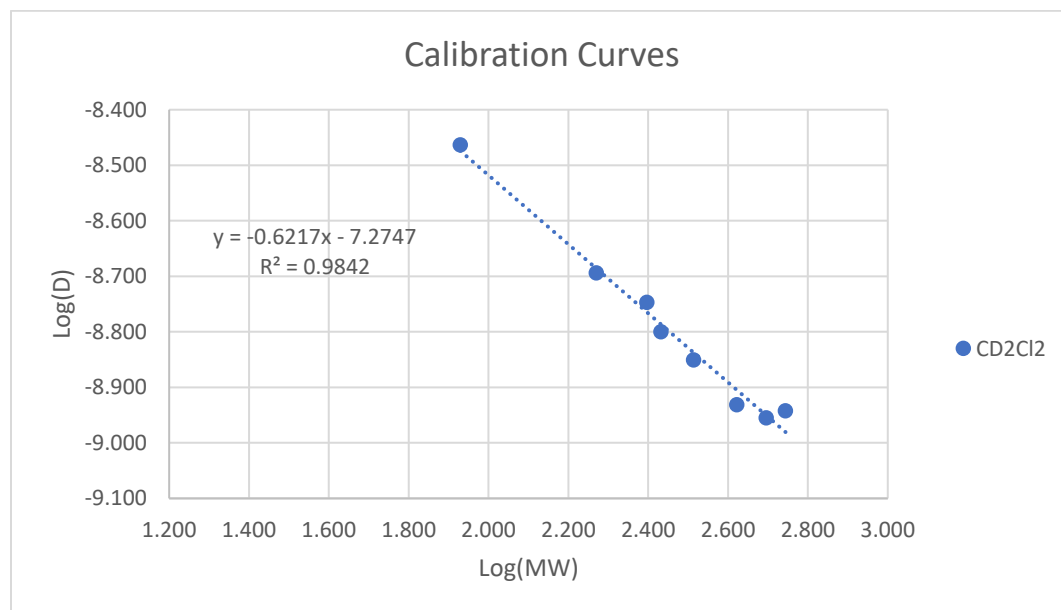
Figure A4 - Calibration Curves

Compound	CD_2Cl_2 Log(D)	log(MW)
Ferrocene	-8.694	2.270
1,1' diacetyl ferrocene	-8.800	2.432
dichloromethane	-8.463	1.929
titanocene dichloride	-8.747	2.396
dppf	-8.942	2.744
dipf	-8.931	2.621
decamethylferrocene	-8.850	2.514
PDIFeCl2	-8.955	2.695

Table A2 - Calibration Compounds

Dichloromethane was the preferred internal standard for generating this calibration curve.

Guidelines for seeing a diffusion signal

After collection of the spectra of a variety of paramagnetic complexes the $w_{1/2}$ and T1s were compiled alongside if there was signal observed for that peak. This data is listed in Table E2.

Shift	Width (Hz)	T1 (s)	Width/T1	Signal observed
-1.7	510	0.0006	825272	n
-24.4	450	0.0012	382500	n
7.9	242	0.0020	121176	n
69.8	1700	0.0189	90134	n
2.8	215	0.0061	35312	n
2.5	150	0.0066	22819	n
1.9	108	0.0067	16200	y
-6.9	400	0.0348	11480	n
-21.6	44	0.0136	3244	br
40.0	720	0.2481	2902	n
82.9	58	0.0219	2656	n
15.9	147	0.0565	2601	y
3.7	90	0.0427	2112	n
11.9	4	0.0042	914	y
1.3	185	0.2775	665	y
3.5	120	0.2857	420	n
36.0	5	0.0144	331	y
6.4	28	0.0869	318	n
4.1	15	0.0478	308	n
4.0	16	0.0604	271	n
-11.1	21	0.0794	269	br
1.1	72	0.6901	105	y

3.2	23	0.2457	95	y
1.2	50	0.5841	85	br
1.2	43	0.5900	73	br
7.4	29	0.5525	53	y
0.9	20	0.3876	51	y
3.9	27	0.5435	50	y
1.4	20	0.5698	36	y
3.5	21	0.5917	35	y
4.9	81	2.4752	33	n
0.8	21	0.6803	31	y
3.0	11	0.5924	19	y
3.1	11	0.6757	16	y

Table A3 - **Peak data**

This data was then used to generated guidelines from our experience on if a signal will be observed for an unknown complex.

Figure A5 - DOSY of Complex 4 –
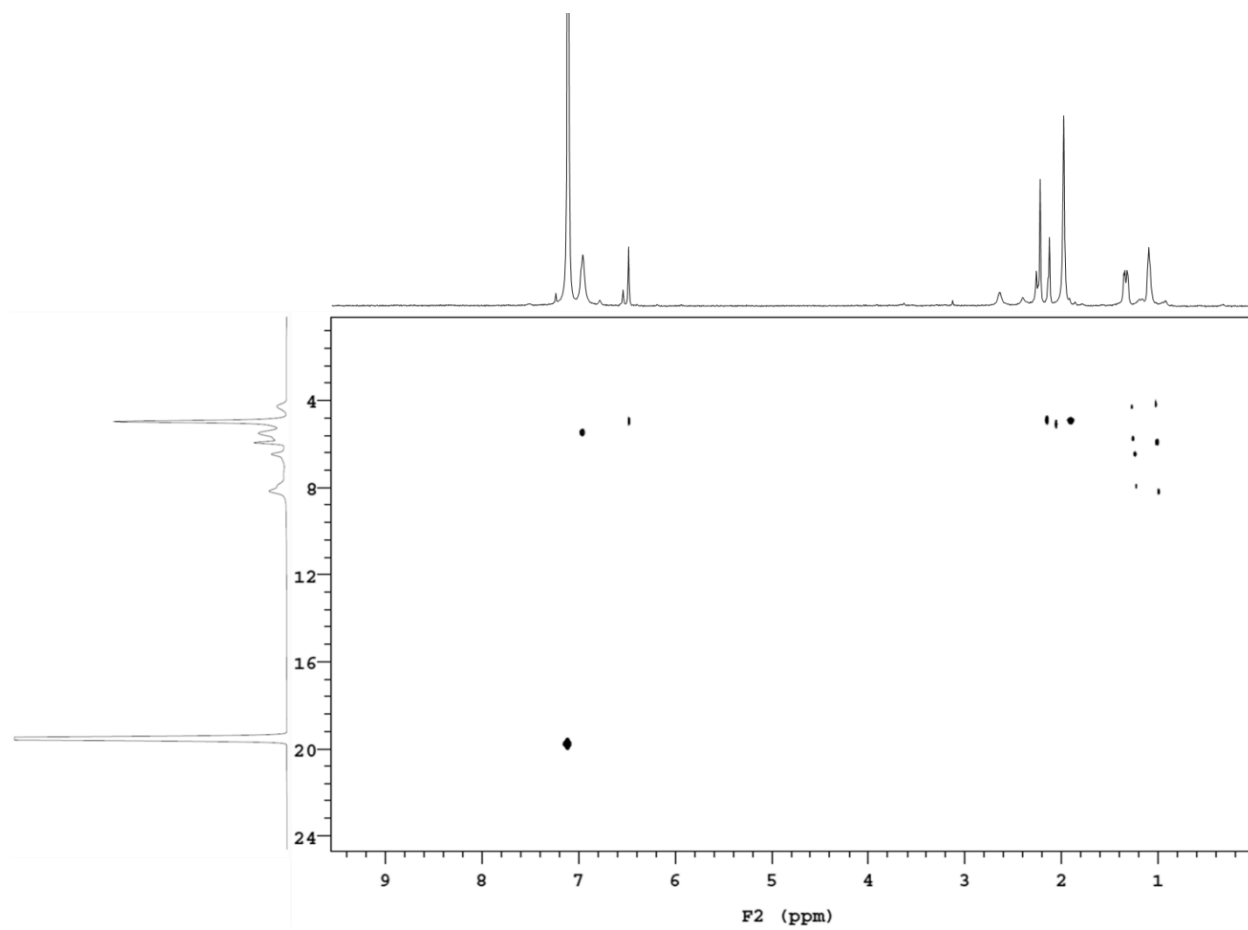
Figure A6 - DOSY of Complex A5 –
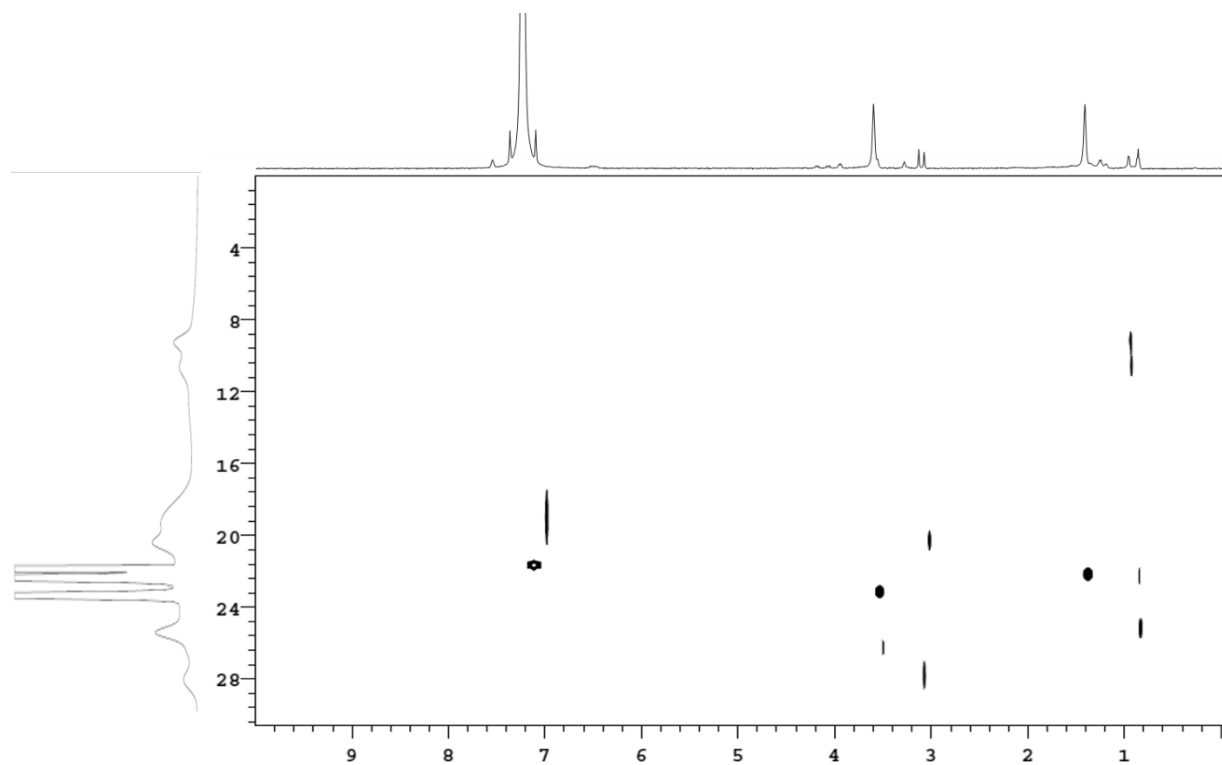
Figure A7 - DOSY of Complex A6 –
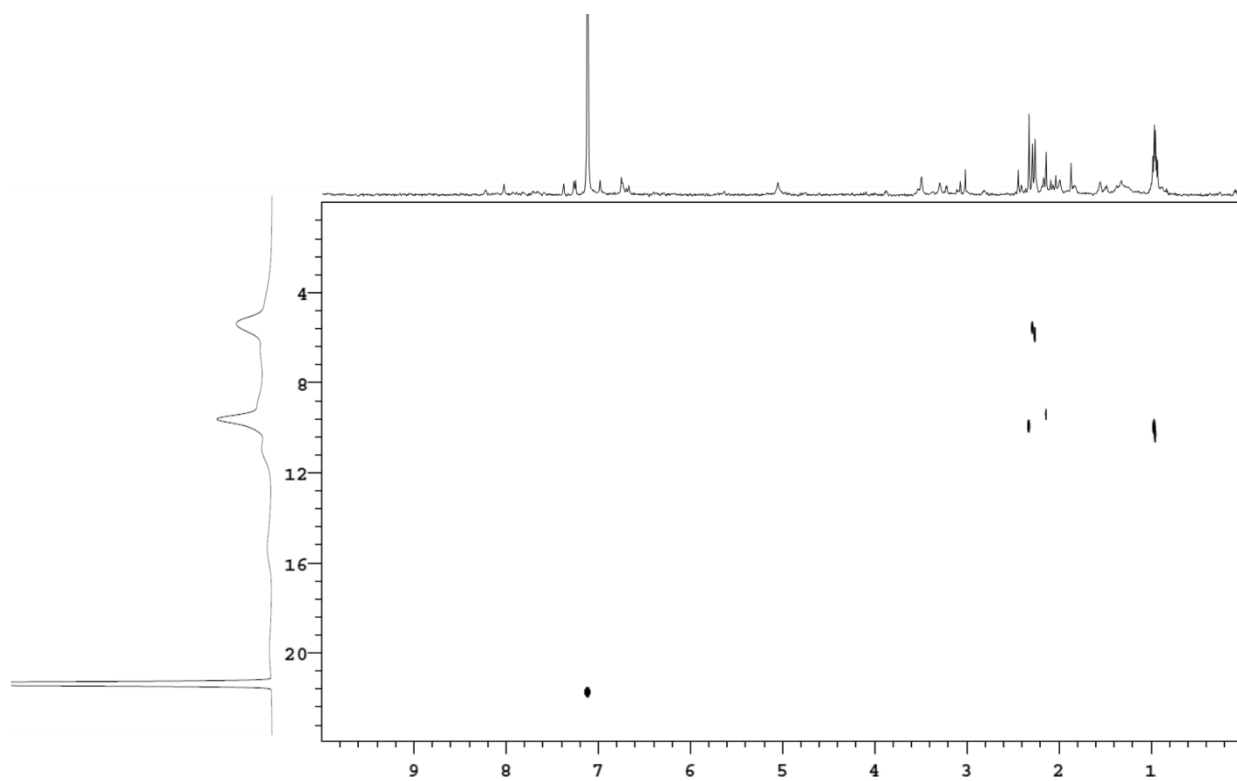
Complex synthesis

Compounds A1 and A2 Synthesized according to literature procedures.[31]

Compounds A3, A4, and A6 from Figure A3 Synthesized according to literature procedures.[32]

Compound A5 from Figure A3 Synthesized according to literature procedures.[33]

A.6   References

1.   Bauer, I.; Knölker, H.-J., Iron Catalysis in Organic Synthesis. *Chem. Rev.* **2015,** *115* (9), 3170-3387.
2.   Bertini, I.; Luchinat, C.; Parigi, G.; Ravera, E., Chapter 7 - Transition metal ions: shift and relaxation. In *NMR of Paramagnetic Molecules (Second Edition)*, Bertini, I.; Luchinat, C.; Parigi, G.; Ravera, E., Eds. Elsevier: Boston, 2017; pp 175-253.
3.   Odom, B.; Hanneke, D.; D'Urso, B.; Gabrielse, G., New Measurement of the Electron Magnetic Moment Using a One-Electron Quantum Cyclotron. *Phys. Rev. Lett.* **2006,** *97* (3), 030801.
4.   Sawicki, M.; Stefanowicz, W.; Ney, A., Sensitive SQUID magnetometry for studying nanomagnetism. *Semicond. Sci. Technol.* **2011,** *26* (6), 064006.
5.   Mössbauer, R. L., Kernresonanzfluoreszenz von Gammastrahlung in Ir191. *Z. Physik* **1958,** *151* (2), 124-143.
6.   Morris, K. F.; Johnson, C. S., Diffusion-ordered two-dimensional nuclear magnetic resonance spectroscopy. *J. Am. Chem. Soc.* **1992,** *114* (8), 3139-3141.
7.   Morris, K. F.; Johnson, C. S., Resolution of discrete and continuous molecular size distributions by means of diffusion-ordered 2D NMR spectroscopy. *J. Am. Chem. Soc.* **1993,** *115* (10), 4291-4299.
8.   Fujita, D.; Ueda, Y.; Sato, S.; Mizuno, N.; Kumasaka, T.; Fujita, M., Self-assembly of tetravalent Goldberg polyhedra from 144 small components. *Nature* **2016,** *540* (7634), 563-566.
9.   Viel, S.; Capitani, D.; Mannina, L.; Segre, A., Diffusion-Ordered NMR Spectroscopy: A Versatile Tool for the Molecular Weight Determination of Uncharged Polysaccharides. *Biomacromolecules* **2003,** *4* (6), 1843-1847.
10.   Paul, S.; Romain, C.; Shaw, J.; Williams, C. K., Sequence Selective Polymerization Catalysis: A New Route to ABA Block Copoly(ester-b-carbonate-b-ester). *Macromolecules* **2015,** *48* (17), 6047-6056.
11.   Viel, S.; Mazarin, M.; Giordanengo, R.; Phan, T. N. T.; Charles, L.; Caldarelli, S.; Bertin, D., Improved compositional analysis of block copolymers using Diffusion Ordered NMR Spectroscopy. *Anal. Chim. Acta* **2009,** *654* (1), 45-48.
12.   Biernesser, A. B.; Delle Chiaie, K. R.; Curley, J. B.; Byers, J. A., Block Copolymerization of Lactide and an Epoxide Facilitated by a Redox Switchable Iron-Based Catalyst. *Angew. Chem. Int. Ed.* **2016,** *55* (17), 5251-5254.
13.   Rocchigiani, L.; Macchioni, A., Disclosing the multi-faceted world of weakly interacting inorganic systems by means of NMR spectroscopy. *Dalton Trans.* **2016,** *45* (7), 2785-2790.
14.   Denis-Quanquin, S.; Riobé, F.; Delsuc, M.-A.; Maury, O.; Giraud, N., Paramagnetic DOSY: An Accurate Tool for the Analysis of the Supramolecular Interactions between Lanthanide Complexes and Proteins. *Chem. Eur. J.* **2016,** *22* (50), 18123-18131.

15.   Pelta, M. D.; Morris, G. A.; Stchedroff, M. J.; Hammond, S. J., A one-shot sequence for high-resolution diffusion-ordered spectroscopy. *Magn. Reson. Chem.* **2002,** *40* (13), S147-S152.

16.   Augé, S.; Schmit, P.-O.; Crutchfield, C. A.; Islam, M. T.; Harris, D. J.; Durand, E.; Clemancey, M.; Quoineaud, A.-A.; Lancelin, J.-M.; Prigent, Y.; Taulelle, F.; Delsuc, M.-A., NMR Measure of Translational Diffusion and Fractal Dimension. Application to Molecular Mass Measurement. *J. Phys. Chem. B* **2009,** *113* (7), 1914-1918.

17.   Neufeld, R.; Stalke, D., Accurate molecular weight determination of small molecules via DOSY-NMR by using external calibration curves with normalized diffusion coefficients. *Chem. Sci.* **2015,** *6* (6), 3354-3364.

18.   Li, D.; Keresztes, I.; Hopson, R.; Williard, P. G., Characterization of Reactive Intermediates by Multinuclear Diffusion-Ordered NMR Spectroscopy (DOSY). *Acc. Chem. Res.* **2009,** *42* (2), 270-280.

19.   Reich, H. J., Role of Organolithium Aggregates and Mixed Aggregates in Organolithium Mechanisms. *Chem. Rev.* **2013,** *113* (9), 7130-7178.

20.   Hamdoun, G.; Sebban, M.; Cossoul, E.; Harrison-Marchand, A.; Maddaluno, J.; Oulyadi, H., 1H Pure Shift DOSY: a handy tool to evaluate the aggregation and solvation of organolithium derivatives. *Chem. Commun.* **2014,** *50* (31), 4073-4075.

21.   Neufeld, R.; Teuteberg, T. L.; Herbst-Irmer, R.; Mata, R. A.; Stalke, D., Solution Structures of Hauser Base iPr2NMgCl and Turbo-Hauser Base iPr2NMgCl·LiCl in THF and the Influence of LiCl on the Schlenk-Equilibrium. *J. Am. Chem. Soc.* **2016,** *138* (14), 4796-4806.

22.   Chapter 3 Relaxation. *Coord. Chem. Rev.* **1996,** *150*, 77-110.

23.   Kruck, M.; Sauer, D. C.; Enders, M.; Wadepohl, H.; Gade, L. H., Bis(2-pyridylimino)isoindolato iron(ii) and cobalt(ii) complexes: Structural chemistry and paramagnetic NMR spectroscopy. *Dalton Trans.* **2011,** *40* (40), 10406-10415.

24.   Pennanen, T. O.; Vaara, J., Nuclear Magnetic Resonance Chemical Shift in an Arbitrary Electronic Spin State. *Phys. Rev. Lett.* **2008,** *100* (13), 133002.

25.   Bachmann, S.; Neufeld, R.; Dzemski, M.; Stalke, D., New External Calibration Curves (ECCs) for the Estimation of Molecular Weights in Various Common NMR Solvents. *Chem. Eur. J.* **2016,** *22* (25), 8462-8465.

26.   Kreyenschmidt, A.-K.; Bachmann, S.; Niklas, T.; Stalke, D., Molecular Weight Estimation of Molecules Incorporating Heavier Elements from van-der-Waals Corrected ECC-DOSY. *ChemistrySelect* **2017,** *2* (24), 6957-6960.

27.   Greenwood, B. P.; Forman, S. I.; Rowe, G. T.; Chen, C.-H.; Foxman, B. M.; Thomas, C. M., Multielectron Redox Activity Facilitated by Metal−Metal Interactions in Early/Late Heterobimetallics: Co/Zr Complexes Supported by Phosphinoamide Ligands. *Inorg. Chem.* **2009,** *48* (13), 6251-6260.

28.   Marquard, S. L.; Bezpalko, M. W.; Foxman, B. M.; Thomas, C. M., Stoichiometric C═O Bond Oxidative Addition of Benzophenone by a Discrete Radical Intermediate To Form a Cobalt(I) Carbene. *J. Am. Chem. Soc.* **2013,** *135* (16), 6018-6021.

29.   Zhou, W.; Marquard, S. L.; Bezpalko, M. W.; Foxman, B. M.; Thomas, C. M., Catalytic Hydrosilylation of Ketones Using a Co/Zr Heterobimetallic Complex: Evidence for an Unusual Mechanism Involving Ketyl Radicals. *Organometallics* **2013,** *32* (6), 1766-1772.

30.   Burger, B. J.; Bercaw, J. E., New Developments in the Synthesis, Manipulation and Characterization of Organometallic Compounds. American Chemical Society: Washington, D.C., 1987.

171

31.   Small, B. L.; Brookhart, M.; Bennett, A. M. A., Highly Active Iron and Cobalt Catalysts for the Polymerization of Ethylene. *Journal of the American Chemical Society* **1998,** *120* (16), 4049-4050.

32.   Saper, N. I.; Bezpalko, M. W.; Foxman, B. M.; Thomas, C. M., Synthesis of chiral heterobimetallic tris(phosphinoamide) Zr/Co complexes. *Polyhedron* **2016,** *114*, 88-95.

33.   Kuppuswamy, S.; Bezpalko, M. W.; Powers, T. M.; Turnbull, M. M.; Foxman, B. M.; Thomas, C. M., Utilization of Phosphinoamide Ligands in Homobimetallic Fe and Mn Complexes: The Effect of Disparate Coordination Environments on Metal–Metal Interactions and Magnetic and Redox Properties. *Inorganic chemistry* **2012,** *51* (15), 8225-8240.

Appendix B: Spectral Data for Chapter 2.

Figure B1. – ^{1}H NMR(500 MHz) spectrum of (CNBox[Ph])FeCl$_2$ (**2.11**).
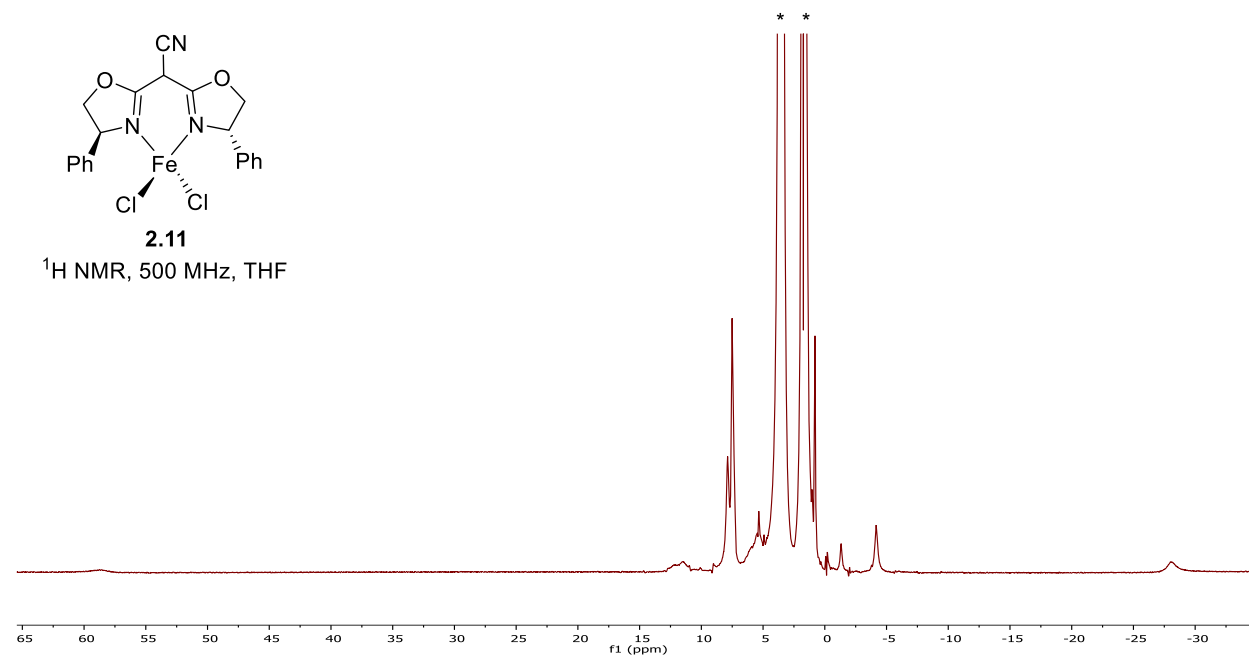
Figure B2. – ^{1}H NMR(500 MHz) spectrum of (CNBox[Ph])FeCl (**2.12**).
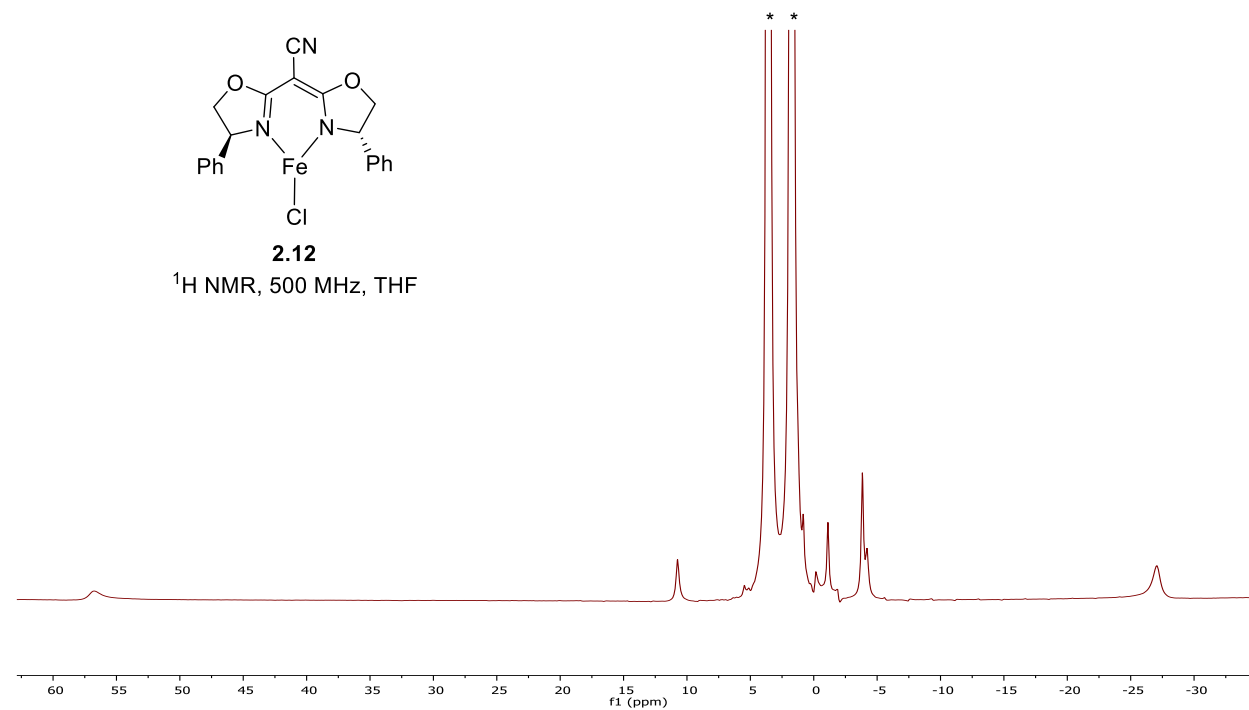
Figure B3.– ^{1}H NMR(400 MHz) spectrum of (CNBox^{Ph})$_2$Fe (**2.13**).

2.13
^{1}H NMR, 400 MHz, THF
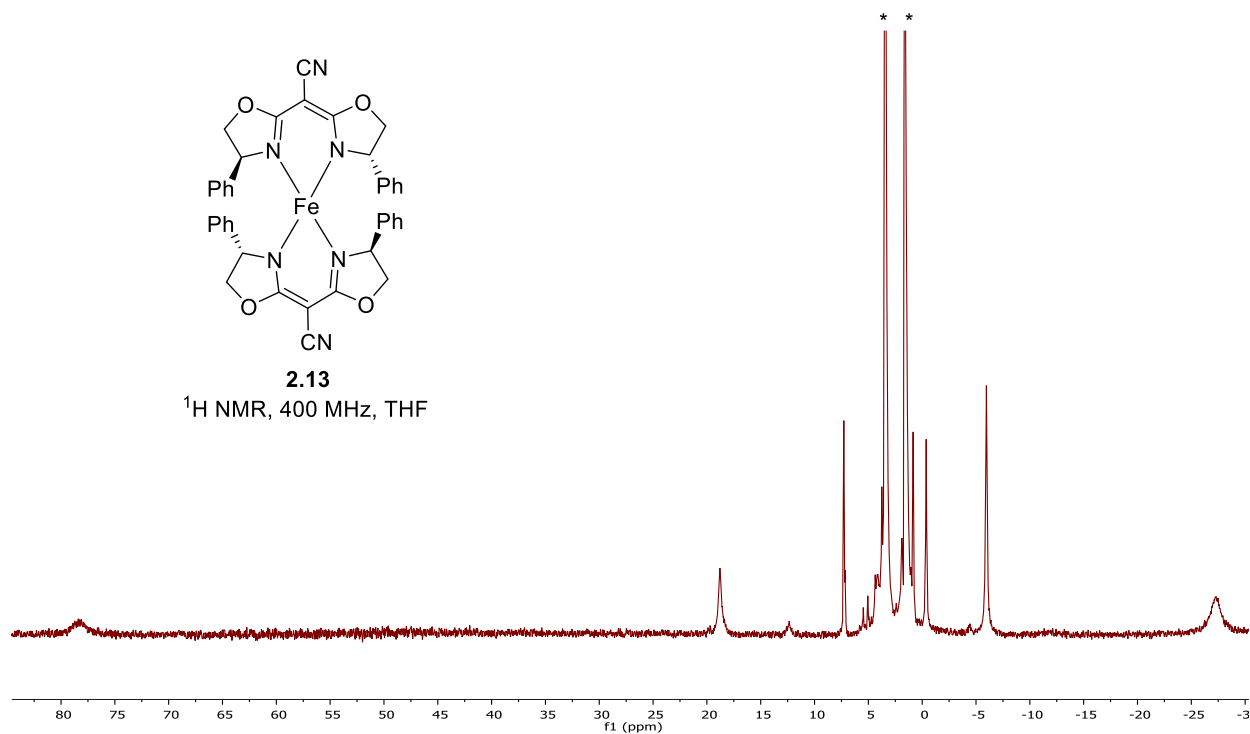
Figure B4.– ^{1}H NMR(500 MHz) of (3-trifluoromethyl)phenyl)cycloheptane (**2.27**).

2.27
^{1}H NMR, 500 MHz, CDCl$_3$
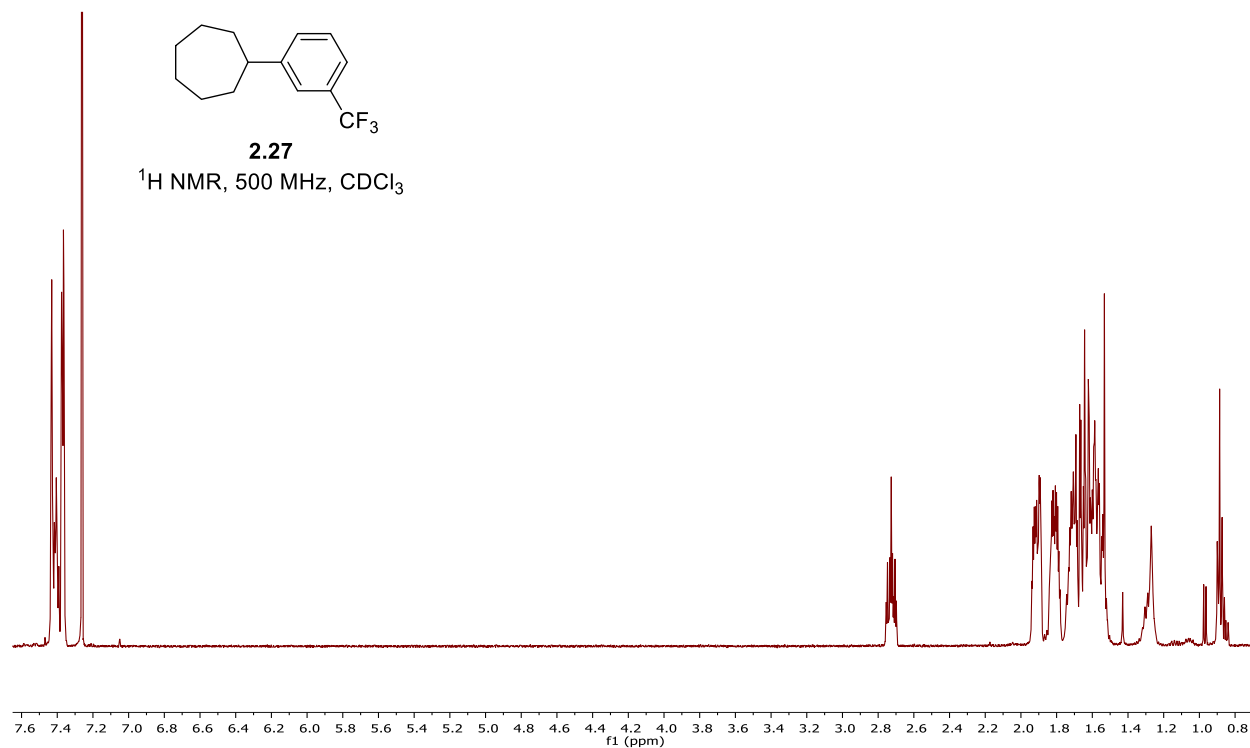
Figure B5.– {¹H}¹³C NMR(125 MHz) spectrum of (3-trifluoromethyl)phenyl)cycloheptane (**2.27**).

¹³C NMR, 125MHz, CDCl₃

2.27
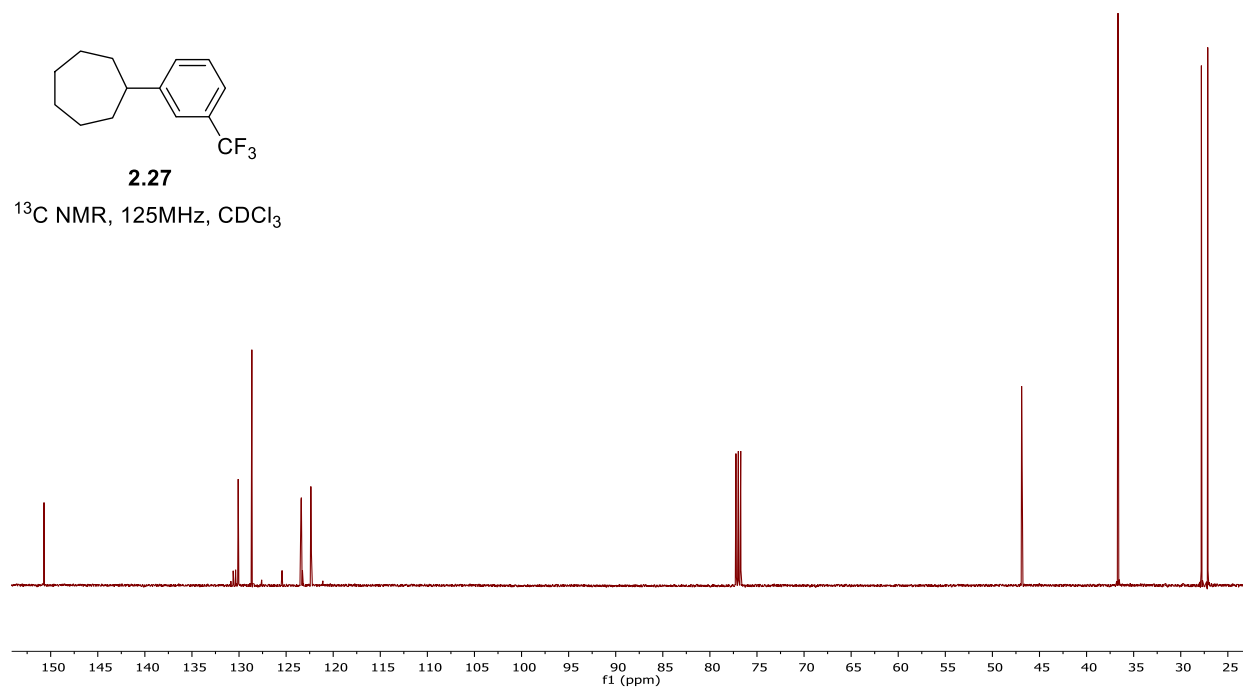
Figure B6. – ¹⁹F NMR(470MHz) spectrum of (3-(trifluoromethyl)phenyl)cycloheptane (**2.27**).

¹⁹F NMR, 470MHz, CDCl₃

2.27
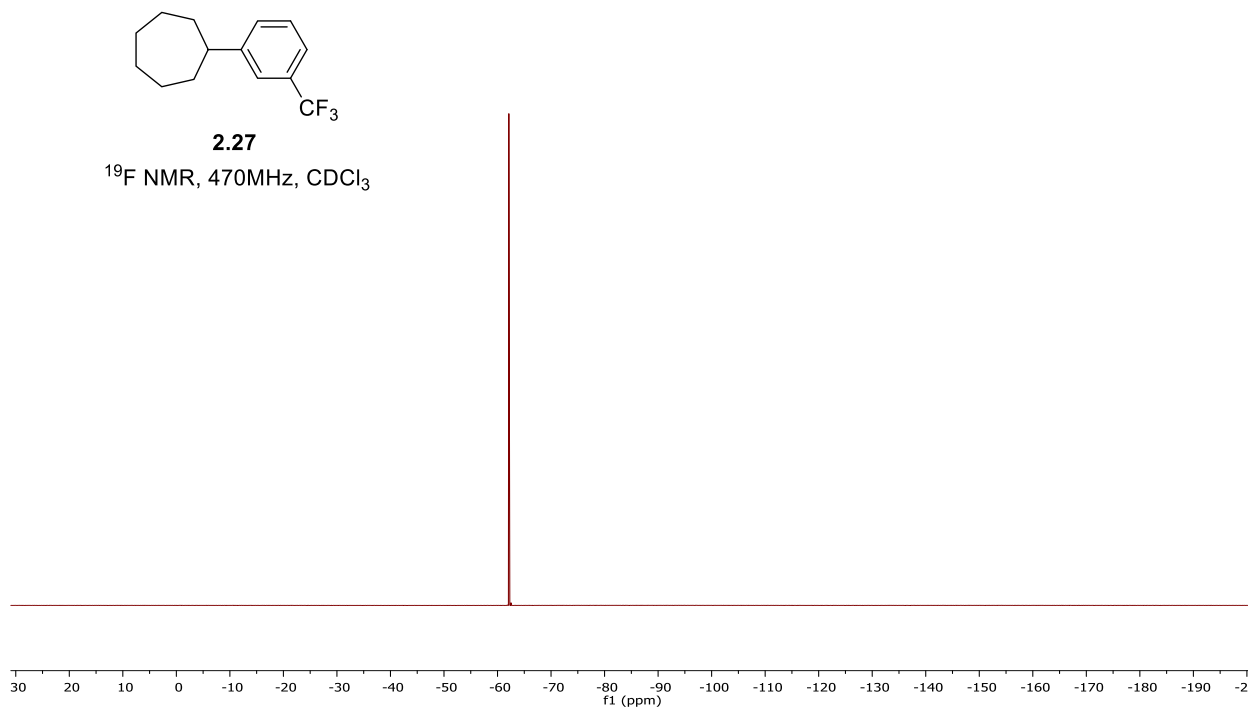
Figure B7.– ^{1}H NMR(500 MHz) spectrum of 1-(3-chloropropyl)-3-(trifluoromethyl)benzene (**2.43**).

2.43

^{1}H NMR, 500 MHz, CDCl$_3$
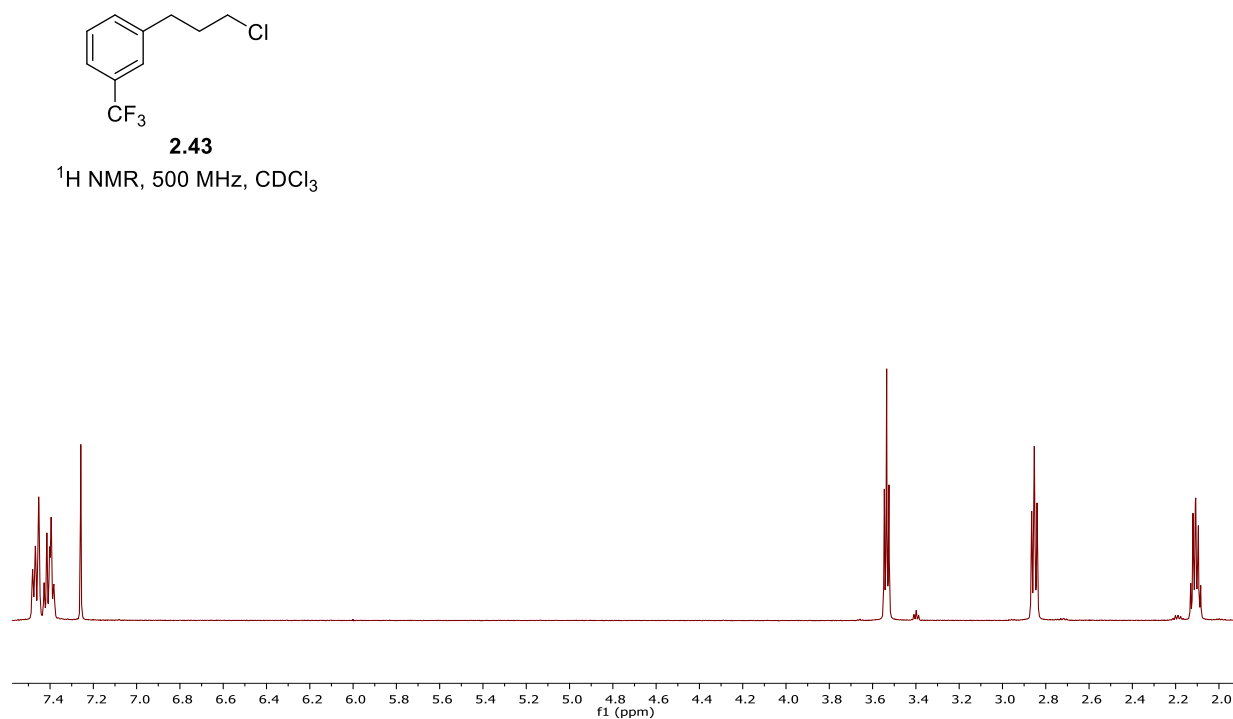
Figure B8.– $\{^1H\}^{13}C$ NMR(125 MHz) spectrum of 1-(3-chloropropyl)-3-(trifluoromethyl)benzene (**2.43**).

2.43

^{13}C NMR, 125 MHz, CDCl$_3$
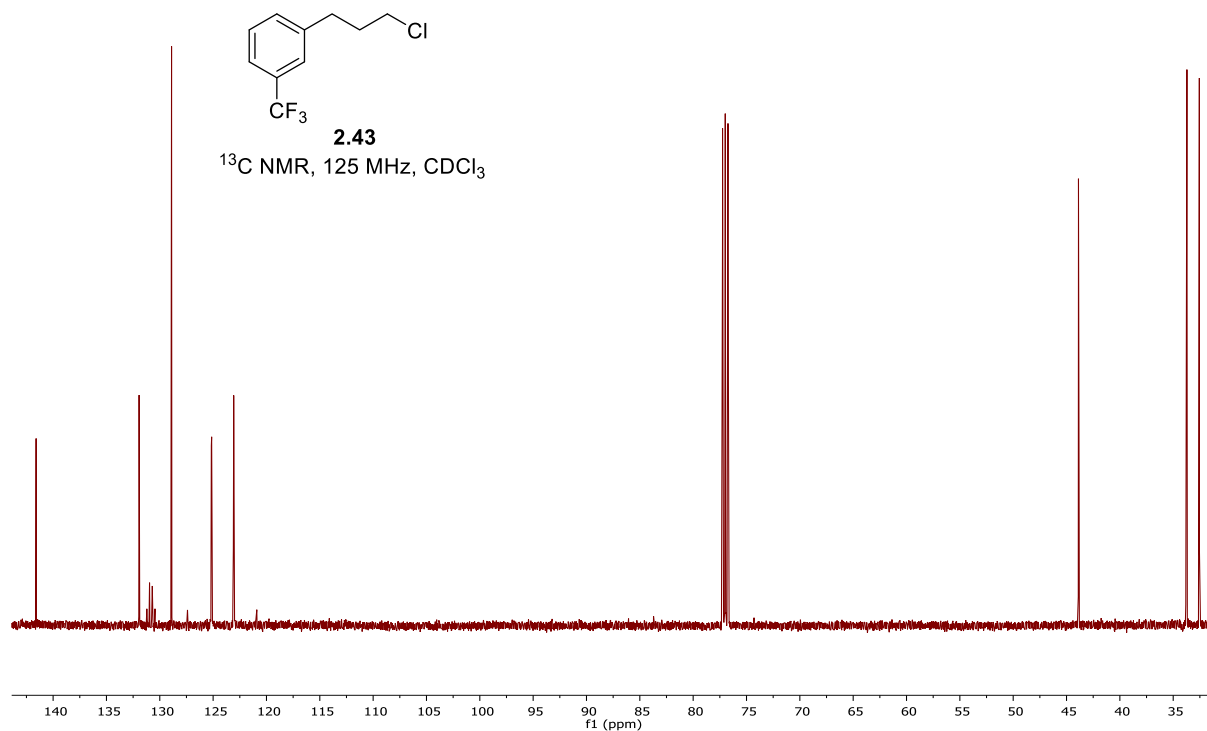
Figure B9.– ^{19}F NMR(470MHz) spectrum of 1-(3-chloropropyl)-3-(trifluoromethyl)benzene (**2.43**).

2.43
^{19}F NMR, 470 MHz, CDCl$_3$
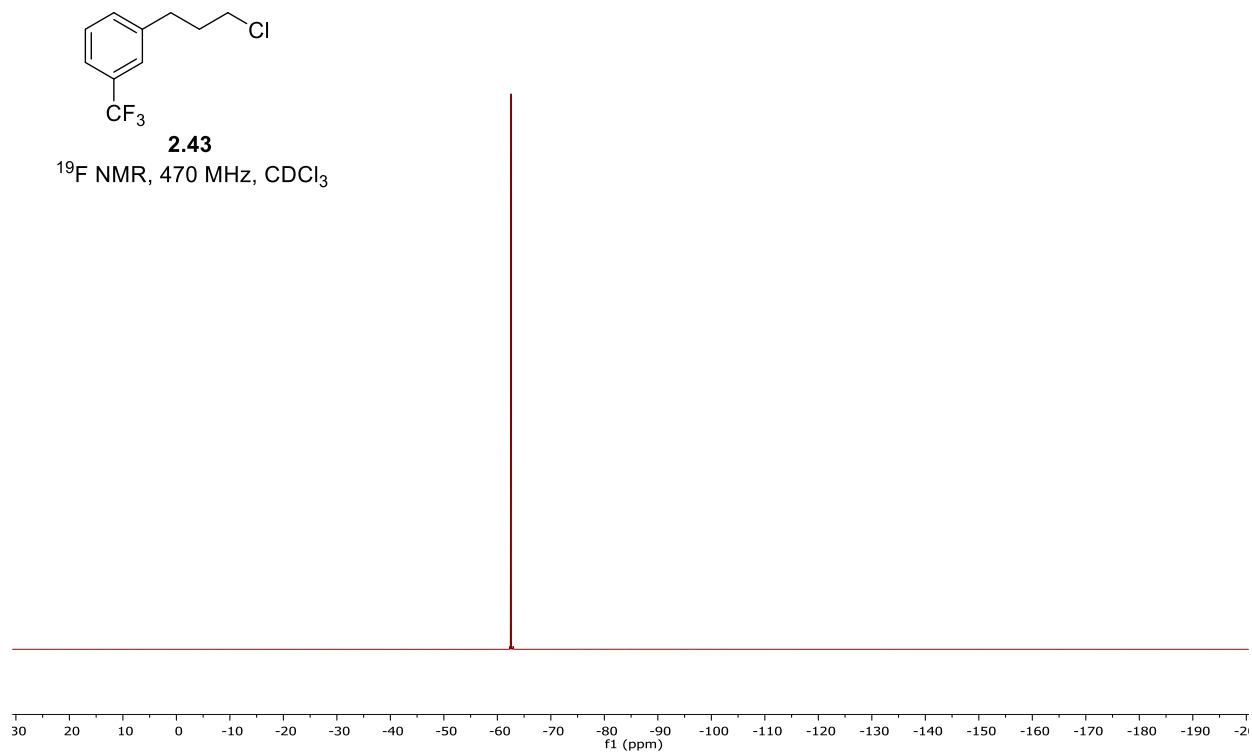
Appendix C: XYZ Coordinates for calculations performed in chapter 2.

(dppe)FeCl₂ - THF Solvation

Ground state calculation. High Spin Fe (II) M = 5

55

H 2.517 1.952 -3.565

H 4.570 1.034 2.989

H 3.113 0.905 1.000

C 3.871 0.209 2.887

H 1.079 1.398 -1.653

C 3.044 0.138 1.766

C 2.673 1.017 -3.033

C 1.856 0.698 -1.945

C 3.802 -0.780 3.873

H 4.450 -0.724 4.743

C 3.685 0.144 -3.432

H 4.319 0.394 -4.278

C 2.138 -0.926 1.621

H 0.245 1.320 0.365

C 2.908 -1.842 3.733

C 2.041 -0.504 -1.248

P 1.008 -1.034 0.177

C 2.079 -1.918 2.611

C -0.226 0.336 0.461

H -0.539 0.239 1.507

C 3.877 -1.057 -2.743

H 2.857 -2.617 4.493

C 3.057 -1.382 -1.664

H 1.396 -2.756 2.503

H 4.660 -1.744 -3.050

C -1.447 0.218 -0.471

H -2.146 1.038 -0.276

H 3.210 -2.322 -1.140

H -1.138 0.284 -1.520

H -1.951 -2.566 2.460

Fe -0.395 -3.081 -0.285

C -2.775 -1.860 2.512

Cl -0.121 -3.626 -2.481

H -3.090 -2.176 4.618

C -3.425 -1.646 3.731

P -2.290 -1.431 -0.226

C -3.196 -1.184 1.357

H -4.120 -3.537 -0.909

C -4.501 -0.762 3.805

C -4.285 -0.300 1.440

C -4.341 -2.713 -1.585

C -4.933 -0.091 2.657

H -5.008 -0.599 4.752

C -3.604 -1.520 -1.501

H -4.636 0.219 0.552

Cl -0.386 -4.647 1.387

H -5.775 0.593 2.709

C -5.358 -2.852 -2.528

H -5.922 -3.779 -2.580

C -3.897 -0.474 -2.388

H -3.343 0.458 -2.348

C -5.645 -1.804 -3.408

C -4.912 -0.619 -3.337

H -6.433 -1.914 -4.147

H -5.129 0.198 -4.020

(dppe)FeClPh – THF Solvation

Ground state calculation. High Spin Fe (II) M = 5

65

H -6.799 -2.304 -3.573

H -5.558 -0.154 -3.711

C -5.891 -2.160 -2.995

C -5.194 -0.954 -3.073

C -5.413 -3.185 -2.173

H -5.948 -4.129 -2.110

C -4.024 -0.766 -2.332

H -3.501 0.182 -2.407

C -4.243 -3.003 -1.437

Cl -0.180 -3.350 -3.461

C -3.539 -1.788 -1.503

H -4.818 -0.440 3.394

C -3.990 -1.046 3.037

H -3.610 -1.949 4.960

C -3.310 -1.895 3.917
C -3.608 -0.976 1.698
H -3.877 -3.808 -0.805
H -4.150 -0.320 1.022
C -2.252 -2.675 3.452
C -2.539 -1.755 1.221
C -1.868 -2.608 2.109
H -1.726 -3.343 4.129
P -1.987 -1.655 -0.533
Fe 0.066 -2.988 -1.173
C -0.239 -5.595 0.349
C 0.175 -6.753 1.016
H -1.055 -3.234 1.751
H -1.303 -5.481 0.139
C 1.527 -6.942 1.312
H -0.556 -7.506 1.306
C 0.666 -4.584 -0.050
C 2.453 -5.966 0.936
H 1.855 -7.840 1.831
C 2.023 -4.814 0.269
H 3.509 -6.103 1.163
H 2.776 -4.073 -0.002
C -1.447 0.124 -0.691
H -1.327 0.348 -1.758
H 1.821 -1.382 -3.420
H -2.212 0.800 -0.295
C 2.167 -0.370 -3.233
P 1.221 -0.791 -0.630

C -0.114 0.337 0.047
H 2.872 -0.090 -5.249
H 1.019 -1.344 2.256
C 2.756 0.363 -4.268
C 2.007 0.201 -1.962
H -0.234 0.114 1.112
C 2.069 -1.187 2.025
C 2.472 -0.862 0.719
H 0.199 1.383 -0.029
C 3.191 1.669 -4.042
C 2.451 1.518 -1.743
C 3.010 -1.322 3.045
H 2.680 -1.567 4.051
C 3.039 2.246 -2.777
H 3.649 2.238 -4.846
C 3.842 -0.703 0.454
H 2.351 1.974 -0.762
H 4.178 -0.462 -0.549
C 4.370 -1.148 2.776
C 4.782 -0.844 1.478
H 3.379 3.261 -2.595
H 5.102 -1.255 3.571
H 5.837 -0.712 1.256

(dppe)FePh$_2$ – THF solvation

Ground state calculation. High Spin Fe (II) M = 5

75

Fe -0.404 -3.479 -0.110
P -2.165 -1.659 0.433
P 1.074 -1.377 -0.517
C -1.413 -0.090 -0.258
C 0.058 0.038 0.171
H 0.472 0.994 -0.165
H 0.134 0.018 1.263
H -1.987 0.781 0.076
H -1.480 -0.127 -1.351
C -2.493 -1.185 2.182
C -3.827 -1.742 -0.354
C -3.331 -0.105 2.512
C -1.859 -1.895 3.211
C -2.055 -1.530 4.547
C -2.886 -0.456 4.864
C -3.527 0.256 3.844
H -3.040 -0.173 5.901
H -4.178 1.091 4.087
H -3.842 0.448 1.728
H -1.215 -2.737 2.971
H -1.559 -2.088 5.335
C -3.991 -1.443 -1.717
C -4.935 -2.214 0.370
C -6.177 -2.364 -0.249
C -6.332 -2.048 -1.600
C -5.235 -1.590 -2.332
H -5.344 -1.346 -3.385
H -3.151 -1.099 -2.312

H -4.833 -2.458 1.423
H -7.023 -2.726 0.328
H -7.300 -2.163 -2.081
C 1.425 -0.808 -2.232
C 2.678 -1.235 0.376
C 2.047 0.426 -2.493
C 1.036 -1.616 -3.311
C 2.271 0.841 -3.805
C 1.261 -1.197 -4.626
C 1.877 0.030 -4.874
H 2.755 1.796 -3.994
H 2.052 0.355 -5.896
H 2.368 1.061 -1.672
H 0.557 -2.573 -3.125
H 0.954 -1.832 -5.452
C 3.902 -1.373 -0.297
C 2.689 -1.093 1.774
C 3.894 -1.063 2.475
C 5.107 -1.348 0.408
C 5.107 -1.187 1.795
H 3.883 -0.944 3.555
H 6.045 -1.165 2.343
H 1.757 -1.013 2.327
H 3.920 -1.494 -1.376
H 6.045 -1.452 -0.130
C -0.954 -4.571 -1.768
C 0.306 -4.604 1.461
C 0.001 -5.157 -2.635

C -2.299 -4.896 -2.062
C -0.347 -5.980 -3.712
C -2.670 -5.717 -3.134
C -1.691 -6.263 -3.968
H -3.721 -5.931 -3.319
H -3.098 -4.492 -1.439
H 1.064 -4.966 -2.472
H 0.428 -6.403 -4.350
C 1.686 -4.815 1.690
C -0.556 -5.317 2.329
C -0.092 -6.156 3.349
C 2.173 -5.648 2.704
C 1.282 -6.323 3.542
H -0.799 -6.680 3.991
H 2.419 -4.306 1.063
H 3.246 -5.771 2.843
H -1.637 -5.217 2.213
H 1.652 -6.973 4.332
H -1.971 -6.903 -4.802

(dppe)Fe(OMe)$_2$ – THF Solvation

Ground state calculation. High Spin Fe (II) M = 5

63

P -1.141 0.861 0.606
P 2.075 0.758 -0.133
C -0.065 2.389 0.654
C 1.045 2.293 -0.409

H 0.379 2.449 1.655
H -0.655 3.299 0.498
H 1.669 3.194 -0.387
H 0.597 2.223 -1.407
C -2.255 1.187 -0.825
C -3.083 2.321 -0.881
C -2.241 1.003 2.071
C 3.145 1.245 1.287
C 2.943 0.629 2.532
C 4.137 2.233 1.160
C 3.235 0.706 -1.558
C 3.224 1.627 -2.616
C -2.275 0.270 -1.888
C -3.916 1.626 -3.043
C -3.907 2.540 -1.984
C -3.060 -0.100 2.368
C -2.300 2.133 2.900
C -3.926 -0.068 3.460
C -3.162 2.160 3.999
C -3.977 1.063 4.280
C 4.119 1.493 -3.681
C 4.160 -0.353 -1.592
C 5.057 -0.480 -2.651
C 5.037 0.443 -3.701
C 3.718 1.006 3.633
C 4.910 2.601 2.260
C 4.699 1.989 3.500
H 5.303 2.277 4.357

H 3.556 0.524 4.594

H 4.314 2.706 0.197

H 5.677 3.363 2.151

H 4.097 2.214 -4.494

H 5.732 0.341 -4.530

H -4.647 1.086 5.136

H -3.195 3.041 4.634

Fe 0.402 -1.081 0.322

O 0.807 -1.781 2.007

C 1.650 -2.867 2.275

O 0.058 -2.084 -1.208

C 0.584 -2.147 -2.501

H 2.523 2.456 -2.620

H -3.016 -0.989 1.743

H -4.554 -0.928 3.676

C -3.103 0.493 -2.993

H -1.650 -0.618 -1.839

H -4.560 1.797 -3.902

H -3.112 -0.222 -3.811

H -3.095 3.030 -0.057

H -4.544 3.419 -2.017

H -1.677 2.999 2.698

H 2.187 -0.149 2.627

H 4.177 -1.081 -0.784

H 5.768 -1.302 -2.660

H 1.474 -3.262 3.290

H 2.718 -2.586 2.222

H 1.502 -3.710 1.577

H 0.366 -3.123 -2.967

H 1.680 -2.016 -2.529

H 0.152 -1.375 -3.166

(dppe)Fe(OMe)Ph – THF Solvation

Ground state calculation. High Spin Fe (II) M = 5

69

Fe -0.655 -3.640 -0.359

P -2.465 -1.866 -0.312

P 0.768 -1.686 0.375

C -1.550 -0.239 -0.219

C -0.432 -0.327 0.836

H 0.080 0.637 0.926

H -0.859 -0.571 1.816

H -2.232 0.587 0.011

H -1.109 -0.042 -1.203

C -3.616 -1.765 1.125

C -3.588 -1.714 -1.761

C -4.592 -0.758 1.222

C -3.514 -2.713 2.153

C -4.364 -2.651 3.262

C -5.326 -1.645 3.350

C -5.440 -0.698 2.327

H -5.989 -1.598 4.210

H -6.192 0.084 2.389

H -4.698 -0.025 0.426

H -2.777 -3.509 2.085

H -4.275 -3.393 4.050

C -3.488 -0.699 -2.724

C -4.563 -2.713 -1.931

C -5.421 -2.692 -3.029

C -5.313 -1.676 -3.983

C -4.346 -0.683 -3.828

H -4.255 0.111 -4.564

H -2.749 0.088 -2.624

H -4.654 -3.509 -1.195

H -6.171 -3.470 -3.142

H -5.978 -1.661 -4.842

C 1.831 -0.878 -0.896

C 1.872 -1.857 1.834

C 2.692 0.183 -0.571

C 1.763 -1.327 -2.225

C 3.468 0.790 -1.558

C 2.542 -0.713 -3.211

C 3.392 0.343 -2.881

H 4.133 1.608 -1.296

H 3.999 0.815 -3.649

H 2.766 0.531 0.456

H 1.107 -2.157 -2.481

H 2.484 -1.066 -4.237

C 2.813 -2.902 1.808

C 1.813 -1.028 2.965

C 2.678 -1.237 4.042

C 3.681 -3.103 2.880

C 3.615 -2.271 4.001

H 2.620 -0.588 4.911
H 4.286 -2.432 4.840
H 1.097 -0.213 3.017
H 2.862 -3.563 0.946
H 4.403 -3.914 2.843
O -0.370 -3.839 -2.190
C -1.144 -4.541 -3.122
H -0.685 -4.495 -4.124
H -2.165 -4.133 -3.215
H -1.245 -5.612 -2.869
C -0.668 -5.210 0.973
C -0.548 -5.116 2.379
C -0.762 -6.526 0.464
C -0.748 -7.661 1.283
C -0.530 -6.238 3.216
C -0.633 -7.519 2.668
H -0.620 -8.396 3.312
H -0.825 -8.654 0.844
H -0.459 -4.135 2.848
H -0.434 -6.114 4.293
H -0.847 -6.681 -0.613

(dppe)Fe(NEt₂) – THF
solvation

Ground state calculation.
High Spin Fe (II) M = 5

77

Fe 0.023 -0.655 1.127

P -1.608 0.235 -0.615

P 1.709 0.023 -0.601
C -0.642 -0.086 -2.184
C 0.744 0.581 -2.115
H 1.306 0.369 -3.030
H 0.630 1.667 -2.056
H -1.183 0.275 -3.066
H -0.535 -1.172 -2.289
C -2.129 1.997 -0.832
C -3.184 -0.687 -0.854
C -2.841 2.435 -1.961
C -1.814 2.926 0.170
C -2.189 4.267 0.043
C -2.888 4.692 -1.087
C -3.215 3.772 -2.089
H -3.182 5.733 -1.187
H -3.766 4.098 -2.967
H -3.117 1.730 -2.740
H -1.280 2.598 1.056
H -1.939 4.973 0.829
C -3.498 -1.426 -2.004
C -4.111 -0.656 0.203
C -5.325 -1.335 0.106
C -5.628 -2.068 -1.045
C -4.712 -2.113 -2.096
H -4.939 -2.682 -2.994
H -2.804 -1.473 -2.838
H -3.879 -0.097 1.106
H -6.031 -1.298 0.931

H -6.571 -2.602 -1.119
C 2.899 -1.229 -1.242
C 2.776 1.478 -0.211
C 3.631 -1.048 -2.428
C 3.096 -2.400 -0.494
C 4.531 -2.022 -2.860
C 4.002 -3.373 -0.926
C 4.717 -3.187 -2.109
H 5.090 -1.871 -3.779
H 5.419 -3.945 -2.447
H 3.512 -0.141 -3.013
H 2.528 -2.552 0.419
H 4.143 -4.276 -0.338
C 4.133 1.316 0.114
C 2.216 2.764 -0.133
C 2.998 3.861 0.233
C 4.911 2.414 0.485
C 4.350 3.691 0.541
H 2.548 4.849 0.278
H 4.958 4.545 0.826
H 1.164 2.923 -0.352
H 4.588 0.332 0.072
H 5.961 2.268 0.728
N -0.428 -2.537 1.010
N 0.343 0.091 2.872
C -0.349 -3.397 -0.153
C -1.353 -3.065 2.004
C 0.387 1.502 3.210

182

C   0.612 -0.751   4.024
H   0.686 -1.800   3.719
H -0.166 -0.701   4.810
H   1.568 -0.485   4.519
H   0.465   2.091   2.285
H   1.306   1.735   3.787
C -0.821   2.024   4.014
H -1.750   1.885   3.448
H -0.713   3.094   4.240
H -0.928   1.494   4.967
H -1.534 -2.292   2.762
C -0.883 -4.337   2.735
H -2.341 -3.282   1.546
H   0.065 -4.156   3.256
H -0.730 -5.173   2.043
H -1.627 -4.655   3.477
H   0.307 -2.961 -0.915
H -1.338 -3.567 -0.627
H   0.064 -4.399   0.065

(dppe)Fe(NEt₂)Ph – THF
Solvation

Ground state calculation.
High Spin Fe (II) M = 5

79

Fe   0.063   0.189   1.169

P   1.612 -0.547 -0.791

P -1.734   0.071 -0.716

C -0.852 -0.847 -2.089

C   0.555 -0.264 -2.308
H   1.025 -0.716 -3.188
H   0.487   0.816 -2.483
H -1.433 -0.793 -3.015
H -0.777 -1.902 -1.804
C -2.300   1.594 -1.592
C -3.271   1.541 -2.608
C -3.292 -0.872 -0.455
C -4.247 -0.323   0.420
C -3.555 -2.119 -1.041
C   3.180   0.351 -1.126
C   4.260   0.129 -0.253
C   3.331   1.290 -2.158
C   2.068 -2.325 -0.961
C   1.405 -3.269 -0.160
C   3.024 -2.767 -1.892
C   4.533   1.986 -2.313
C   5.460   0.820 -0.413
C   5.599   1.754 -1.444
H   6.532   2.296 -1.567
H   4.632   2.708 -3.118
C   3.308 -4.126 -2.019
C   1.689 -4.631 -0.296
C   2.640 -5.061 -1.222
H   2.865 -6.119 -1.322
H   4.052 -4.456 -2.739
C -4.743 -2.799 -0.759
C -5.433 -1.001   0.696

C -5.684 -2.244   0.108
H -6.606 -2.775   0.326
H -6.160 -0.560   1.373
C -3.654   2.700 -3.280
C -1.727   2.830 -1.261
C -2.111   3.991 -1.939
C -3.073   3.928 -2.947
H -3.374   4.832 -3.471
H -1.661   4.943 -1.671
H -3.736   0.593 -2.868
H -4.408   2.648 -4.061
H -0.992   2.887 -0.463
H -2.844 -2.571 -1.725
H -4.931 -3.764 -1.224
H -4.064   0.643   0.884
H   2.520   1.487 -2.851
H   4.164 -0.594   0.554
H   6.284   0.633   0.270
H   0.677 -2.931   0.574
H   1.171 -5.353   0.330
H   3.553 -2.048 -2.511
N -0.212 -1.250   2.425
C   0.903 -1.843   3.156
C -1.510 -1.525   3.036
C   0.498   2.122   1.782
C -0.496   3.039   2.207
C   1.825   2.604   1.902
C   2.140   3.880   2.384

183

C -0.206 4.318 2.696

C 1.121 4.747 2.785

H -1.548 2.753 2.146

H -1.013 4.981 3.006

H 3.179 4.200 2.447

H 1.356 5.740 3.162

H 2.657 1.965 1.602

C -2.047 -2.947 2.789

H -2.245 -0.816 2.631

H -1.498 -1.347 4.127

H 0.710 -2.908 3.384

C 1.285 -1.139 4.473

H 1.786 -1.842 2.501

H -2.192 -3.123 1.717

H -3.011 -3.094 3.294

H -1.356 -3.710 3.167

H 0.443 -1.111 5.175

H 1.596 -0.104 4.286

H 2.112 -1.662 4.970

PhB(pin) – THF solvation

Ground State Calculation

M = 1

32

H -5.135 6.562 1.024

H -5.540 4.168 0.493

C -4.295 5.895 0.844

C -4.524 4.548 0.546

C -2.987 6.382 0.912

H -2.808 7.429 1.144

C -3.444 3.695 0.316

C -1.912 5.523 0.682

H -3.626 2.649 0.082

C -2.119 4.164 0.379

H -0.896 5.906 0.737

H 0.811 1.948 2.145

B -0.919 3.208 0.122

O -1.061 1.860 -0.105

C 1.670 2.151 1.497

H 2.188 3.032 1.888

O 0.390 3.625 0.098

H 0.284 -0.076 1.132

H 2.354 1.299 1.551

C 1.230 2.430 0.054

C 0.240 1.346 -0.524

C 0.412 -0.060 0.047

H -0.336 -0.729 -0.393

C 0.217 1.293 -2.057

C 2.448 2.728 -0.817

H 1.404 -0.457 -0.194

H 0.089 2.290 -2.491

H -0.626 0.673 -2.378

H 3.051 3.513 -0.350

H 3.077 1.836 -0.921

H 2.161 3.068 -1.815

H 1.137 0.855 -2.458

ClB(pin) – THF Solvation

Ground State Calculation

M = 1

22

H 0.698 1.960 2.128

H 2.108 3.015 1.937

C 1.586 2.150 1.517

H 2.249 1.282 1.588

H 0.158 -0.036 1.072

C 0.329 -0.017 -0.006

B -0.898 3.262 0.045

C 1.216 2.450 0.061

O -1.093 1.941 -0.203

O 0.395 3.673 0.088

H -0.417 -0.660 -0.482

H 1.319 -0.439 -0.211

C 0.225 1.395 -0.574

Cl -2.253 4.384 0.298

H 3.065 3.508 -0.260

C 2.469 2.739 -0.760

H 3.086 1.838 -0.848

C 0.258 1.361 -2.105

H 2.225 3.094 -1.763

H -0.584 0.763 -2.466

H 1.184 0.905 -2.471

H 0.172 2.364 -2.534

(MeO)B(pin) – THF
solvation

Ground State Calculation

M = 1

26

B -0.357 4.673 0.374

O 1.016 4.639 0.269

O -0.962 3.452 0.189

C 0.070 2.545 -0.300

C 1.395 3.229 0.221

C -0.041 2.529 -1.830

C -0.205 1.153 0.263

C 1.764 2.821 1.652

C 2.605 3.084 -0.698

H 2.412 3.500 -1.690

H 2.883 2.031 -0.809

H 3.460 3.615 -0.268

H 0.910 2.920 2.330

H 2.563 3.475 2.015

H 2.122 1.787 1.695

H -0.279 1.164 1.353

H 0.586 0.453 -0.026

H -1.152 0.775 -0.137

H 0.154 3.520 -2.255

H -1.057 2.233 -2.111

H 0.659 1.817 -2.278

O -1.088 5.787 0.640

C -0.430 7.031 0.874

H 0.408 6.916 1.570

185

H -1.164 7.718 1.304

H -0.054 7.454 -0.064

(NEt₂)B(pin) – THF Solvation

Ground State Calculation

M = 1

36

B -0.380 -0.085 -0.245

O 0.379 1.066 -0.399

O 0.382 -1.182 0.135

C 1.777 -0.797 -0.009

C 1.706 0.774 0.118

C 1.741 1.264 1.572

C 2.731 1.539 -0.718

C 2.235 -1.271 -1.396

C 2.588 -1.500 1.078

H 2.190 -1.294 2.075

H 3.637 -1.184 1.049

H 2.558 -2.583 0.918

H 1.670 -0.775 -2.192

H 2.064 -2.349 -1.478

H 3.301 -1.080 -1.557

H 1.015 0.726 2.190

H 1.482 2.328 1.594

H 2.733 1.144 2.018

H 2.630 1.316 -1.783

H 3.752 1.293 -0.405

H 2.587 2.616 -0.582

N -1.772 -0.126 -0.464

C -2.520 -1.381 -0.400

C -2.511 1.094 -0.803

H -1.793 -2.198 -0.379

H -3.104 -1.498 -1.325

C -3.460 -1.509 0.805

H -2.903 -1.416 1.744

H -3.957 -2.487 0.795

H -4.240 -0.739 0.793

H -1.926 1.672 -1.529

C -2.836 1.995 0.395

H -3.438 0.801 -1.311

H -1.913 2.316 0.889

H -3.457 1.477 1.133

H -3.375 2.892 0.064

TS for (dppe)Fe(NEt₂)₂ and PhB(pin) TM – THF Solvation

Excited state calculation. High Spin Fe (II) M = 5

Imaginary Frequency = -201.00

115

Fe -0.943 -0.552 -1.066

P 3.346 0.788 -0.050

P 0.363 -1.069 1.205

C 3.004 0.095 1.660

C 1.539 0.087 2.131

H 1.526 -0.228 3.181

H 1.113 1.094 2.096

H 3.613 0.620 2.405

H 3.386 -0.930 1.630

C 3.432 2.619 0.228

C 5.143 0.341 -0.180

C 3.222 3.259 1.460

C 3.679 3.421 -0.903

C 3.736 4.811 -0.801

C 3.523 5.433 0.432

C 3.262 4.653 1.560

H 3.557 6.516 0.512

H 3.095 5.127 2.524

H 3.025 2.680 2.356

H 3.834 2.951 -1.871

H 3.938 5.408 -1.686

C 5.481 -0.782 -0.952

C 6.171 1.047 0.467

C 7.500 0.637 0.347

C 7.822 -0.487 -0.419

C 6.810 -1.198 -1.066

H 7.053 -2.070 -1.667

H 4.699 -1.335 -1.466

H 5.934 1.924 1.062

H 8.284 1.195 0.852

H 8.857 -0.804 -0.512

C 1.377 -2.615 1.172

C -0.863 -1.458 2.537

C 1.749 -3.282 2.353

C 1.869 -3.079 -0.055

C 2.593 -4.391 2.304

C 2.719 -4.189 -0.101

C 3.082 -4.846 1.075

H 2.870 -4.899 3.224

H 3.741 -5.709 1.038

H 1.373 -2.940 3.313

H 1.559 -2.583 -0.973

H 3.091 -4.542 -1.059

C -1.547 -2.686 2.498

C -1.188 -0.544 3.551

C -2.155 -0.858 4.511

C -2.510 -2.999 3.457

C -2.817 -2.086 4.470

H -2.385 -0.140 5.293

H -3.565 -2.330 5.219

H -0.692 0.419 3.608

H -1.315 -3.409 1.721

H -3.019 -3.958 3.414

N -0.214 -1.702 -2.452

N -1.273 1.633 -0.920

C -1.192 2.185 -2.303

C -0.475 2.431 0.053

C 0.435 -1.242 -3.679

C -0.924 -2.969 -2.633

H -6.014 -3.143 -2.286

H -5.050 -1.566 -3.959

C -5.206 -2.471 -2.004

C -4.659 -1.588 -2.943

C -4.703 -2.475 -0.703

H -5.121 -3.152 0.041

C -3.618 -0.735 -2.574

C -3.671 -1.594 -0.349

H -3.224 -0.067 -3.340

C -3.075 -0.699 -1.266

H -3.338 -1.593 0.686

H -3.366 3.764 1.746

B -2.711 1.431 -0.463

O -3.732 2.152 -1.081

C -3.990 2.989 2.196

H -3.463 2.605 3.076

O -2.967 1.250 0.898

H -4.560 4.421 0.011

H -4.923 3.451 2.535

C -4.256 1.822 1.233

C -4.860 2.259 -0.182

C -5.350 3.711 -0.242

H -5.689 3.934 -1.259

C -5.979 1.345 -0.703

C -5.083 0.766 1.976

H -6.195 3.872 0.437

H -5.668 0.301 -0.746

H -6.243 1.660 -1.718

H -4.553 0.470 2.887

H -6.060 1.169 2.266

H -5.238 -0.128 1.371

H -6.877 1.424 -0.080
H -0.021 -1.735 -4.556
C 1.958 -1.456 -3.737
H 0.251 -0.169 -3.828
C 0.232 2.405 -2.816
H -1.751 3.128 -2.364
H -1.712 1.484 -2.962
H 0.586 2.282 -0.166
H -0.668 2.005 1.039
C -0.773 3.935 0.096
H 0.734 3.237 -2.313
H 0.198 2.640 -3.886
H 0.853 1.515 -2.685
H -0.500 4.442 -0.835
H -0.192 4.397 0.902
H -1.833 4.131 0.284
H 2.219 -2.518 -3.660
H 2.450 -0.929 -2.910
H 2.374 -1.070 -4.678
C -0.074 -4.197 -3.004
H -1.710 -2.866 -3.407
H -1.464 -3.200 -1.705
H 0.447 -4.056 -3.958
H -0.718 -5.080 -3.110
H 0.676 -4.414 -2.236

CNBox^{Ph}FeCl₂ – Gas

Ground state calculation. High Spin Fe (II) M = 5

45

H -6.546 -4.954 -1.409
C -6.224 -3.944 -1.645
C -5.716 -3.126 -0.634
H -6.695 -4.107 -3.741
C -6.306 -3.468 -2.953
C -5.293 -1.824 -0.923
C -5.877 -2.173 -3.251
C -5.374 -1.355 -2.242
H -5.929 -1.801 -4.271
H -5.032 -0.352 -2.488
H -5.634 -3.503 0.382
C -3.227 0.684 0.025
N -3.314 -0.587 -0.037
O -4.336 1.401 0.250
C -5.435 0.439 0.328
C -4.749 -0.948 0.186
H -6.126 0.667 -0.485
H -5.928 0.587 1.290
H -4.779 -1.503 1.127
C -0.660 0.818 -0.150
N -0.450 -0.428 0.023
O 0.385 1.630 -0.353
C 1.570 0.774 -0.375
C 1.027 -0.650 -0.073
H 2.261 1.150 0.381
H 2.017 0.866 -1.366
C 1.580 -1.312 1.173

H 1.176 -1.317 -0.926
C -1.990 1.548 -0.137
H -1.971 2.238 0.720
C -2.131 2.378 -1.348
C 2.021 -2.639 1.113
C 1.643 -0.625 2.393
C 2.145 -1.253 3.532
C 2.588 -2.576 3.463
H 2.185 -0.712 4.474
H 1.292 0.402 2.462
C 2.523 -3.268 2.253
H 2.976 -3.066 4.351
H 1.954 -3.184 0.175
H 2.858 -4.299 2.195
N -2.260 3.024 -2.302
Fe -1.795 -2.066 0.092
Cl -2.445 -2.961 2.061
Cl -0.998 -3.202 -1.683

CNBox^{Ph}FeClPh – Gas

Ground state calculation. High Spin Fe (II) M = 5

55

C -3.004 0.481 -0.109
N -3.095 -0.778 0.073
O -4.101 1.242 0.025
C -5.187 0.329 0.377
C -4.524 -1.076 0.405
H -5.962 0.433 -0.385

H -5.575 0.646 1.347
C -5.119 -2.092 -0.550
H -4.520 -1.493 1.415
C -0.444 0.578 -0.328
N -0.234 -0.600 0.115
O 0.604 1.337 -0.683
C 1.790 0.507 -0.492
C 1.245 -0.820 0.108
H 2.464 1.045 0.177
H 2.260 0.381 -1.469
C 1.772 -1.176 1.483
H 1.423 -1.660 -0.570
C -1.776 1.280 -0.502
H -1.758 2.175 0.138
C -1.928 1.753 -1.892
C -5.467 -3.362 -0.078
C -5.317 -1.786 -1.903
C -5.862 -2.734 -2.768
C -6.214 -3.998 -2.288
C -6.015 -4.311 -0.944
H -6.278 -5.295 -0.567
H -5.295 -3.611 0.966
H -5.037 -0.809 -2.291
H -6.007 -2.488 -3.816
H -6.638 -4.737 -2.963
C 2.270 -2.461 1.724
C 1.762 -0.240 2.526
C 2.246 -0.583 3.787

C 2.746 -1.866 4.019
H 2.228 0.149 4.590
H 1.366 0.759 2.359
C 2.756 -2.804 2.987
H 3.121 -2.134 5.003
H 2.263 -3.198 0.926
H 3.135 -3.807 3.163
N -2.065 2.114 -2.985
Fe -1.579 -2.244 0.437
Cl -2.268 -2.764 2.555
C -0.823 -3.657 -0.819
C -0.731 -4.990 -0.359
C -0.330 -3.421 -2.120
C 0.217 -4.434 -2.914
C 0.291 -5.739 -2.422
C -0.186 -6.015 -1.139
H -0.134 -7.029 -0.748
H -1.095 -5.235 0.638
H -0.375 -2.415 -2.543
H 0.582 -4.210 -3.915
H 0.715 -6.532 -3.033

CNBox^{Ph}FePh$_2$ – Gas

Ground state calculation. High Spin Fe (II) M = 5

65

C -2.415 1.056 0.171
N -2.554 -0.133 0.612
O -3.395 1.951 0.381

C -4.471 1.219 1.042
C -3.874 -0.191 1.308
H -5.324 1.202 0.360
H -4.731 1.766 1.950
C -4.735 -1.340 0.827
H -3.653 -0.333 2.370
C 0.025 0.818 -0.612
N 0.249 -0.287 -0.015
O 1.008 1.384 -1.331
C 2.169 0.510 -1.186
C 1.645 -0.695 -0.356
H 2.947 1.080 -0.674
H 2.504 0.242 -2.189
C 2.479 -1.038 0.860
H 1.549 -1.589 -0.981
C -1.256 1.629 -0.620
H -1.023 2.612 -0.184
C -1.692 1.877 -2.009
C -5.224 -2.274 1.747
C -5.068 -1.476 -0.527
C -5.878 -2.528 -0.952
C -6.369 -3.452 -0.026
C -6.040 -3.324 1.323
H -6.410 -4.045 2.047
H -4.955 -2.184 2.797
H -4.681 -0.769 -1.258
H -6.121 -2.629 -2.006
H -6.998 -4.273 -0.359

C 3.044 -2.312 0.975
C 2.713 -0.094 1.869
C 3.497 -0.421 2.973
C 4.063 -1.694 3.078
H 3.662 0.315 3.755
H 2.267 0.896 1.802
C 3.835 -2.639 2.078
H 4.672 -1.949 3.941
H 2.853 -3.055 0.204
H 4.264 -3.634 2.158
N -2.054 2.062 -3.095
Fe -1.088 -1.685 0.945
C -1.111 -1.721 3.008
C -0.946 -3.279 -0.349
C -0.731 -3.137 -1.738
C -1.037 -4.613 0.108
C -0.916 -5.716 -0.742
C -0.697 -5.526 -2.107
C -0.607 -4.226 -2.608
H -0.444 -4.063 -3.672
H -0.662 -2.137 -2.176
H -1.214 -4.806 1.167
H -0.992 -6.725 -0.340
H -0.601 -6.381 -2.774
C -0.973 -2.924 3.735
C -1.271 -0.561 3.799
C -1.298 -0.586 5.197
C -1.163 -1.801 5.871

C -0.999 -2.974 5.132
H -1.185 -1.833 6.959
H -1.376 0.413 3.313
H -1.422 0.338 5.761
H -0.889 -3.927 5.647
H -0.834 -3.862 3.197

CNBox^{Ph}Fe(OMe)$_2$ – Gas

Ground state calculation. High Spin Fe (II) M = 5

53

O -1.118 -2.896 -1.020
H -0.735 -4.442 -2.330
C -1.290 -4.229 -1.400
H -0.921 -4.940 -0.638
H -2.346 -4.485 -1.597
C -2.972 0.982 -0.226
N -3.208 -0.257 -0.051
O -3.990 1.858 -0.143
C -5.177 1.066 0.172
C -4.671 -0.402 0.202
H -5.922 1.266 -0.598
H -5.550 1.411 1.139
C -5.293 -1.361 -0.796
H -4.767 -0.832 1.201
C -0.426 0.726 -0.397
N -0.364 -0.410 0.176
O 0.690 1.255 -0.922
C 1.759 0.302 -0.643

C 1.040 -0.895 0.037
H 2.475 0.810 0.007
H 2.231 0.055 -1.596
C 1.650 -1.361 1.352
H 0.964 -1.752 -0.644
C -1.639 1.628 -0.545
H -1.510 2.463 0.161
C -1.695 2.222 -1.895
C -5.474 -2.698 -0.419
C -5.630 -0.965 -2.096
C -6.162 -1.886 -2.999
C -6.355 -3.214 -2.612
C -6.005 -3.619 -1.323
H -6.141 -4.653 -1.019
H -5.168 -3.014 0.575
H -5.468 0.060 -2.421
H -6.420 -1.567 -4.005
H -6.770 -3.931 -3.316
C 3.026 -1.242 1.587
C 0.857 -1.997 2.317
C 1.424 -2.473 3.498
C 2.793 -2.335 3.732
H 0.789 -2.957 4.235
H -0.205 -2.127 2.136
C 3.594 -1.723 2.768
H 3.233 -2.707 4.653
H 3.676 -0.785 0.844
H 4.663 -1.619 2.930

N -1.771 2.693 -2.951

Fe -1.937 -1.933 0.339

O -2.803 -2.491 1.888

C -2.952 -1.980 3.171

H -3.534 -2.669 3.808

H -3.487 -1.006 3.194

H -1.988 -1.811 3.688

CNBox^{Ph}Fe(OMe)Ph –
Gas

Ground state calculation.
High Spin Fe (II) M = 5

59

C -3.014 0.674 -0.331

N -3.216 -0.578 -0.218

O -3.993 1.532 0.002

C -5.130 0.706 0.398

C -4.590 -0.752 0.331

H -5.935 0.901 -0.314

H -5.429 1.025 1.398

C -5.456 -1.705 -0.480

H -4.438 -1.170 1.334

C -0.467 0.616 -0.609

N -0.325 -0.568 -0.158

O 0.625 1.324 -0.941

C 1.768 0.461 -0.657

C 1.136 -0.867 -0.149

H 2.381 0.963 0.094

H 2.334 0.350 -1.584

C 1.619 -1.330 1.210

H 1.286 -1.675 -0.871

C -1.763 1.371 -0.829

H -1.683 2.318 -0.276

C -1.913 1.721 -2.254

C -6.852 -1.631 -0.371

C -4.895 -2.703 -1.284

C -5.713 -3.592 -1.982

C -7.102 -3.504 -1.879

C -7.670 -2.523 -1.066

H -8.750 -2.448 -0.970

H -7.314 -0.882 0.269

H -3.816 -2.796 -1.356

H -5.256 -4.356 -2.605

H -7.737 -4.198 -2.424

C 2.189 -2.600 1.351

C 1.506 -0.505 2.337

C 1.961 -0.940 3.580

C 2.538 -2.206 3.711

H 1.862 -0.293 4.448

H 1.048 0.478 2.248

C 2.649 -3.035 2.595

H 2.892 -2.545 4.680

H 2.262 -3.253 0.485

H 3.089 -4.024 2.690

N -2.044 1.995 -3.374

Fe -1.760 -2.149 0.192

O -2.406 -2.262 1.931

C -1.101 -3.606 -1.096

C -1.108 -4.961 -0.691

C -0.576 -3.367 -2.386

C -0.095 -4.388 -3.213

C -0.121 -5.711 -2.770

C -0.631 -5.996 -1.501

H -0.658 -7.025 -1.146

H -1.502 -5.224 0.291

H -0.545 -2.347 -2.776

H 0.295 -4.154 -4.203

H 0.251 -6.512 -3.406

C -2.175 -3.239 2.902

H -1.125 -.257 3.245

H -2.418 -4.259 2.549

H -2.798 -3.058 3.794

CNBox^{Ph}Fe(NMeEt)$_2$ –
Gas

Ground state calculation.
High Spin Fe (II) M = 5

67

H -3.569 -4.330 1.221

H -4.216 -3.855 2.794

C -3.295 -3.872 2.180

H -2.602 -4.575 2.688

N -2.704 -2.567 1.963

H -3.934 -2.296 4.492

C -3.267 -1.484 4.181

C -2.195 -1.980 3.188

H -3.886 -0.700 3.726

H -1.542 -2.697 3.728

H -2.805 -1.070 5.087

H -1.549 -1.127 2.934

C -3.239 0.995 -0.031

N -3.504 -0.252 0.002

O -4.198 1.881 0.300

C -5.373 1.086 0.646

C -4.930 -0.387 0.414

H -6.190 1.404 -0.004

H -5.620 1.307 1.687

C -5.746 -1.136 -0.621

H -4.923 -0.958 1.346

C -0.718 0.754 -0.423

N -0.655 -0.454 -0.022

O 0.400 1.357 -0.868

C 1.435 0.326 -0.863

C 0.766 -0.890 -0.165

H 2.297 0.726 -0.327

H 1.702 0.131 -1.904

C 1.367 -1.278 1.172

H 0.742 -1.767 -0.816

C -1.938 1.654 -0.444

H -1.752 2.476 0.263

C -2.108 2.268 -1.776

C -6.421 -2.308 -0.262

C -5.851 -0.666 -1.937

C -6.619 -1.355 -2.875

C -7.294 -2.521 -2.507

C -7.193 -2.997 -1.199

H -7.710 -3.907 -0.907

H -6.334 -2.685 0.754

H -5.321 0.236 -2.238

H -6.687 -0.983 -3.894

H -7.891 -3.059 -3.238

C 1.673 -2.617 1.435

C 1.619 -0.317 2.161

C 2.170 -0.688 3.386

C 2.476 -2.028 3.639

H 2.360 0.067 4.145

H 1.381 0.729 1.978

C 2.225 -2.991 2.662

H 2.904 -2.318 4.594

H 1.469 -3.370 0.678

H 2.455 -4.036 2.853

N -2.270 2.745 -2.821

Fe -2.197 -1.971 0.197

N -1.669 -3.066 -1.294

C -1.554 -2.631 -2.670

C -1.575 -4.508 -1.153

H -0.653 -4.888 -1.642

C -2.767 -5.311 -1.709

H -1.471 -4.744 -0.085

H -1.491 -1.534 -2.720

H -2.403 -2.920 -3.318

H -0.642 -3.030 -3.162

H -2.884 -5.166 -2.789

H -3.700 -4.993 -1.228

H -2.634 -6.387 -1.531

CNBox^{Ph}Fe(NMeEt)Ph –
Gas

Ground state calculation.
High Spin Fe (II) M = 5

66

C -2.985 0.490 -0.219

N -3.060 -0.772 -0.049

O -4.074 1.249 -0.006

C -5.146 0.325 0.342

C -4.457 -1.070 0.372

H -5.913 0.409 -0.431

H -5.550 0.644 1.305

C -5.141 -2.121 -0.490

H -4.379 -1.451 1.397

C -0.439 0.647 -0.525

N -0.180 -0.471 0.030

O 0.572 1380 -1.024

C 1.775 0.570 -0.856

C 1.302 -0.662 -0.035

H 2.518 1.183 -0.344

H 2.132 0.310 -1.855

C 1.917 -0.794 1.344

H 1.467 -1.588 -0.590

C -1.793 1.308 -0.678

H -1.780 2.223 -0.068

C -2.006 1.736 -2.075

C -6.540 -2.223 -0.468

C -4.411 -3.029 -1.264

C -5.068 -4.004 -2.017

C -6.460 -4.090 -2.002

C -7.195 -3.198 -1.219

H -8.280 -3.261 -1.190

H -7.129 -1.544 0.146

H -3.328 -2.988 -1.266

H -4.481 -4.697 -2.614

H -6.969 -4.849 -2.589

C 2.460 -2.019 1.746

C 1.950 0.290 2.231

C 2.521 0.154 3.495

C 3.066 -1.071 3.887

H 2.539 1.001 4.175

H 1.524 1.248 1.938

C 3.034 -2.157 3.012

H 3.511 -1.178 4.873

H 2.422 -2.869 1.070

H 3.451 -3.114 3.312

N -2.193 2.067 -3.170

Fe -1.442 -2.161 0.493

N -1.965 -2.444 2.314

C -0.623 -3.540 -0.806

C 0.081 -4.663 -0.311

C -0.612 -3.402 -2.213

C 0.034 -4.305 -3.064

C 0.715 -5.400 -2.528

C 0.737 -5.576 -1.143

C -1.996 -1.422 3.339

C -2.145 -3.784 2.847

H -1.868 -4.507 2.068

C -3.573 -4.119 3.317

H -1.452 -3.962 3.695

H -1.744 -0.442 2.908

H -1.262 -1.610 4.147

H -2.979 -1.306 3.837

H -4.281 -4.038 2.483

H -3.908 -3.443 4.114

H -3.627 -5.143 3.711

H 1.262 -6.428 -0.714

H 0.120 -4.839 0.765

H -1.135 -2.563 -2.677

H 0.007 -4.157 -4.142

H 1.220 -6.108 -3.182

PhB(pin) – Gas

Ground State Calculation

M = 1

32

B -2.115 1.586 -0.490

C -2.047 0.169 -1.125

C -2.929 -0.204 -2.155

C -2.870 -1.475 -2.726

C -1.924 -2.398 -2.273

C -1.040 -2.048 -1.250

C -1.103 -0.775 -0.684

H -0.413 -0.502 0.110

H -3.666 0.513 -2.506

H -3.559 -1.747 -3.522

H -1.877 -3.390 -2.717

H -0.304 -2.766 -0.898

O -2.980 2.567 -0.914

O -1.317 1.988 0.555

C -1.507 3.421 0.726

C -2.914 3.657 0.048

C -0.351 4.109 -0.012

C -1.441 3.742 2.218

H -0.374 3.888 -1.084

H 0.597 3.736 0.388

H -0.376 5.196 0.119

H -2.160 3.152 2.791

H -1.638 4.805 2.399

H -0.440 3.515 2.598

C -3.059 4.977 -0.707

C -4.094 3.468 1.010

H -2.315 5.074 -1.501

H -2.958 5.831 -0.027

H -4.051 5.028 -1.168

H -4.014 2.523 1.558

H -5.023 3.444 0.432

H -4.161 4.286 1.736

ClB(pin) – Gas

Ground State Calculation

M = 1

22

H 0.696 1.958 2.126

H 2.100 3.020 1.938

C 1.585 2.151 1.517

H 2.251 1.286 1.591

H 0.159 -0.038 1.071

C 0.331 -0.018 -0.008

B -0.900 3.263 0.045

C 1.215 2.452 0.060

O -1.086 1.937 -0.201

O 0.400 3.669 0.084

H -0.419 -0.660 -0.481

H 1.320 -0.443 -0.213

C 0.223 1.396 -0.572

Cl -2.248 4.379 0.296

H 3.064 3.510 -0.260

C 2.471 2.738 -0.759

H 3.090 1.838 -0.846

C 0.257 1.361 -2.105

H 2.228 3.094 -1.762

H -0.591 0.770 -2.465

H 1.180 0.903 -2.475

H 0.173 2.366 -2.531

(MeO)B(pin) – Gas

Ground State Calculation

M = 1

26

B -0.352 4.678 0.353

O 1.026 4.632 0.266

O -0.956 3.456 0.163

C 0.073 2.547 -0.306

C 1.396 3.226 0.233

C -0.013 2.526 -1.839

C -0.218 1.156 0.255

C 1.738 2.821 1.673

C 2.621 3.069 -0.665

H 2.447 3.482 -1.661

H 2.897 2.013 -0.767

H 3.471 3.599 -0.223

H 0.871 2.928 2.332

H 2.532 3.475 2.047

H 2.090 1.785 1.729

H -0.307 1.171 1.344

H 0.571 0.448 -0.023

H -1.164 0.787 -0.154

H 0.198 3.514 -2.261

H -1.029 2.244 -2.132

H 0.686 1.805 -2.276

O -1.076 5.795 0.603

C -0.437 7.042 0.849

H 0.627 6.917 1.074

H -0.934 7.522 1.698

H -0.543 7.689 -0.030

(NMeEt)B(pin) – Gas

Ground State Calculation

M = 1

33

B -2.836 1.707 -0.322

O -3.325 2.881 -0.879

O -1.993 1.937 0.756

C -1.719 3.361 0.781

C -2.972 3.956 0.027

C -0.401 3.581 0.025

C -1.568 3.798 2.237

H -0.491 3.279 -1.023

H 0.379 2.968 0.488

H -0.082 4.628 0.059

H -2.440 3.520 2.834

H -1.426 4.883 2.309

H -0.691 3.313 2.677

C -2.699 5.213 -0.798

C -4.179 4.185 0.950

H -1.943 5.034 -1.567

H -2.361 6.036 -0.158

H -3.619 5.531 -1.299

H -4.387 3.298 1.556

H -5.061 4.388 0.334

H -4.024 5.036 1.621

N -3.167 0.423 -0.798

C -4.110 0.231 -1.895
C -2.580 -0.778 -0.229
H -1.939 -0.508 0.613
H -1.969 -1.328 -0.959
H -3.360 -1.464 0.134
H -4.674 1.159 -2.019
H -4.832 -0.551 -1.610
C -3.450 -0.146 -3.228
H -2.765 0.645 -3.553
H -4.210 -0.282 -4.007
H -2.881 -1.079 -3.153

TS for CNBox^{Ph}Fe(OMe)$_2$ with PhB(pin) – Gas

Excited state calculation. High Spin Fe (II) M = 5

Imaginary Frequency = -210.04

85

O -0.430 -1.448 -0.780
H -2.439 -1.734 -1.044
C -1.540 -2.343 -0.932
H -1.407 -2.959 -1.827
H -1.645 -2.995 -0.060
C -2.010 1.502 -1.900
N -2.133 0.988 -0.742
O -2.957 2.348 -2.353
C -3.939 2.453 -1.277
C -3.393 1.525 -0.155

H -4.904 2.139 -1.680
H -3.989 3.504 -0.984
C -4.333 0.417 0.279
H -3.077 2.092 0.724
C 0.501 1.415 -2.198
N 0.780 1.358 -0.956
O 1.483 1.644 -3.082
C 2.718 1.664 -2.306
C 2.234 1.639 -0.828
H 3.259 2.570 -2.583
H 3.286 0.775 -2.584
C 2.534 2.910 -0.040
H 2.674 0.777 -0.322
C -0.859 1.282 -2.858
H -0.911 2.077 -3.613
C -0.992 0.006 -3.582
C -4.533 0.178 1.643
C -4.999 -0.389 -0.655
C -5.854 -1.408 -0.233
C -6.055 -1.632 1.131
C -5.391 -0.839 2.068
H -5.538 -1.010 3.131
H -4.005 0.788 2.371
H -4.846 -0.231 -1.721
H -6.362 -2.025 -0.969
H -6.723 -2.423 1.461
C 3.827 3.451 -0.094
C 1.575 3.525 0.775

C 1.908 4.674 1.500
C 3.191 5.215 1.429
H 1.154 5.140 2.129
H 0.583 3.095 0.877
C 4.154 4.595 0.632
H 3.442 6.108 1.995
H 4.595 2.972 -0.697
H 5.161 4.998 0.576
N -1.128 -0.972 -4.189
Fe -0.426 0.375 0.596
O -1.095 1.710 1.741
C -0.848 1.914 3.105
H -1.757 2.277 3.617
H -0.063 2.673 3.272
H -0.525 0.997 3.621
B 0.805 -1.995 -0.332
C 0.674 -0.999 1.774
C -0.157 -1.823 2.577
C 0.149 -2.157 3.901
C 1.320 -1.671 4.485
C 2.168 -0.853 3.737
C 1.844 -0.534 2.416
H 2.537 0.102 1.867
H -1.073 -2.238 2.152
H -0.521 -2.799 4.471
H 1.568 -1.927 5.512
H 3.082 -0.467 4.184
O 0.894 -3.343 -0.000

O 1.988 -1.529 -0.922
C 2.978 -2.586 -0.851
C 2.095 -3.879 -0.598
C 3.950 -2.277 0.295
C 3.747 -2.594 -2.176
H 3.444 -2.248 1.260
H 4.404 -1.294 0.124
H 4.759 -3.015 0.340
H 3.074 -2.661 -3.034
H 4.453 -3.431 -2.216
H 4.326 -1.668 -2.271
C 2.701 -4.898 0.369
C 1.664 -4.588 -1.892
H 2.889 -4.456 1.350
H 3.640 -5.306 -0.022
H 2.001 -5.729 0.504
H 1.201 -3.890 -2.596
H 0.922 -5.353 -1.641
H 2.506 -5.079 -2.392

TS for CNBox^Ph^Fe(NMeEt)$_2$ with PhB(pin) – Gas

Excited state calculation. High Spin Fe (II) M = 5

Imaginary Frequency = -214.41

99

H 0.109 -2.855 -0.556
H 1.224 -1.938 -1.591

195

C 0.172 -2.171 -1.405
H -0.241 -2.693 -2.275
N -0.570 -0.927 -1.097
H -1.675 -0.737 -3.673
C -0.672 -0.311 -3.577
C -0.375 0.120 -2.137
H 0.047 -1.052 -3.942
H -1.015 0.963 -1.871
H -0.613 0.561 -4.239
H 0.661 0.464 -2.065
C 3.271 1.539 0.187
N 2.711 0.740 -0.625
O 4.527 1.997 -0.084
C 4.959 1.258 -1.252
C 3.656 0.593 -1.770
H 5.708 0.526 -0.936
H 5.410 1.963 -1.953
C 3.844 -0.829 -2.257
H 3.233 1.181 -2.595
C 1.247 2.402 1.569
N 0.251 1.804 1.025
O 0.990 3.484 2.344
C -0.457 3.524 2.483
C -0.942 2.689 1.286
H -0.768 4.568 2.464
H -0.710 3.069 3.445
C -1.301 3.502 0.052
H -1.782 2.054 1.564

C 2.740 2.176 1.456
H 3.150 3.198 1.430
C 3.321 1.585 2.675
C 3.583 -1.151 -3.594
C 4.310 -1.834 -1.398
C 4.504 -3.132 -1.868
C 4.242 -3.443 -3.205
C 3.781 -2.449 -4.068
H 3.574 -2.681 -5.109
H 3.222 -0.379 -4.270
H 4.507 -1.607 -0.354
H 4.858 -3.902 -1.188
H 4.395 -4.455 -3.569
C -2.398 3.126 -0.732
C -0.557 4.631 -0.322
C -0.908 5.372 -1.449
C -2.008 4.994 -2.222
H -0.323 6.246 -1.723
H 0.301 4.942 0.270
C -2.749 3.868 -1.862
H -2.284 5.574 -3.099
H -2.957 2.231 -0.476
H -3.603 3.563 -2.461
N 3.848 1.261 3.656
Fe 0.088 -0.355 0.869
N 1.470 -0.902 2.110
C 1.157 -0.820 3.532
C 2.268 -2.083 1.813

H 1.755 -3.004 2.166

C 3.693 -2.106 2.395

H 2.348 -2.177 0.722

H 0.465 0.011 3.726

H 2.045 -0.637 4.156

H 0.666 -1.736 3.911

H 3.692 -2.057 3.488

H 4.282 -1.255 2.035

H 4.207 -3.033 2.106

B -2.009 -1.190 -0.691

C -1.730 -1.295 1.602

C -2.679 -0.539 2.325

C -3.320 -1.005 3.479

C -3.049 -2.291 3.949

C -2.134 -3.089 3.257

C -1.495 -2.593 2.120

H -0.785 -3.250 1.619

H -2.969 0.445 1.954

H -4.037 -0.374 4.001

H -3.546 -2.668 4.840

H -1.920 -4.097 3.607

O -2.968 -0.174 -0.794

O -2.557 -2.436 -0.982

C -3.995 -2.332 -1.034

C -4.246 -0.759 -1.153

C -4.578 -2.973 0.234

C -4.458 -3.145 -2.250

H -4.234 -2.477 1.142

H -4.248 -4.016 0.280

H -5.674 -2.964 0.216

H -3.986 -2.803 -3.174

H -5.546 -3.097 -2.372

H -4.181 -4.193 -2.103

C -5.317 -0.214 -0.202

C -4.569 -0.282 -2.578

H -5.082 -0.434 0.840

H -6.301 -0.637 -0.437

H -5.387 0.873 -0.315

H -3.812 -0.602 -3.298

H -4.596 0.813 -2.590

H -5.544 -0.649 -2.917

CNBox^Ph FeCl – Gas

Ground state calculation.
High Spin Fe (II) M = 5

43

C -3.150 0.742 -0.302

N -3.358 -0.466 0.198

O -4.269 1.455 -0.536

C -5.385 0.709 0.004

C -4.823 -0.714 0.235

H -6.197 0.751 -0.723

H -5.695 1.195 0.935

C -5.257 -1.748 -0.790

H -5.096 -1.072 1.232

C -0.673 0.687 -0.484

N -0.445 -0.529 -0.003

O 0.429 1.352 -0.877

C 1.579 0.577 -0.473

C 1.005 -0.817 -0.126

H 2.033 1.068 0.394

H 2.288 0.569 -1.303

C 1.607 -1.445 1.115

H 1.151 -1.503 -0.970

C -1.914 1.358 -0.627

C -1.919 2.695 -1.112

C -5.814 -2.961 -0.372

C -5.104 -1.507 -2.164

C -5.504 -2.462 -3.097

C -6.060 -3.671 -2.670

C -6.214 -3.919 -1.307

H -6.640 -4.858 -0.966

H -5.928 -3.162 0.690

H -4.672 -0.570 -2.507

H -5.381 -2.262 -4.158

H -6.370 -4.415 -3.399

C 2.378 -2.607 1.009

C 1.426 -0.861 2.377

C 2.007 -1.431 3.509

C 2.779 -2.590 3.392

H 1.855 -0.973 4.482

H 0.823 0.038 2.476

C 2.963 -3.177 2.141

H 3.230 -3.035 4.275

H 2.516 -3.073 0.036

H 3.556 -4.082 2.044

N -1.925 3.790 -1.509

Fe -1.891 -1.726 0.629

Cl -2.049 -3.725 1.489

CNBox^{Ph}FePh – Gas

Ground state calculation.
High Spin Fe (II) M = 5

53

C -3.161 0.776 -0.083

N -3.246 -0.527 0.133

O -4.342 1.427 -0.095

C -5.363 0.490 0.311

C -4.680 -0.897 0.207

H -6.216 0.612 -0.358

H -5.658 0.736 1.336

C -5.131 -1.735 -0.979

H -4.852 -1.471 1.123

C -0.700 0.978 -0.349

N -0.361 -0.288 -0.162

O 0.330 1.811 -0.601

C 1.552 1.067 -0.408

C 1.102 -0.414 -0.350

H 2.010 1.400 0.529

H 2.220 1.293 -1.241

C 1.786 -1.222 0.737

H 1.290 -0.903 -1.315

C -1.996 1.553 -0.310

C -2.130 2.958 -0.486

C -5.724 -2.984 -0.771

C -4.977 -1.266 -2.292

C -5.413 -2.033 -3.372

C -6.007 -3.279 -3.154

C -6.161 -3.754 -1.852

H -6.617 -4.724 -1.673

H -5.840 -3.362 0.242

H -4.517 -0.298 -2.472

H -5.289 -1.657 -4.384

H -6.345 -3.876 -3.996

C 2.693 -2.230 0.397

C 1.546 -0.952 2.092

C 2.204 -1.678 3.085

C 3.113 -2.681 2.735

H 2.008 -1.461 4.131

H 0.838 -0.176 2.370

C 3.356 -2.956 1.389

H 3.624 -3.247 3.509

H 2.879 -2.454 -0.651

H 4.054 -3.739 1.109

N -2.241 4.109 -0.631

Fe -1.673 -1.762 0.174

C -1.533 -3.748 0.420

C -2.140 -4.652 -0.480

C -0.827 -4.324 1.500

C -0.735 -5.708 1.676

C -1.348 -6.570 0.765

C -2.052 -6.037 -0.317

H -2.532 -6.701 -1.033

H -0.325 -3.684 2.225

H -0.183 -6.114 2.521

H -1.277 -7.647 0.896

H -2.704 -4.275 -1.332

CNBox^{Ph}Fe(OMe) – Gas

Ground state calculation.
High Spin Fe (II) M = 5

47

C -3.075 1.042 -0.358

N -3.292 -0.250 -0.162

O -4.194 1.794 -0.446

C -5.317 0.890 -0.505

C -4.747 -0.458 -0.007

H -5.662 0.836 -1.544

H -6.112 1.295 0.124

C -5.267 -1.673 -0.751

H -4.971 -0.585 1.061

C -0.592 1.031 -0.358

N -0.384 -0.256 -0.145

O 0.524 1.777 -0.483

C 1.654 0.933 -0.176

C 1.074 -0.505 -0.147

H 2.053 1.240 0.796

H 2.412 1.088 -0.946

C 1.553 -1.333 1.030

H 1.336 -1.035 -1.072

C -1.833 1.713 -0.474

197

C -1.829 3.116 -0.709
C -6.127 -2.574 -0.113
C -4.917 -1.902 -2.090
C -5.419 -3.009 -2.772
C -6.282 -3.900 -2.128
C -6.635 -3.680 -0.797
H -7.301 -4.371 -0.287
H -6.398 -2.410 0.928
H -4.241 -1.217 -2.594
H -5.135 -3.178 -3.808
H -6.672 -4.763 -2.661
C 2.433 -2.400 0.826
C 1.155 -1.022 2.338
C 1.630 -1.765 3.417
C 2.514 -2.826 3.204
H 1.309 -1.516 4.425
H 0.462 -0.202 2.508
C 2.914 -3.143 1.906
H 2.883 -3.405 4.046
H 2.739 -2.658 -0.185
H 3.594 -3.972 1.731
N -1.827 4.265 -0.902
Fe -1.850 -1.623 -0.038
O -1.614 -3.384 0.078
C -2.310 -4.587 0.196
H -1.911 -5.337 -0.505
H -3.387 -4.478 -0.017
H -2.213 -5.003 1.213

CNBox^{Ph}Fe(NMeEt) – Gas

Ground state calculation.
High Spin Fe (II) M = 5

54

C -3.083 0.901 -0.551
N -3.375 -0.249 0.031
O -4.149 1.675 -0.850
C -5.315 1.055 -0.269
C -4.848 -0.378 0.099
H -6.115 1.081 -1.010
H -5.607 1.638 0.611
C -5.391 -1.461 -0.820
H -5.139 -0.618 1.127
C -0.610 0.689 -0.666
N -0.464 -0.482 -0.067
O 0.539 1.257 -1.092
C 1.633 0.465 -0.587
C 0.969 -0.850 -0.106
H 2.107 1.016 0.231
H 2.351 0.324 -1.397
C 1.500 -1.357 1.222
H 1.109 -1.638 -0.857
C -1.807 1.410 -0.906
C -1.724 2.695 -1.510
C -6.298 -2.406 -0.330
C -5.022 -1.513 -2.172
C -5.554 -2.490 -3.013
C -6.462 -3.429 -2.515

C -6.833 -3.385 -1.171
H -7.534 -4.114 -0.773
H -6.586 -2.380 0.719
H -4.316 -0.789 -2.569
H -5.260 -2.519 -4.059
H -6.874 -4.191 -3.170
C 2.219 -2.555 1.281
C 1.304 -0.626 2.402
C 1.819 -1.085 3.614
C 2.540 -2.282 3.661
H 1.659 -0.509 4.521
H 0.739 0.303 2.373
C 2.738 -3.016 2.493
H 2.940 -2.640 4.606
H 2.371 -3.134 0.373
H 3.293 -3.950 2.521
N -1.656 3.748 -2.005
Fe -1.993 -1.597 0.609
N -2.221 -3.241 1.471
C -2.966 -4.346 0.880
C -1.560 -3.601 2.715
H -3.666 -3.946 0.135
H -3.590 -4.828 1.655
C -2.103 -5.425 0.204
H -1.527 -4.991 -0.623
H -2.730 -6.230 -0.201
H -1.394 -5.876 0.907
H -1.065 -2.727 3.153

H -0.785 -4.378 2.594

H -2.283 -3.980 3.461

TS for CNBox^PhFe(OMe) and PhB(pin) – Gas

Excited state calculation. High Spin Fe (II) M = 5

Imaginary Frequency = -210.57

79

C -3.357 0.685 0.549

N -2.346 -0.137 0.767

O -4.512 0.350 1.172

C -4.205 -0.724 2.084

C -2.843 -1.266 1.585

H -5.018 -1.451 2.037

H -4.138 -0.306 3.095

C -2.954 -2.563 0.796

H -2.163 -1.426 2.428

C -2.234 2.294 -0.964

N -1.018 1.781 -0.937

O -2.365 3.410 -1.721

C -1.129 3.566 -2.452

C -0.115 2.720 -1.653

H -0.893 4.630 -2.493

H -1.282 3.180 -3.467

C 0.754 3.524 -0.696

H 0.533 2.147 -2.321

C -3.390 1.837 -0.281

C -4.612 2.552 -0.427

C -2.529 -3.768 1.369

C -3.527 -2.589 -0.483

C -3.669 -3.794 -1.172

C -3.241 -4.991 -0.592

C -2.670 -4.976 0.681

H -2.331 -5.901 1.139

H -2.080 -3.761 2.360

H -3.863 -1.664 -0.943

H -4.117 -3.798 -2.162

H -3.351 -5.929 -1.131

C 2.133 3.293 -0.636

C 0.194 4.505 0.138

C 0.998 5.244 1.004

C 2.375 5.009 1.055

H 0.550 6.003 1.640

H -0.876 4.697 0.106

C 2.939 4.031 0.236

H 3.003 5.585 1.730

H 2.573 2.513 -1.251

H 4.008 3.837 0.274

N -5.612 3.137 -0.551

Fe -0.481 0.068 0.000

O 0.580 -0.795 -1.534

C 0.306 -1.424 -2.794

H -0.674 -1.076 -3.128

H 0.298 -2.512 -2.681

H 1.062 -1.136 -3.532

B 1.854 -1.028 -0.901

C 1.062 -0.660 1.223

C 0.779 -1.890 1.869

C 1.174 -2.159 3.182

C 1.878 -1.197 3.906

C 2.186 0.028 3.309

C 1.785 0.284 1.995

H 2.054 1.239 1.546

H 0.255 -2.671 1.319

H 0.945 -3.121 3.636

H 2.191 -1.400 4.927

H 2.737 0.783 3.867

O 2.350 -2.323 -0.907

O 2.865 -0.075 -1.013

C 4.126 -0.771 -1.183

C 3.788 -2.257 -0.730

C 5.189 -0.070 -0.336

C 4.491 -0.653 -2.671

H 4.889 -0.009 0.712

H 5.337 0.951 -0.706

H 6.150 -0.592 -0.399

H 3.738 -1.130 -3.306

H 5.464 -1.104 -2.891

H 4.536 0.407 -2.942

C 4.104 -2.544 0.744

C 4.410 -3.350 -1.603

H 3.675 -1.793 1.410

H 5.185 -2.591 0.915

H 3.673 -3.514 1.011

H 4.087 -3.272 -2.644

H 4.103 -4.332 -1.228

H 5.505 -3.304 -1.572

TS for CNBox^Ph Fe(NMeEt) and PhB(pin) – Gas

Excited state calculation. High Spin Fe (II) M = 5

Imaginary Frequency = -211.35

86

H 4.299 -3.469 -3.598

H 3.706 -1.068 -3.462

C 4.197 -2.992 -2.627

C 3.861 -1.639 -2.548

C 4.403 -3.727 -1.458

C 3.724 -1.005 -1.308

H 4.667 -4.780 -1.515

C 4.269 -3.103 -0.215

C 3.933 -1.752 -0.140

H 4.423 -3.669 0.699

H 3.827 -1.275 0.831

C 0.729 2.673 1.501

N -0.103 1.780 0.992

O 0.161 3.585 2.325

C -1.194 3.143 2.557

C -1.476 2.199 1.367

H -1.834 4.026 2.592

H -1.224 2.620 3.521

C -2.234 2.893 0.243

H -2.048 1.321 1.681

C 2.806 1.983 0.326

N 2.379 0.895 -0.298

O 4.078 2.349 0.035

C 4.658 1.293 -0.750

C 3.440 0.483 -1.248

H 5.308 0.697 -0.100

H 5.250 1.744 -1.548

H 3.153 0.818 -2.255

C 2.121 2.811 1.253

C 2.844 3.846 1.920

C -3.609 2.664 0.096

C -1.614 3.826 -0.601

C -2.356 4.513 -1.565

C -3.725 4.278 -1.700

C -4.351 3.350 -0.867

H -5.415 3.155 -0.968

H -4.098 1.937 0.741

H -0.548 4.018 -0.506

H -1.860 5.237 -2.207

H -4.300 4.815 -2.450

N 3.435 4.692 2.460

Fe 0.527 0.079 0.049

N -0.645 -0.695 -1.504

C -1.493 0.218 -2.319

C 0.134 -1.611 -2.368

H -2.111 0.786 -1.623

H -2.171 -0.383 -2.946

C -0.705 1.184 -3.201

H -0.036 1.811 -2.600

H -1.403 1.850 -3.721

H -0.108 0.672 -3.964

H 0.701 -2.313 -1.755

H 0.845 -1.054 -2.985

H -0.529 -2.193 -3.020

B -1.453 -1.482 -0.442

C 0.023 -1.690 1.152

C 0.765 -2.893 1.055

C 1.122 -3.652 2.171

C 0.758 -3.229 3.450

C 0.029 -2.050 3.600

C -0.331 -1.309 2.471

H -0.925 -0.407 2.620

H 1.058 -3.267 0.077

H 1.681 -4.575 2.041

H 1.037 -3.816 4.322

H -0.265 -1.710 4.591

O -1.802 -2.796 -0.769

O -2.515 -0.826 0.210

C -3.654 -1.722 0.252

C -3.018 -3.143 -0.072

C -4.644 -1.238 -0.819

C -4.303 -1.614 1.633

H -4.214 -1.302 -1.822

H -4.888 -0.188 -0.628   C -3.853 -4.016 -1.014   H -2.039 -3.399 1.875

H -5.575 -1.817 -0.803   C -2.658 -3.963 1.176   H -2.090 -4.845 0.863

H -3.586 -1.822 2.430   H -4.044 -3.522 -1.969   H -3.558 -4.305 1.698

H -5.146 -2.307 1.730   H -4.814 -4.283 -0.559

H -4.689 -0.598 1.780   H -3.309 -4.944 -1.220

Appendix D: Spectral Data for Chapter 3.
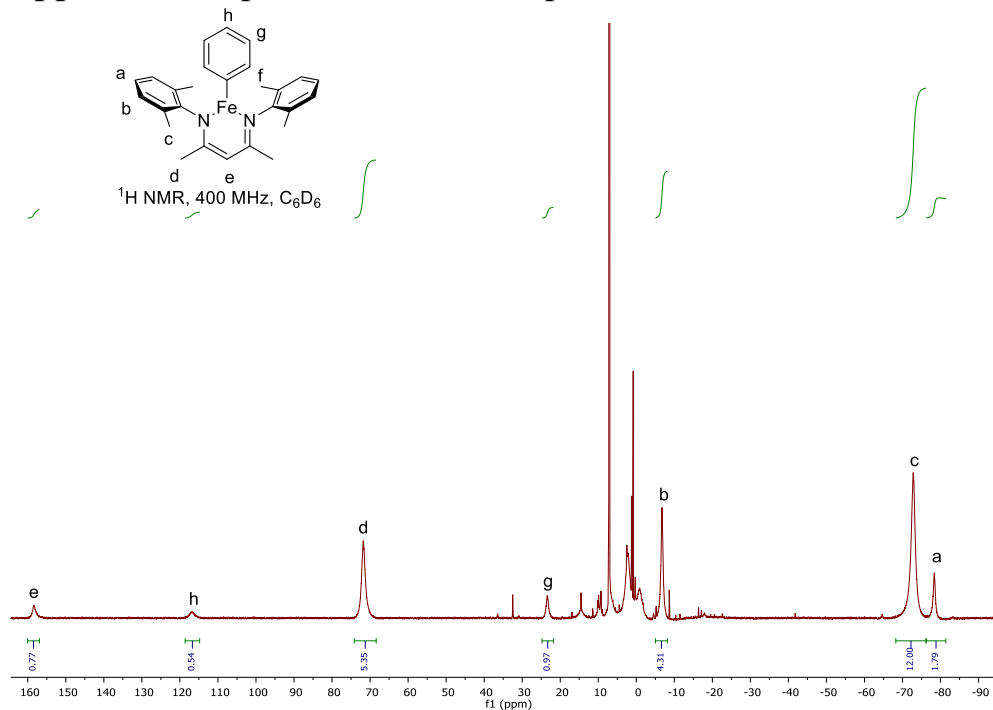
Figure D1. ^{1}H NMR of 2,4-bis[(2,6-dimethylphenyl)imino]pentane iron phenyl complex (**3.4**).
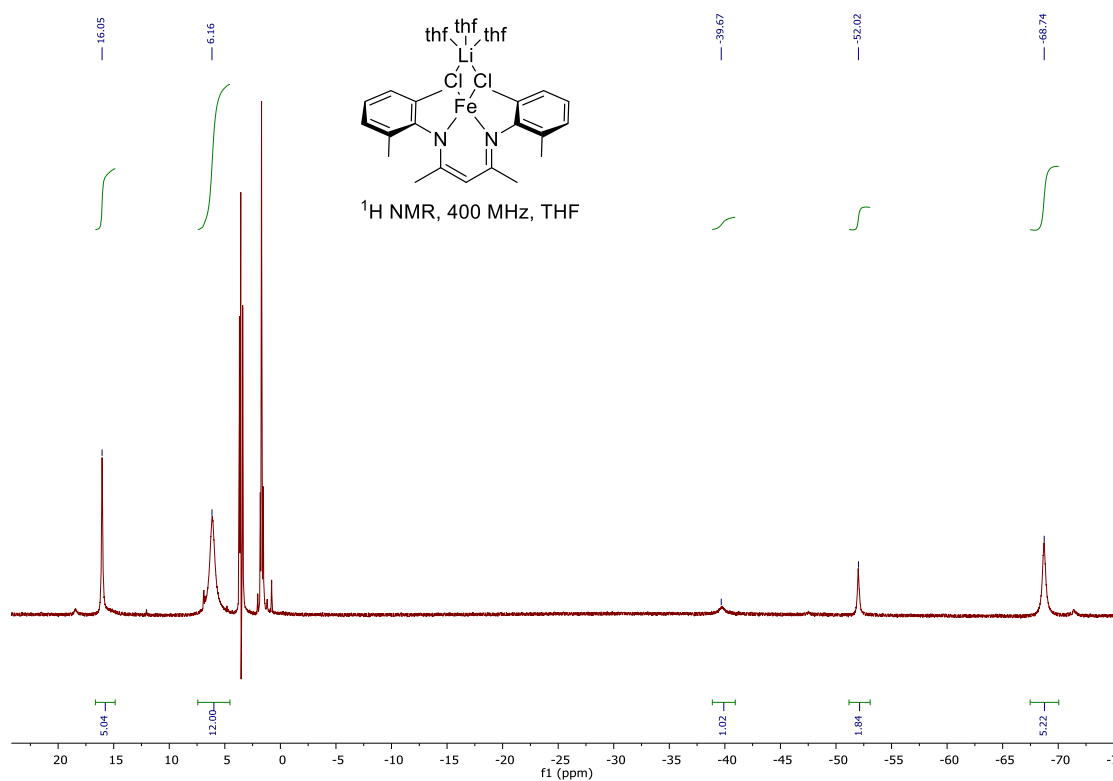
Figure D2. ^{1}H NMR of 2,4-bis[(2,6-dimethylphenyl)imino]pentane iron chloride complex (**3.1**) using solvent suppression for THF peaks.
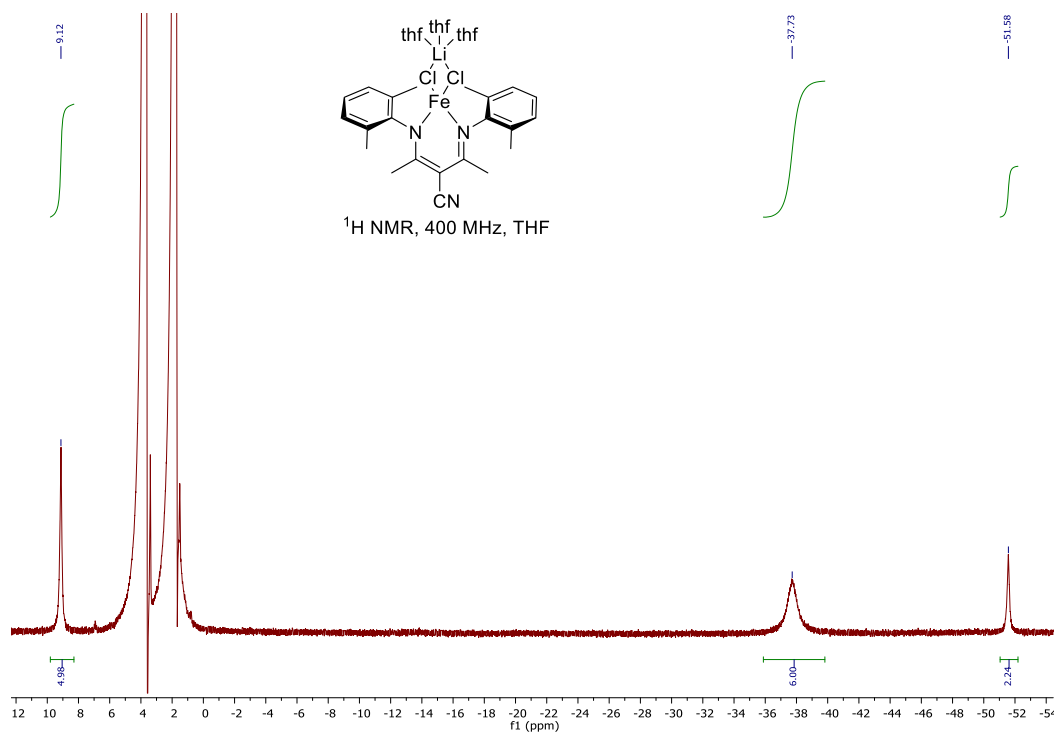
Figure D3. ^{1}H NMR of 3-cyano-2,4-bis[(2,6-dimethylphenyl)imino]pentane iron chloride complex (**3.1b**) using solvent suppression for THF peaks.
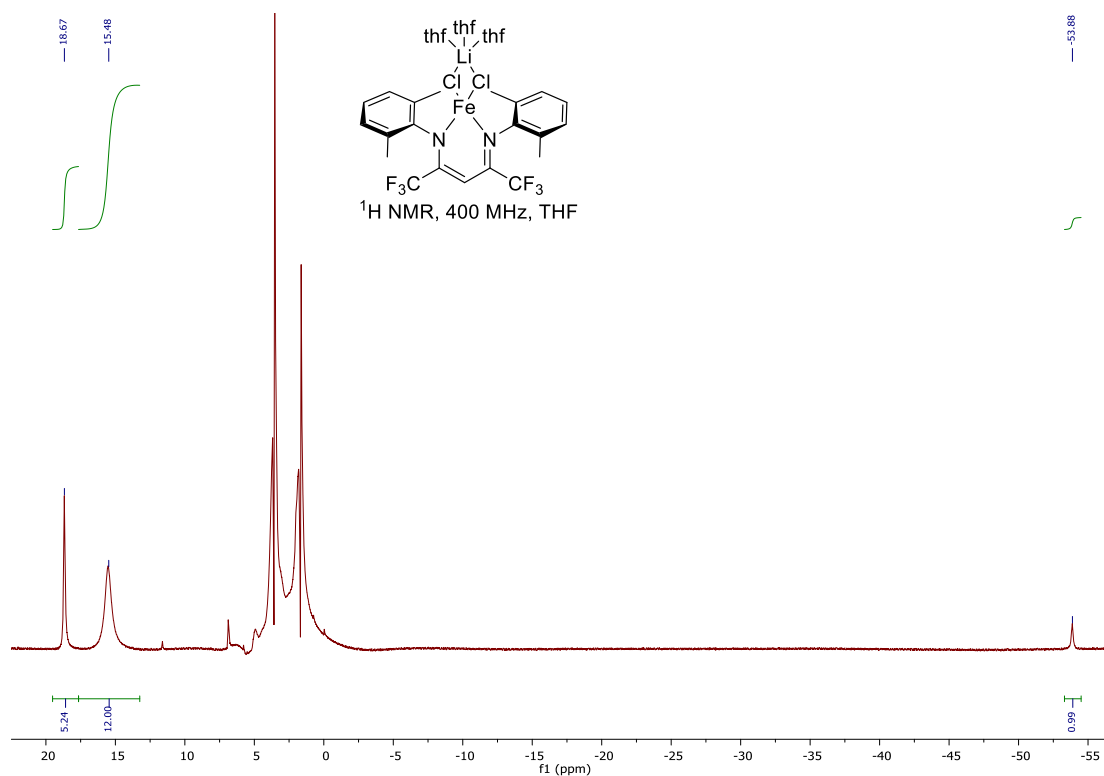
Figure D4. ^{1}H NMR of 1,1,1,5,5,5-hexafluoro-2,4-bis[(2,6-dimethylphenyl)imino]pentane iron chloride complex (**3.6**) using solvent suppression for THF peaks.

203
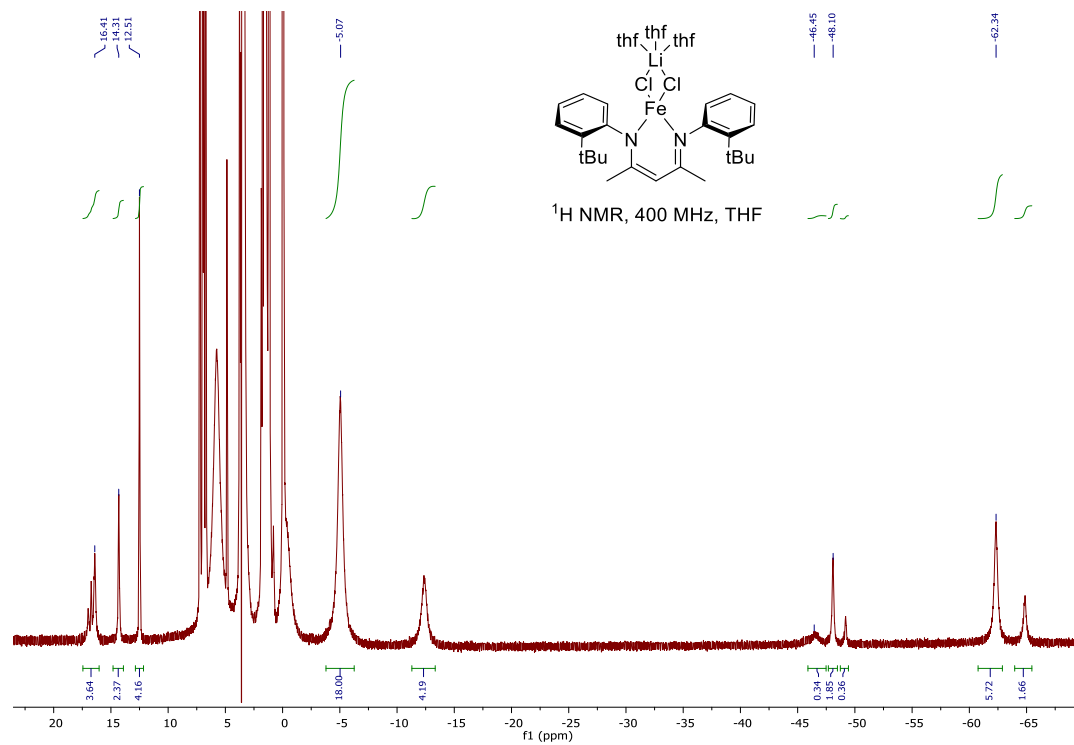
Figure D5. ¹H NMR of 2,4-bis[(2-*tert*-butylphenyl)imino]pentane iron chloride complex (**3.7**) using solvent suppression for THF peaks.
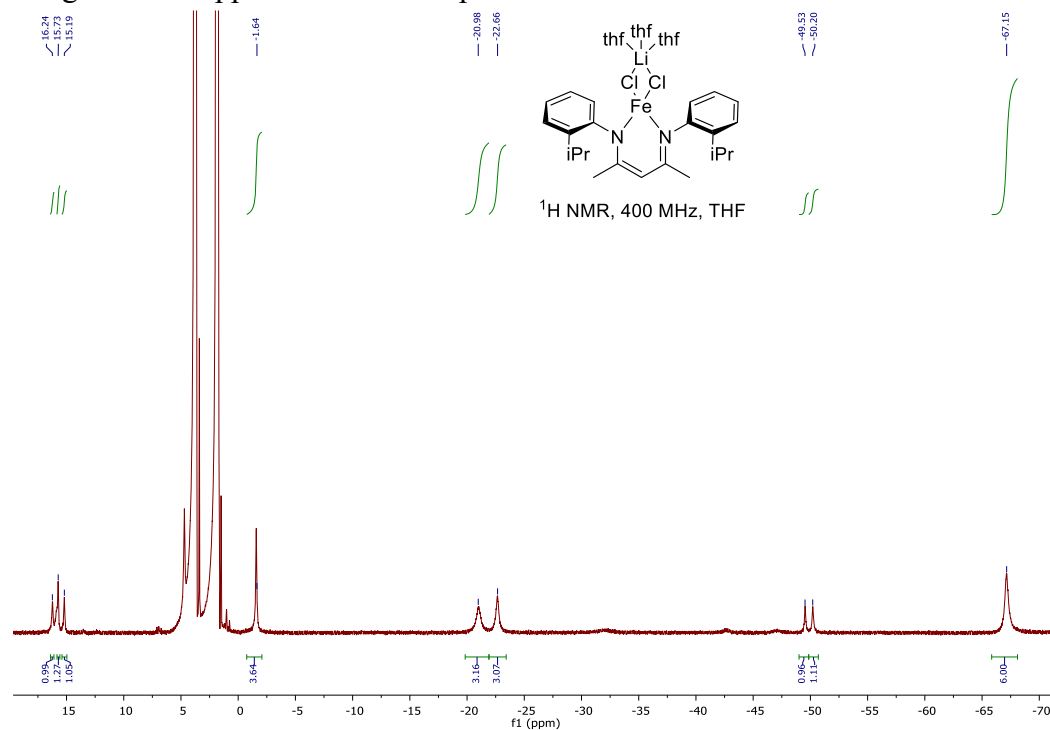
Figure D6. ¹H NMR of 2,4-bis[(2-isopropylphenyl)imino]pentane iron chloride complex (**3.8**) using solvent suppression for THF peaks.
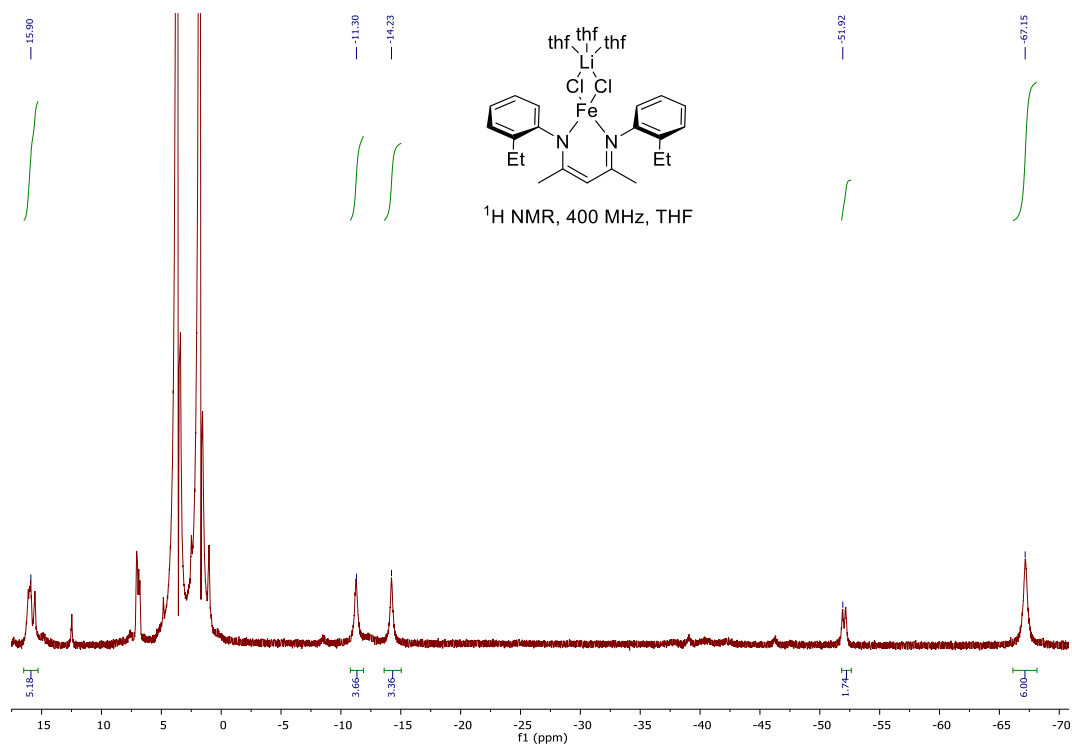
Figure D7. ^{1}H NMR of 2,4-bis[(2-ethylphenyl)imino]pentane iron chloride complex (**3.9**) using solvent suppression for THF peaks.
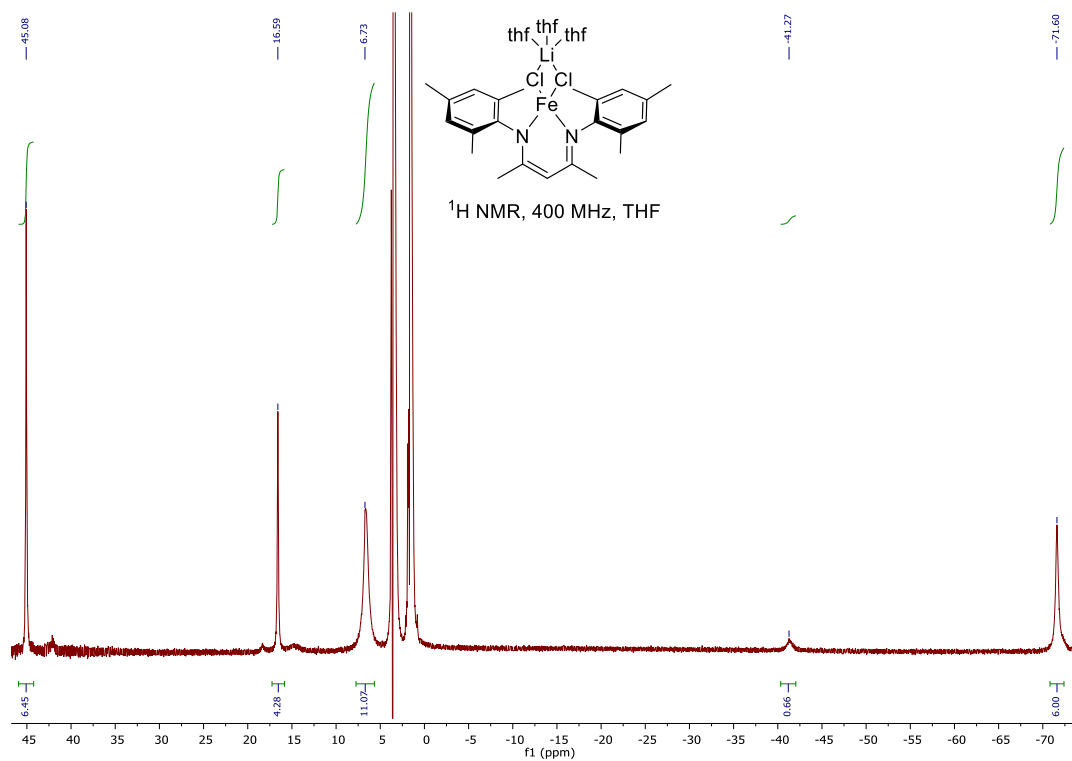
Figure D8. ¹H NMR of 2,4-bis[(2,4,6-trimethylphenyl)imino]pentane iron chloride complex (**3.11**) using solvent suppression for THF peaks.
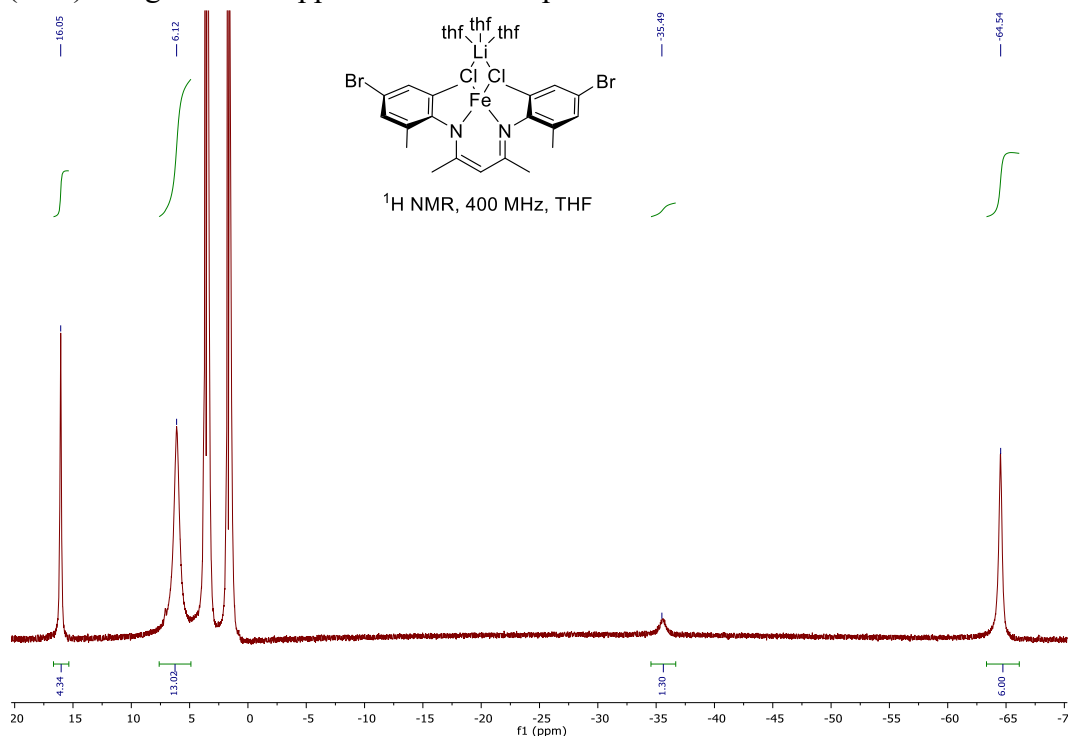
Figure D9. ¹H NMR of 2,4-bis[(4-bromo-2,6-dimethylphenyl)imino]pentane iron chloride complex (**3.12**) using solvent suppression for THF peaks.
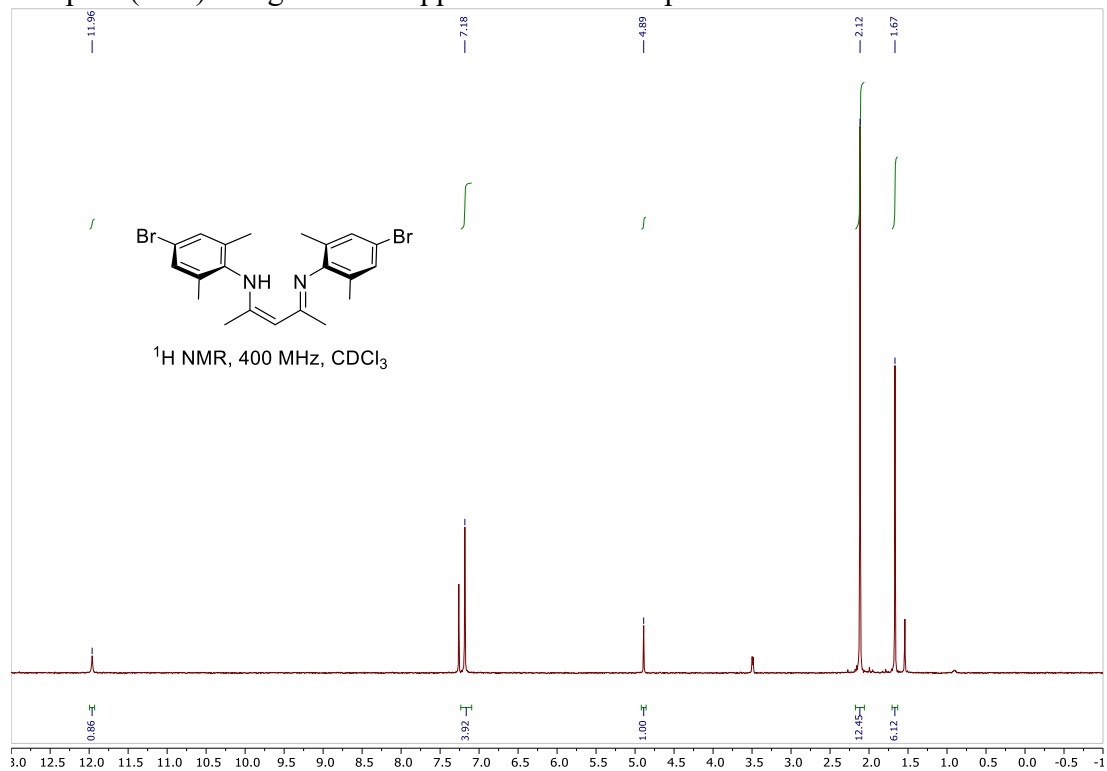
Figure D10. ¹H NMR of 2,4-bis[(4-bromo-2,6-dimethylphenyl)imino]pentane (**3.12a**) ligand
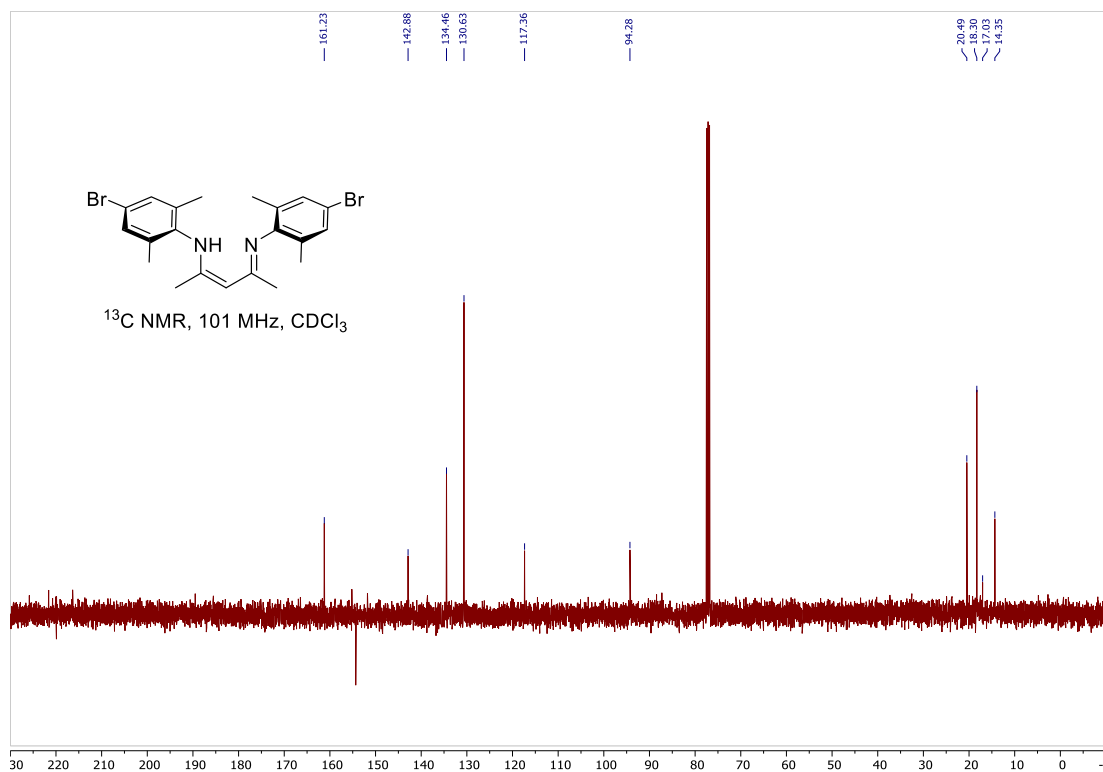
Figure D11. ^{13}C NMR of 2,4-bis[(4-bromo-2,6-dimethylphenyl)imino]pentane (3.12a) ligand
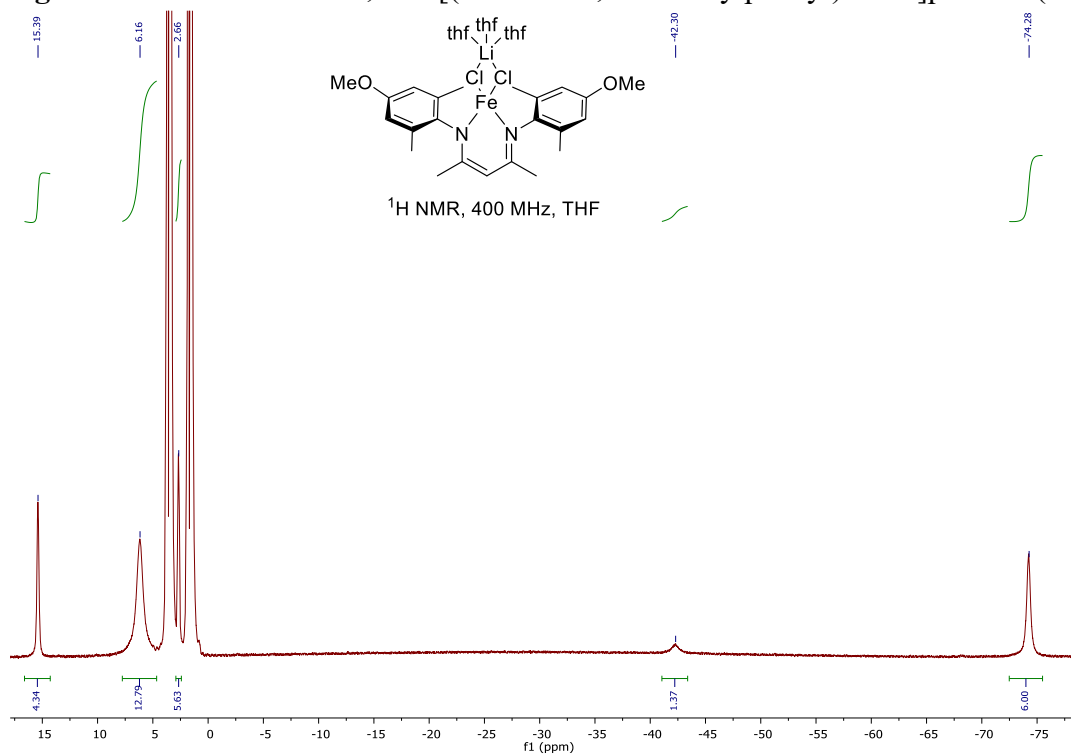
Figure D12. ^{1}H NMR of 2,4-bis[(4-methoxy-2,6-dimethylphenyl)imino]pentane iron chloride complex (**3.13**) using solvent suppression for THF peaks.
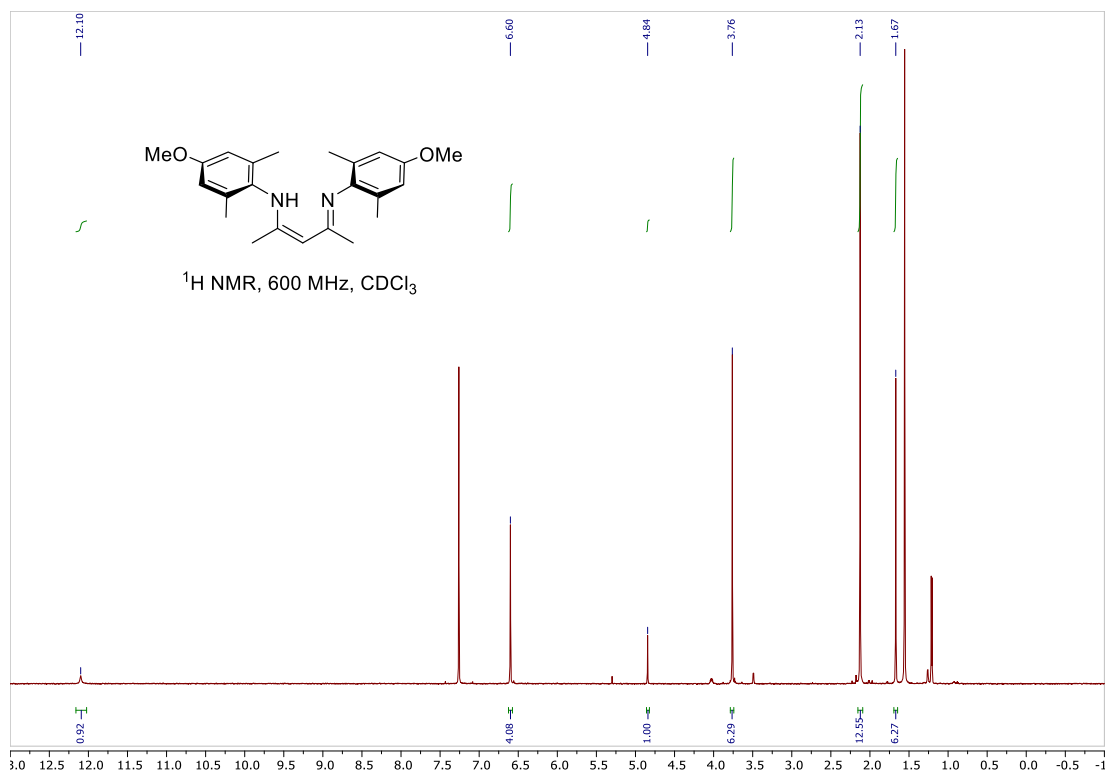
Figure D13. ^{1}H NMR of 2,4-bis[(4-methoxy-2,6-dimethylphenyl)imino]pentane (**3.13a**) ligand.
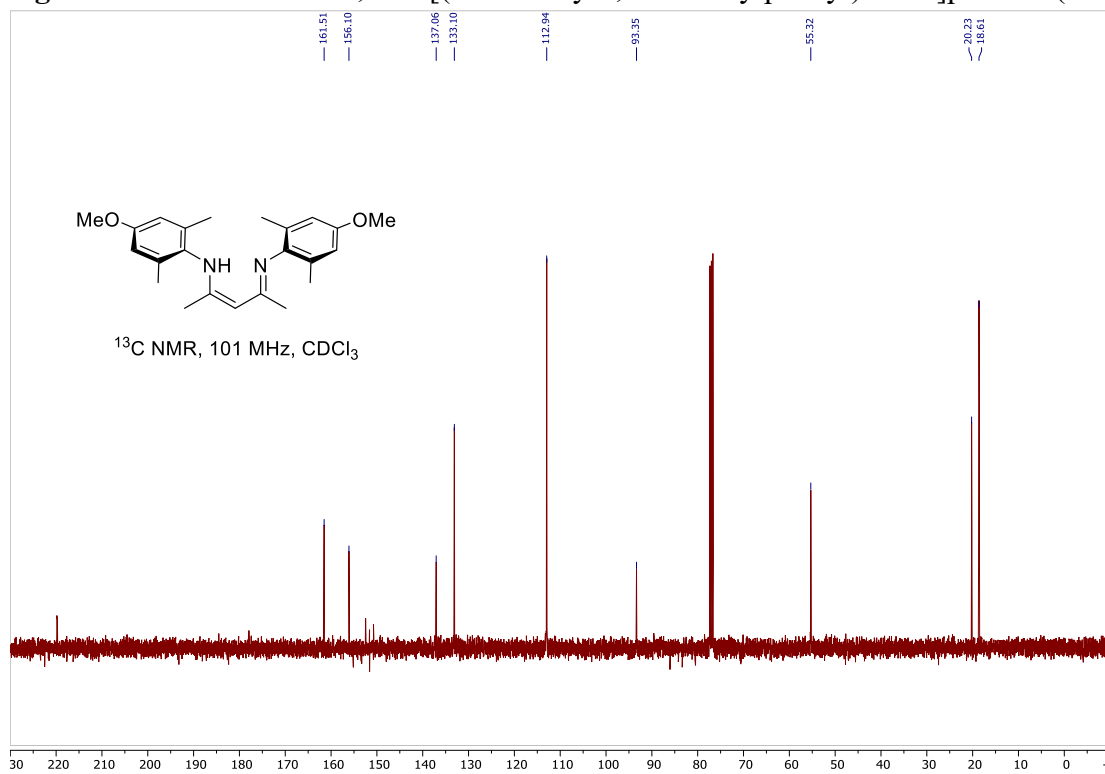
Figure D14. ^{13}C NMR of 2,4-bis[(4-methoxy-2,6-dimethylphenyl)imino]pentane (**3.13a**) ligand.

208
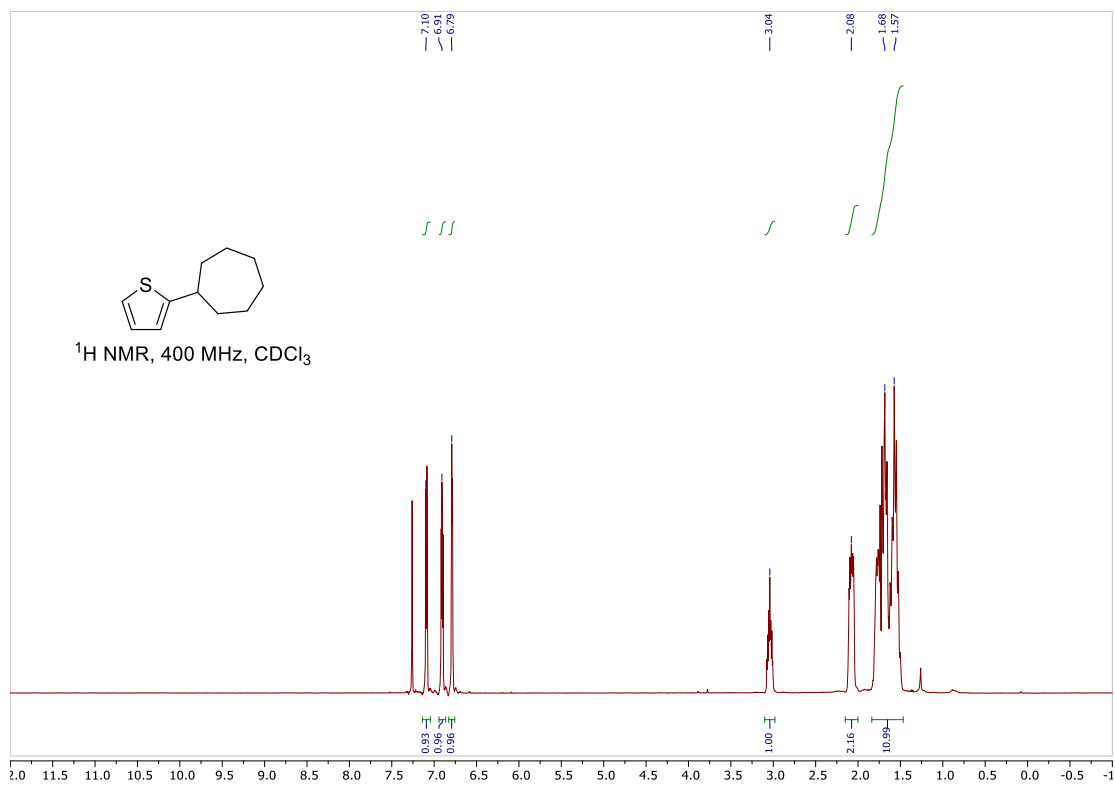
Figure D15. ^{1}H NMR of 2-cycloheptyl thiophene (**3.16**)
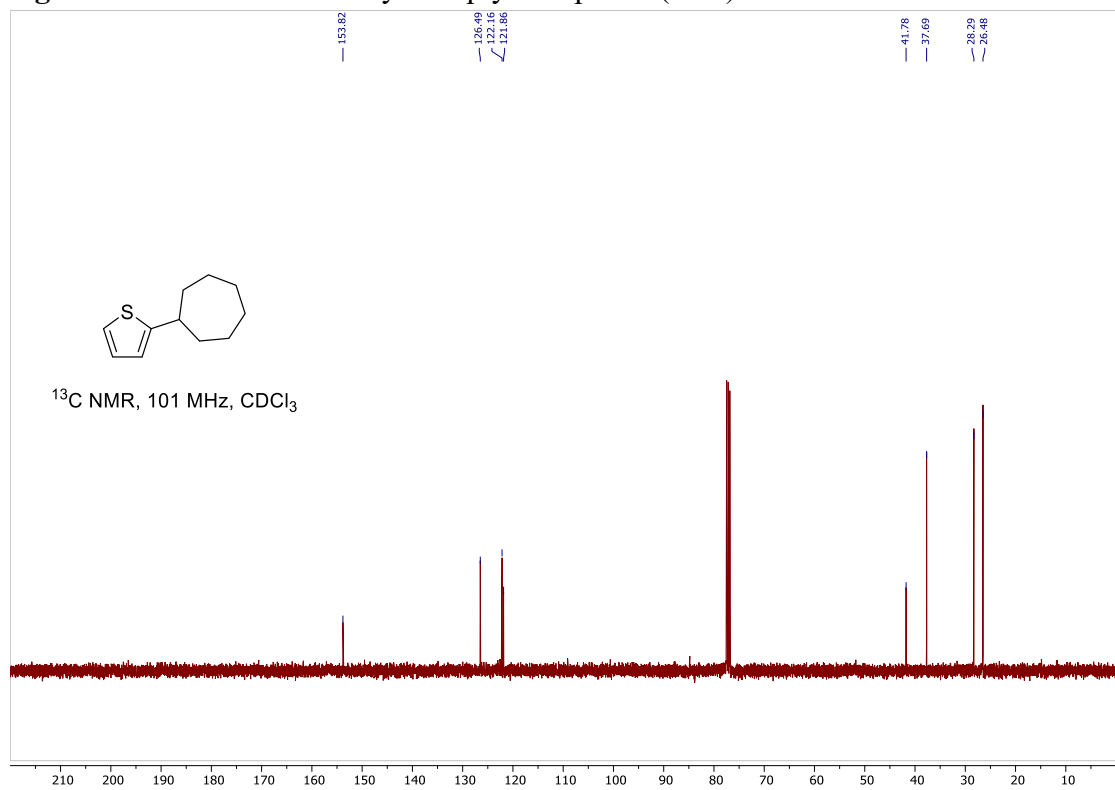
Figure D16. ^{13}C NMR of 2-cycloheptyl thiophene (**3.16**)

209
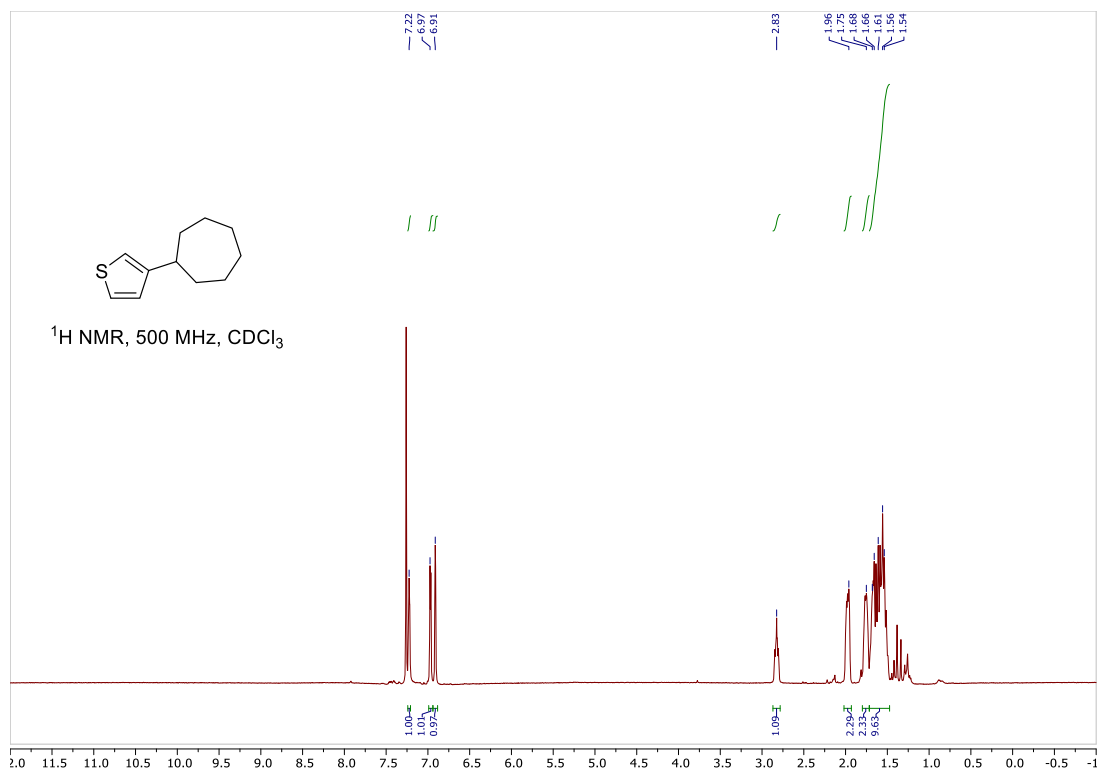
Figure D17. ^{1}H NMR of 3-cycloheptyl thiophene (**3.17**)
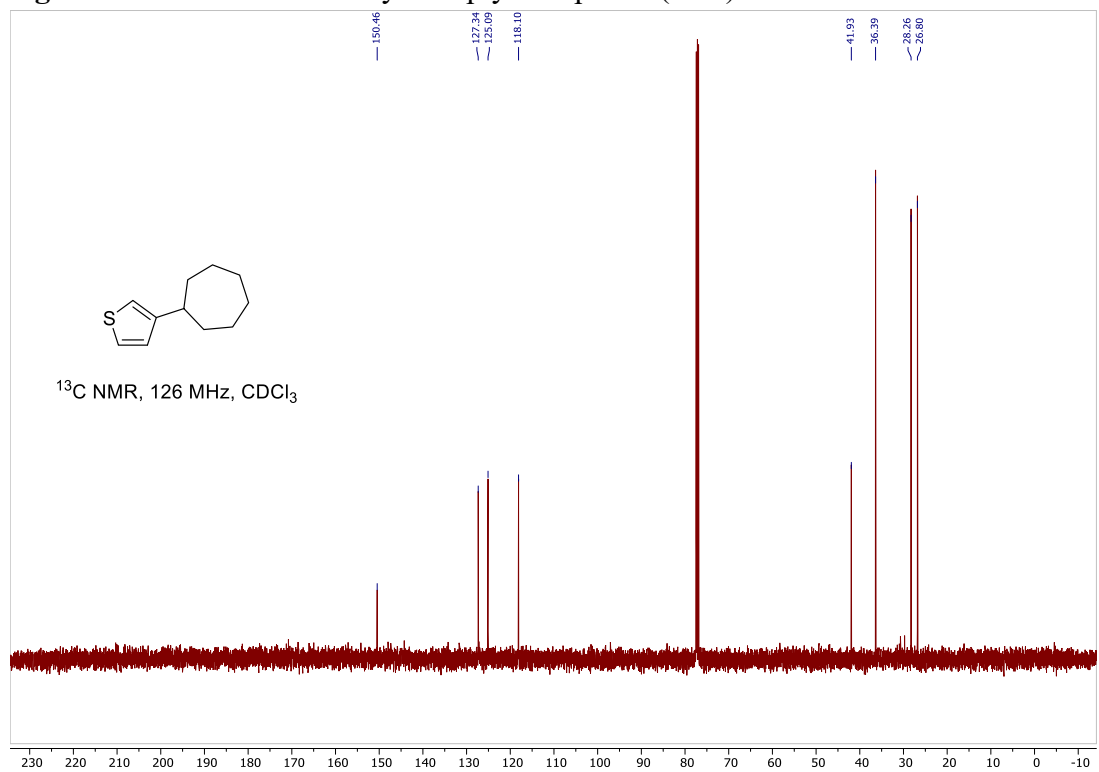
Figure D18. ^{13}C NMR of 3-cycloheptyl thiophene (**3.17**)

210
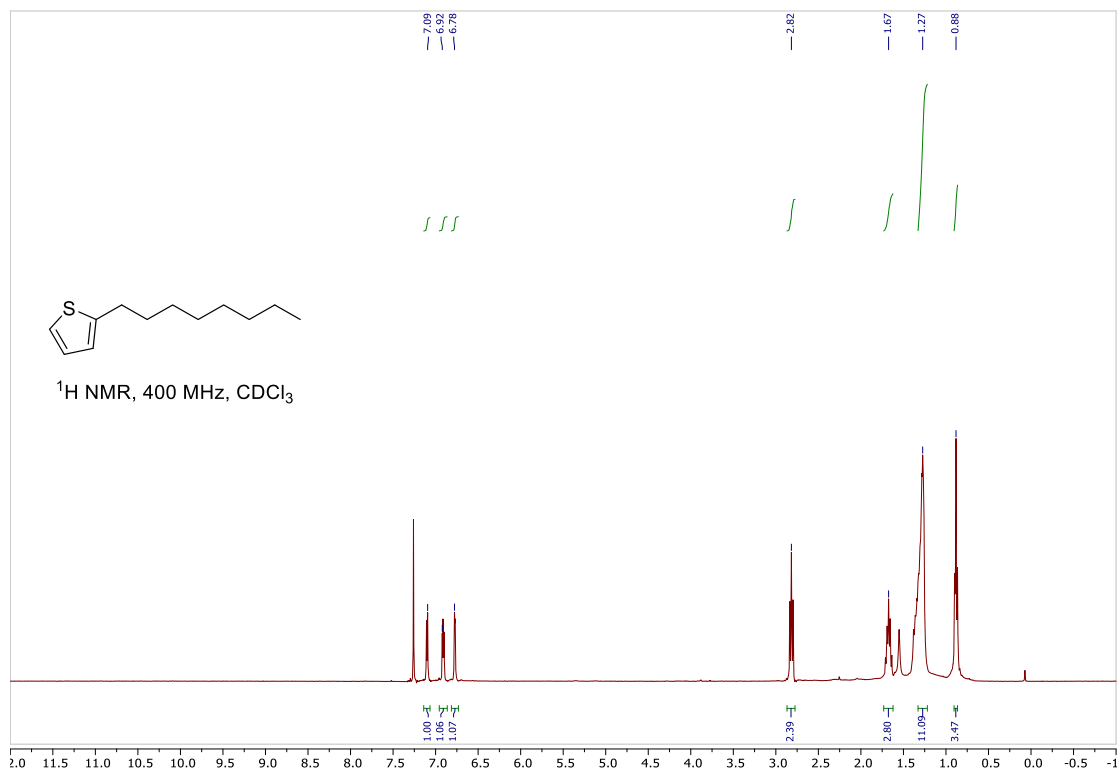
Figure D19. ¹H NMR of 2-octyl thiophene (**3.18**)
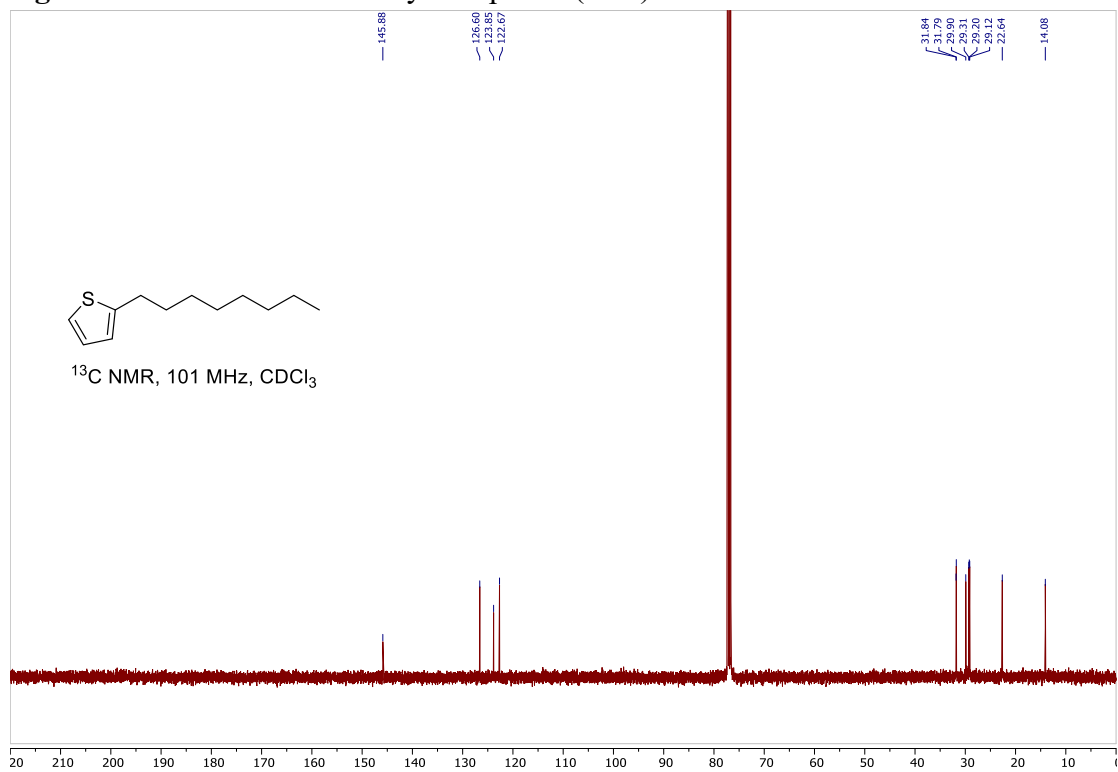
Figure D20. ¹³C NMR of 2-octyl thiophene (**3.18**)

211
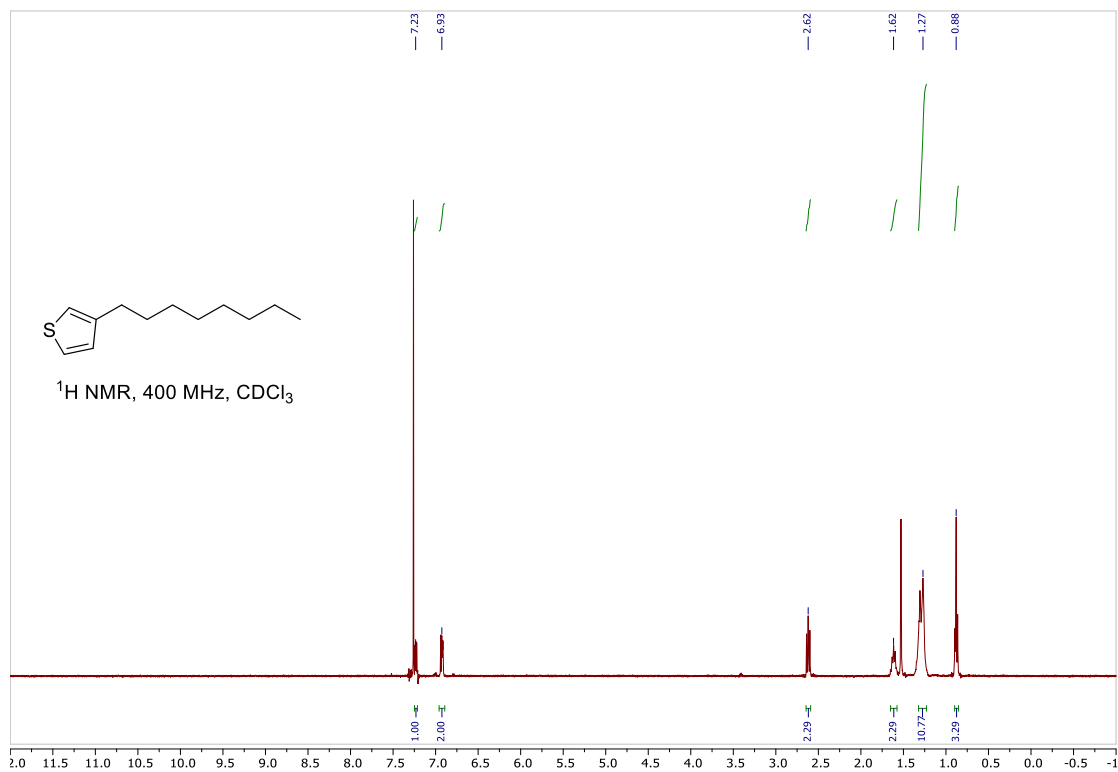
Figure D21. ¹H NMR of 3-octyl thiophene (**3.19**)
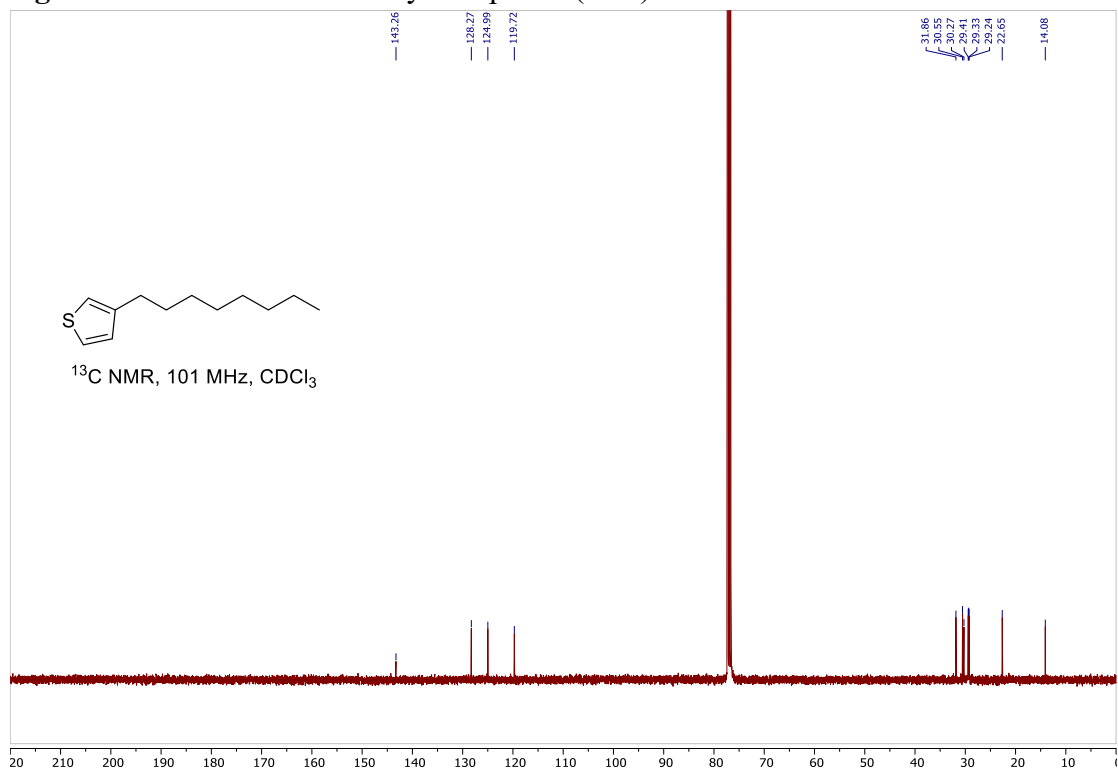
Figure D22. ¹³C NMR of 3-octyl thiophene (**3.19**)
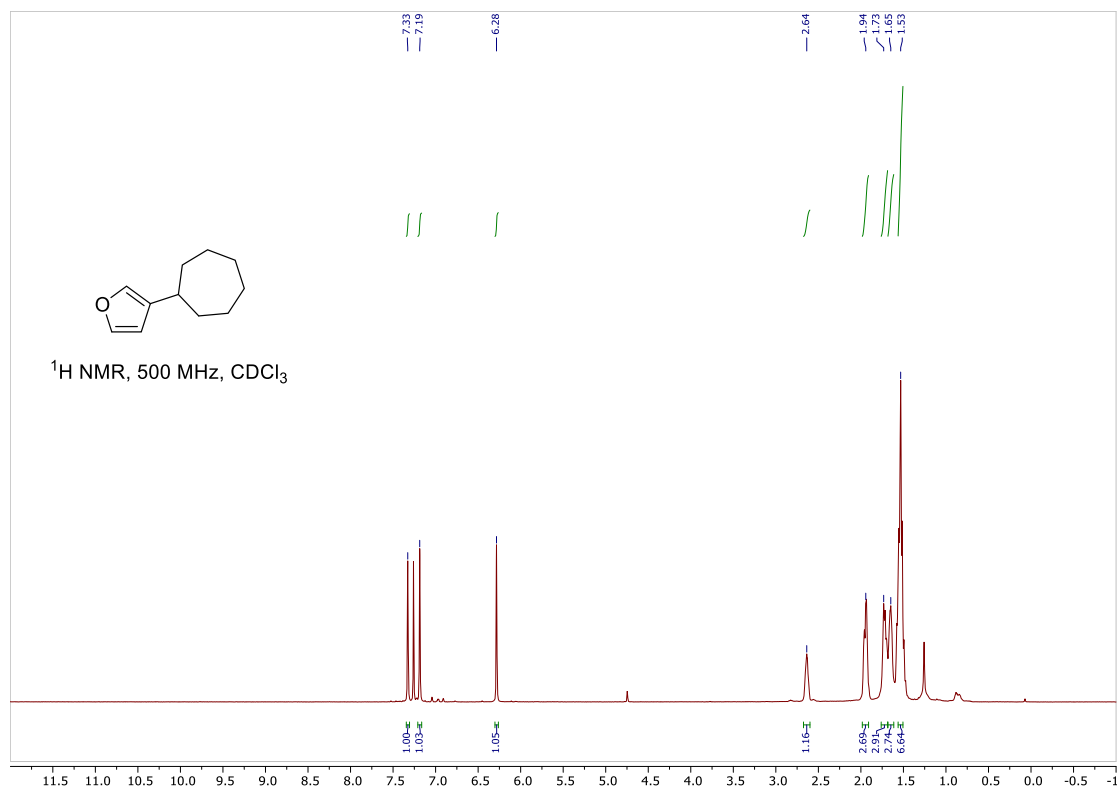
Figure D23. ^{1}H NMR of 3-cycloheptyl furan (**3.20**)
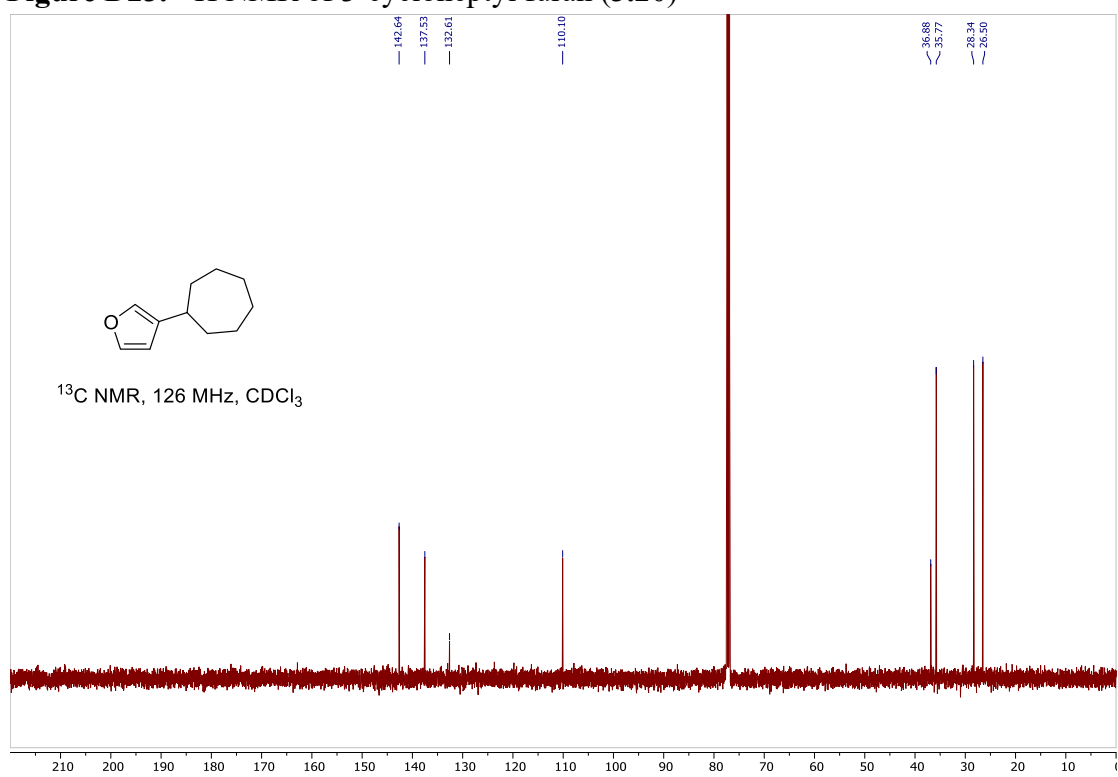
Figure D24. ^{13}C NMR of 3-cycloheptyl furan (**3.20**)

213
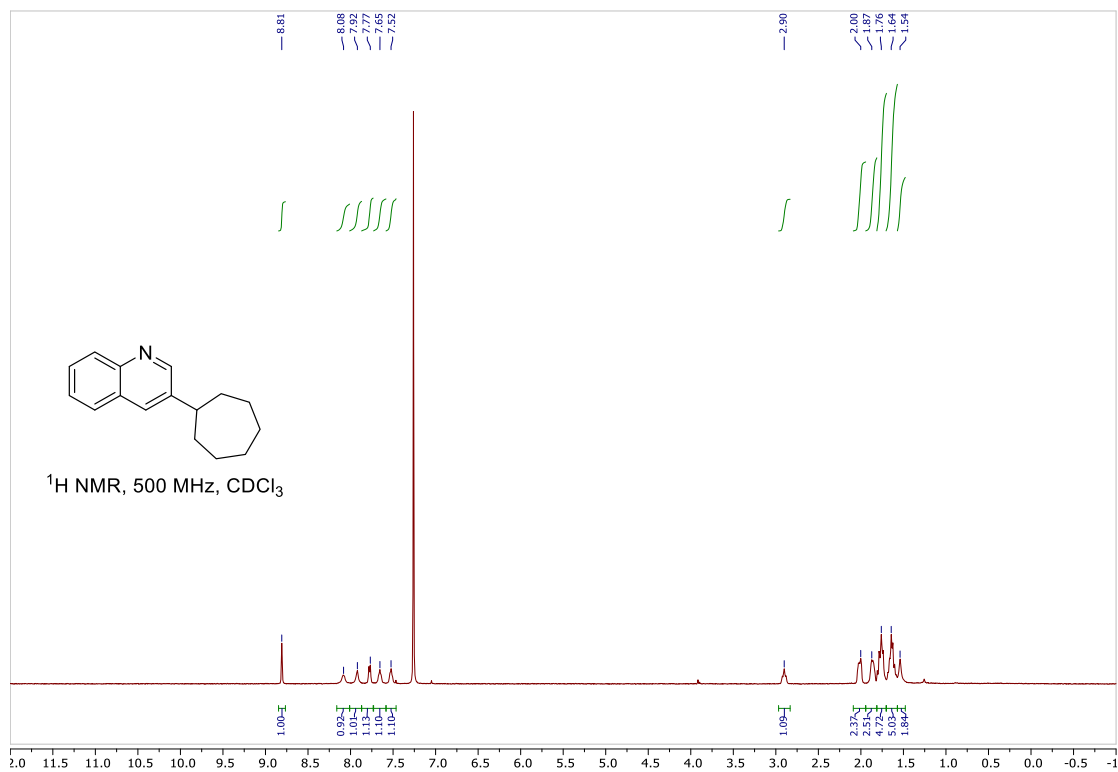
Figure D25. ¹H NMR of 3-cycloheptyl quinoline (**3.22**)
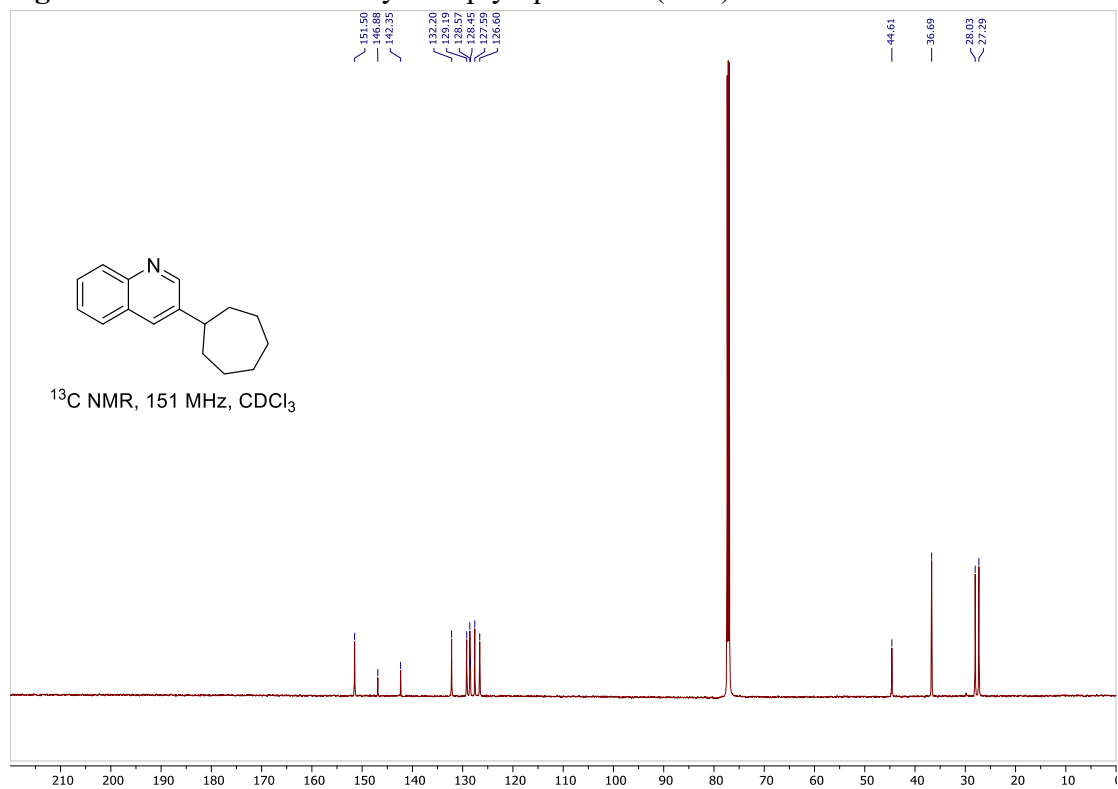
Figure D26. ¹³C NMR of 3-cycloheptyl quinoline (**3.22**)
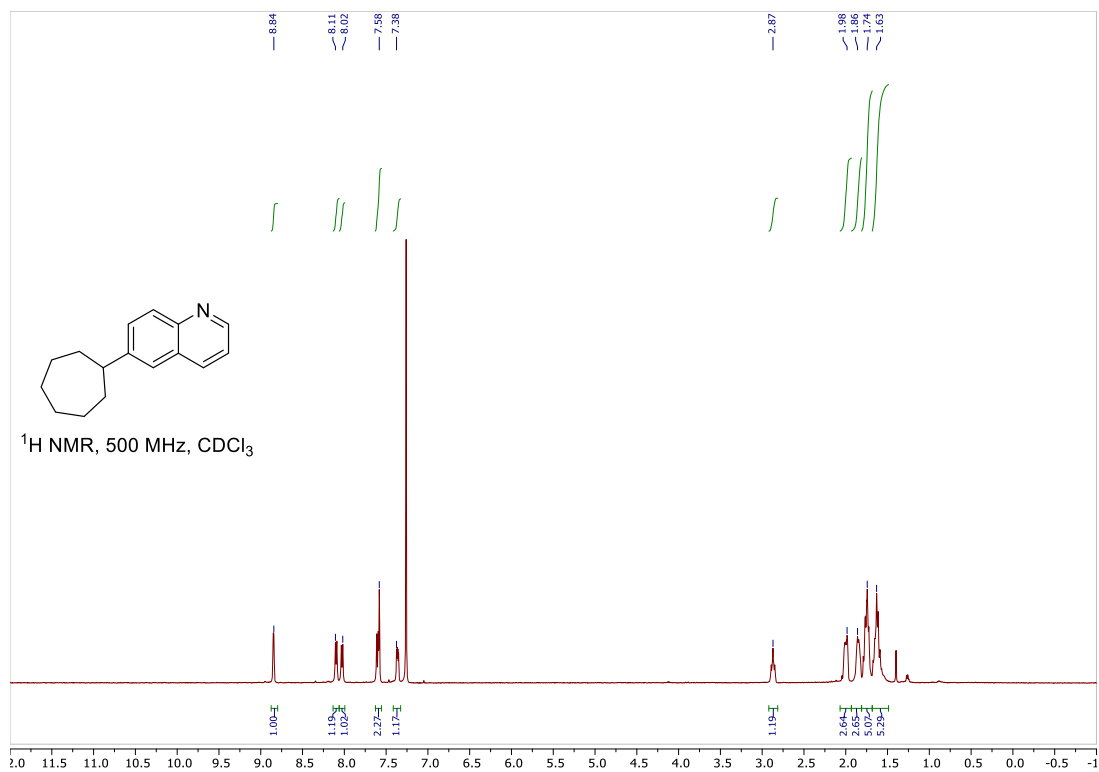
Figure D27. ^{1}H NMR of 6-cycloheptyl quinoline (**3.23**)
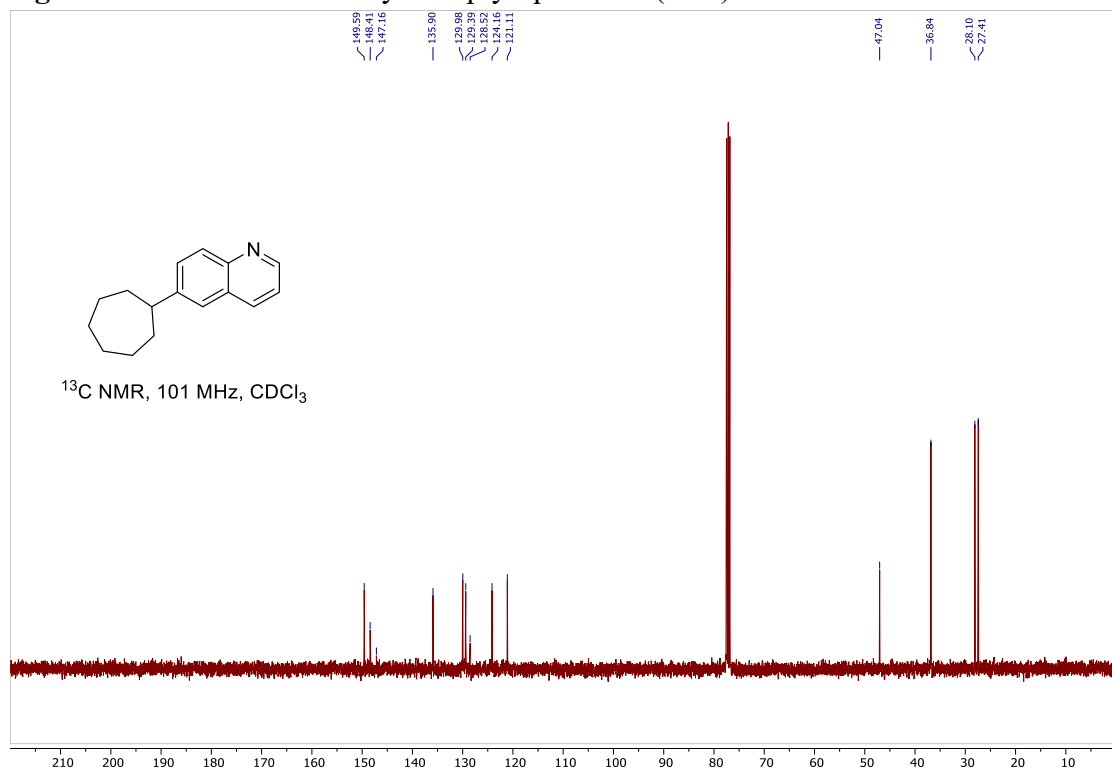
Figure D28. ^{13}C NMR of 6-cycloheptyl quinoline (**3.23**)
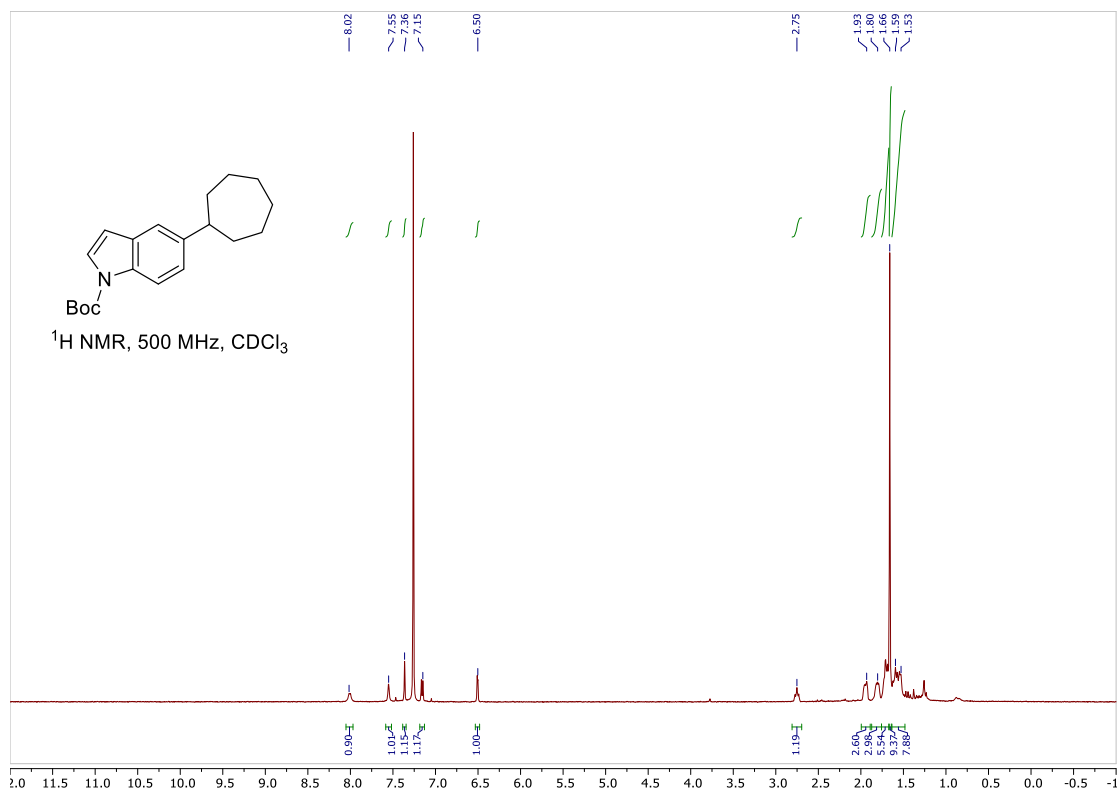
Figure D29. ^{1}H NMR of 5-cycloheptyl-1-*N*-Boc-indole (**3.25**)
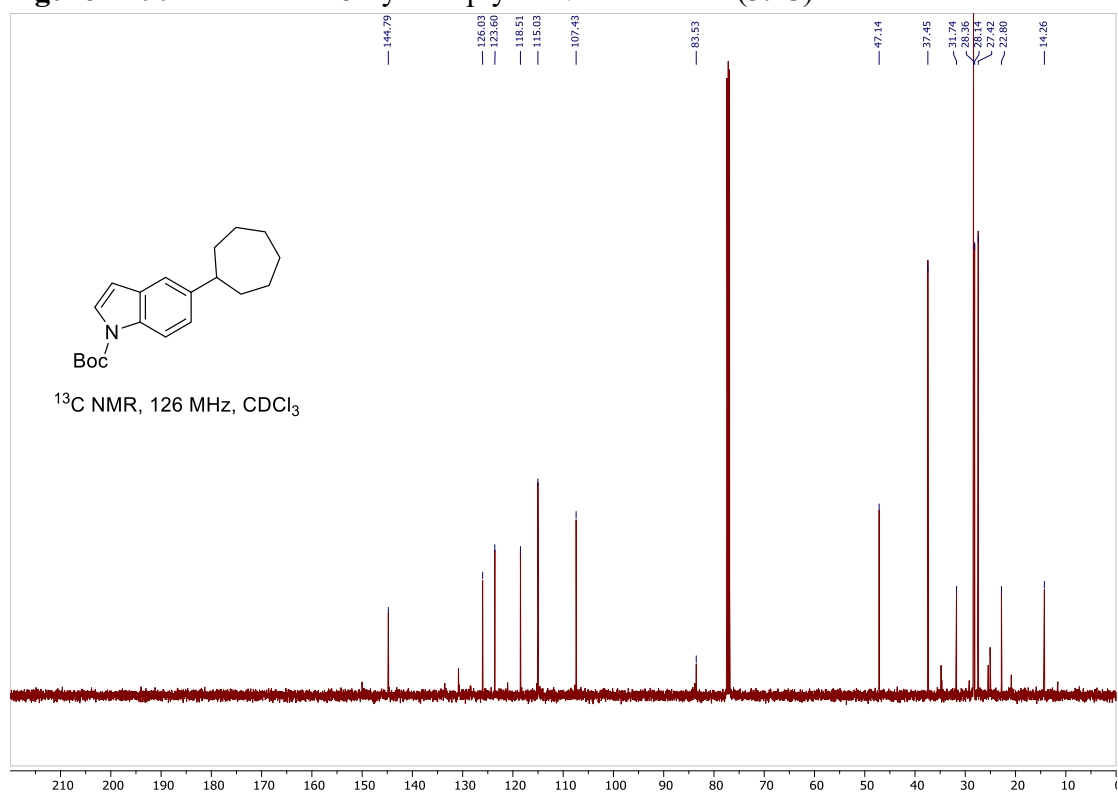
Figure D30. ^{13}C NMR of 5-cycloheptyl-1-*N*-Boc-indole (**3.25**)
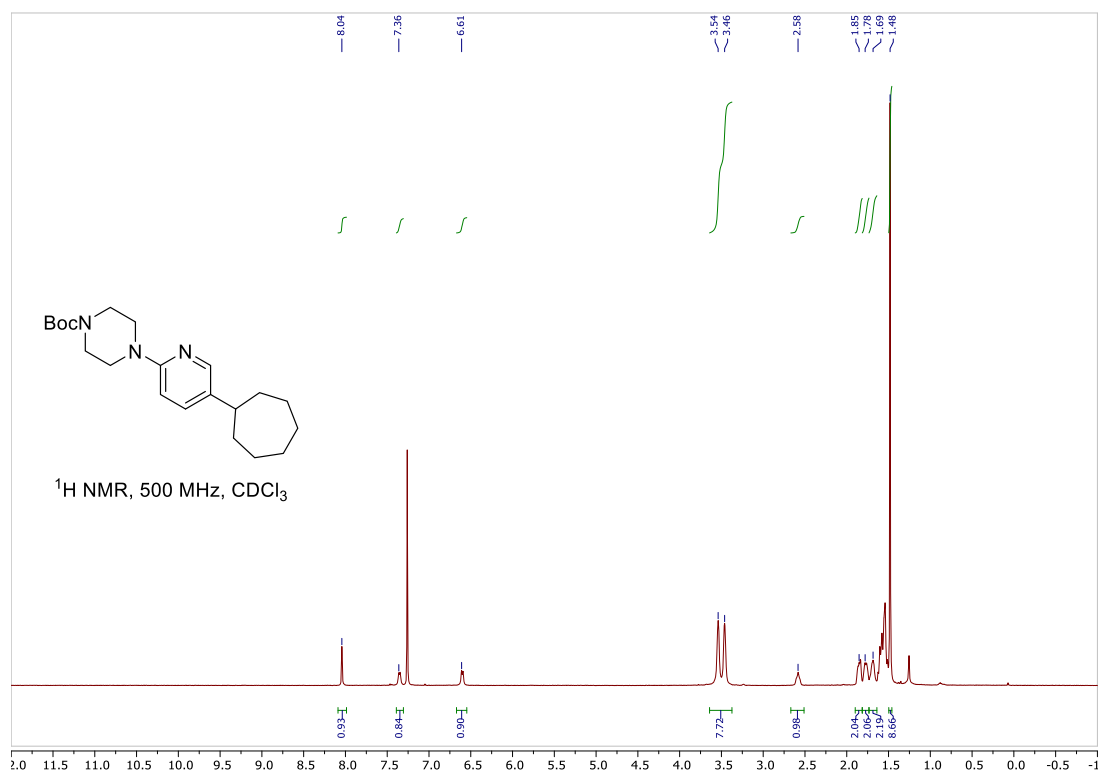
Figure D31. ^{1}H NMR of 6-(4-Boc-piperazin-1-yl)-3-cycloheptyl pyridine (**3.28**)
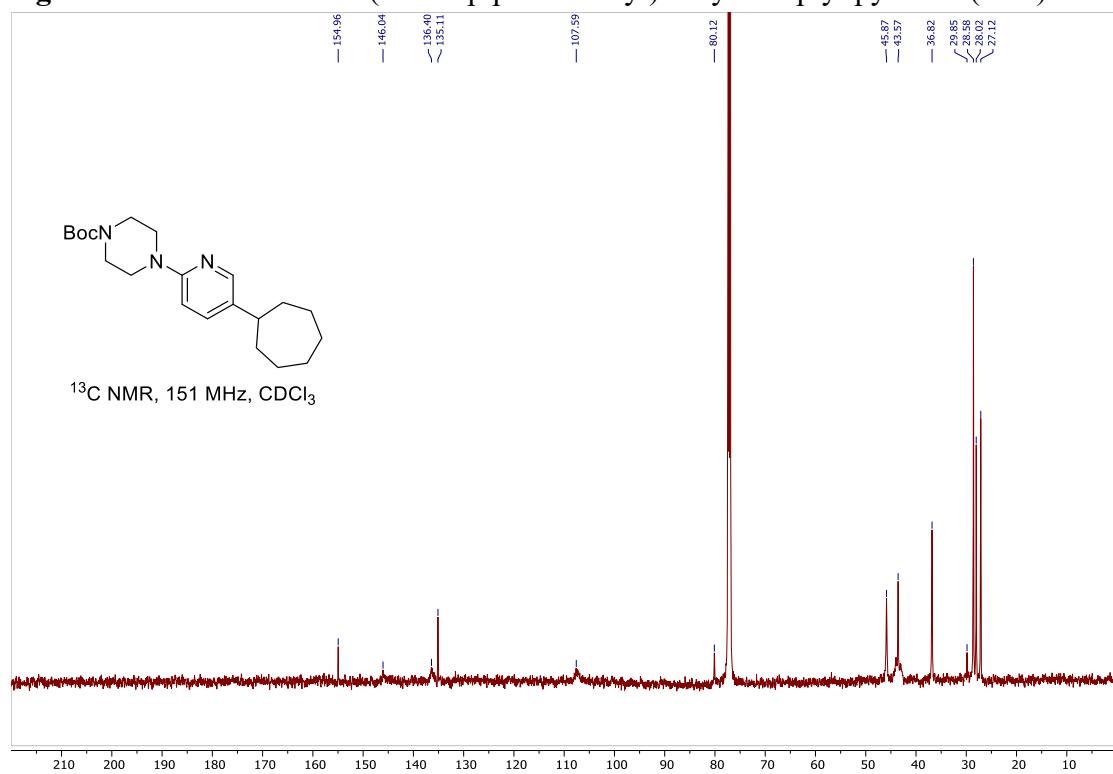
Figure D32. ^{13}C NMR of 6-(4-Boc-piperazin-1-yl)-3-cycloheptyl pyridine (**3.28**)

217
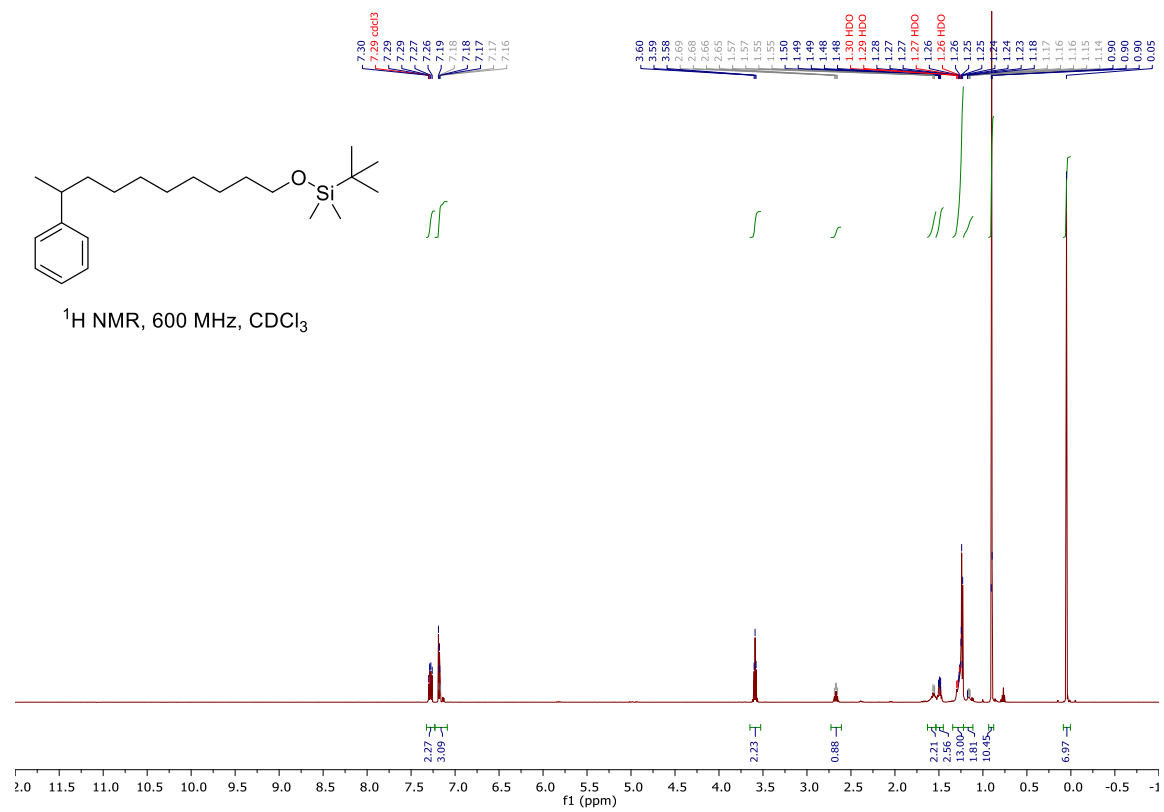
Figure D33. ^{1}H NMR of *tert*-butyldimethyl((9-phenyldecyl)oxy)silane (**3.35**)
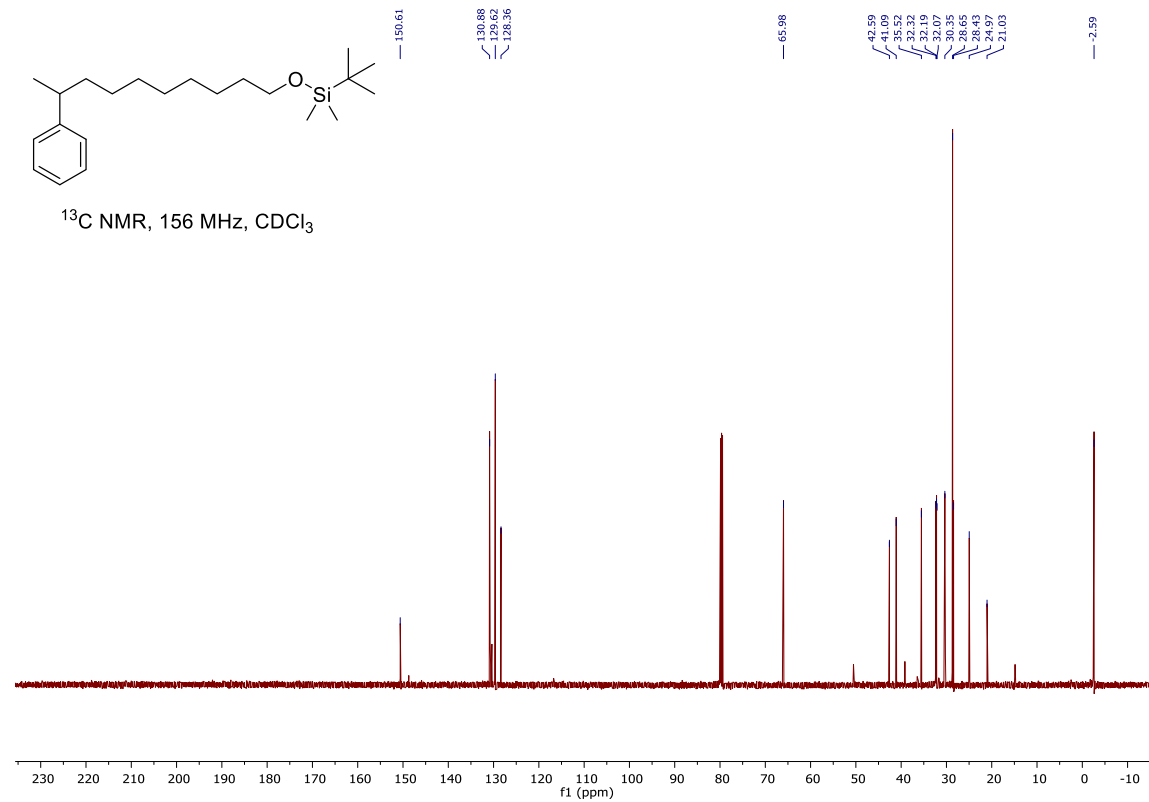
Figure D34. ^{13}C NMR of *tert*-butyldimethyl((9-phenyldecyl)oxy)silane (**3.35**)

218

Appendix E: Crystallographic Data for Chapter 3.

Table E1. Crystal data and structure refinement for dimeric 2,4-bis[(2,6-dimethylphenyl)imino]pentane iron *N,N*-diethylamide complex (**3.3**)

Identification code   C50H70Fe2N6

Empirical formula   C50 H70 Fe2 N6

Formula weight   866.82

Temperature   100(2) K

Wavelength   1.54178 Å

Crystal system   Monoclinic

Space group   **6**/c

Unit cell dimensions   a = 15.8079(5) Å   α= 90°.

b = 14.3502(4) Å   β= 109.8450(10)°.

c = 21.0653(6) Å   γ = 90°.

Volume   4494.8(2) Å^3

Z   4

Density (calculated)   1.281 Mg/m^3

Absorption coefficient   5.480 mm^{-1}

F(000) 1856

Crystal size   0.480 x 0.260 x 0.100 mm^3

Theta range for data collection   4.282 to 66.599°.

Index ranges   -18<=h<=18, -17<=k<=17, -24<=l<=25

Reflections collected   19773

Independent reflections   3960 [R(int) = 0.0363]

Completeness to theta = 66.599°   99.7 %

Absorption correction Semi-empirical from equivalents

Max. and min. transmission   0.7528 and 0.4837

Refinement method   Full-matrix least-squares on F^2

Data / restraints / parameters 3960 / 0 / 273

Goodness-of-fit on F^2 1.067

Final R indices [I>2sigma(I)] R1 = 0.0288, wR2 = 0.0794

R indices (all data)   R1 = 0.0292, wR2 = 0.0798

Extinction coefficient n/a

Largest diff. peak and hole   0.322 and -0.371 e.Å^{-3}

Table E2. Atomic coordinates (x 10^4) and equivalent isotropic displacement parameters ($Å^2$x 10^3) for dimeric 2,4-bis[(2,6-dimethylphenyl)imino]pentane iron *N,N*-diethylamide complex (**3.3**). U(eq) is defined as one third of the trace of the orthogonalized U^{ij} tensor.
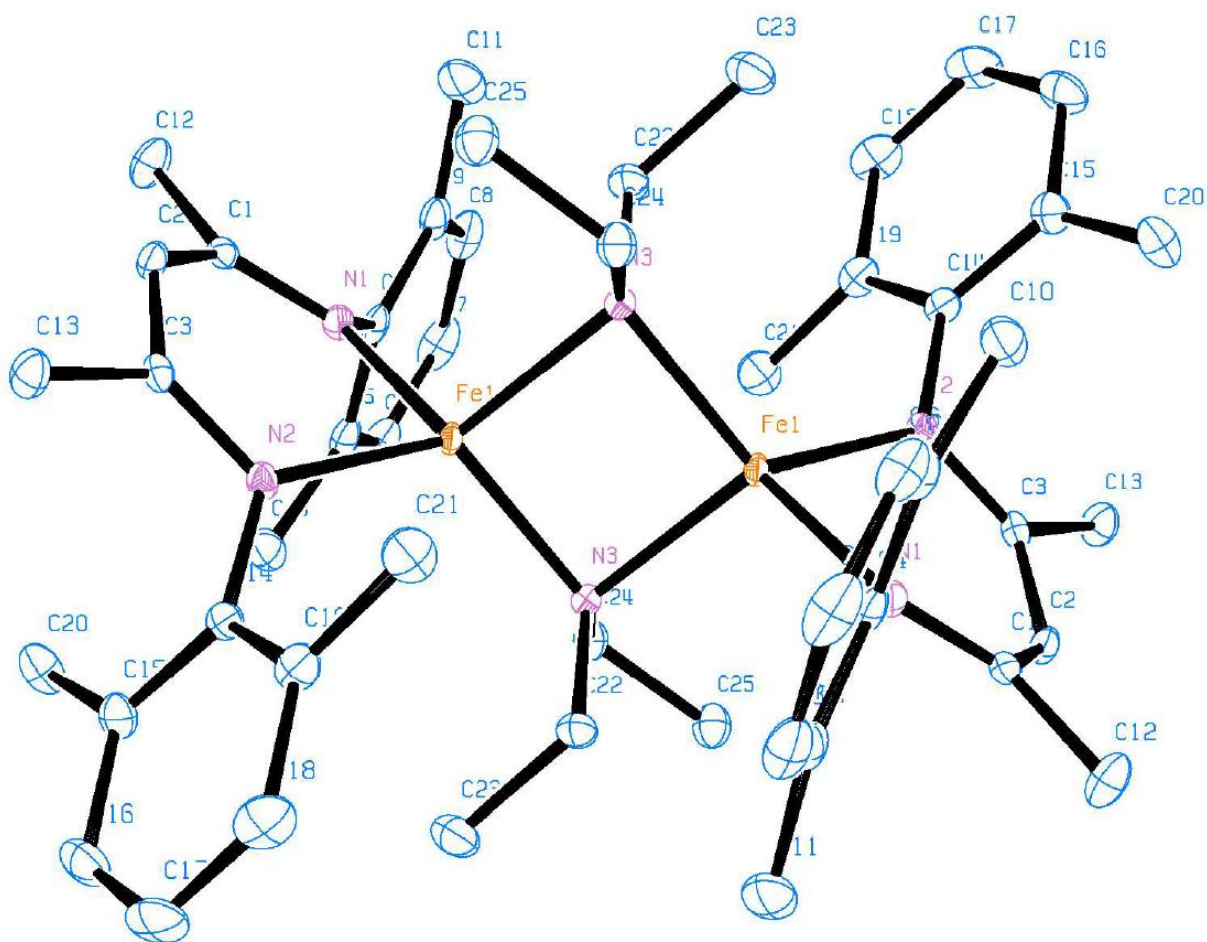
	x	y	z	U(eq)
Fe(1)	7654(1)	3272(1)	5451(1)	9(1)
N(1)	7882(1)	3290(1)	6488(1)	11(1)
N(2)	8003(1)	4654(1)	5448(1)	10(1)
N(3)	6507(1)	2774(1)	4737(1)	10(1)
C(1)	8488(1)	3876(1)	6878(1)	11(1)

C(2)	8929(1)	4563(1)	6626(1)	12(1)
C(3)	8660(1)	4979(1)	5989(1)	11(1)
C(4)	7358(1)	2743(1)	6793(1)	12(1)
C(5)	6474(1)	3048(1)	6692(1)	15(1)
C(6)	5927(1)	2532(1)	6957(1)	21(1)
C(7)	6247(1)	1734(1)	7331(1)	24(1)
C(8)	7119(1)	1456(1)	7447(1)	21(1)
C(9)	7694(1)	1948(1)	7189(1)	16(1)
C(10)	6135(1)	3955(1)	6338(1)	19(1)
C(11)	8655(1)	1614(1)	7385(1)	23(1)
C(12)	8737(1)	3870(1)	7638(1)	19(1)
C(13)	9142(1)	5869(1)	5932(1)	16(1)
C(14)	7604(1)	5317(1)	4916(1)	12(1)
C(15)	7019(1)	6002(1)	5009(1)	15(1)
C(16)	6589(1)	6606(1)	4480(1)	21(1)
C(17)	6732(1)	6544(1)	3870(1)	24(1)
C(18)	7325(1)	5889(1)	3788(1)	22(1)
C(19)	7780(1)	5277(1)	4308(1)	16(1)
C(20)	6841(1)	6098(1)	5664(1)	20(1)
C(21)	8468(1)	4618(1)	4218(1)	21(1)
C(22)	6196(1)	3365(1)	4128(1)	14(1)
C(23)	5625(1)	4207(1)	4166(1)	20(1)
C(24)	5736(1)	2488(1)	4939(1)	14(1)
C(25)	5022(1)	1909(1)	4414(1)	17(1)

Table E3. Bond lengths [Å] and angles [°] for dimeric 2,4-bis[(2,6-dimethylphenyl)imino]pentane iron *N,N*-diethylamide complex (**3.3**)

Fe(1)-N(3)	2.0503(12)
Fe(1)-N(2)	2.0601(12)
Fe(1)-N(1)	2.0909(13)
Fe(1)-N(3)#1	2.1275(12)
Fe(1)-Fe(1)#1	2.8494(4)
N(1)-C(1)	1.328(2)
N(1)-C(4)	1.4412(19)
N(2)-C(3)	1.338(2)
N(2)-C(14)	1.4407(19)
N(3)-C(22)	1.4770(19)
N(3)-C(24)	1.4793(19)
C(1)-C(2)	1.410(2)
C(1)-C(12)	1.513(2)
C(2)-C(3)	1.397(2)
C(2)-H(2)	0.935(19)
C(3)-C(13)	1.512(2)
C(4)-C(9)	1.407(2)
C(4)-C(5)	1.409(2)
C(5)-C(6)	1.393(2)
C(5)-C(10)	1.505(2)
C(6)-C(7)	1.384(3)
C(6)-H(6)	0.9500
C(7)-C(8)	1.375(3)
C(7)-H(7)	0.9500
C(8)-C(9)	1.399(2)
C(8)-H(8)	0.9500

223

C(9)-C(11)   1.510(2)

C(10)-H(10A)   0.9800

C(10)-H(10B) 0.9800

C(10)-H(10C) 0.9800

C(11)-H(11A)   0.9800

C(11)-H(11B) 0.9800

C(11)-H(11C) 0.9800

C(12)-H(12A)   0.9800

C(12)-H(12B) 0.9800

C(12)-H(12C) 0.9800

C(13)-H(13A)   0.9800

C(13)-H(13B) 0.9800

C(13)-H(13C) 0.9800

C(14)-C(19)   1.402(2)

C(14)-C(15)   1.408(2)

C(15)-C(16)   1.393(2)

C(15)-C(20)   1.505(2)

C(16)-C(17)   1.381(3)

C(16)-H(16)   0.9500

C(17)-C(18)   1.378(3)

C(17)-H(17)   0.9500

C(18)-C(19)   1.398(2)

C(18)-H(18)   0.9500

C(19)-C(21)   1.501(2)

C(20)-H(20A)   0.9800

C(20)-H(20B) 0.9800

C(20)-H(20C) 0.9800

C(21)-H(21A)   0.9800

C(21)-H(21B) 0.9800

C(21)-H(21C) 0.9800

C(22)-C(23)   1.527(2)

C(22)-H(22A)   0.9900

C(22)-H(22B) 0.9900

C(23)-H(23A)   0.9800

C(23)-H(23B) 0.9800

C(23)-H(23C) 0.9800

C(24)-C(25)   1.530(2)

C(24)-H(24A)   0.9900

C(24)-H(24B) 0.9900

C(25)-H(25A)   0.9800

C(25)-H(25B) 0.9800

C(25)-H(25C) 0.9800

N(3)-Fe(1)-N(2)   120.34(5)

N(3)-Fe(1)-N(1)   124.49(5)

N(2)-Fe(1)-N(1)   92.24(5)

N(3)-Fe(1)-N(3)#1   94.01(4)

N(2)-Fe(1)-N(3)#1   119.61(5)

N(1)-Fe(1)-N(3)#1   107.82(5)

N(3)-Fe(1)-Fe(1)#1   48.14(3)

N(2)-Fe(1)-Fe(1)#1   137.08(4)

N(1)-Fe(1)-Fe(1)#1   129.49(3)

N(3)#1-Fe(1)-Fe(1)#1 45.87(3)

C(1)-N(1)-C(4)   118.15(12)

C(1)-N(1)-Fe(1)   119.13(10)

C(4)-N(1)-Fe(1)   122.54(9)

C(3)-N(2)-C(14)	116.18(12)
C(3)-N(2)-Fe(1)	117.67(10)
C(14)-N(2)-Fe(1)	126.15(9)
C(22)-N(3)-C(24)	110.21(11)
C(22)-N(3)-Fe(1)	112.78(9)
C(24)-N(3)-Fe(1)	119.73(9)
C(22)-N(3)-Fe(1)#1	106.76(9)
C(24)-N(3)-Fe(1)#1	119.03(9)
Fe(1)-N(3)-Fe(1)#1	85.99(4)
N(1)-C(1)-C(2)	123.69(13)
N(1)-C(1)-C(12)	121.66(13)
C(2)-C(1)-C(12)	114.62(13)
C(3)-C(2)-C(1)	129.18(14)
C(3)-C(2)-H(2)	114.7(11)
C(1)-C(2)-H(2)	114.8(11)
N(2)-C(3)-C(2)	124.37(13)
N(2)-C(3)-C(13)	119.50(13)
C(2)-C(3)-C(13)	116.11(13)
C(9)-C(4)-C(5)	119.82(14)
C(9)-C(4)-N(1)	123.19(14)
C(5)-C(4)-N(1)	116.98(13)
C(6)-C(5)-C(4)	119.54(15)
C(6)-C(5)-C(10)	119.54(15)
C(4)-C(5)-C(10)	120.80(14)
C(7)-C(6)-C(5)	120.80(16)
C(7)-C(6)-H(6)	119.6
C(5)-C(6)-H(6)	119.6
C(8)-C(7)-C(6)	119.44(16)

226

C(8)-C(7)-H(7)   120.3

C(6)-C(7)-H(7)   120.3

C(7)-C(8)-C(9)   121.96(16)

C(7)-C(8)-H(8)   119.0

C(9)-C(8)-H(8)   119.0

C(8)-C(9)-C(4)   118.37(15)

C(8)-C(9)-C(11)   117.31(15)

C(4)-C(9)-C(11)   124.25(15)

C(5)-C(10)-H(10A)   109.5

C(5)-C(10)-H(10B)   109.5

H(10A)-C(10)-H(10B)   109.5

C(5)-C(10)-H(10C)   109.5

H(10A)-C(10)-H(10C)   109.5

H(10B)-C(10)-H(10C)   109.5

C(9)-C(11)-H(11A)   109.5

C(9)-C(11)-H(11B)   109.5

H(11A)-C(11)-H(11B)   109.5

C(9)-C(11)-H(11C)   109.5

H(11A)-C(11)-H(11C)   109.5

H(11B)-C(11)-H(11C)   109.5

C(1)-C(12)-H(12A)   109.5

C(1)-C(12)-H(12B)   109.5

H(12A)-C(12)-H(12B)   109.5

C(1)-C(12)-H(12C)   109.5

H(12A)-C(12)-H(12C)   109.5

H(12B)-C(12)-H(12C)   109.5

C(3)-C(13)-H(13A)   109.5

C(3)-C(13)-H(13B)   109.5

H(13A)-C(13)-H(13B)	109.5
C(3)-C(13)-H(13C)	109.5
H(13A)-C(13)-H(13C)	109.5
H(13B)-C(13)-H(13C)	109.5
C(19)-C(14)-C(15)	119.87(14)
C(19)-C(14)-N(2)	120.90(13)
C(15)-C(14)-N(2)	119.22(13)
C(16)-C(15)-C(14)	119.25(15)
C(16)-C(15)-C(20)	118.99(15)
C(14)-C(15)-C(20)	121.76(14)
C(17)-C(16)-C(15)	121.01(16)
C(17)-C(16)-H(16)	119.5
C(15)-C(16)-H(16)	119.5
C(18)-C(17)-C(16)	119.55(16)
C(18)-C(17)-H(17)	120.2
C(16)-C(17)-H(17)	120.2
C(17)-C(18)-C(19)	121.37(16)
C(17)-C(18)-H(18)	119.3
C(19)-C(18)-H(18)	119.3
C(18)-C(19)-C(14)	118.84(15)
C(18)-C(19)-C(21)	119.93(14)
C(14)-C(19)-C(21)	121.19(14)
C(15)-C(20)-H(20A)	109.5
C(15)-C(20)-H(20B)	109.5
H(20A)-C(20)-H(20B)	109.5
C(15)-C(20)-H(20C)	109.5
H(20A)-C(20)-H(20C)	109.5
H(20B)-C(20)-H(20C)	109.5

228

C(19)-C(21)-H(21A) 109.5

C(19)-C(21)-H(21B) 109.5

H(21A)-C(21)-H(21B)   109.5

C(19)-C(21)-H(21C) 109.5

H(21A)-C(21)-H(21C)   109.5

H(21B)-C(21)-H(21C)   109.5

N(3)-C(22)-C(23)   115.92(13)

N(3)-C(22)-H(22A)   108.3

C(23)-C(22)-H(22A)   108.3

N(3)-C(22)-H(22B)   108.3

C(23)-C(22)-H(22B)   108.3

H(22A)-C(22)-H(22B)   107.4

C(22)-C(23)-H(23A) 109.5

C(22)-C(23)-H(23B) 109.5

H(23A)-C(23)-H(23B)   109.5

C(22)-C(23)-H(23C) 109.5

H(23A)-C(23)-H(23C)   109.5

H(23B)-C(23)-H(23C)   109.5

N(3)-C(24)-C(25)   114.79(12)

N(3)-C(24)-H(24A)   108.6

C(25)-C(24)-H(24A)   108.6

N(3)-C(24)-H(24B)   108.6

C(25)-C(24)-H(24B)   108.6

H(24A)-C(24)-H(24B)   107.5

C(24)-C(25)-H(25A)   109.5

C(24)-C(25)-H(25B)   109.5

H(25A)-C(25)-H(25B)   109.5

C(24)-C(25)-H(25C) 109.5

229

H(25A)-C(25)-H(25C)   109.5

H(25B)-C(25)-H(25C)   109.5

Symmetry transformations used to generate equivalent atoms:

#1 -x+3/2,-y+1/2,-z+1

Table E4. Anisotropic displacement parameters $(\text{Å}^2 \text{x } 10^3)$ for dimeric 2,4-bis[(2,6-dimethylphenyl)imino]pentane iron *N,N*-diethylamide complex (**3.3**). The anisotropic displacement factor exponent takes the form: $-2\pi^2[\ h^2 \ a^{*2}U^{11} + ... \ + 2 \ h \ k \ a^* \ b^* \ U^{12}\ ]$

	U^{11}	U^{22}	U^{33}	U^{23}	U^{13}	U^{12}
Fe(1)	13(1)	6(1)	7(1)	-1(1)	2(1)	-1(1)
N(1)	15(1)	9(1)	8(1)	1(1)	3(1)	0(1)
N(2)	14(1)	8(1)	10(1)	1(1)	4(1)	0(1)
N(3)	10(1)	10(1)	9(1)	-1(1)	2(1)	0(1)
C(1)	13(1)	11(1)	10(1)	-1(1)	3(1)	4(1)
C(2)	12(1)	12(1)	10(1)	-4(1)	2(1)	-1(1)
C(3)	12(1)	9(1)	14(1)	-2(1)	6(1)	0(1)
C(4)	19(1)	12(1)	6(1)	-3(1)	4(1)	-4(1)
C(5)	20(1)	15(1)	10(1)	-4(1)	4(1)	-4(1)
C(6)	20(1)	27(1)	16(1)	-6(1)	7(1)	-9(1)
C(7)	32(1)	26(1)	15(1)	-3(1)	10(1)	-16(1)
C(8)	37(1)	15(1)	10(1)	2(1)	6(1)	-7(1)
C(9)	26(1)	13(1)	9(1)	-2(1)	4(1)	-2(1)
C(10)	18(1)	17(1)	21(1)	-2(1)	7(1)	2(1)
C(11)	32(1)	22(1)	14(1)	6(1)	7(1)	9(1)
C(12)	24(1)	22(1)	11(1)	-3(1)	6(1)	-7(1)
C(13)	19(1)	13(1)	16(1)	-1(1)	5(1)	-5(1)
C(14)	14(1)	8(1)	12(1)	3(1)	3(1)	-3(1)
C(15)	17(1)	10(1)	19(1)	1(1)	6(1)	-3(1)
C(16)	20(1)	12(1)	28(1)	6(1)	7(1)	2(1)
C(17)	26(1)	19(1)	23(1)	13(1)	3(1)	0(1)
C(18)	26(1)	25(1)	15(1)	7(1)	7(1)	-4(1)
C(19)	18(1)	14(1)	14(1)	2(1)	5(1)	-4(1)

231

C(20)	25(1)	15(1)	24(1)	1(1)	12(1)	4(1)
C(21)	27(1)	22(1)	14(1)	2(1)	10(1)	3(1)
C(22)	15(1)	14(1)	12(1)	2(1)	3(1)	2(1)
C(23)	18(1)	15(1)	25(1)	4(1)	5(1)	3(1)
C(24)	16(1)	14(1)	14(1)	-2(1)	7(1)	-1(1)
C(25)	16(1)	16(1)	19(1)	-2(1)	7(1)	-3(1)

Table E5. Crystal data and structure refinement for dimeric 2,4-bis[(2,6-dimethylphenyl)imino]pentane iron phenyl complex (**3.4**).

Identification code   C54H60Fe2N4(C4H10O)

Empirical formula   C58 H70 Fe2 N4 O

Formula weight   950.88

Temperature   100(2) K

Wavelength   1.54178 Å

Crystal system   Orthorhombic

Space group   Pbca

Unit cell dimensions   a = 13.5021(4) Å α= 90°.

    b = 22.3216(6) Å β= 90°.

    c = 33.1135(10) Å γ = 90°.

Volume   9980.0(5) Å^3

Z   8

Density (calculated)   1.266 Mg/m^3

Absorption coefficient   4.990 mm^{-1}

F(000) 4048

Crystal size   0.480 x 0.400 x 0.280 mm^3

Theta range for data collection   2.669 to 69.544°.

Index ranges   -15<=h<=16, -27<=k<=23, -23<=l<=38

Reflections collected   37898

Independent reflections   9062 [R(int) = 0.0398]

Completeness to theta = 67.679°   98.8 %

Absorption correction Semi-empirical from equivalents

Max. and min. transmission   0.7532 and 0.4281

Refinement method   Full-matrix least-squares on F^2

Data / restraints / parameters 9062 / 0 / 598

233

Goodness-of-fit on F^2 1.026

Final R indices [I>2sigma(I)] R1 = 0.0379, wR2 = 0.0886

R indices (all data)   R1 = 0.0453, wR2 = 0.0931

Extinction coefficient n/a

Largest diff. peak and hole   0.459 and -0.583 e.Å^{-3}

Table E6. Atomic coordinates (x 10^4) and equivalent isotropic displacement parameters (Å^{2}x 10^3) for dimeric 2,4-bis[(2,6-dimethylphenyl)imino]pentane iron phenyl complex (**3.4**). U(eq) is defined as one third of the trace of the orthogonalized U^{ij} tensor.
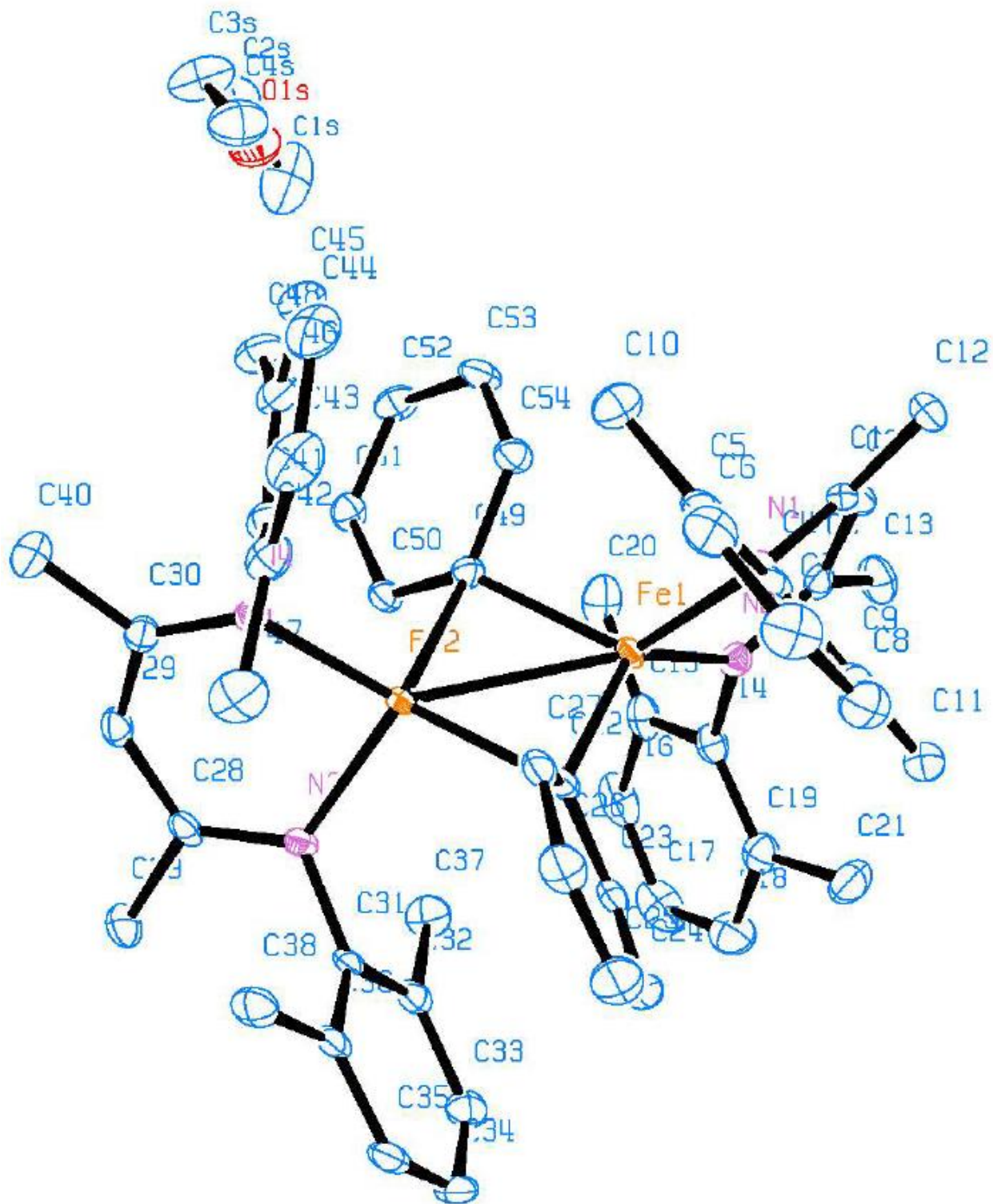
	x	y	z	U(eq)
Fe(1)	3350(1)	3847(1)	4006(1)	12(1)
Fe(2)	1949(1)	3201(1)	3642(1)	12(1)
N(1)	3207(1)	4361(1)	4510(1)	15(1)
N(2)	4770(1)	4115(1)	3917(1)	16(1)
N(3)	2088(1)	2413(1)	3347(1)	14(1)
N(4)	508(1)	3287(1)	3470(1)	15(1)
C(1)	3728(2)	4866(1)	4553(1)	17(1)
C(2)	4542(2)	5015(1)	4308(1)	18(1)
C(3)	5084(2)	4647(1)	4047(1)	17(1)
C(4)	2586(2)	4184(1)	4843(1)	17(1)
C(5)	1572(2)	4323(1)	4840(1)	19(1)
C(6)	978(2)	4114(1)	5154(1)	26(1)
C(7)	1372(2)	3777(1)	5464(1)	30(1)
C(8)	2377(2)	3647(1)	5465(1)	27(1)
C(9)	2994(2)	3843(1)	5156(1)	20(1)
C(10)	1129(2)	4684(1)	4504(1)	26(1)
C(11)	4069(2)	3669(1)	5155(1)	23(1)
C(12)	3484(2)	5300(1)	4888(1)	22(1)
C(13)	6097(2)	4874(1)	3920(1)	26(1)
C(14)	5429(1)	3746(1)	3681(1)	17(1)
C(15)	5541(2)	3837(1)	3265(1)	21(1)
C(16)	6127(2)	3438(1)	3049(1)	28(1)
C(17)	6610(2)	2969(1)	3237(1)	33(1)
C(18)	6532(2)	2900(1)	3650(1)	29(1)
C(19)	5952(2)	3289(1)	3879(1)	21(1)

236

C(20)	5091(2)	4363(1)	3049(1)	28(1)
C(21)	5933(2)	3234(1)	4331(1)	28(1)
C(22)	2685(2)	3046(1)	4193(1)	16(1)
C(23)	3459(2)	2635(1)	4272(1)	18(1)
C(24)	3392(2)	2210(1)	4574(1)	26(1)
C(25)	2525(2)	2155(1)	4794(1)	32(1)
C(26)	1739(2)	2536(1)	4724(1)	26(1)
C(27)	1828(2)	2988(1)	4435(1)	18(1)
C(28)	1571(2)	2300(1)	3011(1)	16(1)
C(29)	748(2)	2641(1)	2893(1)	19(1)
C(30)	200(2)	3053(1)	3123(1)	17(1)
C(31)	2699(2)	1941(1)	3504(1)	14(1)
C(32)	3720(2)	1932(1)	3422(1)	17(1)
C(33)	4302(2)	1491(1)	3602(1)	21(1)
C(34)	3895(2)	1070(1)	3857(1)	23(1)
C(35)	2883(2)	1079(1)	3932(1)	20(1)
C(36)	2275(2)	1509(1)	3756(1)	16(1)
C(37)	4178(2)	2392(1)	3149(1)	24(1)
C(38)	1178(2)	1501(1)	3841(1)	23(1)
C(39)	1839(2)	1767(1)	2752(1)	23(1)
C(40)	-819(2)	3203(1)	2958(1)	30(1)
C(41)	-162(1)	3659(1)	3699(1)	18(1)
C(42)	-666(2)	3405(1)	4027(1)	23(1)
C(43)	-1243(2)	3777(1)	4270(1)	32(1)
C(44)	-1347(2)	4379(1)	4187(1)	32(1)
C(45)	-887(2)	4616(1)	3852(1)	26(1)
C(46)	-296(2)	4264(1)	3599(1)	21(1)
C(47)	-634(2)	2741(1)	4106(1)	32(1)

237

C(48)	131(2)	4542(1)	3226(1)	27(1)
C(49)	2628(1)	4008(1)	3429(1)	15(1)
C(50)	2729(2)	3833(1)	3022(1)	16(1)
C(51)	2683(2)	4239(1)	2704(1)	18(1)
C(52)	2607(2)	4848(1)	2780(1)	21(1)
C(53)	2546(2)	5043(1)	3176(1)	21(1)
C(54)	2521(2)	4633(1)	3492(1)	18(1)
C(1S)	2875(2)	6122(2)	1608(1)	53(1)
C(2S)	1838(2)	6299(1)	1709(1)	36(1)
C(3S)	542(2)	6088(1)	2162(1)	41(1)
C(4S)	333(2)	5799(1)	2562(1)	36(1)
O(1S)	1543(1)	5980(1)	2058(1)	31(1)

238

Table E7. Bond lengths [Å] and angles [°] for dimeric 2,4-bis[(2,6-dimethylphenyl)imino]pentane iron phenyl complex (**3.4**).

Fe(1)-N(2)	2.0301(17)
Fe(1)-N(1)	2.0356(17)
Fe(1)-C(22)	2.096(2)
Fe(1)-C(49)	2.175(2)
Fe(1)-Fe(2)	2.6664(4)
Fe(2)-N(3)	2.0207(16)
Fe(2)-N(4)	2.0368(17)
Fe(2)-C(22)	2.106(2)
Fe(2)-C(49)	2.142(2)
N(1)-C(1)	1.335(3)
N(1)-C(4)	1.440(3)
N(2)-C(3)	1.332(3)
N(2)-C(14)	1.442(3)
N(3)-C(28)	1.335(3)
N(3)-C(31)	1.436(2)
N(4)-C(30)	1.328(3)
N(4)-C(41)	1.445(3)
C(1)-C(2)	1.405(3)
C(1)-C(12)	1.511(3)
C(2)-C(3)	1.400(3)
C(2)-H(2)	0.9500
C(3)-C(13)	1.518(3)
C(4)-C(9)	1.399(3)
C(4)-C(5)	1.404(3)
C(5)-C(6)	1.394(3)
C(5)-C(10)	1.499(3)

239

C(6)-C(7)   1.380(3)

C(6)-H(6)   0.9500

C(7)-C(8)   1.388(3)

C(7)-H(7)   0.9500

C(8)-C(9)   1.389(3)

C(8)-H(8)   0.9500

C(9)-C(11)   1.503(3)

C(10)-H(10A)   0.9800

C(10)-H(10B) 0.9800

C(10)-H(10C) 0.9800

C(11)-H(11A)   0.9800

C(11)-H(11B) 0.9800

C(11)-H(11C) 0.9800

C(12)-H(12A)   0.9800

C(12)-H(12B) 0.9800

C(12)-H(12C) 0.9800

C(13)-H(13A)   0.9800

C(13)-H(13B) 0.9800

C(13)-H(13C) 0.9800

C(14)-C(15)   1.400(3)

C(14)-C(19)   1.404(3)

C(15)-C(16)   1.391(3)

C(15)-C(20)   1.504(3)

C(16)-C(17)   1.381(4)

C(16)-H(16)   0.9500

C(17)-C(18)   1.382(4)

C(17)-H(17)   0.9500

C(18)-C(19)   1.394(3)

240

C(18)-H(18)   0.9500

C(19)-C(21)   1.500(3)

C(20)-H(20A)   0.9800

C(20)-H(20B) 0.9800

C(20)-H(20C) 0.9800

C(21)-H(21A)   0.9800

C(21)-H(21B) 0.9800

C(21)-H(21C) 0.9800

C(22)-C(27)   1.413(3)

C(22)-C(23)   1.414(3)

C(23)-C(24)   1.381(3)

C(23)-H(23)   0.9500

C(24)-C(25)   1.385(4)

C(24)-H(24)   0.9500

C(25)-C(26)   1.380(4)

C(25)-H(25)   0.9500

C(26)-C(27)   1.395(3)

C(26)-H(26)   0.9500

C(27)-H(27)   0.9500

C(28)-C(29)   1.402(3)

C(28)-C(39)   1.511(3)

C(29)-C(30)   1.407(3)

C(29)-H(29)   0.9500

C(30)-C(40)   1.517(3)

C(31)-C(36)   1.398(3)

C(31)-C(32)   1.406(3)

C(32)-C(33)   1.394(3)

C(32)-C(37)   1.500(3)

241

C(33)-C(34)   1.379(3)

C(33)-H(33)   0.9500

C(34)-C(35)   1.389(3)

C(34)-H(34)   0.9500

C(35)-C(36)   1.390(3)

C(35)-H(35)   0.9500

C(36)-C(38)   1.509(3)

C(37)-H(37A)   0.9800

C(37)-H(37B) 0.9800

C(37)-H(37C) 0.9800

C(38)-H(38A)   0.9800

C(38)-H(38B) 0.9800

C(38)-H(38C) 0.9800

C(39)-H(39A)   0.9800

C(39)-H(39B) 0.9800

C(39)-H(39C) 0.9800

C(40)-H(40A)   0.9800

C(40)-H(40B) 0.9800

C(40)-H(40C) 0.9800

C(41)-C(42)   1.401(3)

C(41)-C(46)   1.402(3)

C(42)-C(43)   1.394(3)

C(42)-C(47)   1.507(3)

C(43)-C(44)   1.380(4)

C(43)-H(43)   0.9500

C(44)-C(45)   1.377(4)

C(44)-H(44)   0.9500

C(45)-C(46)   1.397(3)

242

C(45)-H(45)   0.9500

C(46)-C(48)   1.498(3)

C(47)-H(47A)   0.9800

C(47)-H(47B) 0.9800

C(47)-H(47C) 0.9800

C(48)-H(48A)   0.9800

C(48)-H(48B) 0.9800

C(48)-H(48C) 0.9800

C(49)-C(50)   1.410(3)

C(49)-C(54)   1.418(3)

C(50)-C(51)   1.389(3)

C(50)-H(50)   0.9500

C(51)-C(52)   1.386(3)

C(51)-H(51)   0.9500

C(52)-C(53)   1.386(3)

C(52)-H(52)   0.9500

C(53)-C(54)   1.391(3)

C(53)-H(53)   0.9500

C(54)-H(54)   0.9500

C(1S)-C(2S)   1.493(4)

C(1S)-H(1SA)   0.9800

C(1S)-H(1SB)   0.9800

C(1S)-H(1SC)   0.9800

C(2S)-O(1S)   1.415(3)

C(2S)-H(2SA)   0.9900

C(2S)-H(2SB)   0.9900

C(3S)-O(1S)   1.414(3)

C(3S)-C(4S)   1.500(4)

243

C(3S)-H(3SA)	0.9900
C(3S)-H(3SB)	0.9900
C(4S)-H(4SA)	0.9800
C(4S)-H(4SB)	0.9800
C(4S)-H(4SC)	0.9800
N(2)-Fe(1)-N(1)	92.41(7)
N(2)-Fe(1)-C(22)	134.32(7)
N(1)-Fe(1)-C(22)	101.38(7)
N(2)-Fe(1)-C(49)	104.38(7)
N(1)-Fe(1)-C(49)	125.82(7)
C(22)-Fe(1)-C(49)	102.08(8)
N(2)-Fe(1)-Fe(2)	139.87(5)
N(1)-Fe(1)-Fe(2)	127.45(5)
C(22)-Fe(1)-Fe(2)	50.79(6)
C(49)-Fe(1)-Fe(2)	51.30(5)
N(3)-Fe(2)-N(4)	91.98(7)
N(3)-Fe(2)-C(22)	103.48(7)
N(4)-Fe(2)-C(22)	135.21(8)
N(3)-Fe(2)-C(49)	122.15(7)
N(4)-Fe(2)-C(49)	103.68(7)
C(22)-Fe(2)-C(49)	102.84(8)
N(3)-Fe(2)-Fe(1)	128.58(5)
N(4)-Fe(2)-Fe(1)	138.88(5)
C(22)-Fe(2)-Fe(1)	50.44(5)
C(49)-Fe(2)-Fe(1)	52.42(6)
C(1)-N(1)-C(4)	117.24(17)
C(1)-N(1)-Fe(1)	120.78(14)
C(4)-N(1)-Fe(1)	121.91(12)

244

C(3)-N(2)-C(14)	119.17(17)
C(3)-N(2)-Fe(1)	121.09(14)
C(14)-N(2)-Fe(1)	119.53(13)
C(28)-N(3)-C(31)	117.60(16)
C(28)-N(3)-Fe(2)	121.26(13)
C(31)-N(3)-Fe(2)	121.02(13)
C(30)-N(4)-C(41)	118.98(17)
C(30)-N(4)-Fe(2)	120.33(14)
C(41)-N(4)-Fe(2)	120.32(13)
N(1)-C(1)-C(2)	123.45(19)
N(1)-C(1)-C(12)	120.22(19)
C(2)-C(1)-C(12)	116.27(18)
C(3)-C(2)-C(1)	128.80(19)
C(3)-C(2)-H(2)	115.6
C(1)-C(2)-H(2)	115.6
N(2)-C(3)-C(2)	123.77(19)
N(2)-C(3)-C(13)	119.67(19)
C(2)-C(3)-C(13)	116.53(18)
C(9)-C(4)-C(5)	120.6(2)
C(9)-C(4)-N(1)	119.11(18)
C(5)-C(4)-N(1)	120.18(19)
C(6)-C(5)-C(4)	118.8(2)
C(6)-C(5)-C(10)	120.3(2)
C(4)-C(5)-C(10)	120.84(19)
C(7)-C(6)-C(5)	121.1(2)
C(7)-C(6)-H(6)	119.5
C(5)-C(6)-H(6)	119.5
C(6)-C(7)-C(8)	119.5(2)

245

C(6)-C(7)-H(7)	120.3
C(8)-C(7)-H(7)	120.3
C(7)-C(8)-C(9)	121.3(2)
C(7)-C(8)-H(8)	119.3
C(9)-C(8)-H(8)	119.3
C(8)-C(9)-C(4)	118.7(2)
C(8)-C(9)-C(11)	120.0(2)
C(4)-C(9)-C(11)	121.3(2)
C(5)-C(10)-H(10A)	109.5
C(5)-C(10)-H(10B)	109.5
H(10A)-C(10)-H(10B)	109.5
C(5)-C(10)-H(10C)	109.5
H(10A)-C(10)-H(10C)	109.5
H(10B)-C(10)-H(10C)	109.5
C(9)-C(11)-H(11A)	109.5
C(9)-C(11)-H(11B)	109.5
H(11A)-C(11)-H(11B)	109.5
C(9)-C(11)-H(11C)	109.5
H(11A)-C(11)-H(11C)	109.5
H(11B)-C(11)-H(11C)	109.5
C(1)-C(12)-H(12A)	109.5
C(1)-C(12)-H(12B)	109.5
H(12A)-C(12)-H(12B)	109.5
C(1)-C(12)-H(12C)	109.5
H(12A)-C(12)-H(12C)	109.5
H(12B)-C(12)-H(12C)	109.5
C(3)-C(13)-H(13A)	109.5
C(3)-C(13)-H(13B)	109.5

246

H(13A)-C(13)-H(13B)   109.5

C(3)-C(13)-H(13C)   109.5

H(13A)-C(13)-H(13C)   109.5

H(13B)-C(13)-H(13C)   109.5

C(15)-C(14)-C(19)   120.7(2)

C(15)-C(14)-N(2)   121.20(19)

C(19)-C(14)-N(2)   118.14(19)

C(16)-C(15)-C(14)   118.4(2)

C(16)-C(15)-C(20)   119.0(2)

C(14)-C(15)-C(20)   122.5(2)

C(17)-C(16)-C(15)   121.4(2)

C(17)-C(16)-H(16)   119.3

C(15)-C(16)-H(16)   119.3

C(16)-C(17)-C(18)   119.8(2)

C(16)-C(17)-H(17)   120.1

C(18)-C(17)-H(17)   120.1

C(17)-C(18)-C(19)   120.7(2)

C(17)-C(18)-H(18)   119.6

C(19)-C(18)-H(18)   119.6

C(18)-C(19)-C(14)   118.8(2)

C(18)-C(19)-C(21)   120.0(2)

C(14)-C(19)-C(21)   121.1(2)

C(15)-C(20)-H(20A)   109.5

C(15)-C(20)-H(20B)   109.5

H(20A)-C(20)-H(20B)   109.5

C(15)-C(20)-H(20C)   109.5

H(20A)-C(20)-H(20C)   109.5

H(20B)-C(20)-H(20C)   109.5

247

C(19)-C(21)-H(21A) 109.5

C(19)-C(21)-H(21B) 109.5

H(21A)-C(21)-H(21B)   109.5

C(19)-C(21)-H(21C) 109.5

H(21A)-C(21)-H(21C)   109.5

H(21B)-C(21)-H(21C)   109.5

C(27)-C(22)-C(23)   116.23(19)

C(27)-C(22)-Fe(1)   126.64(15)

C(23)-C(22)-Fe(1)   106.93(14)

C(27)-C(22)-Fe(2)   96.78(14)

C(23)-C(22)-Fe(2)   127.96(15)

Fe(1)-C(22)-Fe(2)   78.77(7)

C(24)-C(23)-C(22)   122.0(2)

C(24)-C(23)-H(23)   119.0

C(22)-C(23)-H(23)   119.0

C(23)-C(24)-C(25)   119.9(2)

C(23)-C(24)-H(24)   120.1

C(25)-C(24)-H(24)   120.1

C(26)-C(25)-C(24)   120.4(2)

C(26)-C(25)-H(25)   119.8

C(24)-C(25)-H(25)   119.8

C(25)-C(26)-C(27)   119.7(2)

C(25)-C(26)-H(26)   120.2

C(27)-C(26)-H(26)   120.2

C(26)-C(27)-C(22)   121.7(2)

C(26)-C(27)-H(27)   119.2

C(22)-C(27)-H(27)   119.2

N(3)-C(28)-C(29)   123.02(19)

248

N(3)-C(28)-C(39)	119.73(18)
C(29)-C(28)-C(39)	117.19(19)
C(28)-C(29)-C(30)	128.3(2)
C(28)-C(29)-H(29)	115.9
C(30)-C(29)-H(29)	115.9
N(4)-C(30)-C(29)	124.15(19)
N(4)-C(30)-C(40)	120.61(19)
C(29)-C(30)-C(40)	115.19(19)
C(36)-C(31)-C(32)	120.50(18)
C(36)-C(31)-N(3)	119.20(18)
C(32)-C(31)-N(3)	120.23(18)
C(33)-C(32)-C(31)	118.65(19)
C(33)-C(32)-C(37)	120.56(19)
C(31)-C(32)-C(37)	120.78(19)
C(34)-C(33)-C(32)	121.3(2)
C(34)-C(33)-H(33)	119.3
C(32)-C(33)-H(33)	119.3
C(33)-C(34)-C(35)	119.4(2)
C(33)-C(34)-H(34)	120.3
C(35)-C(34)-H(34)	120.3
C(34)-C(35)-C(36)	121.1(2)
C(34)-C(35)-H(35)	119.5
C(36)-C(35)-H(35)	119.5
C(35)-C(36)-C(31)	119.01(19)
C(35)-C(36)-C(38)	119.59(19)
C(31)-C(36)-C(38)	121.40(18)
C(32)-C(37)-H(37A)	109.5
C(32)-C(37)-H(37B)	109.5

249

H(37A)-C(37)-H(37B)   109.5

C(32)-C(37)-H(37C) 109.5

H(37A)-C(37)-H(37C)   109.5

H(37B)-C(37)-H(37C)   109.5

C(36)-C(38)-H(38A) 109.5

C(36)-C(38)-H(38B) 109.5

H(38A)-C(38)-H(38B)   109.5

C(36)-C(38)-H(38C) 109.5

H(38A)-C(38)-H(38C)   109.5

H(38B)-C(38)-H(38C)   109.5

C(28)-C(39)-H(39A) 109.5

C(28)-C(39)-H(39B) 109.5

H(39A)-C(39)-H(39B)   109.5

C(28)-C(39)-H(39C) 109.5

H(39A)-C(39)-H(39C)   109.5

H(39B)-C(39)-H(39C)   109.5

C(30)-C(40)-H(40A) 109.5

C(30)-C(40)-H(40B) 109.5

H(40A)-C(40)-H(40B)   109.5

C(30)-C(40)-H(40C) 109.5

H(40A)-C(40)-H(40C)   109.5

H(40B)-C(40)-H(40C)   109.5

C(42)-C(41)-C(46)   120.6(2)

C(42)-C(41)-N(4)   118.70(19)

C(46)-C(41)-N(4)   120.70(19)

C(43)-C(42)-C(41)   118.6(2)

C(43)-C(42)-C(47)   120.1(2)

C(41)-C(42)-C(47)   121.2(2)

250

C(44)-C(43)-C(42)   121.4(2)

C(44)-C(43)-H(43)   119.3

C(42)-C(43)-H(43)   119.3

C(45)-C(44)-C(43)   119.3(2)

C(45)-C(44)-H(44)   120.3

C(43)-C(44)-H(44)   120.3

C(44)-C(45)-C(46)   121.6(2)

C(44)-C(45)-H(45)   119.2

C(46)-C(45)-H(45)   119.2

C(45)-C(46)-C(41)   118.3(2)

C(45)-C(46)-C(48)   118.7(2)

C(41)-C(46)-C(48)   122.9(2)

C(42)-C(47)-H(47A) 109.5

C(42)-C(47)-H(47B) 109.5

H(47A)-C(47)-H(47B)   109.5

C(42)-C(47)-H(47C) 109.5

H(47A)-C(47)-H(47C)   109.5

H(47B)-C(47)-H(47C)   109.5

C(46)-C(48)-H(48A) 109.5

C(46)-C(48)-H(48B) 109.5

H(48A)-C(48)-H(48B)   109.5

C(46)-C(48)-H(48C) 109.5

H(48A)-C(48)-H(48C)   109.5

H(48B)-C(48)-H(48C)   109.5

C(50)-C(49)-C(54)   115.11(18)

C(50)-C(49)-Fe(2)   97.09(13)

C(54)-C(49)-Fe(2)   137.37(16)

C(50)-C(49)-Fe(1)   138.60(15)

C(54)-C(49)-Fe(1)   94.48(14)

Fe(2)-C(49)-Fe(1)   76.28(7)

C(51)-C(50)-C(49)   122.53(19)

C(51)-C(50)-H(50)   118.7

C(49)-C(50)-H(50)   118.7

C(52)-C(51)-C(50)   120.5(2)

C(52)-C(51)-H(51)   119.8

C(50)-C(51)-H(51)   119.8

C(51)-C(52)-C(53)   118.9(2)

C(51)-C(52)-H(52)   120.5

C(53)-C(52)-H(52)   120.5

C(52)-C(53)-C(54)   120.45(19)

C(52)-C(53)-H(53)   119.8

C(54)-C(53)-H(53)   119.8

C(53)-C(54)-C(49)   122.3(2)

C(53)-C(54)-H(54)   118.9

C(49)-C(54)-H(54)   118.9

C(2S)-C(1S)-H(1SA) 109.5

C(2S)-C(1S)-H(1SB) 109.5

H(1SA)-C(1S)-H(1SB)   109.5

C(2S)-C(1S)-H(1SC) 109.5

H(1SA)-C(1S)-H(1SC)   109.5

H(1SB)-C(1S)-H(1SC)   109.5

O(1S)-C(2S)-C(1S)   108.3(2)

O(1S)-C(2S)-H(2SA) 110.0

C(1S)-C(2S)-H(2SA) 110.0

O(1S)-C(2S)-H(2SB) 110.0

C(1S)-C(2S)-H(2SB) 110.0

252

H(2SA)-C(2S)-H(2SB)   108.4

O(1S)-C(3S)-C(4S)   108.7(2)

O(1S)-C(3S)-H(3SA) 109.9

C(4S)-C(3S)-H(3SA) 109.9

O(1S)-C(3S)-H(3SB) 109.9

C(4S)-C(3S)-H(3SB) 109.9

H(3SA)-C(3S)-H(3SB)   108.3

C(3S)-C(4S)-H(4SA) 109.5

C(3S)-C(4S)-H(4SB) 109.5

H(4SA)-C(4S)-H(4SB)   109.5

C(3S)-C(4S)-H(4SC) 109.5

H(4SA)-C(4S)-H(4SC)   109.5

H(4SB)-C(4S)-H(4SC)   109.5

C(3S)-O(1S)-C(2S)   112.45(19)

_____

Symmetry transformations used to generate equivalent atoms:

Table E8. Anisotropic displacement parameters (Å^2x 10^3) for dimeric 2,4-bis[(2,6-dimethylphenyl)imino]pentane iron phenyl complex (**3.4**). The anisotropic displacement factor exponent takes the form: $-2\pi^2[\, h^2\, a^{*2}U^{11} + ... + 2\, h\, k\, a^*\, b^*\, U^{12}]$

	U^{11}	U^{22}	U^{33}	U^{23}	U^{13}	U^{12}
Fe(1)	15(1)	9(1)	12(1)	-1(1)	-1(1)	-3(1)
Fe(2)	14(1)	8(1)	14(1)	0(1)	-1(1)	-1(1)
N(1)	20(1)	12(1)	14(1)	0(1)	-1(1)	-1(1)
N(2)	15(1)	16(1)	15(1)	2(1)	-1(1)	-1(1)
N(3)	17(1)	10(1)	14(1)	1(1)	1(1)	0(1)
N(4)	14(1)	13(1)	19(1)	3(1)	-1(1)	-1(1)
C(1)	22(1)	9(1)	18(1)	0(1)	-8(1)	2(1)
C(2)	24(1)	10(1)	21(1)	1(1)	-6(1)	-3(1)
C(3)	18(1)	16(1)	17(1)	5(1)	-6(1)	-4(1)
C(4)	25(1)	12(1)	13(1)	-4(1)	1(1)	-1(1)
C(5)	27(1)	14(1)	18(1)	-4(1)	1(1)	2(1)
C(6)	28(1)	27(1)	24(1)	-4(1)	8(1)	2(1)
C(7)	38(1)	32(1)	22(1)	3(1)	11(1)	0(1)
C(8)	40(1)	24(1)	16(1)	3(1)	1(1)	2(1)
C(9)	27(1)	12(1)	19(1)	-2(1)	-2(1)	0(1)
C(10)	23(1)	28(1)	27(1)	2(1)	1(1)	4(1)
C(11)	28(1)	18(1)	22(1)	1(1)	-5(1)	0(1)
C(12)	29(1)	15(1)	21(1)	-5(1)	-5(1)	0(1)
C(13)	26(1)	26(1)	28(1)	-1(1)	-1(1)	-11(1)
C(14)	15(1)	19(1)	18(1)	-2(1)	1(1)	-6(1)
C(15)	19(1)	26(1)	18(1)	0(1)	2(1)	-11(1)
C(16)	26(1)	35(1)	24(1)	-8(1)	10(1)	-15(1)
C(17)	21(1)	35(1)	43(2)	-15(1)	13(1)	-5(1)

254

C(18)	20(1)	27(1)	40(2)	-2(1)	2(1)	2(1)
C(19)	17(1)	23(1)	24(1)	-1(1)	-1(1)	-3(1)
C(20)	29(1)	37(1)	17(1)	6(1)	1(1)	-10(1)
C(21)	28(1)	31(1)	26(1)	6(1)	-8(1)	4(1)
C(22)	25(1)	10(1)	14(1)	0(1)	-2(1)	-4(1)
C(23)	25(1)	12(1)	16(1)	-5(1)	-5(1)	-2(1)
C(24)	38(1)	17(1)	23(1)	0(1)	-12(1)	5(1)
C(25)	49(2)	24(1)	22(1)	11(1)	-5(1)	-6(1)
C(26)	36(1)	24(1)	18(1)	5(1)	2(1)	-10(1)
C(27)	25(1)	14(1)	15(1)	-4(1)	-2(1)	-2(1)
C(28)	22(1)	11(1)	16(1)	0(1)	0(1)	-6(1)
C(29)	26(1)	18(1)	13(1)	1(1)	-6(1)	-5(1)
C(30)	18(1)	15(1)	19(1)	5(1)	-4(1)	-4(1)
C(31)	21(1)	7(1)	13(1)	-3(1)	-2(1)	0(1)
C(32)	23(1)	14(1)	15(1)	-3(1)	0(1)	-1(1)
C(33)	20(1)	19(1)	25(1)	-6(1)	1(1)	5(1)
C(34)	31(1)	12(1)	25(1)	0(1)	-4(1)	8(1)
C(35)	32(1)	9(1)	19(1)	0(1)	0(1)	-2(1)
C(36)	23(1)	10(1)	16(1)	-3(1)	-1(1)	-2(1)
C(37)	22(1)	24(1)	27(1)	4(1)	4(1)	-2(1)
C(38)	25(1)	17(1)	28(1)	5(1)	2(1)	-4(1)
C(39)	30(1)	22(1)	17(1)	-7(1)	-4(1)	-2(1)
C(40)	24(1)	29(1)	38(2)	1(1)	-12(1)	1(1)
C(41)	13(1)	19(1)	20(1)	2(1)	-2(1)	0(1)
C(42)	17(1)	28(1)	25(1)	6(1)	0(1)	-1(1)
C(43)	20(1)	47(2)	28(1)	5(1)	7(1)	2(1)
C(44)	23(1)	41(2)	31(2)	-6(1)	2(1)	11(1)
C(45)	23(1)	25(1)	31(1)	0(1)	-4(1)	8(1)

C(46)	17(1)	22(1)	25(1)	4(1)	-3(1)	2(1)
C(47)	26(1)	31(1)	37(2)	13(1)	5(1)	-5(1)
C(48)	28(1)	22(1)	30(1)	10(1)	-2(1)	4(1)
C(49)	15(1)	14(1)	17(1)	2(1)	-1(1)	0(1)
C(50)	19(1)	13(1)	14(1)	-2(1)	0(1)	0(1)
C(51)	21(1)	20(1)	13(1)	0(1)	1(1)	-1(1)
C(52)	25(1)	19(1)	20(1)	9(1)	1(1)	1(1)
C(53)	31(1)	10(1)	23(1)	0(1)	1(1)	0(1)
C(54)	25(1)	15(1)	15(1)	1(1)	0(1)	0(1)
C(1S)	37(2)	92(3)	29(2)	-3(2)	6(1)	0(2)
C(2S)	39(1)	36(1)	32(2)	3(1)	1(1)	-4(1)
C(3S)	36(1)	40(2)	47(2)	15(1)	10(1)	13(1)
C(4S)	42(1)	34(1)	33(2)	3(1)	8(1)	9(1)
O(1S)	32(1)	33(1)	27(1)	5(1)	3(1)	7(1)